Durham E-Theses

Phenomenology of long baseline neutrino oscillation Beta Beam experiments and their related technologies

ORME, CHRISTOPHER,DAVD

Phenomenology of long baseline neutrino oscillation Beta Beam experiments and their related technologies

A thesis presented for the degree
of Doctor of Philosophy
by

Christopher David Orme

Department of Physics and Astronomy
December 2009

Durham
University

Abstract

The primary goal of the future experimental program in neutrino oscillation physics is to determine the size of the unknown mixing angle, θ_{13}, whether CP-violation is present in the leptonic sector and the sign of the atmospheric mass squared splitting. If θ_{13} is not found by upcoming experiments, then we must turn to intense sources of neutrinos: the Superbeam, Neutrino Factory or Beta Beams.

The phenomenon and present status of neutrino oscillations is introduced and future experimental options and some of the strategies summarised. A measurement of θ_{13} and the CP-phase δ requires a search of sub-dominant appearance events, such as $\nu_e \rightarrow \nu_\mu$. In general, neutrino appearance data can accommodate up to 8 different solutions. This 'problem of degeneracies' is discussed and some of the strategies to resolve them are highlighted. A Beta Beam is an intense, clean and collimated electron neutrino beam sourced from the the acceleration of radioactive ions. In this thesis, the ability of Beta Beams, using a neutrino run only, to resolve these degeneracies is explored. The energy dependence of the neutrino oscillation probability and degeneracies is exploited to achieve a good overall CP-violation reach. This approach is adapted to the variants on the Beta Beam idea; namely the electron capture beams and hybrid beams. It is found for all cases considered that the reach is heavily dependent on the event rate with degeneracies causing major problems for low luminosity machines. The need for high event rates suggests that electron capture and hybrid machines will not be competitive without extensive R&D. The single ion Beta Beam is a viable alternative to the dual ion Beta Beams considered in the literature. Future studies may indicate that it in fact has a better overall physics reach.

Declaration

This thesis is the result of my own work, except where explicit reference is made to the work of others, and has not been submitted for another qualification to this or any other university.

Chapters 4, 5 and 6 are based on a number of published and archived papers. Specifically, chapter 4 is based on the study

> *An intermediate gamma beta beam experiment with long baseline*, JHEP **0807** (2008) 115 [arXiv:0802.0255 [hep-ph]].

The results presented in that work have been re-simulated under slightly different assumptions to make it consistent with the other phenomenological studies in this thesis. The material presented in chapter 4 should therefore be considered solely the author's. I was also heavily involved in the development of the physics and presentation strategy of the original paper.

Chapter 5 is an analysis of an electron capture machine that extends work of collaborators based at CERN and Valencia. The work in this chapter is solely of the author and most of the material therein has not been submitted to the archive or any journal. The sections discussing the feasibility of using bound beta decays as a source for a Beta Beam type experiment is an abridged account based on

> *On the possibility of sourcing a mono-enegetic $\bar{\nu}_e$ beta beam from bound beta decay* [arXiv:0901.4287];

of which I am the sole author. The content of this chapter will be prepared for publication in late Autumn this year.

Chapter 6 contains a selection of some of the analyses carried out in

> *A combined beta-beam and electron capture neutrino experiment* JHEP **0906** (2009) 040 [arXiv:0902.4903 [hep-ph]].

The idea for this study developed independently from myself and discussions between Sergio Palomares-Ruiz and Jose Bernabeu. The results presented are from the simulations of Catalina Espinoza; a graduate student of Prof Bernabeu. I was influential in the writing of the paper and the overall strategy of the paper. In particular, the opinions expressed in chapter 6 with regards the motivation, feasibility of the idea and its place in the overall long baseline experimental programme are my own.

<div align="right">

Christopher Orme

November 2009

</div>

Between the first submission and the first revision, the content of chapter 5 has been submitted to the archive as the article

CP-violation reach of an electron capture neutrino beam [arXiv:0912.2676];

and will be forwarded to a journal in view of publication. An extended discussion of the resolution of degeneracies appears in this paper which is incorporated into the discussion of chapter 4. The relevant section from the preprint is reproduced verbatim in thesis as Appendix C for reference.

<div align="right">

Christopher Orme

January 2010

</div>

Acknowledgements

Firstly, I would like to thank my supervisor, Silvia Pascoli, for guidance, patience, presistence and the provision of opportunity.

I would like to thank all the office mates I have had over the four years for putting up with me: Sophy Palmer, Callum Durnford, Joao Pires, Nehir Ikizlerli, Jon Tully, Jamie Tattersall, Alison Fowler, Tiago Fleury, Paul Mellor, Dan Roythorne, Alex Merson, Elise Jennings, Nikos Nikoloudakis and Nikos Fanidakis.

This work on Beta Beams was born out of collaborations and discussions with many people: Mats Lindroos, Adrian Fabich, Sergio Palomares-Ruiz, Olga Mena, Davide Meloni, Jose Bernabeu, Catalina Espinoza, Thomas Schwetz, Walter Winter, Patrick Huber, Mauro Mezzetto, and Elena Wildner. I thank Mats for answering all my questions on the technological aspects of the Beta Beam and Thomas Schwetz for his patience in answering questions on statistics in long baseline neutrino oscillation experiments.

I would like thank the CERN ISOLDE and Beta Beam groups for their warm hospitality on a number of occasions; Karsten Riisager, Michael Benedikt, Yorick Blumenfeld for allowing me to stay within the group; and Jenny Weterings for putting up with the CERN administration on my behalf. A special mention needs to go for the Departamento de Física Teórica, Valencia where I worked on the hybrid Beta Beams with Jose Bernabeu and Catalina Espinoza.

Contents

Contents

Chapter 1.

Introduction

Wolfgang Pauli was apologetic when he postulated the existence of the neutrino to save the principle of energy conservation in radioactive decays [1]. He felt that he had set an impossible task for experimentalists; a light particle, possibly with zero mass, that was neutral. This fear was deepened by Bethe and Peierls a few years later when they showed that its cross-section with matter must be extremely small [2]. However, with the advent of nuclear warfare and nuclear power, intense sources of radioactive nuclei became available. Reines and Cowan made use of this advance and discovered the neutrino in a water and Cadmium Chloride detector placed near the nuclear reactor at Savannah river, South Carolina [3].

Neutrinos are spin-1/2 particles that interact with matter via Weak interactions. Experiments examining the helicity of ejected electrons in the decay of Cobalt-60 indicate that neutrinos violate parity maximally [4]; only left-handed neutrinos or right-handed anti-neutrinos appear to interact with matter. Within the Standard Model this is accommodated by placing the left-handed neutrino in an SU(2) doublet with the electron; and treating the right-handed electron as an SU(2) singlet. The right-handed neutrino and left-handed anti-neutrino do not appear in the Standard Model. This has the consequence that neutrino masses cannot be constructed in the same manner as the other fermions, and so neutrinos are assumed to be massless in the Standard Model. There is, however, no exact symmetry that forbids the existence of neutrino mass. Neutrinos are electrically neutral and can therefore be Majorana particles. Majorana mass terms can be constructed with Standard Model fields and the gauge symmetries, however, such terms violate lepton number and are non-renormalisable. These terms relate the neutrino mass to higher energy scales and are a natural way to generate very small neutrino masses consistent with the bounds from laboratory experiments.

Direct searches for neutrino mass concentrate on searching for distortions close to the endpoint of the electron spectrum of a beta decay; however none have returned a non-zero mass.

The current bound is set by the Troitsk [5] and Mainz [6] Tritium experiments: $m_\nu < 2.3$ eV. Within the next decade, the range 0.2 eV $< m_\nu < 2.3$ eV will be explored by the KATRIN [7] and MARE [8] experiments. Indirect searches have been more successful. Experiments set up to measure the neutrino flux from the sun [9] and the interaction of cosmic rays with the upper atmosphere [10, 11, 12] have indicated that neutrinos of a given flavour can transmute into another; a trick that requires the neutrino to be massive. This trick is the phenomenon of neutrino oscillations.

Neutrino oscillations is a physical phenomenon initially conceived by Pontecorvo in the 1950s [13]. The flavour of a neutrino is tagged by the lepton accompanying it at a weak interaction vertex, not by its mass. Consequently, a neutrino of given flavour can be a superposition of mass eigenstates which, if produced and detected coherently, can evolve into a different flavour over distance; an effect dependent on the mass-squared splittings of the neutrino mass states. The neutrino 'mixing' is described by a 3×3 unitary matrix parameterised by 3 mixing angles and 1 (or 3) physical phases [14]. At present, 2 mixing angles and the two mass-squared splittings are known [15]; however, the third mixing angle, the physical phases and the sign of one of the mass-squared splittings are all unknown. The goal of the future neutrino experimental programme is to determine the absolute neutrino mass scale, whether the neutrino is a Dirac or Majorana particle; and make measurements of the unknown mixing and oscillation parameters. The current and near future neutrino oscillation experimental program focuses on conventional accelerator and reactor sources. The far future might require the use of intense neutrino beams such as the Superbeam, Neutrino Factory or Beta Beam.

This thesis is not a study of neutrino masses, nor is it primarily about neutrino oscillations in general. The goal of this thesis is the study of the Beta Beam class of machines that may be part of the future neutrino oscillation experimental program. A Beta Beam is a particle accelerator and storage complex that can source clean, intense and collimated beams of electron neutrinos and anti-neutrinos. Radioactive ions will be produced by existing or specially built nuclear ion facilities and then accelerated to a large Lorentz boost. This action produces an intense neutrino spectrum covering a range of laboratory energies suitable for the future experimental program of long baseline neutrino oscillation experiments. The aim of the thesis is to provide an introduction to the phenomenology of three-neutrino mixing and oscillations and some of the experimental challenges before discussing in detail the physics of a Beta Beam [16] and its related technologies. This work is part of a worldwide collaborative study into a future long baseline neutrino oscillation facility.
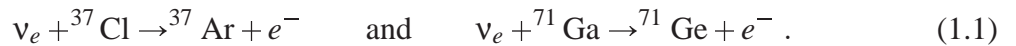
This introductory chapter gives a brief overview of neutrino mixing and oscillations; and reviews the present experimental status of the leptonic mixing matrix. The main facilities that

will attempt to improve current limits and measure the unknown parameters, both in the near and far future, will be introduced. The chapter ends with a detailed outline of the thesis.

1.1. Neutrinos have mass

For a long time neutrinos were thought to be massless. With no right-handed neutrino field in the Standard Model, neutrino mass cannot be generated in the same manner as the other leptons. This view changed suddenly with the discovery that neutrinos can change flavour in the passage from source to detection; a result that requires neutrinos to have a non-zero proper time and hence mass. Our current description of these conversions is within the framework of neutrino mixing and oscillations, suggested theoretically by Pontecorvo in the 1950s [13]. This description has now been confirmed by a series of experiments measuring the atmospheric and solar neutrino fluxes; and a number of groundbreaking terrestrial experiments using neutrinos from nuclear reactors and accelerators.

A drama had been unfolding in the study of solar neutrinos since the first publication of data from the Davis Homestake experiment [17]. This was one of a series of radiochemical experiments designed to capture solar neutrinos via the reactions

$$\nu_e + {}^{37}\text{Cl} \rightarrow {}^{37}\text{Ar} + e^- \qquad \text{and} \qquad \nu_e + {}^{71}\text{Ga} \rightarrow {}^{71}\text{Ge} + e^- \ . \qquad (1.1)$$

The solar neutrinos are produced in the proton-proton chains and the Carbon-Nitrogen-Oxygen (CNO) thermonuclear reactions that generate the sun's energy in its core. The Standard Solar Models (SSM) [18] that calculate the solar neutrino fluxes are extensive and make 'accurate' predictions on the number events in radiochemical experiments. However, there was a persistent mismatch between theory and experiment in this case. After the final run of the Davis experiment (which used Chlorine) the average neutrino rate through the detector was [19]

$$R^{\text{exp}} = 2.56^{+0.23}_{-0.23} \qquad \nu_e \ cm^{-2}s^{-1} \ , \qquad (1.2)$$

which is well below the theoretical prediction of the Standard Solar Model (SSM):

$$R^{\text{theo}} = 7.6^{+1.3}_{-1.1} \qquad \nu_e \ cm^{-2}s^{-1} \ . \qquad (1.3)$$

Gallium experiments, such as SAGE [20] at the Baksan Laboratory in Russia, and GALLEX/GNO [21] based at Gran Sasso, confirmed the deficit that had come to be known

as the 'solar neutrino problem'. The resolution of this problem began with the results from the Sudbury Neutrino Observatory (SNO) [9] - a Water Čerenkov detector (see Sec. 2.3.2) using heavy water. The novelty in this experiment was the ability to detect neutrinos through charge current, neutral current and elastic scattering events. Charge current reactions can only be used to measure the rate of ν_e passing through the detector whereas the neutral current reactions measure the sum rate of all neutrino flavours. Elastic scattering primarily measures the electron neutrino rate. By construction, the SNO detector, therefore, could measure the total neutrino rate of active neutrinos coming from the sun. At the end of the so-called 'salt-phase' [22], the neutral current event rate was reported to be approximately 3 times larger than the charge current rate; the implication being that two thirds of the electron neutrinos have become muon or tau neutrinos by some process on the journey from the Sun's centre to the detector.

To confirm the solar neutrino oscillation hypothesis required the further step of producing the neutrinos terrestrially then observing the change with a distant detector (or mulitple detectors). The first experiment to make this observation was the KamLAND experiment [23] in Japan and Korea. A liquid scintillator detector located in the Kamioka mine was setup to measure the anti-neutrino rates from 53 nuclear power reactors located an average distance of 180 km from the detector. The number of events was 65 % the expected rate with no flavour change in flight. However, the major discovery was that the deviations from the expected number of events from the data sample as a function of the baseline divided by the energy displayed an oscillatory structure (see Fig. 1.1) [23].

Similar to solar neutrinos, an 'anomaly' was present in atmospheric neutrino data samples. Atmospheric neutrinos are final state particles from the decay of charged pions, $\pi^\pm$, and kaons, $K^\pm$ (and subsequently muons, $\mu^\pm$), in the particle cascades following the a cosmic ray interaction with the upper atmosphere, for example

$$
\begin{aligned}
\pi^+ \quad &\rightarrow \quad \mu^+ + \nu_\mu \\
&\hookrightarrow \quad e^+ + \nu_e + \bar{\nu}_\mu \,.
\end{aligned}
\tag{1.4}
$$

In an atmospheric neutrino experiment one can measure the ratio

$$
R = \frac{\left(\frac{N_\mu}{N_e}\right)_D}{\left(\frac{N_\mu}{N_e}\right)_{\text{Theo}}} \,,
\tag{1.5}
$$
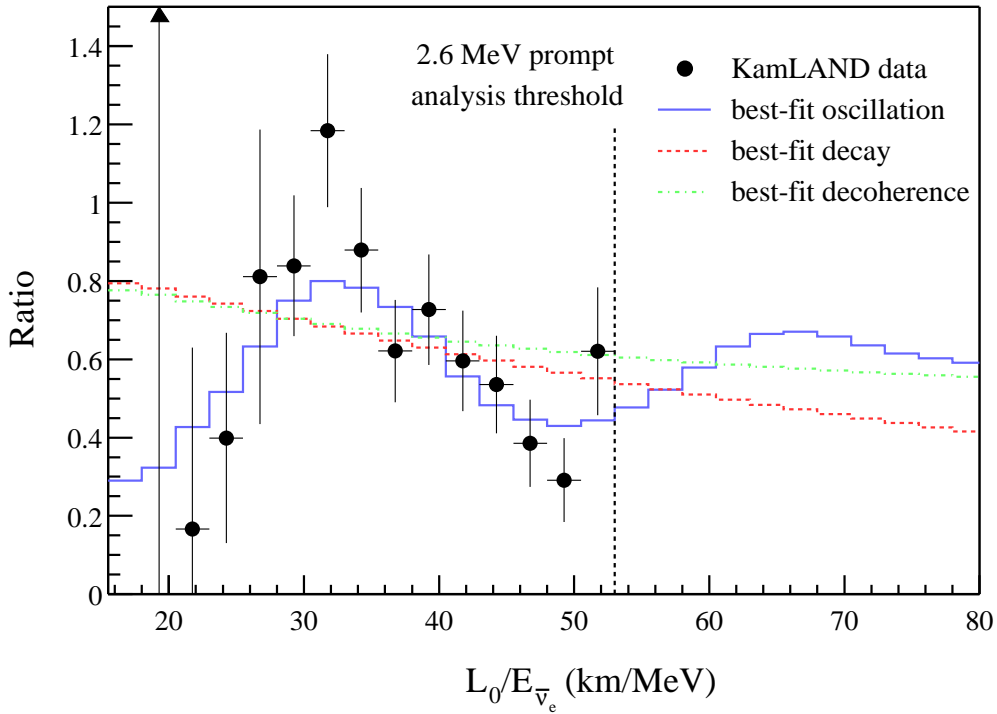
Figure 1.1.: The ratio of the number of events to the expected number for the KamLAND experiment as a function baseline/neutrino energy. The best fits for neutrino oscillations, neutrino decoherence and neutrino decay are shown. Plot reproduced from [23].

where N_α is the number of ν_α and $\bar{\nu}_\alpha$ events in the detector, and the ratios are for the experimental data (top line) and a theoretical prediction taking into account detector response and the predicted atmospheric neutrino flux (bottom line). This ratio was measured by a number of experiments [24, 25, 26, 27, 28] and was consistently found to be less than 1. This 'atmospheric anomaly' was confirmed by the large data sample of Super Kamiokande [10]; the implication being a deficit of either (or both) neutrino flavours. Super Kamiokande was able to ascribe this deficit to the phenomenon of neutrino oscillations by reconstructing the angular dependence of the neutrino flux. The results indicated that the discrepancy between the data and the theoretical prediction grew with the distance between source and detection. The measurement of a 'up-down asymmetry' [11, 12] was consistent with ν_μ oscillating into ν_τ, not sterile neutrinos [29]. The neutrino oscillation hypothesis for atmospheric neutrinos was confirmed by the KEK-to-Kamioka (K2K) [30] experiment which artificially produced ν_μ by firing protons onto a fixed target then using the subsequent pion and kaon decays. A deficit was observed in both the total event rate and the event energy spectrum with no observation of the $\nu_\mu \to \nu_e$ oscillation.

In short, we now know that neutrinos are massive and they mix. This discovery prompts several important questions to be addressed by future theoretical, phenomenological and experimental studies, including:

- Are neutrinos Dirac or Majorana particles?

- What is the absolute scale of the neutrino mass?

- Are neutrino masses related to a new physics scale?

- What are the elements of the mixing?

- Is there CP-violation in the lepton sector?

- What relations exist between the lepton and quark sectors; and wider contexts?

Neutrino physics is a vast subject area combining many different sub-disciplines of high energy physics. This thesis concentrates on the physics of neutrino mixing and CP-violation in long baseline neutrino oscillation experiments. In this thesis, phenomenological work into the physics reach of future long baseline neutrino experiments will be presented with focus on specific aspects of the Beta Beam and its variants. A brief review of the possible facilities that will shape the future of the neutrino long baseline program will be given in Sec. 1.4.

1.2. Neutrino mixing and oscillations

The phenomenon of neutrino oscillations requires neutrinos to be massive but with their identities not tagged by their mass. The requirement of massive neutrinos is straightfroward; for a neutrino to 'change' requires it to have a non-zero proper time, i.e. they travel with speeds less than the speed of light in a vacuum. For neutrinos to oscillate, the flavour basis needs to be rotated from the mass basis. In a weak interaction, the flavour of neutrino produced or destroyed is the flavour of the lepton at the same vertex. On the other hand, the flavour of a charged lepton is identified by examining its kinematic properties and decays, both of which are dependent on its mass. A lepton of definite flavour is a lepton of definite mass. Since the mass of a neutrino is not measured, only the flavour, it is not necessary for the mass basis and flavour basis to be aligned. A neutrino of definite flavour can then be a superposition of neutrinos of definite mass.

The superposition enters the Standard Model (SM) Lagrangian in the charge current interactions as a mixing matrix, $U_{\alpha j}$,

$$\mathcal{L}_{CC}^{\nu} = \frac{g}{\sqrt{2}} \sum_{j=1,2,3} \sum_{\alpha=e,\mu,\tau} \left[\bar{l}^{\alpha} \gamma^{\mu} \frac{1-\gamma^5}{2} U_{\alpha j}^* \nu_j W_{\mu}^+ + \text{h.c.} \right] . \tag{1.6}$$

Here, l, ν and W are the lepton, neutrino and weak boson fields respectively, and g is the weak coupling constant. The neutrino fields are written in the mass basis. For 3-neutrino mixing, this matrix is a 3×3 unitary matrix, $U_{\alpha j}$ which relates the mass states, ν_j, to flavour states, ν_α, via

$$\nu_j = \sum_{\alpha=e,\mu,\tau} U_{\alpha j} \nu_\alpha , \tag{1.7}$$

or conversely, the flavour states to mass states

$$\nu_\alpha = \sum_{j=1,2,3} U_{\alpha j}^* \nu_j . \tag{1.8}$$

This matrix is parameterised by three mixing angles and a single physical phase. If neutrinos are Majorana particles then there are two additional phases present; however, these combine to form an overall irrelevant phase that does not appear in the final oscillation probability. It is therefore sufficient to consider Dirac neutrinos in the following sections. The mixing angles are labelled θ_{12}, θ_{23} and θ_{13}, and together represent a 3-dimensional rotation of the mass basis to the flavour basis. The physical phase δ manifests itself as a distinction between neutrino mixing and anti-neutrino mixing known as CP-violation. With these labels, the standard parameterisation of the mixing matrix is [14]

$$U = \begin{pmatrix} c_{12}c_{13} & s_{12}c_{13} & s_{13}e^{-i\delta} \\ -s_{12}c_{23} - c_{12}s_{13}s_{23}e^{i\delta} & c_{12}c_{23} - s_{12}s_{13}s_{23}e^{i\delta} & c_{23}s_{23} \\ s_{12}s_{23} - c_{12}s_{13}c_{23}e^{i\delta} & -c_{12}s_{23} - s_{12}s_{13}c_{23}e^{i\delta} & c_{23}c_{23} \end{pmatrix} \tag{1.9}$$

and is refered to as the Pontecorvo-Maki-Nakagawa-Sakata (PMNS) matrix. Here, the shorthand c_{ij} and s_{ij} has been used to label the cosine and sine of the mixing angles θ_{ij} between the mass states i and j.

1.2.1. The oscillation probability

As mentioned above, the phenomenon of neutrino oscillations requires massive neutrinos and the flavour states to be a superposition of the mass states. Massive neutrinos evolve in time; neutrino oscillations originate from the difference in the evolution of the individual states [31] and is, in 3-neutrino oscillations, characterised by two phase shifts. To see this, begin by noting that a massive neutrino state $|\nu_j\rangle$ is an eigenstate of the free Hamiltonian

$$\hat{\mathcal{H}}|\nu_j\rangle = E_j|\nu_j\rangle , \tag{1.10}$$

where E_j is the neutrino energy. Such neutrino states are solutions of the Schrödinger equation and thus evolve in time

$$|\nu_j(t)\rangle = e^{-iE_jt}|\nu_j\rangle , \tag{1.11}$$

or, using Eqs. 1.7 and 1.8, a definite flavour state created at time $t = 0$ evolves in time as

$$|\nu_\alpha(t)\rangle = \sum_{\beta=e,\mu,\tau} \left(\sum_{j=1,2,3} U^*_{\alpha j} e^{-iE_jt} U_{\beta j} \right) |\nu_\beta\rangle . \tag{1.12}$$

The amplitude for the transition $\nu_\alpha \to \nu_\beta$ is therefore

$$A_{\nu_\alpha \to \nu_\beta} = \langle \nu_\beta | \nu_\alpha(t)\rangle = \sum_j U^*_{\alpha j} U_{\beta j} e^{-iE_jt} , \tag{1.13}$$

with probability

$$P_{\nu_\alpha \to \nu_\beta} = |A_{\nu_\alpha \to \nu_\beta}|^2 = \sum_{j,k} U^*_{\alpha k} U_{\beta k} U_{\alpha j} U^*_{\beta j} \, e^{-i(E_j - E_k)t} . \tag{1.14}$$

To convert this probability into a form based only on known observables, we note that neutrinos are ultra-relativistic so that $t = L$ in natural units, where L is the source-detection distance known as the baseline. Secondly, for neutrino 3-momentum $\vec{p}$ and mass m_j, we approximate

$$E_jt - p_jL \approx (E_j - p_j)L = \frac{E_j^2 - p_j^2}{E_j + p_j}L = \frac{m_j^2}{E_k + p_k}L \approx \frac{m_j^2}{2E}L , \tag{1.15}$$

so that

$$E_j - E_k \simeq \frac{\Delta m_{jk}^2}{2E} \ .$$

(1.16)

Here, $\Delta m_{jk}^2 = m_j^2 - m_k^2$ and the 'equal-momentum assumption' has been taken. Finally, the $\nu_\alpha \to \nu_\beta$ oscillation probability for source-detection distance L and neutrino energy E is

$$P_{\nu_\alpha \to \nu_\beta} = |A_{\alpha \to \beta}(t)|^2 = \sum_{k,j} U_{\alpha k}^* U_{\beta k} U_{\alpha j} U_{\beta j}^* \exp\left(-i\frac{\Delta m_{jk}^2 L}{2E}\right) \ .$$

(1.17)

Therefore, neutrino oscillation probabilities are dependent on the 4 parameters of the mixing matrix and two independent mass squared differences. The absolute mass scale is not attainable. It is sometimes useful to separate out the real and imaginary parts of Eq. 1.17:

$$P_{\nu_\alpha \to \nu_\beta} = \delta_{\alpha\beta} - 4\sum_{i>j} \Re e\, U_{\alpha k}^* U_{\beta k} U_{\alpha j} U_{\beta j}^* \sin^2\left(\frac{\Delta m_{jk}^2 L}{4E}\right) + 2\sum_{i>j} \Im m\, U_{\alpha k}^* U_{\beta k} U_{\alpha j} U_{\beta j}^* \sin\left(\frac{\Delta m_{jk}^2 L}{2E}\right) \ .$$

(1.18)

This is the 'textbook' derivation of the oscillation probability and should be accompanied by a caveats regarding the last few steps. The assumption that the 3-momentum is the same for all mass states with $E = \vec{p}$ has been made in Eq. 1.15: This is the 'equal-momentum' assumption and is not necessary [32]. The above form of the oscillation probability can be recovered in more careful treatments involving wave packets [33] or full field theory calculations [34] without resorting to this assumption. The approximation $t \simeq L$ is also not valid here since the amplitude of a plane wave is the same irrespective of its location in space-time [35]. This problem is overcome by noting that real localised particles should be described by wavepackets [33]. For neutrino oscillations to occur, the neutrino must be produced as a coherent superposition of the mass states. This is amounts to saying that the uncertainty on the momentum of the neutrino production process must be larger than the momentum difference of the mass states [36]. If the momentum uncertainty of the production process is very small, it may be possible to determine which mass state has been emitted; in which case the neutrinos are emitted incoherently and neutrino oscillations cannot occur. More quantitatively, if we define the oscillation length

$$L_{\text{osc}} = \frac{4\pi E}{\Delta m_{jk}^2} \ ,$$

(1.19)

and let Δx and Δp be the uncertainties on the localisation and momentum of the production process; we have

$$\Delta x \Delta p \gtrsim \hbar \, , \tag{1.20}$$

and for oscillations to occur requires

$$\Delta x > L_{\text{osc}} \, . \tag{1.21}$$

Note from Eq. 1.17 that the oscillation probability has an oscillatory structure which is a function of L and E. For a given baseline L, it is customary to characterise the oscillatory structure in the following manner:

- The probability peak at the highest energy is referred to as the 'first oscillation maximum'.

- Moving to smaller energies, the nth oscillation peak is labelled 'nth oscillation maximum'.

- The trough between first oscillation maximum and second oscillation maximum is the 'first oscillation minimum'.

- The 'nth oscillation minimum' is defined the same manner as the nth oscillation maximum.

For baselines $L \lesssim 1500$ km, the maxima correspond to the maxima of the real part in Eq. 1.18, i.e

$$\frac{\Delta m_{jk}^2 L}{4E_n} \approx \frac{(2n-1)}{2}\pi \, , \tag{1.22}$$

where E_n is the energy of the nth maximum. For longer baselines, this correspondence is no longer correct as the propagation of neutrinos through matter distorts the oscillation probability. In these cases it is necessary to determine the maxima positions numerically.

1.2.2. Two-neutrino oscillations

Most neutrino oscillation data to date is interpreted using 2-neutrino oscillation schemes. Although a full 3-neutrino oscillation analysis is mandatory for future experiments, it is instructive to analyse some of the features of neutrino oscillation probabilities using only 2 neutrinos.

A 2-neutrino mixing matrix is parameterised by a single mixing angle, θ;

$$U = \begin{pmatrix} \cos\theta & \sin\theta \\ -\sin\theta & \cos\theta \end{pmatrix}, \qquad (1.23)$$

and there is also only one mass-squared splitting, $\Delta m^2 = \Delta m_{21}^2 \equiv m_2^2 - m_1^2$ say. Using Eq. 1.17, we distinguish two different cases

1. The 'disappearance' or 'survival' probability

$$P_{\nu_\alpha \to \nu_\alpha} = 1 - \sin^2 2\theta \, \sin^2\left(\frac{\Delta m^2 L}{4E}\right) ; \qquad (1.24)$$

2. The appearance probability (for $\alpha \neq \beta$)

$$P_{\nu_\alpha \to \nu_\beta} = \sin^2 2\theta \, \sin^2\left(\frac{\Delta m^2 L}{4E}\right) . \qquad (1.25)$$

Experiments using the first case are known as 'disappearance experiments', and the latter case as 'appearance' experiments. Note that these vacuum oscillations are not sensitive to the sign of Δm^2.

The above expressions are exact for vacuum oscillations, approximately true for short terrestrial baselines, but insufficient for intermediate to long baselines. As neutrinos pass through matter they interact inducing an effective mass. This process will be discussed in more detail in Sec. 2.1.1. For the following discussion, it is sufficient to note that these interactions introduce a matter potential, $A = \sqrt{2}\, G_F\, n_e$, where G_F is the Fermi constant and n_e is the electron density of matter [37]. The Hamiltonian in the flavour basis is given by

$$
\begin{aligned}
\hat{\mathcal{H}} &= \frac{1}{2E}\left[U \begin{pmatrix} m_1^2 & 0 \\ 0 & m_2^2 \end{pmatrix} U^\dagger + \begin{pmatrix} 2EA & 0 \\ 0 & 0 \end{pmatrix} \right] \\
&= \frac{1}{4E}\begin{pmatrix} -\Delta m^2 \cos 2\theta + 2\tilde{A} & \Delta m^2 \sin 2\theta \\ \Delta m^2 \sin 2\theta & \Delta m^2 \cos 2\theta \end{pmatrix} + \begin{pmatrix} -A/2 & 0 \\ 0 & -A/2 \end{pmatrix},
\end{aligned} \qquad (1.26)
$$

where $\tilde{A} = 2EA$. (This Hamiltonian could result from electron neutrino mixing with some other flavour, and A can be thought of as a charge current coherent scattering potential.) Noting that the addition of a constant diagonal matrix to the Hamiltonian does not alter the neu-

trino evolution and can be discarded, this matter Hamiltonian is equivalent to the vacuum Hamiltonian with effective mixing matrix

$$\tilde{U} = \begin{pmatrix} \cos\tilde{\theta} & \sin\tilde{\theta} \\ -\sin\tilde{\theta} & \cos\tilde{\theta} \end{pmatrix} \tag{1.27}$$

and effective mass-squared splitting

$$\Delta\tilde{m}^2 = \sqrt{(\Delta m^2 \cos 2\theta - \tilde{A})^2 + (\Delta m^2 \sin 2\theta)^2} \ . \tag{1.28}$$

The effective mixing angle can be found by comparing the Hamiltonian with the effective vacuum case

$$\tan 2\tilde{\theta} = \frac{\Delta m^2 \sin 2\theta}{\Delta m^2 \cos 2\theta - \tilde{A}} \ . \tag{1.29}$$

There is thus a resonance when

$$\tilde{A} = \Delta m^2 \cos 2\theta \tag{1.30}$$

which returns maximal mixing $\tilde{\theta} = 45^o$. Note that the existence of a resonance is determined by the signs of $\tilde{A}$ and Δm^2, as well as the value of θ. For neutrinos ($\tilde{A} > 0$) and $\Delta m^2 > 0$, the resonance exists if $\theta < 45^o$. For anti-neutrinos $\tilde{A} < 0$ and so the resonance exists if $\theta > 45^o$. These are reversed if $\Delta m^2 < 0$. Consequently, in the presence of matter, the sign of Δm^2 is accessible to experiment if fitted simultaneously with θ, or θ is known externally from another experiment. This resonance is known as the MSW effect [37] and is important for understanding the passage of solar neutrinos [38] from production at the core of the sun to the surface. Let the density of matter be n_e^{res} at the resonance, then

$$n_e^{\text{res}} = \frac{\Delta m^2 \cos 2\theta}{2\sqrt{2}G_F E} \ . \tag{1.31}$$

An electron neutrino produced in the centre of the sun is predominantly a heavy mass state, m_2 say, and is exposed to a background density $n_e \gg n_e^{\text{res}}$. The neutrino will oscillate with the oscillation length given in Eq. 1.19. If the density gradient is sufficiently small for neutrino conversions to occur adiabatically, as the neutrino crosses the resonance region, the electron neutrino can convert fully into a pure m_1 mass state. The neutrino leaves the sun as this m_1 state which is an eigenstate of the vacuum Hamiltonian. Consequently, the neutrino state does not oscillate on its journey to Earth. A terrestrial detector then measures the ν_e (or ν_μ or ν_τ)

component of this mass state which enables access to the mixing angle. A measurement of the $\Delta m_{\rm sol}^2$ can be made since the resonance condition is dependent on it. Crucially, the existence of the resonance and simultaneous measurement of $\theta_{\rm sol} < 45^o$ implies $\Delta m_{\rm sol}^2 > 0$ and is the reason why the sign of $\Delta m_{\rm sol}^2$ is known but the sign of $\Delta m_{\rm atm}^2$ is not (see next section). In the context of long baseline experiments, the resonance manifests itself as an enhancement of the appearance oscillation probability for very long baselines.

1.3. Present status

The phenomenology of 3-neutrino oscillations will be discussed in detail in the next chapter. With the exception of the LSND experiment [39], the data from all neutrino oscillation experiments [9, 11, 12, 19, 20, 21, 22, 23, 30, 40, 41, 42, 43, 44] can be described with 3-neutrino mixing. Up to now, experiments have studied 'disappearance' oscillation channels of the form $\nu_\alpha \rightarrow \nu_\alpha$ (or $\bar{\nu}_\alpha \rightarrow \bar{\nu}_\alpha$). To a good approximation, the 3-neutrino oscillation framework appears to be hierarchical in nature; the two mass-squared splittings, Δm_{31}^2 and Δm_{21}^2, differ by an order of magnitude [15]:

$$\frac{\Delta m_{31}^2}{\Delta m_{21}^2} \approx 30 \ . \tag{1.32}$$

This result can be viewed as 3-neutrino mixing decoupling into 2 sets of 2-neutrino mixing, each with single mixing angle and mass-squared difference.

- Data from solar [9, 19, 20, 21, 22, 41] and reactor [23, 42, 43] experiments with ν_e or $\bar{\nu}_e$ as their source neutrino are consistent with a small mass squared difference and moderate mixing angle (errors given in Tab. 1.1).

$$\Delta m_{\rm sol}^2 \approx \Delta m_{21}^2 = 7.6 \times 10^{-5} \ {\rm eV}^2 \qquad {\rm and} \qquad \theta_{\rm sol} = \theta_{12} = 34^o \ . \tag{1.33}$$

- Data from atmospheric [11, 12] and accelerator [30, 44] experiments are described with a larger mass-squared difference, albeit with unknown sign, and maximal mixing

$$|\Delta m_{\rm atm}^2| \approx |\Delta m_{32}^2| = 2.4 \times 10^{-3} \ {\rm eV}^2 \qquad {\rm and} \qquad \theta_{\rm atm} = \theta_{23} = 45^o \ . \tag{1.34}$$

The unknown sign is a consequence of the $\sin^2 \Delta m_{jk}^2/4E$ dependence of a 2-neutrino disappearance probability.

The third mixing angle is currently bounded from above [15],

$$\sin^2\theta_{13} < 0.04 \quad (0.056) \qquad \text{at} \qquad 2\sigma \quad (3\sigma) \, , \tag{1.35}$$

although some collaborations claim a slight hint that it is non-zero [45]:

$$\sin^2\theta_{13} = 0.016^{+0.010}_{-0.010} \qquad \text{at} \quad 1\sigma \, . \tag{1.36}$$

This result is also present at 1.5σ in a different analysis that excludes the atmospheric data [46]. In disappearance experiments, θ_{13} will manifest itself as a tension between the data of the two separate 2-neutrino regimes. (If $\theta_{13} = 0^o$ then the two sectors decouple and 2-neutrino oscillations is exact.) Any interference can be resolved in a full 3-neutrino analysis with non-zero θ_{13}. This can be seen by breaking down the mixing matrix into a product of three rotation matrices:

$$U = \begin{pmatrix} c_{12} & s_{12} & 0 \\ -s_{12} & c_{12} & 0 \\ 0 & 0 & 1 \end{pmatrix} \begin{pmatrix} c_{13} & 0 & s_{13}e^{-i\delta} \\ 0 & 1 & 0 \\ -s_{13}e^{i\delta} & 0 & c_{13} \end{pmatrix} \begin{pmatrix} 1 & 0 & 0 \\ 0 & c_{23} & s_{23} \\ 0 & -s_{23} & c_{23} \end{pmatrix} . \tag{1.37}$$

The mixing matrix can be thought of as a product of the atmospheric, interference and solar regimes with any CP-violation manifesting itself in the interference. For small θ_{13}, the interference is small and there is an approximate decoupling of the atmospheric and solar sectors. A non-zero θ_{13} will thus show up as a conflict between the fits of two separate 2-neutrino sectors.

The claims are not statistically significant [15] and data from upcoming experiments [47, 48, 49, 50] is eagerly anticipated to help resolve this issue. In fact, it has recently been pointed out that the presence of non-standard interactions [51] can account for these effects [52].

At present, an accelerator experiment known as MINOS is taking data in the US. MINOS is a conventional beam experiment that fires ν_μ and $\bar{\nu}_\mu$ towards a 5.4 kton far detector 735 km distant from Fermilab. The neutrinos are sourced from the decay of focussed pions taken from the NuMI[1] beamline and directed down a long decay tunnel (see next section). The goal of MINOS is primarily to improve precision on Δm^2_{atm} and θ_{23}. Although in principle a measurement of θ_{13} can be made by searching for sub-dominant $\nu_\mu \to \nu_e$ and $\bar{\nu}_\mu \to \bar{\nu}_e$ events, this is left for near and far future experiments such as the reactor experiments [49, 50, 53] and Superbeams [47, 48]. T2K will be the first 'Superbeam' experiment (essentially an upgrade

---

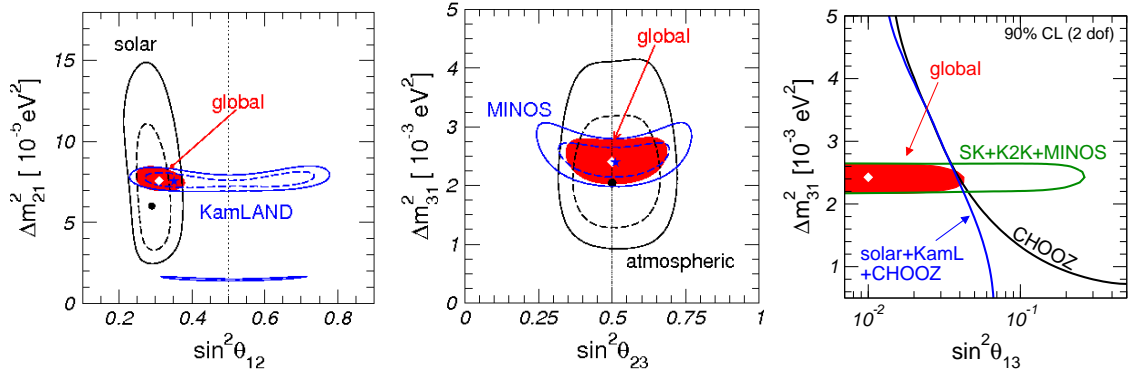[1]Nu represents ν, and MI is an abbreviation for Main Injector.

Figure 1.2.: The global fit to all presently available neutrino oscillation data. The left panel shows the 95 % and 99 % confidence levels for the correlation between θ_{12} and Δm_{21}^2. The fit is preformed using all available solar data and the latest results from KamLAND. The middle panel shows the 95 % and 99 % confidence levels for the correlation between θ_{23} and Δm_{31}^2. All available atmospheric and accelerator data has been used. The right panel shows the current global bound on θ_{13}. Atmospheric and accelerator data on θ_{13} are strongly correlated with the atmospheric mixing angle. Data from solar and reactor experiments are only weakly correlated and therefore provide the strongest bounds. Plots taken from [15].

in power of a 'conventional' accelerator beam experiment) which will fire ν_μ and $\bar{\nu}_\mu$ from J-PARC to the SuperKamiokande Water Čerenkov detector at the Kamioka mine (L=295 km). Muon-events will be used to confirm and improve results on Δm_{atm}^2 and θ_{23}, and measure θ_{13} by searching for electron-type events. T2K is also the first accelerator neutrino experiment to use the off-axis technique - the exploitation of the kinematics of pion decay to reduce the background (see next section). A Superbeam experiment, using the NUMI beamline, known as NOvA [48] has just recently started construction.

All experiments to date have examined neutrino disappearance channels and have demonstrated that neutrinos predominantly oscillate into ν_τ or $\bar{\nu}_\tau$; no electron-like or muon-like appearance events have been observed. The high energy threshold for τ production means that dedicated detectors are necessary to search for ν_τ and $\bar{\nu}_\tau$ appearance events. A neutrino beam from CERN known as CNGS[2] is currently being shot at a emulsion detector known as OPERA [54] located at Gran Sasso (L=730 km). The purpose of the experiment is the confirmation of neutrino oscillations using a terrestrial experiment, i.e. observation of an appearance event. The global fit on all the oscillation parameters using all available data, including the latest MINOS experiment data set, is summarised in Tab. 1.1 and Fig. 1.2.

---

[2]CERN Neutrinos to Gran Sasso

parameter	best fit	2σ	3σ
Δm^2_{21}	7.65×10^{-5} eV^2	7.25-8.11	7.05 - 8.34
$|\Delta m^2_{31}|$	2.40×10^{-3} eV^2	2.18-2.64	2.07 - 2.75
$\sin^2 \theta_{12}$	0.30	0.27-0.35	0.25 -0.37
$\sin^2 \theta_{23}$	0.50	0.39-0.63	0.36 -0.67
$\sin^2 \theta_{13}$	0.01	$\leqslant 0.040$	$\leqslant 0.056$

Table 1.1.: Best fit values, 2σ and 3σ intervals for the neutrino mixing and oscillation parameters. The results are for global fits to all atmospheric, solar, reactor and accelerator experiments. Table adapted from [15].

1.4. Future technologies

All long baseline neutrino oscillation experiments consist of the following components

- A neutrino source with some theoretically known or simulated neutrino spectrum. In virtually all cases, this spectrum will span a range of energies. The neutrino energy is written either E or E_ν.

- The neutrino propagation from source to detection. This distance is known as the 'baseline' and given the symbol L.

- The detection: the neutrino events are counted or reconstructed at the detector. How this is done is dependent on the detector technology chosen (Sec. 2.3.2).

There are currently two categories of terrestrial neutrino beam: reactors and accelerators. The latter can be further divided into 'beam dump' and 'storage ring' beams. In this section, a brief review of each type of neutrino beam will be given. A complete review of the technologies, results to date and projected sensitivities of future beams is an extensive undertaking and will not be attempted here. For this information, one is directed to the many optimisation studies [55]; or, for a general overview, the International Scoping Study reports [56].

Reactor experiments: Reactor experiments use the high luminosity, but low energy ($\langle E_\nu \rangle \sim$ 3.5 MeV), $\bar{\nu}_e$'s released as nuclear reactor fission products beta decay towards stability. The approach adopted is to investigate $\bar{\nu}_e \rightarrow \bar{\nu}_e$ disappearance at short baselines [42, 43, 57] or short-long baselines [23]. Multiple short-long baselines were used by the KamLAND collaboration to search for disappearance events in the solar regime. The primary interest for future experiments is the use of short baselines to search for sub-dominant atmospheric effects and,

in particular, make a clean measurement of θ_{13}. The relevant 3-neutrino disappearance probability is given by

$$P_{\bar{\nu}_e \to \bar{\nu}_e} \approx 1 - \sin^2 2\theta_{13} \sin^2\left(\frac{\Delta m_{31}^2 L}{4E}\right) - \cos^4\theta_{13}\sin^2 2\theta_{12}\sin^2\left(\frac{\Delta m_{21}^2 L}{4E}\right) . \qquad (1.38)$$

The baseline is typically chosen to match the first solar oscillation maximum, i.e.

$$\frac{\Delta m_{21}^2 L}{4E} \approx \frac{\pi}{2} \quad \Rightarrow \quad L \sim 1 \text{ km} , \qquad (1.39)$$

with a θ_{13} measurement made by searching for additional superimposed atmospheric oscillations. There are currently three planned reactor neutrino experiments: RENO [49], Daya Bay [50] and Double Chooz [53]. These experiments will be the first to test θ_{13} below the current bound, however their reach is severely restricted by systematics [58] - the physics reach cannot be boosted significantly further by pushing for higher luminosities. Even if experimental uncertainties can be kept under control, there is a sensitivity limit to this approach since one is searching for a subdominant 3-neutrino effect on top of a dominant 2-neutrino effect. To push below reactor sensitivities requires the signal to be solely a 3-neutrino effect. This can be achieved by searching for appearance events in an accelerator based experiment.

Conventional beams and Superbeams A conventional beam sources high energy ν_μ and $\bar{\nu}_\mu$ by a technique referred to here as the 'beam dump' method. Conventional beams and Superbeams source neutrinos from the decay of charged pions and kaons produced when high luminosity proton beams are fired onto a fixed target. These mesons are then collected and focussed before directed towards a far detector via a decay tunnel. The mesons that do not decay, and the muons and electrons, are absorbed by a beam dump at the far end. The neutrinos of interest are sourced from the following reactions

$$\pi^+ \to \mu^+ + \nu_\mu \quad \text{and} \quad K^+ \to \mu^+ + \nu_\mu , \qquad (1.40)$$

whose fluxes need to be calculated using a Monte Carlo simulation of the production, focussing and decay. Anti-neutrinos can be sourced from the CP-conjugate decays with the magnetic polarity of the focussing horns reversed. Conventional beams like K2K [30] and MINOS [44] use disappearance measurements to confirm and constrain atmospheric neutrino oscillations. MINOS, which is currently running; T2K [47], which is due to start taking data in near future; and NOvA [48], which has just started construction; wish to also search for θ_{13}. They attempt this by searching for sub-dominant ν_e and $\bar{\nu}_e$ events. Searches of this type

are limited by an intrinsic contamination of the neutrino beam. Additional decay channels of the kaons and the decay of the daughter muons in the decay channel source ν_e's:

$$\mu^+ \to e^+ + \nu_e + \bar{\nu}_\mu \qquad \text{and} \qquad K^+ \to \pi^0 + e^+ + \nu_e \ . \qquad (1.41)$$

The $\nu_\mu \to \nu_e$ appearance channel can therefore be confused with the $\nu_e \to \nu_e$ disappearance channel.

Near future Superbeams, such as T2K and NOvA, are not expected to take the $\sin^2 2\theta_{13}$ sensitivity reach much lower than the reactor experiments. To gain an order of magnitude requires Superbeams to be upgraded further. The main difference between the two classifications is that the next generation Superbeams aim for much higher luminosities. Such a facility requires the design and construction of powerful proton drivers and targets that can withstand such bombardments. A number of projects are ongoing in view of this such as the development of the Super Proton Linac (SPL) at CERN [59], and Project-X at Fermilab [60].

There are two principle strategies for conventional beams and Superbeams:

1. The Wide Band Beam (WBB) [61]. In proposals of this type, the detector is located on-axis with the un-oscillated neutrino flux covering a wide range of energies. Depending on the site, baselines up to 2500 km are possible. The broad spectrum means that detectors are required to reconstruct the neutrino energies with good precision and keep backgrounds to a minimum. Fluxes of this type allow for study of multiple oscillation maxima with a single beam.

2. Off-axis beams [47, 48, 62] aim to reduce backgrounds from ν_e in the beam (which are energy dependent). By placing the detector off-axis, with respect to the vector in the centre of the beam, one produces a smaller flux with a narrow range of energies. This is a consequence of the properties of the pion decays and is discussed further in Appendix B. The ν_e's, are sourced from 3-body decays and do not share this property. The benefits of this technique are that the flux can be tuned to a oscillation maximum and more restrictive cuts can be introduced to reduce background events from the beam contamination.

Neutrino Factories The Neutrino Factory [63] was born out of the Muon Collider proposal [64]. The basic idea is to extend the Superbeam principle by extracting the muons produced in pion and kaon decay and then cool, bunch and accelerate them. These muons are then injected into a storage ring in which the muon decays in the long straight sections,

pointing towards distant detectors, source the neutrinos. The two decays are

$$\mu^+ \to e^+ + \nu_e + \bar{\nu}_\mu \qquad \text{and} \qquad \mu^- \to e^- + \bar{\nu}_e + \nu_\mu \,; \qquad (1.42)$$

so that a large set of CP-conjugate and T-conjugate oscillation channels are in principle available. The high luminosity and acceleration of the muons produces intense and collimated beams of ν_e and $\bar{\nu}_\mu$ (or $\bar{\nu}_e$ and ν_μ). There is an inherent problem with sourcing neutrinos in this manner which has important consequences on the strategy adopted. Neutrino events are tagged by the observed lepton. Without a magnetised detector, $\nu_e \to \nu_\mu$ 'right-sign' μ^- events are indistinguishable from $\bar{\nu}_\mu \to \bar{\nu}_\mu$ 'wrong sign' μ^+ events.

There are currently two magnetised detector proposals to extract the sub-dominant appearance events from the signal [63, 65]

1. The High Energy Neutrino Factory (HENF) [63] using Magnetised Iron Neutrino Detectors (MIND) [66]. This is the basis for the International Design Study for the Neutrino Factory (IDS-NF) [67]. In order to remove backgrounds from muon-sign misidentification and charmed-meson decays [66], restrictive cuts on the signal are necessary. This has the side-effect of removing large fractions of the appearance events at low energies, in turn preventing the use of these detectors at short baselines. At present, the optimal setup for this facility is two detectors at $L_1 = 4000$ km and $L_2 = 7500$ km [68].

2. The Low Energy Neutrino Factory (LENF) [65] using a magnetised Totally Active Scintillator Detector (TASD). Initial studies suggest that relatively large detection efficiencies down to 0.8 GeV can be achieved. Studies have been carried out into the phenomenology of such a machine for the FNAL - Homestake (1280 km) and FNAL - Henderson Mine (1480 km) baselines [65].

Beta Beams The Beta Beam [16] is a variant on the Neutrino Factory that instead uses the neutrinos from beta emitting ions. Beta Beams have the advantage over other technologies of sourcing uncontaminated beams that are well collimated and are of high energy. Magnetised detectors are therefore not necessary; large Water Čerenkovs (WC), Liquid Argon detectors (LAr), Totally Active Scintillator Detectors (TASD) and Iron Calorimeters (IC) are all options. A restrictive energy threshold is not a problem with neutrino energies from 200 MeV up to several GeV accommodated. The Beta Beam can therefore use the full range of long baselines: CERN-Frejus (130 km) up to CERN-INO (~ 7000 km). A Beta Beam does not need to be built from scratch; current proposals all aim to take advantage of existing or suggested upgrades

to the accelerator complexes at CERN and Fermilab (and maybe DESY). A more complete overview of the Beta Beam will be given in Chap. 3.

1.5. Outline of the thesis

The goal of future long baseline neutrino oscillation experiments is to continue the exploration of the mixing matrix; specifically

- Improve the precision on the known oscillation parameters;

- Make a measurement of θ_{13};

- Determine if there is CP-violation in the lepton sector and, if possible, measure it;

- Determine the sign of the atmospheric mass-squared splitting;

- Determine whether $\theta_{23} = 45^o$. If not, in which octant does it reside?

- Search for beyond 3-neutrino oscillation effects such as non-standard interactions and sterile neutrino mixings.

The unravelling of the neutrino mixing matrix and neutrino masses is important for understanding the origins of flavour and relations between the lepton and quark sectors. With our incomplete knowledge, there is scope for many different neutrino mass and mixing models consistent with the available data [69]. It is important that these gaps in our understanding are filled so that the models can be discriminated. Long baseline experiments are a rich source of results not available or easily attainable with mass searches [5, 6, 7, 8, 70, 71, 72] neutrinoless double beta decay experiments [73, 74, 75, 76] or astrophysics [77].

The goal of this PhD has been to study in detail the physics reach of Beta Beams and their related technologies: electron capture beams, bound beta beams and electron capture and Beta Beam hybrids. This thesis serves as a summary of these studies with the focus on studies of CP-violation in the lepton sector and the ability of long baseline neutrino oscillation experiments using this technology to observe and measure it. A number of phenomenological studies into the physics reach of Beta Beams have been carried out to varying degrees of sophistication prior to this thesis [78, 79, 80, 81, 82, 83, 84, 86, 87, 88, 89, 90]. The goal of this thesis is the analysis of electron neutrino beams sourcing European baselines with the technologies mentioned above, but without using a CP-conjugate channel. Concrete facility setups

will not be considered; the objective being the study of the CP-violation reach properties of these machines.

Big decisions are looming in the neutrino community. Around 2012-2013 will be the culmination of an intense period of experimental R&D on the Superbeams, the Neutrino Factory and the Beta Beams. To plot the future of the long baseline neutrino oscillation programme requires a phenomenological analysis of all the available beams and their variants with care to make realistic assumptions but, at the same time, to give the experimentalists optimistic targets to aim for. The work contained within this thesis contributes to this on-going decision and revision process. Specifically, studies examining a non-standard approach to a Beta Beam facility [89]; an expansion of an introductory study into the electron capture machine concept [91]; and a novel idea using a neutrino flux that contains both Beta Beam and electron capture beam neutrino spectra [92] is presented, as is a critique [93] of a recent suggestion of using bound beta decays to source mono-energetic anti-neutrino fluxes [94]. Neutrino facilities of this kind and/or the strategy they employ may not be possible or be built for a number of reasons. Never-the-less, they need to studied so that the neutrino community can make a decision based on sound physical analyses and the status of the R&D. The potential to measure CP-violation will be discussed in all cases and will be put in a context through discussion of the technology and the necessity of the approach adopted.

The thesis is essentially in two parts; Chaps. 2 and 3 provide a summary of the background to the thesis. In Chap. 2, the phenomenological task for future long baseline neutrino facilities will be set out. The ultimate goal of the future experiments is to determine the values of the third mixing angle θ_{13} and CP-violation phase δ; and to settle the unresolved questions from pervious experiments: what is the sign of the atmospheric mass-squared difference, Δm^2_{atm}; does θ_{23} deviate from 45 degrees and, if so, in which octant does it reside? The subdominant appearance channels $\nu_e \rightarrow \nu_\mu$ and $\bar{\nu}_e \rightarrow \bar{\nu}_\mu$ have been identified as the best experimental signals for future experiments. Analysis of these channels will be through a perturbative expansion which provides a wealth of insight on the behaviour on long baseline experiments, in general, and specific setups, in particular. The problem of degenerate solutions will be introduced along with its ramifications. The statistical procedures will also be discussed at this point so that the seriousness of degenerate solutions can be made manifest. In Chap. 3, the Beta Beam technology and proposed facility setup will be tendered. Detailed discussion is beyond the scope of this thesis, however, a sketch of a Beta Beam facility will be given and the salient features relevant for the following studies highlighted.

The final three chapters contain the phenomenological studies for single ion Beta Beams and their related technologies. The content of Chap. 4 is based on the study [89] conducted

to examine the properties of a Beta Beam that only uses neutrinos. The rationale behind this strategy is the current uncertainty on the number of neutrinos and anti-neutrinos that can sourced for a given baseline. The absolute numbers and the ratio of the source rates are both unknown; all Beta Beam studies either have to use target numbers or arbitrary rates (of varying degree of realism). In this chapter, a strategy involving only neutrinos will be motivated semi-analytically with the suggested conclusions investigated using a full simulation of a case study baseline.

The study of electron capture machines in Chap. 5 naturally adopts the same approach by the absence of an equivalent anti-neutrino flux. The study presented in this chapter is an extension of the work carried out by collaborators at CERN and Valencia [91]. The analysis presented is the first optimisation of the electron capture machine. The number of ion decays, the boosts and the run times will be all be looked at to ascertain their importance. The atmospheric neutrino background will also be included for the first time. The chapter will end with a critique of the bound beta beam. Bound beta decays have been put forward [94] as a possible source of mono-energetic anti-neutrinos to accompany the electron capture fluxes. I will argue that this is not possible in any realistic manner.

The final chapter looks at an idea that was initially born out of the original electron capture beam papers. Finding electron ions with suitable decay energies is tricky since for the energies required in the laboratory frame, there is typically a beta decay 'background' to the electron capture with equivalent or greater strength. The chapter examines whether there is any benefit to using this non-standard hybrid neutrino flux as opposed to the standard Beta Beam spectrum or the mono-energetic neutrino from electron capture decays.

Chapter 2.

Contemporary long baseline phenomenology

In the last chapter, several goals for future experiments were identified. The present data can be described by two distinct mass-squared differences, $\Delta m_{\text{sol}}^2 \approx \Delta m_{21}^2$ and $\Delta m_{\text{atm}}^2 \approx \Delta m_{31}^2$; and two mixing angles, θ_{12} and θ_{23}. The labeling of the mass-squared differences is suggestive of two regimes: atmospheric and solar. The lack of any electron or muon appearance events means that the third mixing angle allowed by the theory must be small. The atmospheric and solar regimes can be thought of as two approximately disjoint 2-neutrino oscillation schemes. If exact, i.e. $\theta_{13} = 0^o$, then there can be no CP-violation in the neutrino sector. To search for CP-violation requires a search for the sub-dominant interference effects between the two regimes whose strength depends on the size of θ_{13}.

2.1. 3-neutrino oscillations

The search for CP-violation requires a measurement of one of the appearance channels and is a 3-neutrino effect. This is a consequence of the CPT invariance of a quantum field theory and/or the subdominant nature of the effect. First suppose one wished to attempt a measurement of CP-violation by looking for a discrepancy between CP-conjugate channels. At a given energy and baseline, the neutrino and anti-neutrino disappearance probabilities are the same. To see this consider a neutrino oscillation from flavour α to flavour β: $\nu_\alpha \to \nu_\beta$. A CP transformation exchanges the neutrino and anti-neutrino channels

$$\nu_\alpha \to \nu_\beta \xleftrightarrow{CP} \bar{\nu}_\alpha \to \bar{\nu}_\beta \ . \tag{2.1}$$

Similarly, a T transformation is the change

$$\nu_\alpha \to \nu_\beta \xleftrightarrow{\ T\ } \nu_\beta \to \nu_\alpha\ , \tag{2.2}$$

so that the complete CPT transformation is the exchange

$$\nu_\alpha \to \nu_\beta \xleftrightarrow{\ CPT\ } \bar{\nu}_\beta \to \bar{\nu}_\alpha\ . \tag{2.3}$$

CPT is a symmetry of a local quantum field theory. Assuming neutrino oscillations to be formulated in such a theory, we must have

$$\nu_\alpha \to \nu_\beta = \bar{\nu}_\beta \to \bar{\nu}_\alpha\ . \tag{2.4}$$

For the case $\alpha = \beta$, we see that neutrino and anti-neutrino channels for a disappearance event are identical. However, note this does not mean that the probabilities are independent of δ. If $\theta_{13} \neq 0^o$ then δ is part of the Hamiltonian and can affect neutrino evolution. One can then ask whether it is feasible to attempt a measurement of δ by reconstructing the energy dependence of the signal. This is in principle possible for disappearance events, however, the effect is subdominant with the signal dwarfed by the 2-neutrino oscillation effects. The best approach is therefore is use appearance events as the CP-conjugate probabilities are different for $\delta_{13} \neq 0^o$ and the subdominant effects *are* the signal. Future experiments will in general use both energy reconstruction of the signal and a comparison of CP-conjugate channels in each bin. In this thesis, neutrino runs alone will be used and CP-violation measurements will rely on energy reconstruction of the signal. Note that it is also possible to seek a discrepancy from T-conjugate channels; CP-violation is equivalent to T-violation for CPT to remain conserved. For example,the combination of Superbeams and Beta Beams over the same baseline [82, 87, 95, 96] will partly adopt this strategy.

The physics reach of future long baseline experiments focusses on the so-called *'golden'* $\nu_e \to \nu_\mu$ oscillation channel and its CP-conjugate partner. Charge current (CC) ν_μ events are typically long, clean tracks accompanied by a hadronic shower and are easy to identify and reconstruct [66]. CC ν_e events, on the other hand, shower electromagnetically in a manner similar to a hadronic shower, but without the long track of the muon. Such a track is necessary to reconstruct the charge and momentum of the lepton, and hence the flavour and helicity. A calorimetric measurement of the hadronic shower combined with the lepton measurement allows for the reconstruction of the incident neutrino energy. Without the track, the electromagnetic shower makes the CC ν_e events look like neutral current (NC) events. These points are especially true for the large magnetised calorimeters proposed for Neutrino Factories.
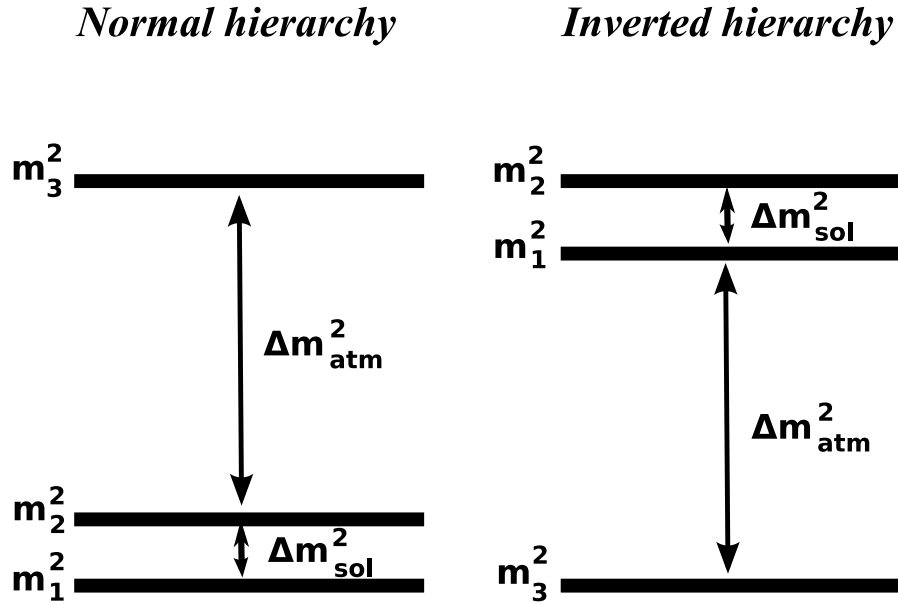
Normal hierarchy   Inverted hierarchy

Figure 2.1.: Neutrino mass orderings relevant for neutrino oscillations. Taking the solar mass squared splitting to be between the mass states 1 and 2, the normal neutrino mass ordering has m_1 as the smallest state. If m_3 is the smallest state then we have an inverted ordering.

In addition to the golden channel, the following channels (and their CP-conjugates) are also considered in CP-violation analyses:

- $\nu_e \to \nu_\mu$ the *'golden'* channel ,

- $\nu_e \to \nu_\tau$ the *'silver'* channel ,

- $\nu_\mu \to \nu_e$ the *'platinum'* channel .

The golden channel is the main physics channel for Beta Beams and Neutrino Factories. The silver channel has been considered as a source of additional information to help resolve degeneracies (see Sec. 2.2) [97, 98, 99], or to improve sensitivity to non-standard interaction effects and searches for oscillations into sterile neutrinos [100]. Observation of the $\nu_e \to \nu_\tau$ channel is only possible for neutrino energies greater than the τ production threshold. The platinum channel is the principle appearance channel available to conventional beams and Superbeams. It is also available to the Neutrino Factory but is little considered for the reasons described above. The physics in this thesis concentrates on the golden channel. Searches for θ_{13} and CP-violation need appearance oscillation channels. For the other unknown oscillation parameters, the appearance channels are not mandatory; and, in particular, the sign of Δm_{atm}^2 could in principle be measured with the $\nu_e \to \nu_e$ and $\nu_\mu \to \nu_\mu$ channels for a sufficiently large matter

potential. Recall that neutrino mass splittings are hierarchal since

$$\frac{\Delta m_{31}^2}{\Delta m_{21}^2} \approx 30 \ . \tag{2.5}$$

In the context of neutrino oscillations[1] , we can identify two cases (depicted in Fig. 2.1)

Normal hierarchy $\quad \text{sign}(\Delta m_{31}^2) > 0 \ : \qquad m_1 < m_2 < m_3 \ ,$

Inverted hierarchy $\quad \text{sign}(\Delta m_{31}^2) < 0 \ : \qquad m_3 < m_1 < m_2 \ .$

If the mass splittings are small in relation to the absolute mass scale, the neutrino masses have a degenerate spectrum ($m_1 \approx m_2 \approx m_3$). Since the absolute neutrino mass is not observable in a neutrino oscillation experiment, it is customary to refer to the mass orderings as the normal and inverted hierarchy, irrespective of the absolute mass scale.

To extract the sign of Δm_{31}^2, recall that the mixing angle and mass-squared splitting in matter are dependent on the sign of the vacuum Δm^2. In the absence of CP-violation, there will still be a discrepancy between CP-conjugate channels since the external matter fields are CP-invariant. For 3-neutrino oscillations appearance events in a vacuum, however, the discrepancy is only present in the sub-leading effects. For a pure 2-neutrino vacuum oscillation analysis in the atmospheric regimes, the oscillation probabilities are invariant with respect to this change (hence why it is currently unknown): Eq. 1.24. The mass hierarchy can be determined by searching for this effect, although the presence of $\delta \neq 0^o$ is a problem (see Sec. 2.2).

Far future facilities will focus on the appearance channels and will search primarily for θ_{13}, δ and the sign of Δm_{31}^2. It is expected that the other mixing parameters will be measured to a better precision with running and near future facilities. The physics reach of a new facility rests on the size of θ_{13} since this controls the size of the interference between the solar and atmospheric sectors. The solar contributions to the appearance probability have no dependence on the sought parameters (see Sec. 2.1.2). If θ_{13} is too small, then few statistically significant results are possible for any given facility. The overall physics reach, and the smallest θ_{13} for which statistically significant results can be returned, is dependent on the facility type and the particular setup (or combination of experiments). The physics reach of an experiment can be seriously hampered by the unknown $\text{sign}(\Delta m_{31}^2)$ and the octant of θ_{23} (see Sec. 2.2).

---

[1]The hierarchal nature of neutrinos is also important for direct neutrino mass searches using beta decays, and for neutrinoless double beta decay experiments. Such experiments use effective mass observables whose behaviour as a function of the true mass scale is hierarchy dependent.

2.1.1. The appearance probability

The evolution of the neutrino state $|\nu\rangle$ is determined by the Schrödinger equation

$$\hat{\mathcal{H}} |\nu\rangle = i\frac{\partial |\nu\rangle}{\partial t} \,, \tag{2.6}$$

where $\hat{\mathcal{H}}$ is the Hamiltonian

$$\hat{\mathcal{H}} = \frac{1}{2E} \left[U \begin{pmatrix} m_1^2 & 0 & 0 \\ 0 & m_2^2 & 0 \\ 0 & 0 & m_3^2 \end{pmatrix} U^\dagger + \begin{pmatrix} 2EA & 0 & 0 \\ 0 & 0 & 0 \\ 0 & 0 & 0 \end{pmatrix} \right] . \tag{2.7}$$

Here, the m_i are the neutrino masses, E is the neutrino energy, U is the mixing matrix defined in Eq. 1.2, and A is the potential defined below. The first term is the evolution of the neutrino field, in the flavour basis, in a vacuum. The second term is the contribution to the evolution from forward coherant scattering of the neutrinos in matter (Fig. 2.2). These scatterings introduce the effective Hamiltonians

$$\hat{\mathcal{H}}_{\text{eff}}^{CC} = \frac{G_F}{\sqrt{2}} \left[\bar{\nu}_e \gamma^\sigma (1 - \gamma^5) e \right] \left[\bar{e} \gamma_\sigma (1 - \gamma^5) \nu_e \right] \tag{2.8}$$

and

$$\hat{\mathcal{H}}_{\text{eff}}^{NC} = \frac{G_F}{\sqrt{2}} \sum_{\alpha=e,\mu,\tau} \sum_f \left[\bar{\nu}_\alpha \gamma^\sigma (1 - \gamma^5) \nu_\alpha \right] \left[\bar{f} \gamma_\sigma (g_V^f - g_A^f \gamma^5) f \right] . \tag{2.9}$$

Here, G_F is the Fermi constant, ν, e and f are the neutrino, electron and fermion fields respectively. g_V^f and $_A^f$ for fermion f with charge q_f are given by

$$g_V^f = I_3^f - 2q_f \sin\theta_W \qquad \text{and} \qquad g_A^f = I_3^f . \tag{2.10}$$

θ_W is the Weinberg angle and I_3^f is the weak isopin of fermion f.

To obtain an average of the effective potential ($\bar{\mathcal{H}}_{\text{eff}} = \bar{\mathcal{H}}_{\text{eff}}^{CC} + \bar{\mathcal{H}}_{\text{eff}}^{NC}$), it is necessary to integrate over all variables associated with the electron. On doing so, one obtains [101]

$$\bar{\mathcal{H}}_{\text{eff}} = \sum_{\alpha=e,\mu,\tau} A_\alpha \bar{\nu}_{\alpha L} \gamma^0 \nu_{\alpha L} \,, \tag{2.11}$$

where

$$A_\alpha = A_{CC}\,\delta_{\alpha e} + A_{NC} = \sqrt{2}G_F\left(n_e\,\delta_{\alpha e} - \frac{1}{2}n_n\right)\,. \tag{2.12}$$

n_e and n_n are the electron and neutron densities in matter. The electron and proton contributions to the neutral current potential cancel since they have opposite charge and opposite weak isospin. The contribution from the neutron can also be removed as a constant factor added to each diagonal element of the Hamiltonian introduces an overall phase in the evolution which has no significance in the oscillation probabilities[2]. We are therefore left with the potential introduced in Eq. 1.2.2.

$$A = \sqrt{2}\,G_F\,n_e\,. \tag{2.13}$$

Passage through matter changes the oscillation probabilities as the potential modifies the mixing angles and effective energy of the neutrinos. It is common to rewrite the Hamiltonian as

$$\hat{\mathcal{H}} = U_{23}\left[U_{13}U_{12}\begin{pmatrix}0 & 0 & 0\\ 0 & \Delta_{21} & 0\\ 0 & 0 & \Delta_{31}\end{pmatrix}U_{12}^\dagger U_{13}^\dagger + \begin{pmatrix}A & 0 & 0\\ 0 & 0 & 0\\ 0 & 0 & 0\end{pmatrix}\right]U_{23}^\dagger\,. \tag{2.14}$$

Here, m_1^2 has been factored out as it will introduce an irrelevant phase to the probability, and the common notation

$$\Delta_{ij} \equiv \frac{\Delta m_{ij}^2}{2E} \tag{2.15}$$

has been introduced. The matter term is invariant under the U_{23} transformation.

In Fig. 2.3, the $\nu_e \to \nu_\mu$ appearance probabilities are presented for the CERN-Boulby baseline ($L = 1050$ km) for various assumptions on the oscillation parameters. In all plots, the matter effect has been included assuming a constant density along the baseline of 3 g/cm^3, or

---

[2]This is also the reason that atmospheric data can be attributed to $\nu_\mu \to \nu_\tau$ oscillations, and the CP-conjugate channel, since if sterile neutrinos are included, there will be an obsverable matter effect in the signal. Since sterile neutrinos do not interact with matter, the neutral current can not be removed in this manner. Put another way, this is the reason atmospheric neutrinos are treated as vacuum oscillations even though there is substantial passage through matter.
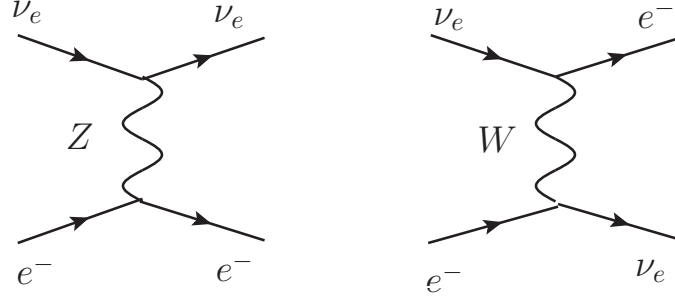
Figure 2.2.: Coherent scattering Feynman diagrams that generate the charge current and neutral current matter potentials for the electron neutrinos interacting with an electron background. Neutral current diagrams can also be drawn for all neutrino flavours and on proton and neutron backgrounds.

in terms of the potential:

$$\sqrt{2}\, G_F\, E\, n_e \simeq 1.15 \times 10^{-4} \text{ eV}^2 \left(\frac{\rho}{3\,\text{gcm}^{-3}} \right) \left(\frac{E}{1\,\text{GeV}} \right) , \qquad (2.16)$$

where ρ is the matter density. On the top line of Fig. 2.3, the $\nu_e \rightarrow \nu_\mu$ appearance probabilities are shown for $\delta = 0^o$, $\delta = -90^o$ and $\delta = 90^o$ for two choices of θ_{13}. On the bottom line, the difference between neutrino and anti-neutrinos probabilities, and the effect of the choice of hierarchy are shown. To find a probability for anti-neutrinos, note that the appropriate weak currents are

$$j_{W;L}^{\sigma} = 2 \sum_{\alpha} \sum_i U_{\alpha i}^* \bar{\nu}_{\alpha L} \gamma^\sigma l_{\alpha L} , \qquad (2.17)$$

$$j_{W;L}^{\sigma\dagger} = 2 \sum_{\alpha} \sum_i U_{\alpha i} \bar{l}_{\alpha L} \gamma^\sigma \nu_{\alpha L} . \qquad (2.18)$$

 Vacuum neutrino and anti-neutrino oscillations therefore are the same up to the switch $\delta \rightarrow -\delta$. In matter, the sign of the potential also needs to be reversed as the neutrino and anti-neutrino have opposite weak isospins. The procedure used to numerically evolve the Hamiltonian is presented in Appendix A.

   From the top line of Fig. 2.3, the appearance probability appears to have an underlying $1/E^2$ form which is modified by an oscillatory structure; the strength of which depends on the size of θ_{13}. The value of the CP-phase modifies the size and location of these oscillations. In the next section, it will be shown that these features are due to solar, atmospheric and interference effects respectively. Further, the solar trend does not appear to change with θ_{13}. For small θ_{13}, the solar contribution is dominant; the atmospheric and interference contributions can be
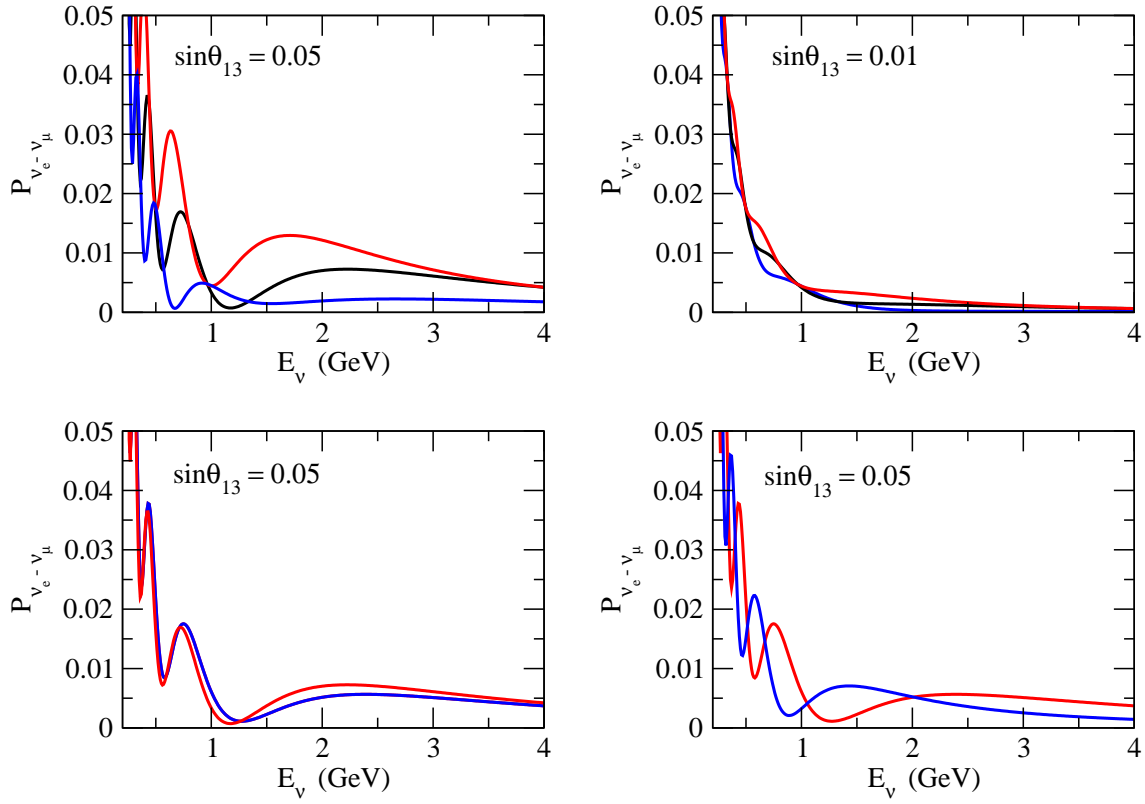
Figure 2.3.: $\nu_e \rightarrow \nu_\mu$ appearance probabilities for the CERN-Boulby baseline (1050 km) as a function of energy. On the top row, the effect of the CP-phase and the size of θ_{13} is demonstrated. In each case the probabilities for $\delta = 0^o$ (black), $\delta = -90^o$ (blue) and $\delta = 90^o$ (red) are calculated. On the bottom row, $\sin \theta_{13} = 0.05$ and $\delta = 0^o$ are taken. On the left, the red line represents $\nu_e \rightarrow \nu_\mu$ and the blue $\bar{\nu}_e \rightarrow \bar{\nu}_\mu$. On the right, the red line is for the normal hierarchy whilst the blue is for the inverted.

thought of as corrections to the $1/E^2$ trend. An inverted hierarchy suppresses the probability for neutrinos but enhances it (not shown) for anti-neutrinos for large matter effects. For small matter effect, the inverted hierarchy shifts the probability form to lower energies.

2.1.2. Perturbative expansion of the probability

The goal of this section is to find an analytical form for the appearance probability. To do this note that the Hamiltonian (Eq. 2.14) is equivalent to a 'vacuum' Hamiltonian with modified mixing angles and mass eigenstates:

$$\hat{\mathcal{H}} = \tilde{U} \begin{pmatrix} \lambda_1 & 0 & 0 \\ 0 & \lambda_2 & 0 \\ 0 & 0 & \lambda_3 \end{pmatrix} \tilde{U}^\dagger \, , \tag{2.19}$$

where $\tilde{U} = U_{23}\tilde{U}_{13}\tilde{U}_{12}$ is the modified mixing matrix and the λ_i are the effective neutrino masses squared divided by energy. To find analytic forms for the 3-neutrino oscillation probabilities one needs to find $\tilde{U}$ and the λ_i and then use Eq. 1.17 with $U \to \tilde{U}$ and $m_i^2/2E \to \lambda_i$. This has been done [102] but the results are not physically intuitive. An alternative is to use the hierarchal nature of the neutrino mass splittings, and other small parameters in the problem, to perform a perturbative expansion [66, 103, 104].

For a given mass-squared difference Δm_{ij}^2, baseline L and neutrino energy E, the first oscillation maximum (for small matter effects or vacuum) satisfies

$$\frac{\Delta m_{ij}^2 L}{2E} \approx \frac{\pi}{2} \, . \tag{2.20}$$

Neutrino event cross-sections are dependent on incident neutrino energies, with preference for high energies to achieve useful rates. From the above equation, we therefore wish to configure a facility to examine the oscillatory structure of the atmospheric regime as it has the larger Δm_{ij}^2. Following [66], a perturbative expansion is made by treating the atmospheric regime as zeroth order with the solar regime as a correction, viz:

$$\hat{\mathcal{H}} = U_{23} \left[\mathcal{M} + U_{13}U_{12} \begin{pmatrix} 0 & 0 & 0 \\ 0 & \Delta_{21} & 0 \\ 0 & 0 & 0 \end{pmatrix} U_{12}^\dagger U_{13}^\dagger \right] U_{23}^\dagger \, , \tag{2.21}$$

where

$$
\mathcal{M} = U_{13}U_{12} \begin{pmatrix} 0 & 0 & 0 \\ 0 & 0 & 0 \\ 0 & 0 & \Delta_{31} \end{pmatrix} U_{12}^{\dagger}U_{13}^{\dagger} + \begin{pmatrix} \pm A & 0 & 0 \\ 0 & 0 & 0 \\ 0 & 0 & 0 \end{pmatrix} \tag{2.22}
$$

is a 2-neutrino oscillation matrix in matter that we wish to diagonalise. It is easy to find the 3 eigenvalues of $\mathcal{M}$

$$
\lambda_1^{(0)} = \frac{1}{2}\left(\Delta_{31} \pm A - B_{\mp}\right) , \tag{2.23}
$$

$$
\lambda_2^{(0)} = 0 , \tag{2.24}
$$

$$
\lambda_3^{(0)} = \frac{1}{2}\left(\Delta_{31} \pm A + B_{\mp}\right) ; \tag{2.25}
$$

where

$$
B_{\mp} \equiv \sqrt{\left(\Delta_{31}\cos 2\theta_{13} \mp A\right)^2 + \left(\Delta_{31}\sin^2 2\theta_{13}\right)^2} \tag{2.26}
$$

is an effective mass in matter. The effective mixing angle in matter, θ_M, for this leading order effect, therefore satisfies

$$
\tan 2\theta_M = \frac{\tan 2\theta_{13}}{\Delta_{31}\cos 2\theta_{13} \mp A} \tag{2.27}
$$

and has a resonance when

$$
A = \Delta_{31}\cos 2\theta_{13} . \tag{2.28}
$$

For very long baseline oscillation experiments, the resonance is is important since the enhancement of the probability compensates for the divergence of the neutrino flux.
The diagonalised matrix to first order is

$$
\mathcal{M}^{(0)} = \bar{U}_{\mp} \begin{pmatrix} \lambda_1^{(0)} & 0 & 0 \\ 0 & 0 & 0 \\ 0 & 0 & \lambda_3^{(0)} \end{pmatrix} \bar{U}_{\mp}^{\dagger} , \tag{2.29}
$$

and the first order correction in the basis of the non-perturbed eigenvectors is

$$M_{\mp}^{(1)} = \bar{U}_{\mp}^{\dagger} U \begin{pmatrix} 0 & 0 & 0 \\ 0 & \Delta_{21} & 0 \\ 0 & 0 & 0 \end{pmatrix} U^{\dagger} \bar{U}_{\mp} \; . \tag{2.30}$$

Here $\bar{U}_{\mp} = U_{23}(\theta_{23}) U_{13}(\bar{\theta}_{M\mp})$ and $\bar{\theta}_{M\mp} = \theta_{13} - \theta_{M\mp}$. The eigenvectors to first order are now

$$\lambda_1^{(1)} = \lambda_1^{(0)} + s_{12}^2 \Delta_{21} \cos^2 \bar{\theta}_{M\mp} \; , \tag{2.31}$$

$$\lambda_2^{(1)} = \lambda_2^{(0)} + c_{12}^2 \Delta_{21} \; , \tag{2.32}$$

$$\lambda_3^{(1)} = \lambda_3^{(0)} + s_{12}^2 \Delta_{21} \sin^2 \bar{\theta}_{M\mp} \; . \tag{2.33}$$

With these eigenvalues, and their corresponding eigenvectors, the neutrino probabilities can be found using Eq. 1.17 keeping terms up to Δ_{21}. It is known that θ_{13} is small, so the resulting probability is given a further expansion in θ_{13}, keeping Δ_{21} and θ_{13} terms up to second order. The probability is not complete however as the expansion in θ_{13} does not return the second order terms $O(\Delta_{21}^2)$. To find the extra term note that it is the second order contribution in the $\theta_{13} \to 0$ limit. To find this term, the best approach is to diagonalise $\mathcal{M}$ exactly in this limit.

Finally, the probability is found to be

$$\begin{aligned} P_{\nu_e \to \nu_\mu}(\theta_{13}, \delta)^{\pm} &= \sin^2 2\theta_{13} \sin^2 \theta_{23} \left(\frac{\Delta_{31}}{B_{\mp}} \right)^2 \sin^2 \left(\frac{B_{\mp} L}{2} \right) \\ &+ \mathcal{J} \frac{\Delta_{21}}{A} \frac{\Delta_{31}}{B_{\mp}} \sin \left(\frac{AL}{2} \right) \sin \left(\frac{B_{\mp} L}{2} \right) \cos \left(\pm \delta - \frac{\Delta_{31} L}{2} \right) \\ &+ \cos^2 \theta_{23} \sin^2 2\theta_{12} \left(\frac{\Delta_{21}}{A} \right)^2 \sin^2 \left(\frac{AL}{2} \right) \; , \end{aligned} \tag{2.34}$$

where $\mathcal{J} = \cos \theta_{13} \sin 2\theta_{13} \sin 2\theta_{23} \sin 2\theta_{12}$ and $B_{\mp} = |\Delta_{31} \mp A|$. Up to notation, this expression is equivalent to the form derived in [103]. That study also contained a detailed comparison with a full numerical analysis. These perturbative expansions are only valid for small matter effects. With increasing baselines, and hence A, non-pertubative effects need to be included [105]. Although the above expression remains finite close to the resonance, the result is too large. For the baselines considered in this thesis, it is sufficient.

Most features of long baseline neutrino oscillation experiments can be understood, to some degree, with this formula: both the motivation of strategy or the interpretation of results. Indeed, this formula is fundamental to the understanding of the 'problem of degeneracies'

which will be discussed in the next section. To finish this section, the important features of the probability will be pointed out.

- The expansion consists of three terms: the zeroth-order atmospheric term, the Δ_{21} first order interference term and the Δ_{21}^2 second order solar term.

- The atmospheric and solar terms represent the regimes in which atmospheric and solar features dominant respectively. These regimes are essentially 2-neutrino mixing schemes and so no CP-phase is present in these terms. All CP-violation manifests itself through the interference term which has components of both regimes.

- Both the atmospheric and interference terms are θ_{13} dependent. For small θ_{13}, the solar term dominates making it hard to measure CP-violation. This is the effect seen on the top line of Fig. 2.3.

- In the absence of matter, the leading order term is invariant under the change of hierarchy. In matter, the hierarchy modifies the amplitude of the atmospheric and interference terms. The effect is felt strongest from the atmospheric contribution at high energies and/or long baselines. The solar term can be approximated to

$$\cos^2\theta_{23}\sin^2 2\theta_{12}\left(\frac{\Delta_{21}L}{2}\right)^2 \tag{2.35}$$

for small matter effect and/or baseline and therefore does not contribute to the discrepancy.

- In the presence of matter, there will always be CP-violation even if $\delta = 0^o$ or 180° as the external matter fields are CP-invariant. Therefore, the effective potentials in the Hamiltonian are different for neutrinos and anti-neutrinos. The evolution of the flavour states is therefore different, even for CP-conserving values of δ.

- Both the atmospheric and interference terms are invariant under the change $\theta_{23} \to 90^o - \theta_{23}$. Determining the octant of θ_{13} therefore needs small energies and/or small θ_{13} so that the solar term dominates.

- The coefficients of the oscillatory parts of each term have different energy dependencies. Therefore the relative strength of each term varies according to which region of the neutrino spectrum is being investigated. Exploiting the oscillatory structure of the probability is therefore equivalent to exploring different feature of the oscillation probability.

- When the condition $AL = 2\pi$ holds, only the atmospheric term remains. The baseline for which this is true is known as the '*Magic baseline*'. This particular choice of baseline is important in the breaking of degeneracies and will be discussed further in Sec. 2.2.2 .

All the neutrino oscillation parameters are correlated in the sense that a single measurement of the probability is insufficient for the determination of the unknown parameters. Trivially, multiple measurements and/or experiments need to be performed to extract θ_{13} and δ. It is expected that at the time of any measurement, the current errors on the solar and atmospheric parameters will be much smaller. Never-the-less, any uncertainties on these parameters impact on θ_{13} and δ measurements, especially if θ_{13} is small. For small θ_{13}, the probability is essentially the solar term corrected by the interference term. The sought θ_{13} and δ effects at small θ_{13} can be mimiced by the uncertainty on the solar parameters. For relatively large and moderate θ_{13}, the uncertainties on the atmospheric parameters can modify the overall size of the probability and shift the oscillation peaks. In fact, with both θ_{13} and δ currently unknown, the problem is more severe. This is the '*problem of degeneracies*' to which we now turn.

2.2. The problem of degeneracies

Typically, future long baseline oscillation experiments aim to extract the unknown parameters using both a neutrino and anti-neutrino run. Since we are searching for the two parameters θ_{13} and δ, naively one would expect that the two runs should be sufficient to break the correlation and measure both. It was pointed out in [106], however, that this is a false expectation. If one makes just a single measurement of the probability in each of the polarities, then up to 7 fake solutions can also fit that data [107, 108, 109].

The intrinsic degeneracy

Consider the $\nu_e \to \nu_\mu$ appearance probability, $P^+_{\nu_e \to \nu_\mu}(\theta_{13}, \delta)$, for fixed baseline L and fixed energy E. The correlation between θ_{13} and δ means that for the true pair $(\theta_{13}^{\text{tr}}, \delta^{\text{tr}})$, a measurement of the appearance probability can return a continuum of solutions, viz

$$P^+_{\nu_e \to \nu_\mu}(\theta_{13}^{\text{tr}}, \delta^{\text{tr}}) = P^+_{\nu_e \to \nu_\mu}(\theta_{13}, \delta) \ . \tag{2.36}$$

Likewise, for an anti-neutrino run under the same assumptions, there is a second continuum

$$P^-_{\nu_e \to \nu_\mu}(\theta^{tr}_{13}, \delta^{tr}) = P^-_{\nu_e \to \nu_\mu}(\theta_{13}, \delta) \ . \tag{2.37}$$

In general, this system has two solutions. This can be seen in the the left panel of Fig. 2.4 where, for the CERN-Boulby baseline (1050 km), the two equiprobability curves defined by the above equations have been plotted for the case $\sin\theta_{13} = 0.05$, $\delta = 0^o$, normal hierarchy, and neutrino energies $E = 2.1$ GeV (first oscillation maximum) and $E = 2.5$ GeV. The neutrino equiprobability (solid lines) and anti-neutrino equiprobability (dashed lines) both pass through the true solution by construction. There is an addition solution at similar θ_{13} but larger δ. The second measurement has broken the correlations but left a discrete degeneracy: an additional solution that is also consistent with the data. This is the *'intrinsic degeneracy'*.

The location of the intrinsic degeneracy can be determined analytically using the perturbative expansion in Eq. 2.34 and simultaneously solving the two equations above. This is done in practice by rewriting the equations with θ_{13} as the subject then equating [106]. Attempting this in general results in involved algebra and is not very instructive. However, the exercise simplifies greatly in the atmospheric and solar extremes. Following [106], for large θ_{13}, Eq. 2.2 can be rewritten

$$\theta_{13} = \theta^{tr}_{13} - \frac{Y_\pm}{2X_\pm}\left[\cos\left(\delta - \frac{\Delta_{31}L}{2}\right) - \cos\left(\delta^{tr} - \frac{\Delta_{31}L}{2}\right)\right] \ , \tag{2.38}$$

where the non-essential information is contained in coefficients $X_\pm$ and $Y_\pm$:

$$X_\pm = \sin^2\theta_{23}\left(\frac{\Delta_{31}}{B_\mp}\right)^2\sin^2\left(\frac{B_\mp L}{2}\right) \ , \tag{2.39}$$

$$Y_\pm = \cos\theta_{13}\sin 2\theta_{23}\sin 2\theta_{12}\frac{\Delta_{21}}{A}\frac{\Delta_{31}}{B_\mp}\sin\left(\frac{AL}{2}\right)\sin\left(\frac{B_\mp L}{2}\right) \ . \tag{2.40}$$

'+' corresponds to neutrinos and '-' to anti-neutrinos. Even in this approximation the resulting solutions are complicated. For baselines at the shorter end of the spectrum, in the vacuum limit:

$$\theta_{13} \approx \theta^{tr}_{13} \qquad \text{and} \qquad \delta \approx \pi - \delta^{tr} \ . \tag{2.41}$$

This result is consistent with the left panel of Fig. 2.4; any deviations are the result of matter corrections. The possibility of returning multiple valid fits to the data is clearly a problem. From the left panel of Fig. 2.4, a possible solution presents itself. The location of the intrinsic
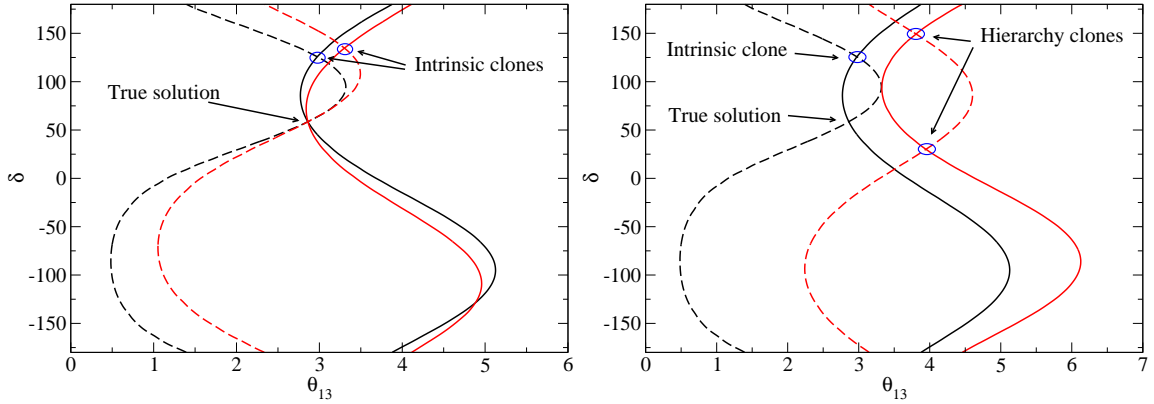
Figure 2.4.: The problem of degeneracies. All curves use the the CERN-Boulby baseline (1050 km) and true values $\sin\theta_{13}^{tr} = 0.05$ and $\delta^{tr} = 50^o$. *Left panel:* The neutrino (solid lines) and anti-neutrino (dashed lines) equiprobability curves for $E_\nu = 2.1$ GeV (black) and $E_\nu = 2.5$ GeV (red). The curves were plotted assuming the normal hierarchy. *Right panel:* For $E_\nu = 2.5$ GeV, the normal hierarchy (black lines) and inverted hierarchy (red lines) equiprobability curves for neutrinos (solid lines) and anti-neutrinos (dashed lines).

degeneracy is energy dependent for a given θ_{13}^{tr} and δ^{tr}. In a realistic experiment, one does not measure the probability directly; the parameters are extracted by reconstructing event spectra which are dependent on the initial flux, the detector technology, the interaction cross-sections and the probability (see next section). Since, in general, we extract information from a range of energies, the intrinsic degeneracy is easily resolved. Problems may arise at large θ_{13} where atmospheric uncertainties are felt more strongly and/or the energy range range is restricted by large energy thresholds and systematics (for example, in a high energy Neutrino Factory).

The energy degeneracy

There is an additional intrinsic degeneracy present in the left panel of Fig. 2.4 that is not discussed in the literature. It is seen that the two equiprobability curves for neutrinos at different energies have a second solution at $\theta_{13} \approx 5^o$ and $\delta \approx -125^o$. This degeneracy is not present in most experiments since the corresponding anti-neutrino runs do not share the same solution. (In fact, for the case above, the anti-neutrino runs do not have this extra degeneracy.) For the single helicity experiments discussed in this thesis, this degeneracy is in general present since a different energy changes the overall magnitude of the contributions and shifts the sinusoidal maximum of the interference term (as seen in Fig. 2.4). Henceforth this degeneracy shall be referred to as the *'energy degeneracy'* to distinguish it from the intrinsic degeneracy originating from neutrino and anti-neutrino runs.

The hierarchy degeneracy

If the neutrino hierarchy is unknown at the time of a (θ_{13}, δ) measurement; for both the true and intrinsic (or energy) degeneracy there can exist an additional solution known as a hierarchy clone [108]. In the right hand panel of Fig. 2.4, the equiprobability curves

$$P^+_{\nu_e \to \nu_\mu}(\theta^{\text{tr}}_{13}, \delta^{\text{tr}}, |\Delta m^2_{32}|) = P^+_{\nu_e \to \nu_\mu}(\theta_{13}, \delta, -|\Delta m^2_{32}|) \qquad \text{and} \qquad (2.42)$$

$$P^-_{\nu_e \to \nu_\mu}(\theta^{\text{tr}}_{13}, \delta^{\text{tr}}, |\Delta m^2_{32}|) = P^-_{\nu_e \to \nu_\mu}(\theta_{13}, \delta, -|\Delta m^2_{32}|) \qquad (2.43)$$

are presented. The change $|\Delta m^2_{32}| \to -|\Delta m^2_{32}|$ lowers the appearance probability for a given energy and pair (θ_{13}, δ). This change can be compensated with an increase in θ_{13}, shifting the equiprobability curves to the right. The two equiprobability curves for the wrong hierarchy intersect in two places as before. The size of these changes is dependent on the size of the matter effect (i.e. the neutrino energy and the baseline) and θ_{13}. For the vacuum case, there is no discrepancy between the probabilities to leading order and so the clones are sited with the true solution and the intrinsic clone (or energy clone). There are therefore four solutions that now fit the data: the true solution, its intrinsic (or energy) clone, and two hierarchy clones. As before, the location of the hierarchy clones are dependent on the energies. The existence of hierarchy clones can be turned to our advantage, however. These clones originate in the unknown sign of Δm^2_{32}. If these clones can be ruled out in favour of the true solution and its intrinsic solution, the mass hierarchy can be determined. The ability of an experiment to do this is controlled by the size of the matter effect and θ_{13}.

The octant degeneracy

Finally, it is not known whether $\theta_{23} \neq 45^o$. If $\theta_{23} = 45^o$ by assumption, then there are no additional fake solutions. If $\theta_{23} \neq 45^o$ by assumption, then it is necessary to consider 4 sets of equations

$$P^\pm_{\nu_e \to \nu_\mu}(\theta^{\text{tr}}_{13}, \delta^{\text{tr}}, |\Delta m^2_{32}|, \theta_{23}) = P^\pm_{\nu_e \to \nu_\mu}(\theta_{13}, \delta, |\Delta m^2_{32}|, \theta_{23}) \,, \qquad (2.44)$$

$$P^\pm_{\nu_e \to \nu_\mu}(\theta^{\text{tr}}_{13}, \delta^{\text{tr}}, |\Delta m^2_{32}|, \theta_{23}) = P^\pm_{\nu_e \to \nu_\mu}(\theta_{13}, \delta, -|\Delta m^2_{32}|, \theta_{23}) \,, \qquad (2.45)$$

$$P^\pm_{\nu_e \to \nu_\mu}(\theta^{\text{tr}}_{13}, \delta^{\text{tr}}, |\Delta m^2_{32}|, \theta_{23}) = P^\pm_{\nu_e \to \nu_\mu}(\theta_{13}, \delta, |\Delta m^2_{32}|, 90^o - \theta_{23}) \,, \qquad (2.46)$$

$$P^\pm_{\nu_e \to \nu_\mu}(\theta^{\text{tr}}_{13}, \delta^{\text{tr}}, |\Delta m^2_{32}|, \theta_{23}) = P^\pm_{\nu_e \to \nu_\mu}(\theta_{13}, \delta, -|\Delta m^2_{32}|, 90^o - \theta_{23}) \,; \qquad (2.47)$$

so that there are in general 8 solutions that can fit the data. In order, the first set of equations results in the 'intrinsic clone'; the second returns the 'hierarchy clones'; the third gives the 'octant' clones; and the fourth equation allows for 'mixed' clones.

2.2.1. Resolution of degeneracies

The existence of degenerate solutions, trivially, does not allow good sensitivity reach for θ_{13} and/or δ. A pair of measurements could return multiple valid solutions which, when combined, can occupy large regions of parameter space. How these degenerate solutions are incorporated in a CP-violation sensitivity plot and how they affect the sensitivity will be discussed in Sec. 2.3.3. To finish this section, a number of strategies suggested to combat the problem of degeneracies will be highlighted.

The location of degenerate solutions is energy dependent. The principle weapon available is therefore the reconstruction of the data in energy bins. The number of events in a given bin is the convolution of the un-oscillated neutrino flux, the appearance probability, the interaction cross-section and the event reconstruction efficiency. For a given experimental setup, the binned data is generated for a given oscillation hypothesis (see next section). χ^2 functions are then calculated to quantify the discrepancy between two hypotheses. Clone solutions manifest themselves as extra allowed regions at some confidence level in the (θ_{13}, δ) plane. Degeneracies are resolved by introducing extra information into the analysis such that the statistical significance of the clone solutions is reduced. This is the power of binning the data - much more information can be incorporated into a fit without the need for extra channels or experiments. Information from the oscillatory structure of the appearance probability is often sufficient to remove any intrinsic or energy degeneracies. This is the approach that is investigated in the Chaps. 4, 5 and 6. Below, some of the other approaches suggested in the literature are listed

- **Wide band beams:** One way to include energy dependence is to use a 'wide band beam'. Near future Superbeams [47, 48] place detectors off-axis to reduce backgrounds and concentrate the flux in narrow energy ranges [112]. Such setups suffer badly from the intrinsic degeneracy since they are close in design to the idealised discussion of degeneracies at single energies. An alternative approach is to use high energy Superbeams on axis so that the flux at the detector covers a large energy range [61]. Binning the data, even conservatively, is an effective strategy at resolving degeneracies.

- **Include extra oscillation channels:** Different oscillation channels have slightly different correlations between the unknown parameters. Analyses of this type focus on the use of $\nu_e \to \nu_\mu$ and $\bar{\nu}_e \to \bar{\nu}_\mu$ but with the inclusion of the silver [97, 98], platinum [113] or $\nu_\mu \to \nu_\tau$ channels. The silver channel is often helpful in dealing with the octant degeneracy [99], non-standard interactions or sterile neutrino oscillations [100]. The platinum channel is the T- conjugate channel of the golden channel. The combination of the golden and platinum and their CP-conjugates is a good strategy in resolving the mass hierarchy at shorter baselines where the matter effect is small [96]. This idea has been studied explicitly for Beta Beam and Superbeam combinations in Europe and the US [82, 87, 95]. The $\nu_\mu \to \nu_\tau$ channel is currently being investigated by the CNGS experiments [54] and is sensitive to the atmospheric parameters. The gain in including this extra channel is tempered by the difficulty in measuring ν_τ appearance (τs decay rapidly, hence not leaving a track, and produce many particle is the following casades). Inclusion of the appearance ν_τ events sometimes adds little to the overall sensitivity [114].

- **Multiple baselines:** The major degeneracy concern for future very long baseline experiments is the hierarchy degeneracy. In the high energy Neutrino Factory, the efficiency profile of the MIND detector forces the shortest baseline to be long (> 3000 km). At such long baselines, the matter effect is large and the degeneracy with θ_{13} and δ is severe. To break this degeneracy requires a clean measurement of one or a pair of the three parameters. This can be achieved with a second detector located at or near the magic baseline, where all but the atmospheric contribution to the probability vanishes, giving a clean measurement of θ_{13} (see Sec. 2.2.2). In addition, since the neutrino has to pass through the dense outer core of the earth, the MSW resonance enhances or suppresses the probability. This effect can be used to determine the hierarchy. The information from the magic baseline reduces the significance of the clone solutions at the short baseline. This approach has been copied for a number of recent Beta Beam proposals [79, 80, 84]. Beta Beams of this type are at the hard limit of what is possible - their technical and practical feasibility are open questions. Beta Beams have short baselines available where a clean measurement of θ_{13} and δ can be made. The use of the magic baseline is therefore not mandatory.

Several suggestions have been put forward for using multiple baselines for Superbeams that use the off-axis approach. The most prominant of these is T2KK [62]. The current beam line for T2K can also source detectors in South Korea and Okinoshima Island in the Sea of Japan [115]. The idea is to upgrade the T2K beam line to a Superbeam irradiating a new Mton Water Čerenkov, known as Hyper Kamiokande [116], close to the current

Kamiokande site at Kamioka (L=295 km) at first oscillation maximum. This beam could also source a detector 2.5^o off-axis in Korea covering second oscillation maximum at ~ 1000 km. The combination of different maxima and baselines is fertile ground for resolving degeneracies [117].

A similar idea has been put forward to supplement the planned NOvA experiment [48]. This is an off-axis experiment which uses neutrinos from the NUMI beamline with a far detector 810 km away at Ash river (Minnesota). In a proposal coined SuperNOvA [118], it was pointed out that introducing a second off-axis detector with neutrino energy at the same L/E but a much shorter baseline was beneficial in resolving the hierarchy degeneracy.

- **Multiple fluxes at the same baseline:** In the 'alternating ions' Beta Beam [88], two different ion pairs are used with similar boosts. The different Q-values of the ions (see Chap. 3) allow for multiple energy ranges to be explored with the same baseline which is helpful for breaking intrinsic and octant degeneracies for short baselines. It is also useful if one wishes to optimise the fluxes for each baseline in a multiple baseline Beta Beam since the flux is quadratic in the boost; low Q-value ions are best for the shorter baselines, and high Q- value ions are needed for the magic baseline [79, 80, 84].

2.2.2. The magic baseline

Although not a feature of this thesis, the use of the magic baseline is an important strategy in the resolution of degeneracies. As mentioned previously, at the magic baseline

$$\sin\left(\frac{AL}{2}\right) = 0 \qquad \Longleftrightarrow \qquad \sqrt{2}G_F n_e L = 2\pi \,. \tag{2.48}$$

Assuming a constant matter density ρ and two electrons per atom on average [119],

$$L_{\text{magic}}[km] \simeq 32726 \frac{1}{\rho[\text{g/cm}^3]} \,. \tag{2.49}$$

Using the Preliminary Reference Earth Model (PREM) [120], which describes the Earth's density as a function of depth, the baseline is numerically found to be $L_{\text{magic}} = 7250$ km [119]. The importance of this baseline lies in the reasonably clean measurement of θ_{13} and the hierarchy without any degeneracy with δ. This baseline needs to be combined with a shorter baseline to search for CP-violation.

It was pointed out in [121] that the probability expansion is not correct when close to the resonance. Nevertheless, the existence of a magic baseline is born out with a full numerical simulation and the simple argument above serves as a demonstration. The probabilities are calculated and presented in [79]. In addition to not having access to the CP-phase, the magic baseline also suffers because of its length. An un-oscillated neutrino flux scales as $1/L^2$ and so the event rate at a detector at the magic baseline is expected to be low. This expectation can be compensated by the matter resonance (see Sec. 1.2.2), which for the CERN-INO baseline (7152 km) is at [79]

$$E_{\text{res}} = \frac{|\Delta m_{31}^2| \cos 2\theta_{13}}{2\sqrt{2} G_F n_e} \simeq 6 \text{ GeV} . \qquad (2.50)$$

For small values of θ_{13}, the event rate per unit decay is approximately constant around the first oscillation maximum as a function of baseline - the increase in the cross-section and the resonance in the oscillation probability compensates for the heavy reduction in the un-oscillated flux for the magic baseline.

The magic baseline is a stable feature of Neutrino Factory proposals due to unavailability of short baselines. The baselines in the range 2000 km $< L <$ 6000 km suffer badly from the hierarchy degeneracy and need to accompanied by a clean measurement of δ and/or sign(Δm_{31}^2) to achieve good physics reach. A number of Beta Beam proposals have been put forward incorporating the magic baseline in a dual baseline setup in a similar manner to the Neutrino Factory. However, with the availability of short baselines, and hence a clean measurement on θ_{13} and δ with little or no matter degeneracy, the use of the magic baseline for a Beta Beam is certainly not mandatory.

2.3. Anatomy of an analysis

The core of any analysis for the physics reach of a long baseline neutrino experiment is the calculation of the neutrino event rate at the detector and its subsequent use in a χ^2 analysis. In this section, an outline of the event rate calculation will be given as will an overview of the χ^2 analysis for use in 2-parameter fits, CP-violation sensitivity plots and hierarchy determination plots. With this information, it will be seen explicitly how the presence of degenerate solutions affects the sensitivity of the experiment.

2.3.1. The simulation

The event rate for a given bin and detector channel is a convolution of the source neutrino flux; propagation effects: oscillations, matter enhancement or suppression, any new physics, such as non-standard interactions; and the event reconstruction at the far detector. A 'channel' is a possible source of events for a given initial neutrino flavour and helicity. For example, consider the Beta Beam oscillation $\nu_e \rightarrow \nu_\mu$. Each of the following contribute events to the total muon event rate and are individual channels

1. The $\nu_e \rightarrow \nu_\mu$ appearance oscillation channel through detection of muons;

2. Neutral current ν_e events misidentified as muons;

3. Charge current $\nu_e \rightarrow \nu_e$ disappearance events with a muon in the final state.

The number of events in the ith energy bin for the appearance channel for true pair $(\theta_{13}^{\text{tr}}, \delta^{\text{tr}})$ is given by the following expression

$$N_i(\theta_{13}^{\text{tr}}, \delta^{\text{tr}}) = \mathcal{N}_T \, t \int_{E_i}^{E_i + \Delta E_i} \varepsilon(E_\nu) \, \sigma_{\nu_\mu}(E_\nu) \, P_{e\mu}(E_\nu, \theta_{13}^{\text{tr}}, \delta^{\text{tr}}) \, \Phi_{\nu_e}(E_\nu) \, dE_\nu \, . \tag{2.51}$$

Here $\mathcal{N}_T \, t$ is an overall normalisation that represents the size of the detector and running time for the particular channel. Physically, $\mathcal{N}_T$ is the number of nuclei 'targets' within the detector. The integrand is composed of 4 experimental distributions; the neutrino flux at production $\Phi_{\nu_e}(E_\nu)$, the oscillation probability $P_{e\mu}(E_\nu, \theta_{13}^{\text{tr}}, \delta^{\text{tr}})$, the event cross-section $\sigma_{\nu_\mu}(E_\nu)$, and the event reconstruction efficiency $\varepsilon(E_\nu)$.

The neutrino flux at production is parameterised by the front-end[3] of the facility. The shape and normalisation of $\Phi_{\nu_e}(E_\nu)$ is dependent on the type of decay and its maximum rest frame energy (Q-value), the boost of the source particle, and a normalisation in the guise of some production rate. The shape of the beta decay flux and its parameterisation will be introduced in Chap. 3. For the Beta Beam, the normalisation is the number of useful ion decays per year; for Superbeams and Neutrino Factories, one often refers to the number of protons on target or more simply the power of the proton source. It is conventional to include the neutrino source-far detector distance (the baseline) in the flux $\Phi_{\nu_e}(E_\nu)$, as opposed to the propagation, making it the un-oscillated neutrino flux at the detector.

---

[3] 'Front-end' is a term often used to describe the production stage of a neutrino facility. Specifically, I take it to mean all technology prior to the propagation over the long baseline. Some people might use it to mean prior to acceleration.

The probability, at a given laboratory neutrino energy E for true pair $(\theta_{13}^{tr}, \delta^{tr})$, is simulated numerically by time evolving the initial neutrino state, as described in appendix A. This probability is also a function of the baseline L, the matter potential, and all the other oscillation parameters. For brevity, these are not labelled.

The convolution of the un-oscillated neutrino flux and oscillation probability gives the differential rate of appearance neutrinos at the detector. The number of neutrino events is then determined by the size of the interaction cross-section and interaction identification efficiency. The neutrino flavour is tagged by the interaction lepton. The identification cross-sections are therefore always charge current cross-sections. Neutral current reactions are flavour blind and therefore can provide a background if misidentified. There are three types of charge current interaction used in event reconstruction:

1. **Quasi-elastic events (QE)**

   These are events in which the target nucleon changes but does not break up. The flavour of the neutrino is through identification of the lepton in the final state. Examples include

   $$\nu_\mu + n \longrightarrow \mu^- + p \qquad \text{and} \qquad \bar{\nu}_\mu + p \longrightarrow \mu^+ + n \ . \qquad (2.52)$$

   Events of this type dominate for neutrino laboratory energies below 1 GeV and are important in Beta Beam studies using large Water Čerenkov detectors (WC).

2. **Pion production events (PD)**

   These events are essentially QE events but with an excited final state nucleon, possibly with a N^* or Δ. Depending on the resonance, pions typically appear in the final state; for example

   $$\nu_\mu + n \longrightarrow \mu^- + p + \pi^o \qquad \text{or} \qquad \nu_\mu + p \longrightarrow n + \pi^+ \ . \qquad (2.53)$$

   Pion production events make a substantial contribution to the total cross section for energies around 1 GeV, but are suppressed at higher energies much like QE events.

3. **Deep inelastic scattering events (DIS)**

   For energies of several GeV upwards, DIS events dominate the charge current cross-section. Events of this type break up the initial state nucleon leaving hadrons in the final
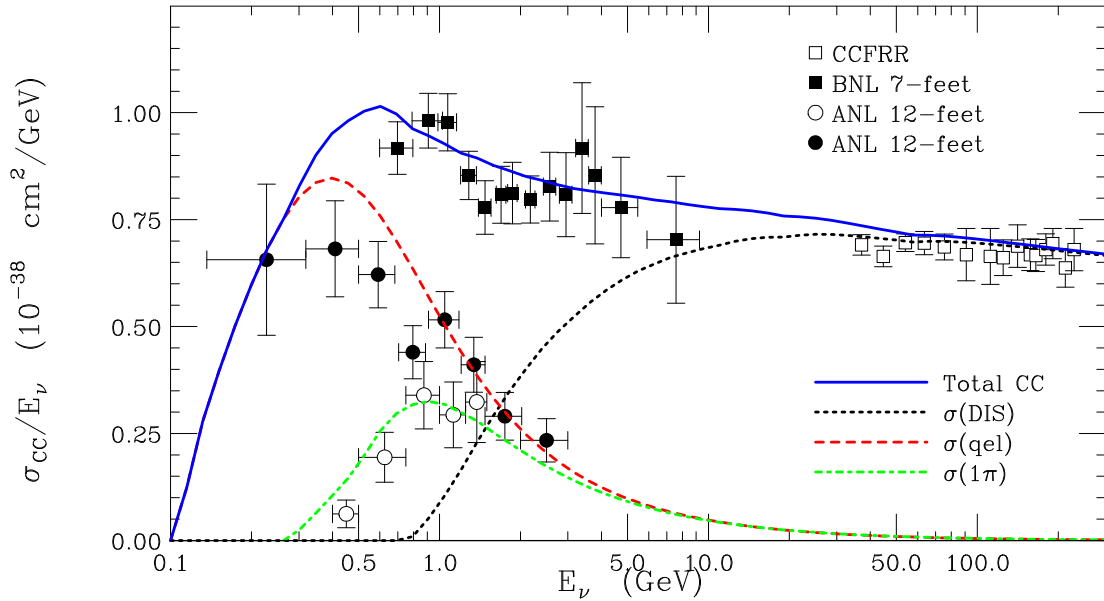
Figure 2.5.: Contributions to the charge current neutrino cross section for muon identification events. Current experimental data [122, 123] is shown with the relevant theoretical predictions. Figure reproduced from [123].

state. Energy reconstruction relies heavily on the ability of the detector technology to account for and reconstruct the final state hadron energies.

The individual contributions to the total charge current cross-section as a function of energy is shown in Fig. 2.5. The ability of a particular detector technology to satisfactorily reconstruct the incident neutrino energy is dependent on the neutrino energy. For example, Water Čerenkov detectors (WC) use QE events but are extremely poor at reconstructing hadronic events. Consequently, WC detectors are optimal for facilities in which the bulk of the neutrino flux is at low energies. The size of a realistic detector is dependent on the choice of the technology. Therefore, the physics reach of a given facility is heavily dependent on the choice of detector technology.

Event reconstruction has two important aspects: the efficiency in which a given event can be identified, and the energy resolution of its reconstruction. The efficiency is the final distribution in the integrand of Eq. 2.51. The reconstruction efficiency is a function of the neutrino energy, but is not theoretically known. This function needs to be determined from a detector Monte Carlo assuming a particular incident neutrino spectrum. Only for a small number of cases have such simulations been carried out; for some technologies, no efficiency curves are available. The standard approach in such cases is to either extrapolate known results or to base the efficiencies on advice from experimental collaborations. Typically, however, the

efficiency is expected to be constant over large energy ranges. An often applied strategy is to then assume a experimental cuts which introduce an energy threshold in the facility simulation. A constant efficiency can then be factored into the normalisation allowing for studies examining generic detector technologies with some 'exposure'.

The evaluation of the integral in Eq. 2.51 returns the number of neutrino events in bin i for a given facility, neutrino parameter hypothesis and perfect energy reconstruction of the detector. In reality, a further step is required to compensate for the imperfect energy reconstruction. The differential event flux, dN_i/dE needs to be appended with a resolution function which (physically) is the probability density function of returning event energy $\tilde{E}$ when the true neutrino energy is E. In this thesis, any energy resolution is treated as Gaussian and the event rate integral is modified to

$$N_i(\theta_{13}^{\mathrm{tr}}, \delta^{\mathrm{tr}}) = \mathcal{N}_T \, t \int_{E_i}^{E_i + \Delta E_i} \frac{dN_i}{dE} \, K_i(E) dE \; , \tag{2.54}$$

where $K(E)$ is the energy resolution kernel for the ith bin and is given by

$$K_i = \mathcal{N}_T \, t \int_{E_i}^{E_i + \Delta E_i} R(E, \tilde{E}) d\tilde{E} \; . \tag{2.55}$$

Here, $R(E, \tilde{E})$ is the energy resolution function

$$R(E, \tilde{E}) = \frac{1}{\sigma(E)\sqrt{2\pi}} e^{-\frac{(E - \tilde{E})^2}{2\sigma^2(E)}} \; . \tag{2.56}$$

This approach to energy reconstruction is adopted by the GLoBES [124] software and is outlined in detail in the manual [125].

The above outline represents the bulk of the computational effort in evaluating the event rates for a given neutrino oscillation hypothesis. The total event rate for a given bin is the rate sum of the channels and backgrounds that can produce or mimic the sought oscillation event. For a Beta Beam, this is the sum of the appearance channel; neutral current events involving ν_e's that can mimic the signal; disappearance charge current events that can be misidentified; and ν_μ atmospheric neutrino events that survive directional cuts.

$$\frac{dN_i^{\mathrm{tot}}}{dE} = \frac{dN_i}{dE} K_i(E) + \sigma_{\nu_e}^{NC} \eta_{NC} \frac{d}{dE} \Phi_{\nu_e} + \sigma_{\nu_e}^{CC} \eta_{CC} P_{ee} \frac{d}{dE} \Phi_{\nu_e} + \frac{dB_{\mathrm{atm}}}{dE} \; . \tag{2.57}$$

In this equation, η_{NC} and η_{CC} are the fraction of neutral current and charge current events that are misidentified as ν_μ appearance events. P_{ee} is the $\nu_e \rightarrow \nu_e$ disappearance probabilty. The atmospheric background events are skewed towards sub-GeV energies and provide technological problems for the Beta Beams and related technologies. These are the ν_μ that are produced in the particle cascades from cosmic rays collision in the upper atmosphere. This issue will be discussed further in Sec. 3.7.

2.3.2. Detectors

Future neutrino facilities will be set up to search for the sub-dominant $\nu_e \rightarrow \nu_\mu$ or $\nu_\mu \rightarrow \nu_e$ appearance channels and their CP-conjugates. Since Beta Beams only search for ν_μ appearance with no intrinsic contamination of the beam, the following discussion restricts itself to muon events. To help resolve the degeneracies inherent to a future long baseline facility, it is important to reconstruct the energy spectrum of the events. Excellent energy reconstruction of muon events is therefore mandatory over a large range of energies. If θ_{13} is small, the background events will dominate the signal if left unchecked. It is therefore important to be able to separate charge current events from neutral current events and to identify and subtract non-beam backgrounds such as atmospheric neutrino events. Finally, since the appearance signals are small, maybe incredibly so, it is important to have the largest detector volume available so to possess a huge number of nucleon targets. This is critical point for a Beta Beam as the available number of events is the main limitation (see Sec. 3.7).

From Fig. 2.5, QE events dominate charge current cross-section at low neutrino energies. For high neutrino energies, a detector needs to reconstruct mainly DIS events. A number of different detector types have been identified for a Beta Beam facility and are split into two categories based on the event types they reconstruct

1. Massive Water Čerenkov detectors that can only use QE events in the reconstruction. From Fig. 2.5, these are only useful if the neutrino flux is concentrated below 1.5 GeV.

2. Smaller tracking calorimeters and Time Projection Chambers (TPC) that, in addition, reconstruct the inelastic events. These are useful at high energies where the QE events are sub-dominant. Although detectors of this type can be used at low energies, they are often not considered since their smaller size returns much smaller event rates than a WC.

A Water Čerenkov detector is a large cavern filled with water surrounded by photo-multiplier tubes (PMT). Neutrino events are identified from the Cerenkov light from the final state lepton as it transverses the detector. WCs are ideal for muon events since muons do not scatter

electromagnetically. Instead a muon event is a Cerenkov ring with sharp edges. Electrons, on the other hand, do scatter electromagnetically and produce very fuzzy Cerenkov rings. (Muons have the same electromagnetic interactions with their environment as electrons, but their much larger mass means that the deviation from their trajectory is very much smaller.) WC Cerenkovs up to 1 Mton have been proposed [78] which corresponds to a fiducial mass of around 440 kton. Such a size constitutes the main advantage of building a WC. However, WC detectors are only good options for quasi-elastic events. For multi-particle final state processes, neutral particles or low energy particles are often present, but cannot be reconstructed. Particles below the Cerenkov threshold are lost. For high energy events with multiple particles above the threshold, there will be more than one Cerenkov ring preventing an accurate event tag. From Fig. 2.5, they are only feasible when a large portion of the neutrino flux is below 1.5 GeV. The large fiducial volumes cannot compensate for energies much beyond 2 GeV.

Neutrino events at high energies are dominated by deep inelastic scattering (DIS) events (Fig. 2.5). To satisfactorily reconstruct the neutrino energy, a measurement of the energy deposited from DIS hadrons is necessary. Detectors typically employ TPC techniques, such as proposed Liquid Argon (LAr) detectors, or traditional tracking calorimetry, such as Iron Calorimeters (IC) or Totally Active Scintillator detectors (TASD). Detectors of this type are assumed to be no more than 100 kton in mass; often they are assumed much smaller.

IC detectors are typically considered magnetised, although this is not a necessary feature for a Beta Beam. The proposed India Neutrino Observatory [126] is of this type, and is used as the far detector in magic baseline Beta Beam studies [79, 80, 84]. INO will consist of three modules each containing several layers of active detector material sandwiched by iron plates. The whole detector volume will be magnetised with a 1.3 Tesla field.

TASD detectors are established technology and are currently considered for the NOvA Superbeam [48] and low energy Neutrino Factories [65]. TASD detectors will be modules of liquid scintillator with long fibers passing through each one. Reconstruction is then through the analysis the particle tracks. TASD detectors possess excellent energy resolution and background rejection.

In LAr detectors [127, 128], a uniform electric field can transport particle tracks undistorted over many meters. An electrical signal can then be read at the end of the drift. R&D has been carried out on small scale detectors, the largest of which is 3 tons. A much larger 600 tonne detector has been built and installed in the Gran Sasso laboratory, and will search for neutrino oscillations (from solar, atmospheric and long baseline events); and nucleon de-

cays. For a next generation neutrino oscillation experiment, detector masses of 50-100 kton are sought. Such a leap needs a major extrapolation of the technology [128].

2.3.3. The statistical analysis

With the number of events in each bin calculated, the next step in the analysis is the calculation of a χ^2 function. For this purpose, we distinguish the *'true'* event rate from a *'test'* event rate. In statistical parlance, the analyses to be carried out are based on the following statistical test:

$$H_0: \quad \theta_{13} \text{ and } \delta \text{ assume their true values} \quad (\theta_{13}, \delta) = (\theta_{13}^{tr}, \delta^{tr})$$

$$H_1: \quad \theta_{13} \text{ and } \delta \text{ assume different values} \quad (\theta_{13}, \delta) = (\theta_{13}^{test}, \delta^{test})$$

All analyses in this thesis work on this raw basis. For a given pair $(\theta_{13}^{test}, \delta^{test})$, can we distinguish the resulting event distribution at a given confidence level from the true event spectrum? The statistical test carried out is a maximum likelihood fit. Consider an experiment with N bins and let n_i be the number of events in the ith bin for a given parameter vector $\vec{\theta}$, so that an experiment returns the event vector

$$\vec{n} = (n_1, n_2, ..., n_N) . \tag{2.58}$$

Here the vector $\vec{\theta}$ holds all the oscillation parameters:

$$\vec{\theta} \equiv \vec{\theta}(\theta_{12}, \theta_{13}, \theta_{23}, \Delta m_{31}^2, \Delta m_{21}^2, \delta) . \tag{2.59}$$

The number of events in a given bin will follow some probability distribution function (p.d.f.), $f(n_i, \vec{\theta})$ with the likelihood function defined to be the joint p.d.f. of the number of events for all the bins

$$L(\vec{n}) = \prod_{i=1}^{N} f(n_i, \vec{\theta}) . \tag{2.60}$$

The task at hand is to compare the event rate vector $\vec{n}$ with $\vec{\xi} = (\xi_1, \xi_2, ..., \xi_N)$ computed under a different hypothesis. To this end, the ratio

$$\lambda = \frac{L(\vec{\xi})}{L(\vec{n})} \tag{2.61}$$

is constructed. To make this statistic applicable for our purposes, we make use of a theorem [129, 130]: "The likelihood χ_λ^2 defined by

$$\chi_\lambda^2 = -2\log\lambda = -2\log L(\vec{\xi}) + 2\log L(\vec{n}) \tag{2.62}$$

asymptotically obeys a chi-square distribution." The χ^2 statistic required is therefore

$$\chi^2 = 2\sum_i^N \left[\xi_i - n_i + n_i \log\left(\frac{n_i}{\xi_i}\right) \right] , \tag{2.63}$$

and is referred to as the 'Poisson form'. Alternatively, one may choose to use the 'Gaussian form' of the χ^2;

$$\chi^2 = \sum_i^N \frac{(\xi_i - n_i)^2}{\xi_i} , \tag{2.64}$$

which is valid in the large sample limit (typically taken as n_i, $\xi_i > 5$), irrespective of the distribution. Both these statistics can form the basis for the maximum likelihood method used to construct sensitivity plots. There are two approaches to include systematics and external information in the analysis:

1. **Covariance matrix method:** We are comparing the event spectrum $\vec{\xi}$ with the true event spectum $\vec{n}$. In a given bin, the variance is simply the number of events in that bin as the number of events follows a Poisson distribution. Consider the Gaussian form of the χ^2: the expression is the simply the squared difference between the two hypotheses normalised by the statistical variability. The inclusion of systematic errors and imperfect external information reduces the χ^2 by adding non-statistical components to the normalisation. With these additions, the χ^2 now takes the form [129, 131]

$$\chi^2 = \sum_i \sum_j (\xi_i - n_i) C_{i,j}^{-1} (\xi_j - n_j) , \tag{2.65}$$

where $C_{i,j}$ is the covariance matrix

$$C_{i,j} = \xi_i + \sum_\alpha \frac{\partial \xi_i}{\partial \alpha} \frac{\partial \xi_j}{\partial \alpha} \sigma^2(\alpha) , \tag{2.66}$$

and α is a systematic parameter. The second term allows one to include external information and systematic errors in the form of correlations. The cross term appears since we are examining the square of the distribution $(\xi_i - n_i)$.

2. **The pull method:** Consider some experimental parameter ζ with uncertainty σ_ζ. One introduces a new parameter π_ζ and modifies the 'test' event vector

$$\xi' = (1 + \pi_\zeta)\xi \,, \tag{2.67}$$

then adds the contribution

$$\left(\frac{\pi_\zeta}{\sigma_\zeta}\right)^2 \tag{2.68}$$

to the error-free χ^2. The required χ^2 function, $\hat{\chi}^2$, is then found by minimising over π_ζ:

$$\hat{\chi}^2 = \min_{\pi_\zeta} \left[2\sum_i^N \left\{ \xi_i' - n_i + n_i \log\left(\frac{n_i}{\xi_i'}\right) \right\} + \left(\frac{\pi_\zeta}{\sigma_\zeta}\right)^2 \right] \,. \tag{2.69}$$

For many systematics, the approach just described is duplicated with the minimisation performed simultaneously over all pull parameters. To include external information on the experimental parameters, one adds the contribution in Eq. 2.68, but does not modify the test vector. This 'prior' can be thought of as adding a penalty to the χ^2 function if the minimisation strays too far from the central values imposed externally.

It can be shown [132] that these two procedures are equivalent. To include an overall systematic error on the flux, σ_f; note that it will not alter the shape of the oscillation probability. The total event rate in each bin is modified by the same factor, $(1 + f_{sys})$, say. Consequently, there are no correlations between bins in this respect so the off-axis terms are all zero. An error on the normalisation of the flux modifies the statistical error by $(f_{sys} \cdot \xi_i)^2$. The inclusion of the known errors on the measured oscillation parameters is not so straightforward. Although the parameters themselves have no energy dependence, the relative strengths of the atmospheric, solar and interference contributions are different for each bin. Their effect is therefore energy dependent even though the parameters themselves are not. For the inclusion of the external information, the cross terms need to computed and the covariance matrix needs to be inverted. In general, this needs to be done numerically.

In any realistic simulation of a future neutrino facility, the uncertainties on the unknown oscillation parameters will have to be included in the analysis using the technique above. In this thesis, the goal is to demonstrate the characteristics of Beta Beam and their related technologies, not to present final sensitivities, and so they are not included. The experimental parameters of the Beta Beam are far from certain and so their is little gain including the details outside a comprehensive optimisation study. The results and the features raised in this thesis

will be largely unchanged with their inclusion. This is also for consistency between the codes used for the phenomenological studies of this thesis.

With the calculation of the χ^2 function, one is now in the position to perform the statistical test. Suppose an experiment has been carried out that returns the binned data $\vec{n}$. The first step would be to fit the oscillation model to the data by minimising over all oscillation parameters and other important experimental uncertainties, given a certain hypothesis. This procedure will return a χ^2_{min} which in general does not equal zero. From this, one can then fit the data keeping some of the parameters fixed, but minimising over the remaining parameters, using the $\Delta\chi^2$ statistic

$$\Delta\chi^2 = \chi^2 - \chi^2_{\text{min}} \,. \tag{2.70}$$

In the absence of data we must artificially generate the vector $\vec{n}$. To do this we pick 'true' values for the parameters that are to be fixed in the fit. Some simulations then smear this data to mimic statistical fluctuations and generate a $\chi^2_{\text{min}} \neq 0$. It is usual, however, to neglect this feature so that $\chi^2_{\text{min}} = 0$ and $\Delta\chi^2 = \chi^2$. With this clarification, each type of sensitivity plot will be considered in turn.

- **Two parameter fits**

  These are the standard sensitivity plots in which the event spectrum for the *'true'* pair $(\theta_{13}^{\text{tr}}, \delta^{\text{tr}})$ is compared to alternative *'test'* pairs across the (θ_{13}, δ)-plane. They show the region of parameter space in which the event spectrum for given pair is indistinguishable from the true event spectrum at given confidence levels. These plots are useful for understanding the behaviour of degenerate solutions. Boundary lines are typically drawn for 90 %, 95 % and 99 % confidence levels with 2 degrees of freedom. An example of such a plot is shown in Fig. 2.6. In this figure[4], the features relevant here are the two regions bounded by black lines.

- **Two parameter fits - hierarchy degeneracy**

  To include the degenerate solutions within any analysis, it is necessary to first fit the data to the opposite hierarchy. This procedure is essentially the same, however, there are some minor differences that need pointing out. Suppose the true hierarchy is normal and the true event rates are $n_i = n_i(\theta_{13}^{\text{tr}}, \delta^{\text{tr}}, |\Delta m_{31}^2|)$. We assign the event vector $\vec{\xi}$ to the

---

[4]This is an old version of a figure that appears later in this thesis. The experimental details are not important for this discussion and are neglected.
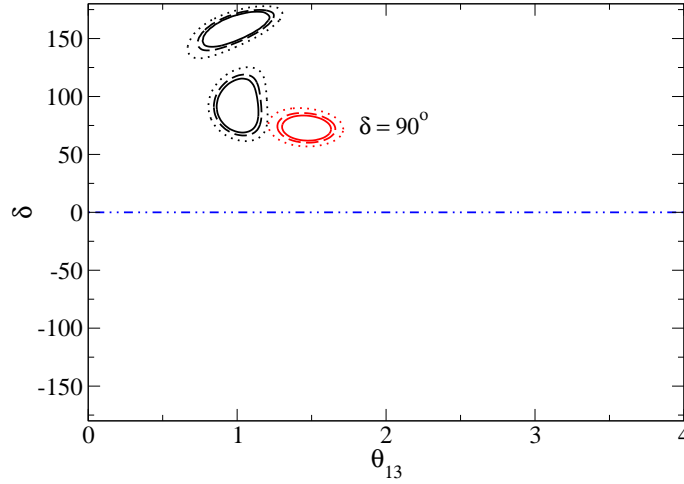
Figure 2.6.: 90 %, 95 % and 99 % for true pairs (shown in black) $(1^o, 90^o)$ and $(1^o, 160^o)$. A hierarchy clone exists for the $(1^o, 90^o)$ pair and is shown in red.

inverted hierarchy and attempt to fit it to the true solution using the χ^2 statistic intro-duced above, returning a $\chi^2_{min} \neq 0$ in general. The 90 %, 95 % and 99 % contours for the degenerate solution are drawn for the χ^2 function using only one degree of freedom. An example of a hierarchy clone are the regions bounded by the red lines in Fig. 2.6.

- **Hierarchy exclusion plots**

The above procedure automatically determines whether a measurement of the sign(Δm^2_{31}) can be made for a given facility. If χ^2_{min} is greater than the required confidence level threshold then the hierarchy is said to be resolved. Since the hierarchy is not known beforehand, hierarchy exclusion plots are constructed in the following way

1. Assume the true hierarchy to be normal. Locate the inverted hierarchy degenerate solution and assign $\chi^2_{min} = \chi^2_{NH}$

2. Repeat with normal and inverted hierarchies interchanged. Assign $\chi^2_{min} = \chi^2_{IH}$

3. For a given $(\theta^{tr}, \delta^{tr})$ the hierarchy χ^2 is $\chi^2_{hier} = \min \{\chi^2_{NH}, \chi^2_{IH}\}$

The hierarchy is said to be resolved at some confidence level if χ^2_{hier} exceeds the threshold for that confidence level with 1 degree of freedom. If the octant degeneracy is included in the analysis, then all solutions consistent with the wrong hierarchy need also to be checked. The final χ^2 is then the minimum of all those calculated.

- **CP-violation sensitivity plots**

To analyse the ability of a facility to measure CP-violation, the simulation of many two parameter fits is not helpful. The presence and location of degeneracies; and the size and shape of the sensitivity regions make such an approach qualitative; lacking simple quantitative statements. The strategy typically employed is to determine whether or not a given true pair can be distinguished from CP-conservation. This amounts to plotting the true solution, and all the degenerate solutions, and checking whether the $\delta = 0^o$ and/or $\delta = 180^o$ lines cross the sensitivity region at some confidence level. This is then repeated for the opposite hierarchy. To automate this numerically, one does the following.

1. Calculate the event rate vector for the true pair with the normal hierarchy as true. Calculate the χ^2's with the usual test rate vector ξ but fixing $\delta = 0^o$.

2. Find the minimum χ^2 along the $\delta = 0^o$ line and label it $\chi^2_{0;NH}$.

3. Repeat the above steps but fixing $\delta = 180^o$, the other CP-conserving case. Label the minimum $\chi^2_{180;NH}$.

4. Locate the hierarchy degeneracy. If the degeneracy is not resolved, one needs to check that it is also not consistent with CP-conservation. Before, the true solution regions were calculated with 2 degrees of freedom but the clones were drawn with only 1. To resolve this incompatibility, one now recalculates the true rate vector but assuming the wrong hierarchy and using the clone location as the true pair. 2 degrees of freedom can now be used.

5. Test the $\delta = 0^o$ and $\delta = 180^o$ lines as before and label the χ^2's $\chi^2_{0;IH}$ and $\chi^2_{180;IH}$.

6. 1-5 are repeated but starting from the assumption that the true hierarchy is inverted. This will generate a further 4 χ^2's.

7. The final χ^2 is the minimum of all 8.

The contour separating the discovery of CP-violation from failure to rule out CP-conservation at a given confidence level is then drawn. These analyses have the benefit of including all the degenerate effects in a sensible way and allows for easy comparison between facilities.

In this thesis, the policy of constructing these plots with 2 d.o.f. is adopted. A significant statistical result should therefore be interpreted as "for a given pair $(\theta^{tr}_{13}, \delta^{tr})$, the allowed region in (θ_{13}, δ) parameter space does not include CP-conserving values of δ".

It is now seen explicitly how degenerate solutions affect the sensitivity of a facility. To determine the effect of any degeneracy, we need to consider the following issues

1. Where is the clone solution?

2. How big is the allowed region surrounding the clone solution?

3. In what energy ranges does the clone solution manifest itself?

If we wish to rule out CP-conservation then no solution must cross the $\delta = 0^o$ or $\delta = 180^o$ lines. For degenerate solutions close together - for example the true and hierarchy clone solution for short baselines - this poses not problem. If true solution can be distinguished from CP-conservation then, in general, so can the hierarchy clone. For large matter effects, the hierarchy clone can be located far from the true solution. If the displacement involves a substantial shift in δ, then there is a risk that the the clone is consistent with CP-conservation even if the true solution is significantly different in a statistical sense. For intrinsic degeneracies, we know that in the atmospheric limit the the true and fake CP-phases are related by $\delta^{\text{tr}} = \pi - \delta^{\text{clone}}$. True solutions that can be distinguished from the CP-conservating $\delta = 0^o$ (or $\delta = 180^o$) might be accompanied by large intrinsic clones that are consistent with the CP-conserving $\delta = 180^o$ (or $\delta = 0^o$).

2.4. The GLoBES simulation package

GLoBES stands for 'General Long Baseline Experiment Simulator' and is a public code for long baseline neutrino oscillation experiments, or any experiment with a stationary neutrino point source [124]. The source code for GLoBES is written in C and allows for the computation of oscillation probabilities, event rates and $\Delta\chi^2$ for a given experimental setup. It is then the responsibility of the user to write code that constructs the plot types discussed in the previous section. The details of a GLoBES simulation are discussed in detail in the manual [125]. In short, a simulation consists of a detector definition thats does not change during run time. The calls to the C and GLoBES libraries; and the statistical analysis make up the main scope of C program. The calculation of the event rates is carried out using the method outlined in Sec. 2.3.1.

All simulations performed for Chap. 4 used the built-in Beta Beam fluxes by adapting the Totally Active Scintillator Detector experimental file used for [133]. The simulations in Chap. 6, belonging to Catalina Espinoza, were calibrated using the same file. The results of the

two chapters are therefore consistent. The codes used for the electron capture machine used in Chap. 5 are based on the fortran 77 files used to generate the oscillation probabilities. The code is far simpler as there is no need for energy reconstruction. These codes just generate the event rates for a given hypothesis using the flux given in Chap. 5 and code for the oscillation probability (see Appendix A).

Chapter 3.

The Beta Beam

In the previous chapters, the challenges for future long baseline neutrino oscillation experiments were introduced; in particular, the problem of degeneracies. The three facility options, and some of the strategies associated with them, were summarised. The Beta Beam is one such machine option and, with its related technologies (to be defined shortly), will be the focus of the remainder of this thesis. More specifically, in this chapter, a more detailed overview of the Beta Beam will be given with particular emphasis on the technological aspects relevant for phenomenology. Feasibility studies for the construction and operational of such a machine are presently being carried out in Working Package 2 of the EUROnu design study. Beta Beam technology will be summarised but the majority of the fine details are beyond the scope of this thesis and will not be discussed.

3.1. Introduction

Before going into the detail of a future Beta Beam facility, it is necessary to deconstruct the phrase "Beta Beam and its related technologies". As introduced in Chap 1, a Beta Beam sources a flux of neutrinos through the production, acceleration and storage of ions with a 100 % or dominant beta decay channel. Such a beam, consisting solely of electron neutrinos or electron anti-neutrinos, will be intense and well collimated. The goal of the facility would be to measure the unknown oscillation parameters and resolve any degeneracy of the setup through the reconstruction of the muon (or anti-muon) event spectrum as a function of energy. However, note that there are four possible ion decays with a neutrino or anti-neutrino in the

final state. For a parent ion I_P and daughter ion I_D, these are

$$\beta^+ - \text{decay} \qquad\qquad I_P \longrightarrow I_D + e^+ + \nu_e \;,$$

$$\beta^- - \text{decay} \qquad\qquad I_P \longrightarrow I_D + e^- + \bar{\nu}_e \;,$$

$$\text{Electron capture decay} \qquad e^- + I_P \longrightarrow I_D + \nu_e \;,$$

$$\text{Bound beta decay} \qquad\qquad I_P \longrightarrow I_D + \bar{\nu}_e \qquad .$$

In a β^+ (β^-) decay a proton (neutron) is converted to a neutron (proton) and a positron (electron) is ejected from the nucleus in combination with a electron neutrino (electron anti-neutrino). These are three-body decays and so the neutrino spectrum is continuous with energies ranging from zero up to the maximum kinetic energy available to the decay, the Q-value. The neutrino energy spectrum takes the following form in the ion rest frame

$$\frac{dN^{\text{rf}}}{d\cos\theta \, dE_{\text{rf}}} \sim E_{\text{rf}}^2 \, (E_0 - E_{\text{rf}}) \sqrt{(E_0 - E_{\text{rf}})^2 - m_e^2} \;. \tag{3.1}$$

Here, E_{rf} is the rest frame neutrino energy and E_0 is the total energy available to the decay and differs from the Q-value by the mass of the electron. The total available energy is sometimes referred to as the 'endpoint energy'. Virtually all studies of Beta Beams choose pairs of ions that decay through these processes, typically one ν_e and one $\bar{\nu}_e$ emitter. Indeed, it was after these processes that the name 'Beta Beam' was coined [16]. A nucleus that is proton rich may also decay through electron capture. This is a process in which an orbital electron is captured by the nucleus with a conversion of a proton into a neutron and emission of a ν_e. This is a two body decay and so the neutrino, for a given transition, is mono-energetic. For a parent nucleus with proton number Z and mass number A, the maximum energy release for a proton rich nucleus of mass $M_A(Z,N)$ is given by

$$\Delta M_A = M_A(Z,N) - M_A(Z-1,N+1) \;. \tag{3.2}$$

For an electron capture decay, this is just the Q-value: $Q_{\text{EC}} = \Delta M_A$. For the competing decay mode of positron decay, however, an excess positron is produced. The maximum kinetic energy available for this decay mode is thus $Q_{\beta^+} = \Delta M_A - 2m_e$. Clearly, for $\Delta M_A < 2m_e$, positron decay is kinematically forbidden with electron capture decay the only allowed process, in general. For $\Delta M_A > 2m_e$, the two processes compete with their respective branching ratios dependent on ΔM_A and the existence, or not, of non weak-interaction decay modes such as α-decay. The use of electron capture decays in long baseline neutrino physics will form the discussion of Chap. 5.

The bound beta decay process can be considered as the inverse of electron capture. In a bound beta decay, a neutron is converted to a proton with the created electron not ejected but instead captured into one of the electron orbitals. This is also a two body decay with the electron anti-neutrinos mono-energetic in energy for each nuclear transition. The rate of bound beta decay is dependent on the orbital wave-functions and is thus only a significant effect for fully, or almost fully stripped, ions. In fact, the process has only be observed in a handful of ions [134, 135, 136, 137, 138] even though it has been known theoretically for 50 years [139]. A second difference with the electron capture decays is that the β^- is not kinematically forbidden and will always constitute a background to the bound beta decay process except in the limit $Q \to 0$. An idea was put forward to combine beams sourced from this process with electron capture decay modes [94]. There are a number of physical and technological drawbacks which render this idea implausible; these will be discussed at the end of Chap. 5.

Although all four processes could be considered *'Beta Beams'*, one is usually referring to a proposal using the first two decays as the source. Beta Beams sourced from electron capture decays and bound beta decays shall be referred to as *'electron capture machines'* and *'bound beta beams'*. Beams sourced from ions that both decay through both β^+ and electron capture modes shall be referred to as *'hybrids'* and shall be discussed in Chap 6. Collectively, these three are the *'related technologies'*.

3.2. The Beta Beam concept

The Beta Beam was originally introduced as a reworking of the Neutrino Factory idea using radioactive ion decays with the production and subsequent acceleration using the existing or potential upgrades of the CERN accelerator complex [16]. The Beta Beam proposes to produce high energy, collimated ν_e and $\bar{\nu}_e$ beams from the decay of radioactive ions. The Beta Beam's primary interest are the

$$\nu_e \to \nu_\mu \qquad \text{and} \qquad \bar{\nu}_e \to \bar{\nu}_\mu \tag{3.3}$$

oscillation appearance channels. By opting to source the neutrino flux from radioactive decays, the Beta Beam differs from coventional beams, Superbeams and Neutrino Factories in one crucial respect: the neutrino flux consists of only one flavour and helicity. Recall that Superbeams, which are sourced from the two-body decay of pions and kaons, are contaminated by neutrinos from the three body decay of kaons and the decay of the muons in the decay tun-

nel. Neutrino Factories require magnetised detectors to separate out the right-sign muons and wrong-sign muons. For high energy Neutrino Factories using the MIND detector technology, two very long baselines are required owing to poor efficiencies at low energies. Low energy Neutrino Factories do not have the problem of poor efficiencies but the need for magnetisation rules out the use of large Water Čerenkov detectors which are ideal for the shorter baselines (see Sec. 2.3.2). The Beta Beam does not possess these problems as only one neutrino flavour and either neutrino or anti-neutrino is present in the beam at production. Magnetised detectors are therefore not necessary; Water Čerenkov, Liquid Argon and Iron Calorimeters are all candidate far detectors, in addition to the magnetised detectors such as MIND and Totally Active Scintillator Detectors. The only requirement is good muon event identification to observe the $\nu_e \to \nu_\mu$ or $\bar{\nu}_e \to \bar{\nu}_\mu$ appearance channels. Consequently, depending on the choice of detector technology, a Beta Beam could be used to source the entire range of long baseline neutrino oscillation experimental baselines; from CERN-Frejus (130 km) to the Magic Baseline (~ 7200 km).

The physics reach of a Beta Beam is highly dependent on the Lorentz boost factor, γ, of the source ion and the ion Q-value, $Q_{\mathrm{ion}} = E_0 - m_e$, where E_0 is the decay endpoint and m_e is the mass of the electron. The maximum boost attainable is constrained by the maximum magnetic rigidity (to be defined in Sec. 3.5) of the final stage of the acceleration. Beta Beams are sometimes described as 'statistics limited' machines. This means the physics reach is high dependent on the magnitude of the un-oscillated event rate; changes in the overall rate can induce large changes in the physics reach. (High luminosity Superbeams and Neutrino Factories are described 'systematics dominated' machines. The high rates accentuate the systematics contributions which behave as $(f_{\mathrm{sys}} \cdot n)^2$.) The principle reason for this limitation is the intrinsic difficulty in producing the required number of radioactive ions and transiting them through the acceleration and storage chain. This feature of the Beta Beam will be revisited in later sections.

3.2.1. Neutrino flux

The neutrino spectrum in the ion rest frame is given by the expression in Eq. 3.1. The flux of interest is this expression, but in the laboratory frame. Write the flux in the ion rest frame as Φ_{rf} and the same in the laboratory frame as Φ_{lab}. It is shown in Appendix B that these fluxes,

for boost γ, are related by

$$\Phi_{\mathrm{lab}}(E_\nu, \theta) = \frac{\Phi_{\mathrm{rf}}(E_\nu \gamma [1 - \beta \cos \theta])}{\gamma [1 - \beta \cos \theta]} \;. \tag{3.4}$$

Here, E_ν is the on-axis neutrino energy in the laboratory frame and β is the velocity of the ion in natural units. γ is the Lorentz boost defined by

$$\gamma = \frac{1}{\sqrt{1 - \beta^2}} \;. \tag{3.5}$$

To calculate the flux in the laboratory frame, it is customary to define a new parameter, y, such that [86]

$$0 \leqslant y = \frac{E_\nu}{2\gamma E_0} \leqslant 1 - y_e \;, \tag{3.6}$$

where $y_e = m_e / E_0$. The expression for the flux in the laboratory frame, per solid angle Ω, at a detector located at baseline L and boost factor γ is then given by

$$\left. \frac{dN^{\mathrm{lab}}}{d\Omega dy} \right|_{\theta \approx 0} \approx \frac{N_\beta}{\pi L^2} \frac{\gamma^2}{g(y_e)} y^2 (1 - y) \sqrt{(1 - y)^2 - y_e^2} \;, \tag{3.7}$$

where N_β is the number of useful ion decays per year and

$$g(y_e) \equiv \frac{1}{60} \left\{ \sqrt{1 - y_e^2} \, (2 - 9y_e^2 - 8y_e^4) + 15 y_e^4 \log \left[\frac{y_e}{1 - \sqrt{1 - y_e^2}} \right] \right\} \tag{3.8}$$

is the normalisation

$$g(y_e) = \int_0^{1 - y_e} y^2 (1 - y) \sqrt{(1 - y)^2 - y_e^2} \;. \tag{3.9}$$

Using the small angle approximation for θ and that the velocity and boost (for large boost) are related by $\beta \approx 1 - \frac{1}{2\gamma^2}$, a neutrino energy in the laboratory frame with off-axis angle θ is (see appendix B)

$$E_\nu(\theta) = \frac{2\gamma E_\nu^{\mathrm{rf}}}{1 + \gamma^2 \theta^2} \;. \tag{3.10}$$

The maximum neutrino energy in the laboratory frame for a given ion and accelerator is thus

$$E_\nu^{\mathrm{max}} = 2\gamma^{\mathrm{max}} Q \;. \tag{3.11}$$

Most Beta Beam studies make the assumption that the production environment and accelerator complex will be located at CERN. Ion production naturally fits into the planned expansion of the nuclear physics facilities known as EURISOL [140] which will use the Isotope Separation Online (ISOL) technique. This aspect will be discussed in Sec. 3.4. The acceleration could be carried out by the existing linacs and synchrotrons or the potential additions and refurbishments required primarily for LHC upgrades. In principle, the LHC itself could be used, however, the availability of any run time is unlikely. The pre-LHC accelerators culminating in the Super Proton Synchrotron (SPS), does not impinge on LHC operations and therefore its characteristics determine the maximum energy of a Beta Beam. Other possibilities are the Main Injector and Tevatron at Fermilab and the HERA ring at DESY. The maximum energies in principle available for Beta Beam are

Current SPS	450	GeV
Upgraded SPS	1000	GeV
FNAL Main Injector	150	GeV
Tevatron	980	GeV
HERA ring	960	GeV

There are currently 4 main ion choices: ^{18}Ne and ^{8}B for neutrino production and ^{6}He and ^{8}Li for anti-neutrino production. ^{18}Ne and ^{6}He are normally paired and have low Q-values in this context. ^{8}B and ^{8}Li have Q-values ~ 4 times larger. Although the neutrino spectra shapes are the same, the difference in Q-values results in different energy ranges in the laboratory frame. In Tab. 3.1, the maximum γ's (to be calculated in Sec. 3.5) for each ion are presented for the current SPS, upgraded SPS and the Fermilab Main Injector. The Tevatron and HERA ring have similar energies to the upgraded SPS and are not included in the table[1]. High energies in the laboratory frame need high-Q ions. However, for the same maximum neutrino laboratory energy and baseline, high-Q ions need a larger number of useful decays a year to produce an equivalent flux to the low-Q ions, as seen from Eq. 3.7. (Larger Q-values need smaller boosts to reach the same laboratory energies and therefore need to be scaled appropriately by the number of useful decays to produce the same flux.) The physics reach is therefore a balancing act between these two experimental parameters.

---

[1]There are currently no published numbers of the maximum ion energy of a Beta Beam based at DESY. The idea is to use the HERA ring as the decay ring and to use the linac and pre-HERA storage rings as the acceleration. The figure of a 960 GeV comes from an advertised $\gamma = 500$ Beta Beam from DESY to Frejus ($L \sim 960$ km) for ^{18}Ne [141]. An energy of at least the size quoted is necessary

		Current SPS		Upgraded SPS		Main Injector	
Isotope	E_P (MeV)	γ	E_ν (GeV)	γ	E_ν (GeV)	γ	E_ν (GeV)
^{18}Ne	1.86	270	1.0	590	2.2	90	0.3
^{6}He	1.94	160	0.6	355	1.4	53	0.2
^{8}B	7.37	300	4.4	670	9.8	100	1.4
^{8}Li	6.72	180	2.4	400	5.4	223	3.2

Table 3.1.: Energy at the peak of the Beta Beam spectrum in the rest frame (E_P) and in the boosted frame for the current (maximum proton energy of 450 GeV), upgraded (maximum proton energy of 1 TeV) SPS and the Fermilab Main Injector. Also shown the maximum achievable γ factor in both cases for each isotope.

This feature of the flux can be seen more explicitly in Fig. 3.1 where the un-oscillated neutrino flux for ^{18}Ne ions ($E_0 = 3.9$ MeV) boosted to $\gamma = 100, 200$ and 300 is shown. The CERN-Canfranc baseline is used assuming $1.1 \cdot 10^{18}$ useful decays per year. In addition, the flux for the equivalent baseline and decays has been shown for ^{8}B, which has $E_0 = 18.4$ MeV, for the same baseline and useful decays for $\gamma = 200$.

The choice of baseline, or combination of baselines, is typically chosen on basis of the properties of the appearance probability and the size of the signal. For example, short baselines such as CERN-Canfranc (650 km) or CERN-Gran Sasso (730 km) have good sensitivity to θ_{13} and δ since there is little degeneracy from sign(Δm_{31}^2) and the un-oscillated neutrino rate is high because of the $1/L^2$ flux dependence. Another example is the magic baseline (Sec. 2.2.2) which is often used for a clean measurement of θ_{13} and the hierarchy. For a measurement of CP-violation, if the magic baseline is chosen, it is necessary to choose an additional baseline whose probability has strong CP-violating features and has a event rate large enough to make use of the synergy between baselines.

The maximum energy in the laboratory frame using ^{18}Na is 4.0 GeV. If this is being paired with ^{6}He, the maximum energy at which ones has both helicities is 2.5 GeV. Therefore, if the required oscillatory structure of the appearance probability is much higher than this, one is forced to use the pairing ^{8}B and ^{8}Li. For short baselines, the pairing ^{18}Na and ^{6}He is preferred as the larger boost needed to cover the same energy range as ^{8}B and ^{8}Li returns a larger un-oscillated flux for a given baseline (from Eq. 3.7). With the ions available and maximum boosts in principle attainable, baselines up to the magic baseline can be sourced. Depending on the choice of boost and source ions, the Beta Beams to date can be split into
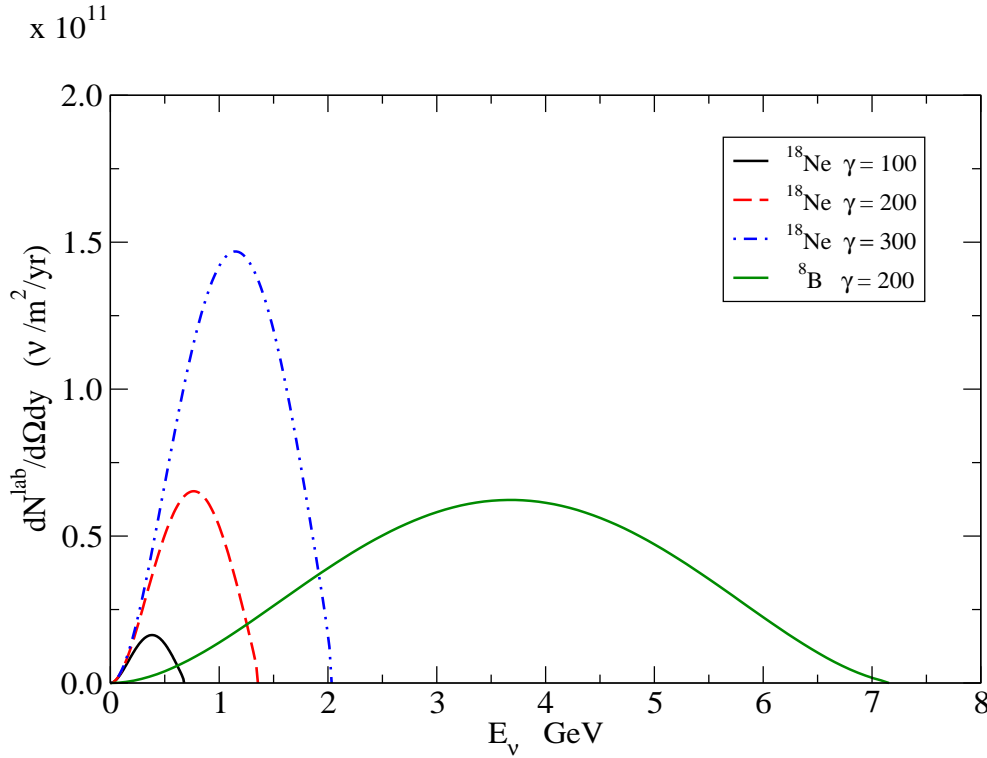
Figure 3.1.: Un-oscillated neutrino fluxes per year at a far detector for the CERN-Canfranc baseline
(650 km). $1.1 \cdot 10^{18}$ useful ion decays per year have been assumed in all cases.

two categories: Continental and inter-continental. I define continental Beta Beams as facilities
for which production, acceleration and the detectors are within the same continent. Although
most Beta Beam studies use CERN as their source site, this definition allows one to include
Fermilab and DESY based proposals. All other Beta Beams are inter-continental.

3.2.2. Continental Beta Beams

Most studies of Beta Beams fall into this category and typically use the ^{18}Na and ^{6}He ion
pair. There is no advantage in using the high-Q ions for continental baselines unless the
number of useful decays can be increased by a factor of 16 to compensate for the lower boosts.
Continental Beta Beams can be sub-divided into low γ and high γ machines.

Low γ: The original Beta Beam proposals assumed only the SPS in its current configuration
is to be available. The boosts were chosen to be[2] $\gamma_{Ne}/\gamma_{He} = 100/60$ or $100/100$. These initial

---

[2]At the time, the possibility of circulating both neutrino and anti-neutrino producing ions together in the storage
ring was common. Timing at the detector could then be used to separate out the right and wrong sign muons.
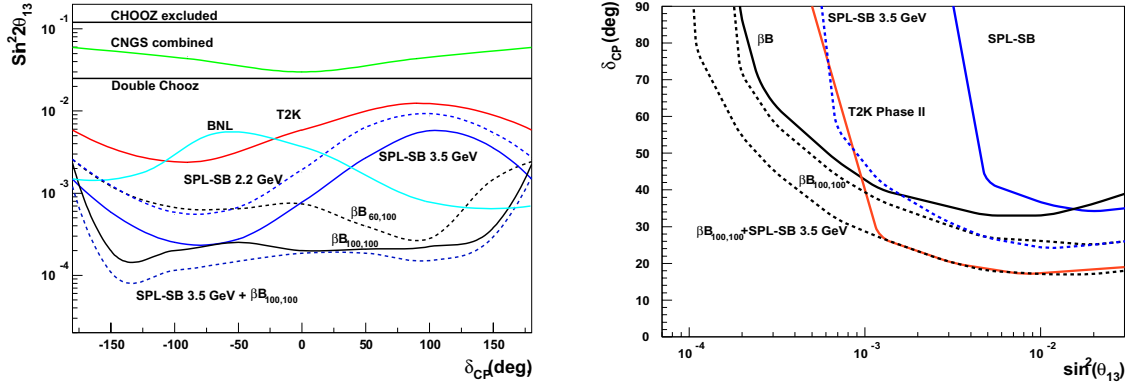
Figure 3.2.: θ_{13} discovery reach (left) - the smallest $\sin^2 2\theta_{13}$ for a given δ for which $\theta_{13} = 0$ can be ruled out - and CP-violation sensitivity, as defined in Sec. 2.3.3, (right). The plots show the reach for the 2 CERN-Frejus Beta Beams described in the text and also in combination with a SPL Superbeam for two energies (labelled on left plot). The plots also include the equivalent analyses for T2K [47] and the Brookhaven wide band beam. Plot taken from [86].

studies suggested the use of a large Water Čerenkov detector known as MEMPHYS [78] with a fiducial detector volume of 440 kton. For the first case, the average neutrino energies are $\langle E_\nu \rangle = 0.36$ GeV and $\langle E_{\bar{\nu}} \rangle = 0.24$ GeV. Owing to nuclear motion effects, energy reconstruction is not possible at these energies; the facility is a 'counting experiment'. Beta Beams will only use a small fraction of the available protons to be produced at CERN. A Superbeam can therefore be constructed for the same baseline without affecting the physics reach of the Beta Beam. The physics reach of the two Beta Beams just described and in combination of a Superbeam sourced from a proposed new Super Proton Linac (SPL) at CERN is shown in Fig. 3.2. The 100/100 Beta Beam in combination with a 3.5 GeV SPL Superbeam can reach θ_{13} and δ sensitivity down to $\sin^2 2\theta_{13} \sim 10^{-4}$. At short baselines, there is very little sensitivity to the mass hierarchy.

In [142] it was suggested that the Fermilab Main Injector could be used to source ^{8}B and ^{8}Li ions for the FNAL-Soudan baseline (L=730 km) using boosts of $\gamma = 80$. The equivalent boosts for ^{18}Na and ^{6}He will be ~ 4 times larger with the flux ~ 16 times larger due to the quadratic dependence on the boost. For the use of ^{8}B and ^{8}Li, the total number of decays will need to be increased by this factor to achieve an equivalent physics reach. This is plausible [142]. The use of ^{8}B and ^{8}Li only needs the Main Injector whilst ^{18}Na and ^{6}He would need the Tevatron (possible in principle but its slow ramps are not ideal for a Beta Beam). No comprehensive study of this idea has been carried out.

For this to work, the boosts have to be in the ratio of the two charge to mass ratios which for ^{18}Ne and ^{6}He is 3/5.
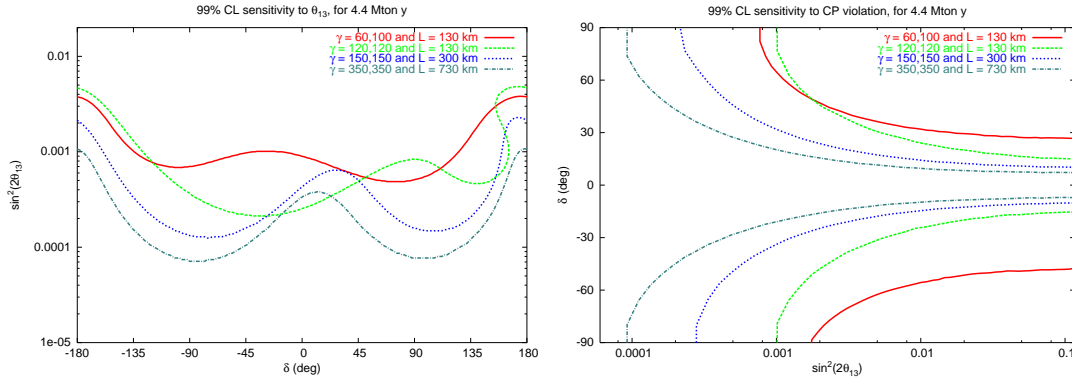
Figure 3.3.: θ_{13} discovery reach (left) and CP-violation sensitivity (right) for a number of Beta Beam proposals. The 350/350 aimed down the CERN-Gran Sasso baseline requires the SPS to be upgraded to 1 TeV. $\gamma = 350$ is the maximum boost possible for ^{6}He in such a machine. Figure reproduced from [86].

High γ: As part of proposed LHC upgrades, the SPS could be equipped with fast cycling superconducting magnets. These will provide fast ramps to reduce ion losses in the acceleration and increase the maximum proton energy to 1 TeV. The maximum boosts available are presented in Tab. 3.1. A number of proposals exist in the literature for Beta Beam facilities using an upgraded SPS to source the CERN-Canfranc (L=650 km), CERN-Gran Sasso (L=730 km) and CERN-Boulby (L=1050 km) baselines. The CERN-Slanic (L=1500 km) and CERN-Phyalsalmi (L=2248 km) baselines are also available but have not been studied in detail. They are not expected to perform better than the previous baselines owing to the stronger degeneracies between θ_{13}, δ and sign(Δm^2_{31}) and the $1/L^2$ flux dependence. Water Čerenkov, Iron Calorimeters, Liquid Argon detectors and Totally Active Scintillator Detectors have all been considered as far detectors; in the first two cases, detector responses given an incident flux have been simulated. The sensitivity for θ_{13} and δ for a 350/350 boost setup is shown in Fig. 3.3.

Just recently, the physics reach of a high boost Beta Beam from Fermilab aimed at the DUSEL site at Homestake (L=1280 km) was examined. The baseline was simulated for a 300 kton Water Čerenkov and a 100 kton liquid argon detector and was compared to a FNAL-Homestake wide band beam without assuming the Project X proton driver upgrade. The results are presented in Fig. 3.4.
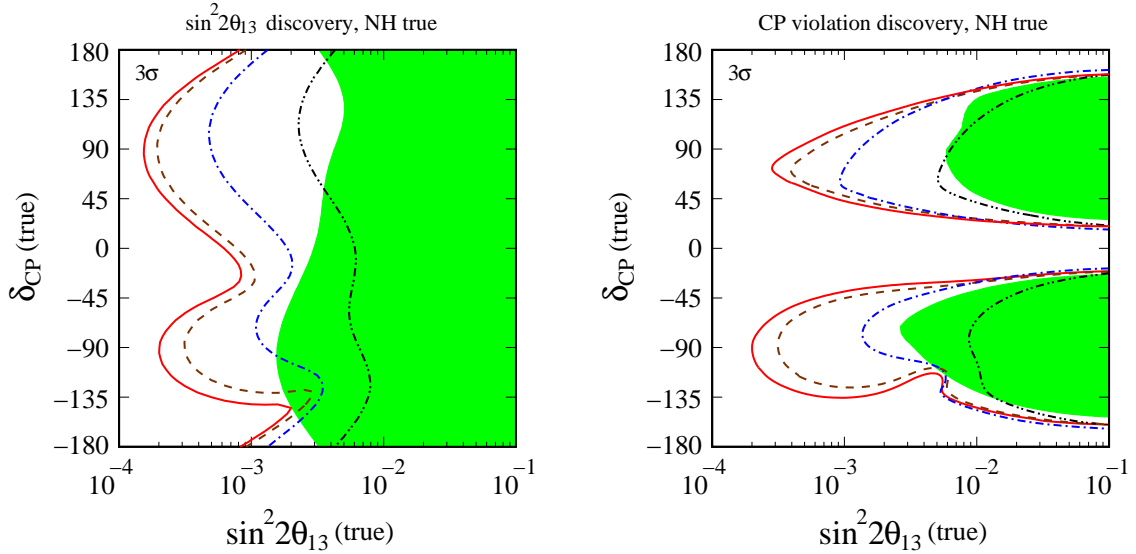
Figure 3.4.: θ_{13} discovery reach (left) and CP-violation sensitivity (right) for the FNAL-DUSEL Beta Beam proposals. Show are the results for a 100 kton liquid argon detector with 10^{-4} background rejection (red) and 10^{-3} background rejection (brown dashed); and a 300 kton water Čerenkov with 10^{-3} background rejection (blue dot dashed) and 10^{-2} background rejection (black double-dot dashed). The green region marks the sensitivity for the wide band beam consider in [143]. Plots taken from [143].

3.2.3. Inter-continental Beta Beams

With a high energy accelerator and the high Q-value ions ^{8}B and ^{8}Li, it is possible to source a useful neutrino flux for inter-continental baselines. The oscillatory structure of these baselines is found at energies unattainable with ^{18}Na and ^{6}He. In general, at very long baselines both CP-violation and hierarchy effects are large. The best choice in this context is the magic baseline where all CP-violation effects vanish from the appearance probability. If the magic baseline is chosen, another (shorter) baseline needs to be considered if the facility is to have any sensitivity to CP-violation. This is the approach adopted by the current International Design Study for a Neutrino Factory [67] proposal.

The interest in using the magic baseline for a Beta Beam centres around the proposed large magnetised iron calorimeter known as the India-based Neutrino Observatory (INO). Its expected location at Pushep is 7152 km distant from CERN - very close to the magic baseline. A number of studies have examined the physics of a 'magical Beta Beam' as a single baseline [79, 80] or in combination with a shorter baseline [84]. Typically boosts of $\gamma = 350 - 650$ are chosen. To achieve good physics reach from these setups one needs to compensate for the loss of events owing to the $1/L^2$ dependence of the flux. There are serious feasibility concerns over such a facility which will be discussed further in Sec. 3.7. In Fig. 3.5, the θ_{13},
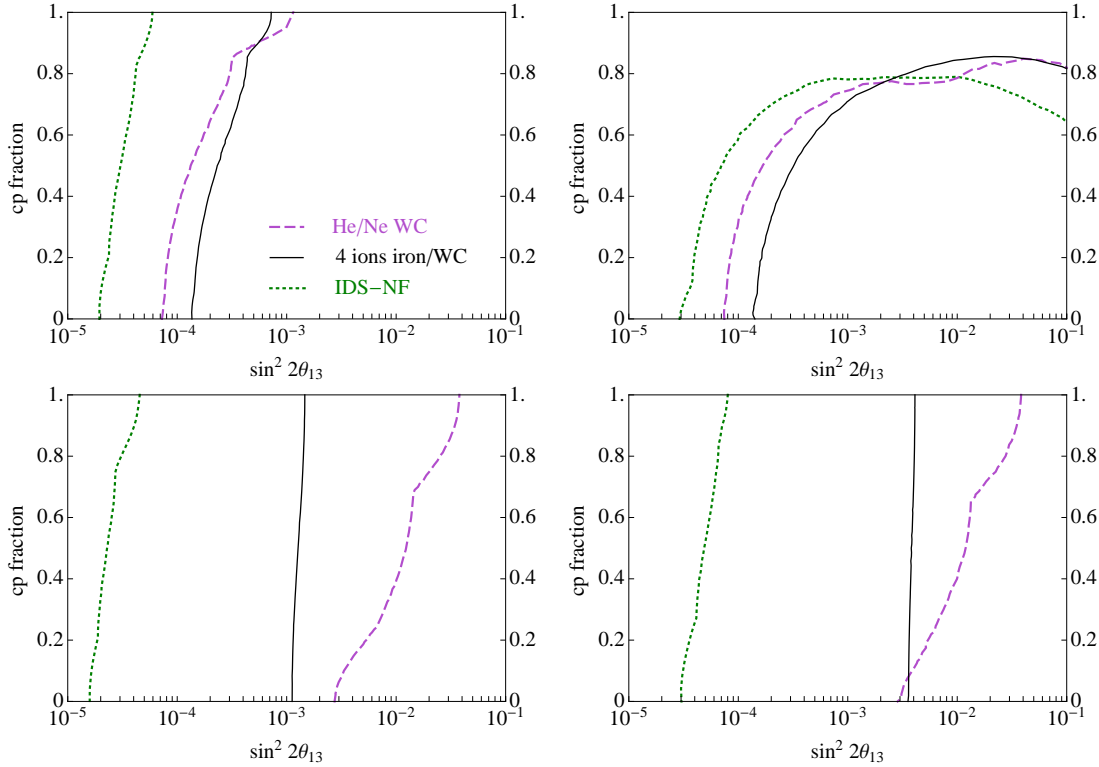
Figure 3.5.: Physics reach of magic baselines Beta Beams [84] compared to the ISS Neutrino Factory [56]. The top-left panel shows the θ_{13} discovery reach; and top-right the CP-violation reach. The bottom panels show the ability to rule out the wrong hierarchy assuming normal to be true (left) and inverted to be true (right). Note all plots show 3σ with 1 degree of freedom. (In this thesis, 2 degrees of freedom are used at 99 % confidence level.) The green doted line is the IDS-Neutrino Factory; the purple a Beta Beam setup only using ^{18}Ne and ^{8}He and a Water Čerenkov at 730 km; and the solid black line shows the combination of a Water Cerenkov at 650 km with a magic baseline high-gamma Beta Beam. Figures reproduced from [84].

CP-violation and mass hierarchy reaches are shown for the latest magical Beta Beam proposal and compared to the equivalent analyses for the a high-γ Beta Beam in Europe and the IDS Neutrino Factory proposal. It shows improvement over a single baseline high boost European Beta Beam, but is not competitive, in general, with the high energy Neutrino Factory.

3.3. The Beta Beam complex

In this and the following sections, a description of a Beta Beam facility will be given. Three distinct phases in a Beta Beam complex can be identified:

1. Radioactive ion production,
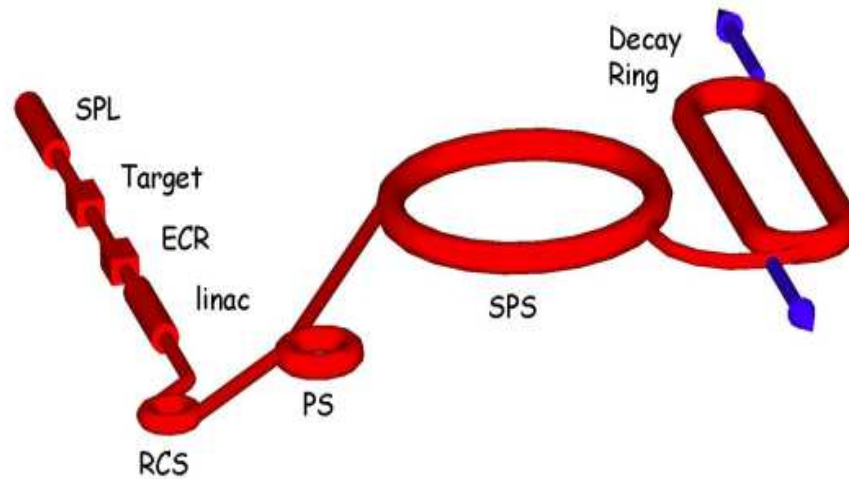
Figure 3.6.: The EURISOL Beta Beam based at CERN. The Beta Beam would use the proposed EU-RISOL facility and existing acceleration infrastructure to produce then accelerate radioactive ions. The construction of a storage ring is necessary to accumulate the ions and to direct the neutrinos towards a distant detector. Figure reproduced from [144].

2. An acceleration chain,

3. A storage ring.

The schematic of a EURISOL Beta Beam complex at CERN is shown in Fig. 3.6. The production of radioactive ions is a well established field - the production mechanism of ~ 3000 different ion species is both known and actively exploited for nuclear physics studies. In particular, the ISOLDE group at CERN are world leaders in both the production and subsequent acceleration of ions to energies $\sim$ MeV. It was suggested in [16] that the ISOL (Isotope Separation On-Line) technique is "the most suitable for high intensity ^{6}He production". The CERN heavy ion programme routinely accelerates ions to ~ 150 GeV/nucleon; however, the ion intensities are much lower. Preliminary studies of the Beta Beam indicated that $\sim 10^{18} - 10^{19}$ useful ion decays per year would be necessary for a physics programme competitive with Superbeams and Neutrino Factories [81, 86]. To source this quantity of neutrinos would require a significant upgrade in the ion production rates and significant R&D on upgrading PS and SPS which, at present, cannot deal with the large intensities of ions [145, 146]. The major in-

frastructure addition required at CERN would be the construction of a storage ring. Typically, storage rings would either be a 'racetrack' or triangular in design; the straight sections direct the neutrinos towards the detector. The neutrinos that decay in the bends or in a straight section not aligned to a baseline would be lost. The design of the storage ring will be discussed in 3.6.

An initial study was carried out [146] soon after the Zucchelli proposal which considered ions given a relativistic boost of $\gamma \sim 100$ using the accelerators currently available; in particular, the SPS with its current configuration and magnetic rigidity. This will be made more explicit in the Sec 3.5. The study examined in detail for the first time the broad requirements on the production and acceleration chain. A long list of potential ions for both ν_e and $\bar{\nu}_e$ emittence were identified with ^{6}He and ^{18}Ne identified as the best candidate ions.

Since the front-end of the Beta Beam had many synergies with a potential upgrade to the CERN nuclear production facilities, it was decided to incorporate a design study for a Beta Beam based at CERN within the EURISOL design study, the project name for the R&D on a future radioactive beam facility based on the ISOL production technique. The EURISOL design study finished at the end of 2008 with a conceptual report for a Beta Beam facility expected in the near future. Almost all R&D on a Beta Beam facility to date was carried out within EURISOL, and hence ion production R&D has been centred on ISOL techniques. This R&D is continuing as Working Package 4 (WP4) of EUROv, "A High Intensity Neutrino Oscillation Facility in Europe", which is a European Commission FP7 design study incorporating R&D on superbeams (WP2) and neutrinos factory (WP3) technologies, neutrino detectors (WP5), and the physics reach of the facilities (WP6).

The present status of the R&D of a Beta Beam facility will be summarised in the next three sections. In Sec. 3.4, the ISOL technique of radioactive ion production will be introduced. This will be accompanied by a description of two alternative possibilities. In Sec. 3.5, an overview of the CERN acceleration infrastructure (and its upgrades) relevant to a Beta Beam facility will be given. The storage ring and the useful number of ion decays will be finally discussed in Secs. 3.6 and 3.7.

3.4. Ion production

The initial feasibility study for Beta Beam [146] outlined several characteristics of potential source ions. There is a narrow range of half-lives if one is to successfully exploit the accel-

eration chain in addition to sourcing a sufficient number of neutrinos for phenomenologically competitive facility. It is important that the ions do not have too short a half-life otherwise the losses in the acceleration chain will be too great (the cycle time of the CERN accelerator complex is around 8 seconds). On the other hand, too long a half-life, although it minimise losses during acceleration, severely restricts the neutrino rate production rate in the storage ring. Half-lives of about 1 second are optimal [145, 146]. Ions are expected to be fully stripped of their electrons. Space charge restrictions (discussed in more detail in Sec. 5.1.1), especially at the required intensities, point to low-Z ions if very large numbers are to be accelerated and stored at any one time. Based on these criteria, ^{6}He is the best candidate ion for $\bar{\nu}_e$ production. For ν_e emission, ^{8}B appears to be the ideal candidate [146], however, this nuclide cannot be produced in large quantities with ISOL techniques. Boron is a very reactive element, especially with the carbon, nitrogen, oxygen and metallic components of the production setup. The optimal ion identified for ν_e production was ^{18}Ne; an inert gas (as is ^{6}He) that can diffuse out of the target areas with little loss. Most R&D on ion production, up to the present, has focused on these two ions with the target rates

- $2.9 \cdot 10^{18}$ $\bar{\nu}_e$ yr^{-1} sourced from ^{6}He

- $1.1 \cdot 10^{18}$ ν_e yr^{-1} sourced from ^{18}Ne

from each straight section of the storage ring. Since the proposed ions are close to the line of stability, there is a possibility that production of large numbers of ions through direct reactions may be possible; for example, bombardment of ^{3}He onto a ^{16}O based target has ^{18}Ne in the final state. Independent of the EURISOL design study, a proposal was put forward by Rubbia *et al.* [142] for the production of large quantities of ^{8}B and ^{8}Li. The idea is to use a 'production ring' that can recirculate and re-accelerate ions that otherwise would be lost in a beam dump. This design also circumvents the reactivity problems associated with ^{8}B in ISOL target regions. In addition, there is also a proposal to produce ^{6}He and ^{8}Li in a two-step process involving fast secondary neutrons on ^{9}Be and ^{11}B targets. These three approaches shall now be summarised in turn.

3.4.1. ISOL

Production of ^{6}He and ^{18}Ne at the future EURISOL facility has been the focus of the R&D on ion production. The centrepiece of the EURISOL design study is a new 2.2 GeV Super Proton Linac (SPL). Although such an intense source of high energy protons is not a requirement for a Beta Beam facility, a proton source is required to start the nuclear reactions in ISOLDE. At

present, ISOLDE is integrated into the current CERN infrastructure; it is fed 1 GeV protons from the Proton Synchrotron Booster (PSB). ISOL techniques make use of thick targets in this high energy beam. The different isotopes are then produced via spallation, fragmentation or fission reactions in or around this thick target. The daughter particles are then magnetically separated so as to select beams with a given mass range and direct them towards the experimental halls.

To produce ^{6}He with ISOL techniques, [146] states that "it is preferable to use a direct reaction with high cross-section and little power dissipation of the primary beam". Examples would be

$$^6\text{Li}\,(n,p)\,^6\text{He} \qquad E_n > 2.7 \text{ MeV}, \qquad \text{and}$$
$$^9\text{Be}\,(n,\alpha)\,^6\text{He} \qquad E_n > 0.6 \text{ MeV}.$$
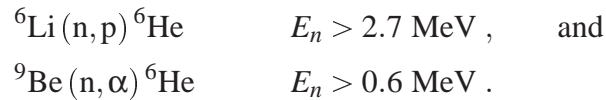
The second reaction is preferred as an ISOL target since ^{9}Be is chemically and physically stable at the high temperatures. Specifically, when bound as BeO, the stresses and thermal shocks can be withstood. Fast neutrons are produced by high-energy proton induced spallation on heavy metal targets such as lead or water-cooled tungsten. This target is situated close to the actual target, or even inside a hollow of the target as depicted in Fig. 3.7. As of summer 2008, $> 1 \cdot 10^{13}$ ^{6}He ions per second could be produced this way. A further factor of 2 is needed to reach the target rate [148].

Production of ^{18}Ne does not need the fast neutrons; instead, it can be produced through spallation on target compounds of Na, Mg, Al and Si. The expulsion of the neutrons from the reaction leaves a final state of the desired nuclide. Target candidates include MgO, MgS, Al_2O_3, Al_4C_3 and SiC [146]. MgO appears to be favoured.

3.4.2. Direct production

Candidate ions for the Beta Beam are low-Z nuclides and are therefore close to the line of stability on a Segre chart. Such nuclides are desirable as they are easier to produce - the parent nuclides have similar numbers of neutrons and protons. This is in contrast to nuclides that are far from the stability line. These are much harder to produce because of the proton number - neutron number mismatch. In fact $\bar{\nu}_e$ candidate ions can normally be produced in larger quantities than ν_e candidate ions as production methods favour neutron rich nuclides. Production methods that do not use neutron or proton type reactions are referred to as 'direct production' methods. For many ions close to the line of stability, such approaches are possible.
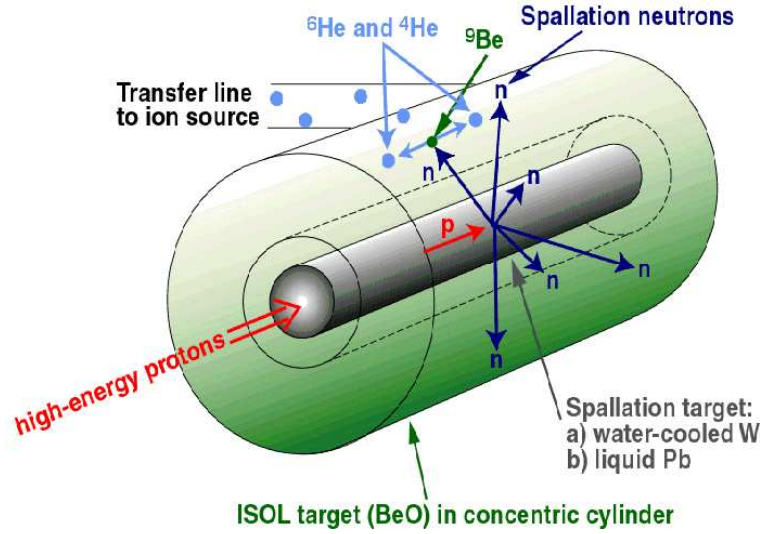
Figure 3.7.: ^{6}He production using ISOL techniques. A high energy proton beam is incident on a spallation target surrounded by a BeO cylinder. The neutrons produced participate in the ^{9}Be (n,α) ^{6}He to form the ^{6}He. Figure reproduced from [147].

For example, the reaction

$$^{16}\text{O} \left(^3\text{He},n\right) {}^{18}\text{Ne} \tag{3.12}$$

is a possible route to ^{18}Ne. The disadvantage of direct production methods is that the target usually also serves as the beam dump. In the above example, the ^{3}He ions that do not go on to source ^{18}Ne are lost and the high intensities required for a Beta Beam facility will possibly destroy the target. Non-ISOL techniques to produce $\bar{\nu}_e$ candidates typically use a direct reaction activated by fast neutrons. Specifically, a second scheme [149] proposes to use fast secondary neutrons from a 40 MeV deuteron beam which are directed onto a 'converter target'. A very high yield of ^{6}He and ^{8}Li can be produced this way. The design is a two-target system. The first target converts the deuterons into fast neutrons. Li, Be, C and D$_2$O compounds have been identified as possible candidates. The second target, to be made from BeO or BN materials, is placed within the forward fast neutron flux. Production then proceeds via the

$$^9\text{Be} \left(n,\alpha\right) {}^6\text{He} \qquad \text{and} \qquad {}^{11}\text{B} \left(n,\alpha\right) {}^8\text{Li} \tag{3.13}$$

reactions. A sketch of the design is shown in Fig. 3.8. Initial investigations pointed to a production, for an optimised geometry for BeO and BN, of

- $1 \cdot 10^{13}$ $\bar{\nu}_e \,\text{s}^{-1}$ sourced from ^{6}He ,
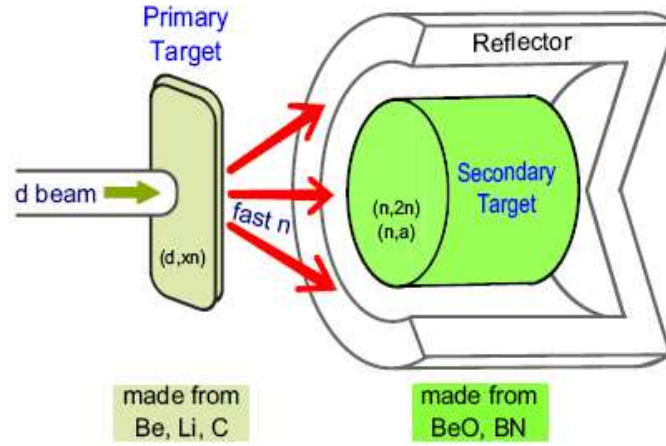
Figure 3.8.: Sketch of the two target method. A deuteron beam is incident on a primary target which
sources fast neutrons. Beryllium and Boron compounds are then placed in the forward
neutron flux. The sought ions are produced via the reactions in the text. Figure reproduced
from [149].

- $2 \cdot 10^{12} \; \bar{\nu}_e \, \text{s}^{-1}$ sourced from ^8Li .

The authors of [149] feel that these numbers can in principle be increased by an order of
magnitude for anti-neutrino production if the ions are to be sourced for a Beta Beam.

3.4.3. Production ring

As previously mentioned, in direct production facilities, the beam that does not source a new
ion through a nuclear reaction is often lost in a beam dump. This severely limits production
rate as large portions of the primary particles are wasted. In a production ring, the idea is to
re-circulate and re-accelerate the primary particles before sending them to the target again. In
the context of Beta Beam facilities, this was initially suggested in [142] and it was proposed
to use the reactions

$$^7\text{Li} \, (d, p) \, ^8\text{Li} \qquad \text{and} \qquad ^6\text{Li} \, (\text{He}, n) \, ^8\text{B} \tag{3.14}$$
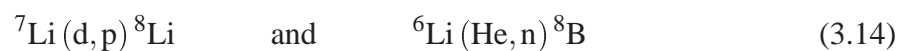
to produce

- $1 \cdot 10^{14} \; ^8\text{Li} \, \text{s}^{-1}$,
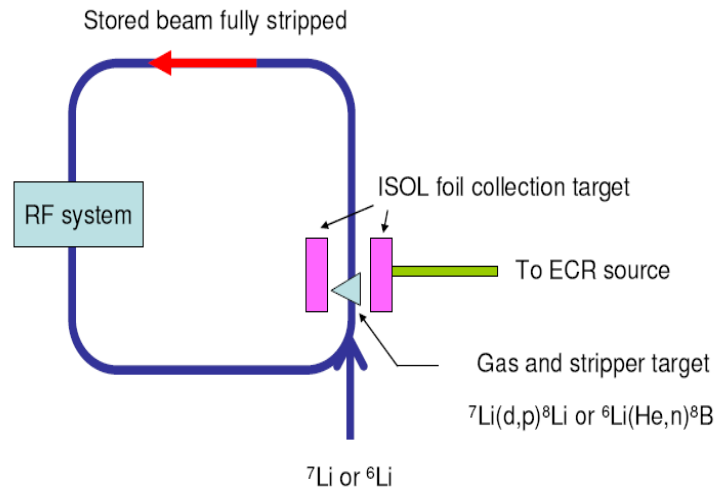
Figure 3.9.: Illustration of the production ring method. ^{7}Li and ^{6}Li are fired towards a target as in direct production with the sought nuclides collected and sent to an ionisation source. Lithium nuclei that do not source source ^{8}Li and ^{8}B nuclei are re-circulated and re-accelerated before being sent to the target area once more. Figure reproduced from [148].

- $2 \cdot 10^{12}\ ^8$B s^{-1} .

A schematic of the initial design is shown in Fig. 3.9. The re-circulation of the beam greatly increases the nuclear reaction probability for a given parent particle. To exploit this technique, heavy ions incident on a gas-jet target are preferred [142]. Initial estimates suggest the above rates could be achieved with a small 'table-top' ring rather than a large device in an experimental hall. The daughter particles are typically neutral and therefore need to pass through an ion source before injected into the accelerator chain.

3.5. Acceleration

Once the ions have been produced, there are several stages of the CERN accelerator complex to transverse before the SPS is used to boost the ions to the required γ. The production techniques do not actually produce ions. The nuclides will still have their full (or almost full) compliment of electrons on exiting from the production area. Ionisation is necessary since neutral atoms cannot be accelerated. The preferred technique is too use a Electron Cyclotron Resonance (ECR) ion source. A moving charge will gyrate with some frequency, ω say, around magnetic field lines in a cavity - this is simply the $\mathbf{v} \times \mathbf{B}$ form of the Lorentz force. When microwaves are propagated through such a cavity, the electrons can be made to

resonate. When neutral atoms are passed through these hot plasma regions, they can ionised into a high charge state. For the low-Z candidate nuclides of the Beta Beam, this amounts to full ionisation. There are substantial losses of ^{18}Ne atoms at this stage (efficiency 29 %); ^{6}He fairs much better (efficiency 93 %).

There are two further stages before the ions are injected into the Proton Synchrotron (PS) and then the Super Proton Synchrotron (SPS). First a linac is used to boost the ions to $\gamma = 1.1$ before being passed to the Rapid Cycling Synchrotron (RCS). Here the ions will be boosted slightly further to around $\gamma \sim 2 - 3$ depending on the ion; however, about 50 % of the ions will be lost at this stage. The ions reach different boosts at this stage because the machine is circular in design. It will be shown below that, for a given machine, the maximum boost available to a particular ion is a function of the maximum boost possible for a proton, the proton number of the ion and the mass number of the ion. The acceleration time of this stage is short. Therefore, there are no significant ion losses owing to space charge effects (see Chap. 5) even though the boosts are still low. This changes with the injection of the ions into the PS.

On leaving the PS, the ions will have boosts $\gamma \sim 9 - 18$; the reason for the variation the same as for the RCS. However, there will be large losses at this stage if the old PS is to be used [146]. The proposal to replace the PS with a new 50 GeV synchrotron will help greatly in this respect.

The last stage of the acceleration is the SPS. The role of the SPS is to take the ions from the PS and accelerate to the boost required by the experiment. Once this is done, the ions are bunched further before injected into a storage ring with sections pointing towards the far detectors. The maximum boost attainable with a synchrotron is dependent on the ion, the radius of the accelerator and the maximum magnetic field available. The calculation of the maximum boosts available will be summarised below.

The maximum boost obtainable for a given ion is determined by the magnetic rigidity of the synchrotron. For a particle with charge e, mass m, velocity $\mathbf{v}$ and with a circular trajectory in a magnetic field $\mathbf{B}$, (following [150]), the Lorentz force is the centripetal force:

$$m\gamma v^2 \kappa + e(\mathbf{v} \times \mathbf{B}) = \mathbf{0} \ . \tag{3.15}$$

Here, $\kappa = (\kappa_x, \kappa_y, 0)$ is the local curvature vector of the trajectory defined by

$$\kappa_{x,y} = \frac{1}{\rho_{x,y}} \ , \tag{3.16}$$

where $\rho_{x,y}$ is the local bending radius of the trajectory[3]. If we take the magnetic field to be perpendicular to the particle velocity so as to only consider transverse fields, and write $q = \gamma m v$ as the momentum, we obtain:

$$|B\rho| = \frac{q}{e} \, . \tag{3.17}$$

The quantity on the left hand side is known as the *'magnetic rigidity'*. For a given rigidity, it is then straightforward to calculate the maximum boost for a proton:

$$\gamma_p = \frac{1}{m_p} \sqrt{q^2 + m_p^2} \, . \tag{3.18}$$

For an ion with charge Z and mass A, the boost for a given magnetic rigidity is found by appending the equivalent proton boost with the relevant charge to mass ratio, viz:

$$\gamma_{ion} = \frac{Z}{A} \gamma_p \, . \tag{3.19}$$

The maximum boost for the four standard Beta Beam ions with the current Super Proton Synchrotron (SPS) and a possible ungraded version are presented in Table. 3.1. The SPS currently has a magnetic rigidity of 1344 Tm corresponding to a maximum proton energy of 450 GeV. Upgrades to the CERN accelerator complex and in view of possible LHC upgrade scenarios, indicate the possibility of a 3335 Tm machine, capable of pushing protons up to 1 TeV at injection into the LHC ring.

3.6. The storage ring

Finally, it is necessary to inject the ions into a storage ring with straight sections directed towards the far detectors sourcing the neutrino flux. The configuration of the ring is important, not only for technical and engineering reasons, but also since neutrinos that decay in the curved sections or the straight sections pointing away from the far detectors are lost. The principle ring designs are equivalent to those of the Neutrino Factory where two configurations have been proposed

---

[3]Note that this is not the same as the radius of the synchrotron. For example, the Large Hadron Collider (LHC) occupies the old LEP tunnel which is approximately 27 km in circumference and hence has a radius of about 4.2 km. The LHC comprises 1200 bending magnets, each 15 m in length. This corresponds to a bending circumference of only 18 km and a bending trajectory radius of approximately 2.8 km.

1. *The racetrack design*

   This design consists of two long straight section parallel to each with a (as small as possible) curved section connecting them. The useful fraction of neutrinos in the storage is known as the 'livetime', l, defined as the fraction of neutrinos that decay in one straight section:

$$l_r = \frac{L_{\text{str}}}{2L_{\text{str}} + 2\pi R} \,, \tag{3.20}$$

   where L_{str} is the length of a straight section and R is the radius of the curved sections.

2. *The triangle design*

   This is a design initially considered for the high energy Neutrino Factory as it is, in principle, capable of sourcing two baselines simultaneously. Assuming that the design is an equilateral triangle, the livetime is

$$l_t = \frac{L_{\text{str}}}{3L_{\text{str}} + 2\pi R} \,. \tag{3.21}$$

The storage ring design for the 'baseline' Beta Beam using ^{18}Ne and ^{6}Ne is ongoing [152]. The study focuses on a racetrack design with 3100 m straight sections and 5 Tesla magnets for the curved sections. These corresponds to a radius of $R \sim 300$ m. The total circumference of this design is approximately 7000 m with a livetime, $l_r = 0.36$. Clearly, the design of the decay ring, and hence livetime, is dependent on both the boost of the injected ions and the magnetic fields available.

3.7. The number of useful ion decays

The neutrino flux at the detector is dependent upon the following 4 experimental parameters:

- The number of useful ion decays, N_β ;

- The ion boost, γ ;

- The baseline, L ;

- The Q-value of the ion .

Boost	Rigidity [Tm]	Ring Length $T = 5$ Tesla, $l_r = 0.36$	Dipole Field $\rho = 300m$
100	935	4197	3.1
150	1403	6296	4.7
200	1870	8395	6.2
350	3273	14691	10.9
500	4676	20987	15.7

Table 3.2.: Magnetic rigidities and racetrack storage ring lengths for a range of boosts. In the third column the length of the storage ring assuming a 5 Tesla field and a live time of 0.36 is shown. The fourth column shows the size of the dipole field required for the storage ring to be equivalent to the baseline design.

The first three are dependent on each other, although they are often considered as independent. The rate of useful ion decays, R, is given by

$$R = \frac{I_{\text{in}}l}{T_{\text{rep}}} \left(1 - e^{-\frac{mT_{\text{rep}}}{\gamma}} \right) T_{\text{run}} \; ; \tag{3.22}$$

where I_{in} is the ion intensity injected into the decay ring; l is the livetime defined in the previous section, T_{rep} is the repetition period for ion fills in the ring; m is the number of bunch merges possible without significant losses; and T_{run} is the length in seconds of the experimental run. The experimental details are beyond the scope of this thesis; the important point to note here is that to first order

$$R \quad \propto \quad \frac{1}{\gamma} , \tag{3.23}$$

so that, with everything else remaining the same, the rate falls with increasing γ. To assume the same number of useful decays with increasing γ therefore requires the implicit assumption that the the number of injected ions is increased; the circumference of the decay is increased to compensate; the magnetic rigidity of the curved sections is increased so to increase the livetime of the ring; or a combination of the previous suggestions. The changes needed in the magnetic rigidity or the circumference of the ring are made explicit in Tab. 3.2. The magnetic rigidity of the curved sections is shown for a series of boosts with the required circumference of the ring, assuming 5 Tesla fields and $l = 0.36$, and the magnetic fields to maintain the baseline design.

The length of the baseline is important since it determines the tilt of the storage ring with respect to the ground. For the CERN-Frejus baseline, this angle is 0.6^o. For the standard decay ring design (each straight section is 3100 metres), this corresponds to a maximum depth of 32 metres. For the CERN-Canfranc baseline (650 km), the angle increases to 6° giving a maximum depth of 324 metres. A baseline of 7000 km, as used in [84], needs a tilt of 34.5^o a has a maximum depth of 1756 metres. Therefore geological, engineering and cost factors will come into play, especially for the very long baselines. Any limitation on the maximum depth will have to be compensated by a reduction of the length of each straight section of the decay ring which in turn will lower the useful rate, all else remaining unchanged.

All the previous points have to be born in mind when discussing the useful decay rate for a given facility. However, these are not the main limitation on the useful decay rate. Events from atmospheric ν_μ and $\bar{\nu}_\mu$ mimic the oscillation appearance signal. Approximately 30 such events per kton-year will pass all the event selection cuts imposed [86]. For large θ_{13} these do not pose a problem since the appearance event rate is high. At the sensitivity boundary and low θ_{13}, however, these events dominate the signal and destroy the sensitivity. To alleviate this problem, the ions are bunched in the decay ring so as to give a good time correlation between the signal at the detector and at the decay ring. The fraction of the decay ring filled by ions is known as the 'suppression factor' or 'duty factor' defined as

$$S_f = \frac{v\, N_b\, \Delta t_b}{L_r} \; ; \tag{3.24}$$

where v is the ion velocity, N_b is the number of bunches, and Δt_b is the length of the bunch (in time). For Beta Beams at low energies (i.e. low γ ^{18}Ne/^{6}He machines), a suppression $S_f \sim 10^{-3}$ is required [81]. With at least $\sim 10^{18}$ useful decays needed, this is very restrictive indeed and is the main limitation of the physics reach for the Beta Beam at low energy. The atmospheric neutrino flux for $S_f = 2 \cdot 10^{-3}$ is shown in Fig. 3.10 and is normalised to 32 atmospheric events. For bins at high energies, the number of atmospheric events is considerably fewer. For the longer baselines and larger boosts, the suppression factor can therefore be relaxed. This loosening can in full or in part compensate for the $1/\gamma$ dependence on the rate and any restrictions on the maximum depth and the available magnetic rigidity of the curved sections. The easing of the suppression to increase the rate is never considered as a method to improve physics reach for these reasons.

Recently, concerns have been made about the feasibility of having a decay ring with maximum depth ~ 2 km [85]. Rather than attempting to improve the physics reach, it was suggested to alter some of the experimental parameters to maintain the same physics reach so that the
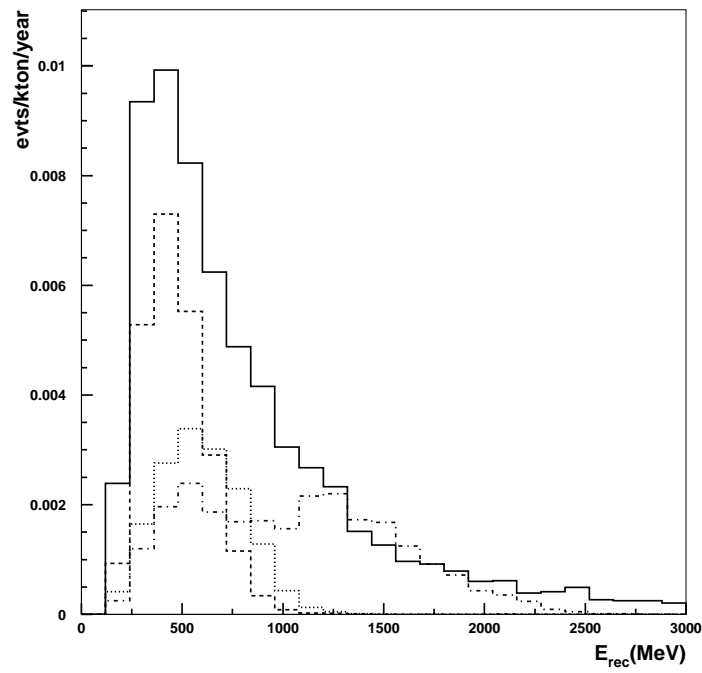
Figure 3.10.: $\nu_\mu + \bar{\nu}_\mu$ atmospheric neutrino events per kiloton-year assuming a duty factor of $2 \cdot 10^{-3}$ (solid lines). The other lines are the event rates for setups considered in [86]. The figure is taken from this reference.

decay ring could be shrunk. The observation made is that a modest increase of the ion boost can return much large increases in the event rate. An increase in the boost can then be used to compensate for a decrease the length of the straight sections of the decay ring. For this strategy to work requires the availability of superconducting magnets up to 15 Tesla.

Chapter 4.

Beta Beams with a neutrino run only

This chapter examines the CP-violation reach of a Beta Beam that uses only a neutrino run. The content of this chapter is based on the work [89] where we used the CERN-Boulby baseline (1050 km), a 10 year run with a high-γ ^{18}Ne beam only, and a generic detector with excellent energy resolution. Whereas all previous Beta Beam studies for short baselines had used conservative energy resolutions and both a neutrino and anti-neutrino run to break degeneracies and boost sensitivities; we pointed out that if the energy resolution of a detector is sufficiently good, so that the energy binning could be narrower, the spectral nature of the appearance probability could be used to break degeneracies and improve the physics reach. Specifically, the behaviour of the probability at (and around) first and and second maximum is sufficiently different that their combination can be used to achieve sensitivity similar to dual-ion Beta Beams.

In this chapter, our motivations for the above scheme will be presented. The simulations presented in this chapter are different from those in [89]. The re-simulation of the setup is for the consistency with the other chapters with regards the assumptions made and the code used.

4.1. The CERN-Boulby case study

This study had both site-practically motivations and technological motivations. At the time, recent studies had indicated that expansion of the Boulby mine, on the north-east coast of England, had excellent potential with relatively modest costs [151]. Specifically, there were plans to dig below the current mine level and laboratory levels into a harder rock stream. Caverns up to 30 m high were suggested as plausible. Such excavations are therefore capable

of hosting massive detectors of several tens of ktons. With multiple caverns, detector masses around 100 ktons could be housed at Boulby.

Secondly, a baseline of 1050 km is longer than most other options considered in the literature, but not significantly more so. This means the matter effect is larger, improving sensitivity to the mass hierarchy, but not sufficiently longer to amplify the degeneracy between the CP-phase δ and the sign of the Δm_{32}^2, catastrophically reducing the CP-violation sensitivity. This increase in baseline length, but not extravagant increase, is sufficient merit to study this baseline.

There is a third motivation not available to the shorter baselines. As the baseline increases, the oscillation probability functional form shifts to higher energies. For small matter effect, this is essentially linear in the baseline. For example, the first oscillation maximum for the CERN-Canfranc (650 km) baseline is ~ 1.3 GeV. The equivalent energy for CERN-Boulby is 2.1 GeV $\approx 1.3 \times 1050/650$. This is important because for a given detector energy threshold, more of the oscillation structure is available to the experiment. Specifically, for the CERN-Boulby baseline and an energy threshold of 400 MeV, appearance events from both first and second oscillation maximum are available. In addition, the oscillatory structure spreads out so that with a given energy resolution and binning, better resolution of the oscillatory structure is possible. The combination of these two effects suggested the possibility of using the oscillatory structure alone (sometimes referred to 'using multiple L/E s') to resolve the degeneracies and achieve a good physics reach.

The motivation for this study is complete with an observation about the potential number of useful ion decays. As mentioned in the previous chapter, the EURISOL target numbers for the useful number of ion decays per year along a straight section of the baseline storage ring are $1.1 \cdot 10^{18}$ ^{18}Ne decays and $2.9 \cdot 10^{18}$ ^{6}He decays. As of summer 2008 (with no update in 2009), the number of ^{18}Ne decays was a factor of 20 short, with ^{6}He still a factor of 2 short. R&D is on-going for the other ion production mechanisms. The numbers available are within the baseline design study but, these will vary with choice of boost and storage ring configuration. In short, the useful number of ion decays for each species are not known with any certainty. A possibility to consider would be that the useful number of neutrinos could greatly outnumber the number of anti-neutrinos, or vice versa. In which case, a facility with a neutrino (or anti-neutrino) run only would need to be considered. Such a facility would have to use the oscillatory structure of the appearance probability as outlined in the previous paragraph to achieve competitive physics reach. The simulations we carried out in [89] are the only studies to consider this possibility.

In [89], a flux of electron neutrinos sourced from the decay of ^{18}Ne ions accelerated to a boost $\gamma = 450$ was considered. The choice of ion is not important here; the same results would be obtained with ^{8}B ions as the source at the lower boost $\gamma = 115$ provided 16 times as may useful decays could be achieved. Sourcing neutrinos with ^{18}Ne ions at $\gamma = 450$ assumes that a 1 TeV SPS will be realised in the future; ^{8}B ions would not need such an upgrade. The choice of neutrino or anti-neutrino run is also not important. In fact, it was noted earlier that the production of anti-neutrino emitters is generally easier as an excess of neutrons is required. With anti-neutrinos, though, the cross-sections are approximately a factor of 3 lower than for neutrino events. It is therefore quite possible that any excess number of anti-neutrinos would be used up compensating for this. The neutrino and anti-neutrino appearance vacuum probabilities differ only through the change $\delta \rightarrow -\delta$. This makes no change to the results in this chapter. For the CERN-Boulby baseline, however, the matter effect is sufficiently strong to induce a measurable splitting of the two probabilities. This effect is roughly mimicked by a change in the sign of Δm_{32}^2 so, overall, the CP-violation sensitivity analysis will return similar results up to a reflection . The motivation above has focused on the three different aspects: location, phenomenological and technological. In the following section, the probability expansion will be used to take a closer phenomenological look at the benefits of the single helicity strategy. In particular, for idealised assumptions, the combination of first and second oscillation maximum will be examined in the context of its degeneracy breaking ability. The following analysis is also relevant for electron capture beams and hybrid facilities to be discussed in the following chapters. Indeed, the following analysis is essentially approximating a neutrino flux to two mono-energetic beams, one at first maximum and the other at second.

4.2. Resolving degeneracies with a neutrino run only

A detailed analysis of the neutrino run only approach requires a full numerical simulation taking into account the energy dependence of the incident flux, ν_μ-appearance probability, cross-sections and efficiencies (see Chap. 2). Never-the-less, it is possible to understand some of the general trends through semi-analytical calculations for a simplified case. Using the oscillation probability expansion (Eq. 2.34), it is possible to get a measure on how this strategy will resolve (or not) the degeneracies.

Recall that the number of neutrino events in a bin i for the pair $(\bar{\theta}_{13}, \bar{\delta})$ is given by

$$N_i(\bar{\theta}_{13}, \bar{\delta}) = \mathcal{N}_T \, t \int_{E_i}^{E_i + \Delta E_i} \varepsilon(E_\nu) \, \sigma_{\nu_\mu}(E_\nu) \, P_{e\mu}(E_\nu, \bar{\theta}_{13}, \bar{\delta}) \, \Phi_{\nu_e}(E_\nu) \, dE_\nu \, , \qquad (4.1)$$

where $\mathcal{N}_T$ is the detector mass, t is the run time of the experiment in years and ε is the detector efficiency. The cross-section, appearance probability and the un-oscillated flux complete the integrand. The potential benefits of this approach can then be established by considering the combination of event information from first and second oscillation maximum. Consider the idealised case of infinite energy resolution so that the integral in Eq. (4.1) reduces to a product. The number of events at the neutrino energy of the first oscillation maximum, E_1, is to be compared to the number at the second oscillation maximum, E_2. Introducing proportionality constants (the product of the number of targets, time of data taking, efficiency, the neutrino flux and cross section) c_1 and c_2 for each energy, in this approximation $N_1(E_1) = c_1 P_{e\mu}^+(E_1)$ and $N_2(E_2) = c_2 P_{e\mu}^+(E_2)$.

As a first case, the location of the energy degeneracy is sought. For the true pair $(\bar{\theta}_{13}, \bar{\delta})$, the clone solution (θ_{13}, δ) is located by solving [110]

$$N_1(\bar{\theta}_{13}, \bar{\delta}, \text{sign}(\Delta m_{31}^2), \bar{\theta}_{23}) = N_1(\theta_{13}, \delta, \text{sign}(\Delta m_{31}^2), \bar{\theta}_{23}) , \qquad (4.2)$$

$$N_2(\bar{\theta}_{13}, \bar{\delta}, \text{sign}(\Delta m_{31}^2), \bar{\theta}_{23}) = N_2(\theta_{13}, \delta, \text{sign}(\Delta m_{31}^2), \bar{\theta}_{23}) . \qquad (4.3)$$

It is straightforward to show that only one solution is allowed for θ_{13} for a measured number of events N_1 and N_2. To see this, write the appearance probability at oscillation maximum m in the following form

$$P^m = I_1^m \sin^2 2\theta_{13} + I_3^m \cos\theta_{13} \sin 2\theta_{13} \sin\delta + I_4^m , \qquad (4.4)$$

so as to concentrate on the θ_{13} and δ dependency at a given energy and baseline. The I_i^m incorporate the non-essential constants in the probability expansion in this respect. Note that since we are considering the appearance probability at oscillation maxima, the $\cos\delta$ contribution to the interference term is absent and so there is no need for a I_2^m. In this notation, the first equation in Eq. 4.2 becomes

$$I_3^1 \sin\delta = \frac{\bar{I}_1^1 \sin^2 2\bar{\theta}_{13} - I_1^1 \sin^2 2\theta_{13}}{\cos\theta_{13}\sin 2\theta_{13}} + \bar{I}_3^1 \frac{\sin\bar{\delta}\cos\bar{\theta}_{13}\sin 2\bar{\theta}_{13}}{\cos\theta_{13}\sin 2\theta_{13}} + \frac{\bar{I}_4^1 - I_4^1}{\cos\theta_{13}\sin 2\theta_{13}} . \qquad (4.5)$$

Here, the $\bar{I}_i^m$ correspond to the true values. However, it is clear that $\bar{I}_i^m = I_i^m$, at a given baseline, energy and mass hierarchy, so the above expression can, for functions f and g, be neatened to

$$I_3^1 \sin\delta = I_1^1 f(\theta_{13}, \bar{\theta}_{13}) + I_3^1 \sin\bar{\delta} g(\theta_{13}, \bar{\theta}_{13}) ; \qquad (4.6)$$

and equivalently for the second oscillation maximum:

$$I_3^2 \sin\delta = I_1^2 f(\theta_{13}, \bar{\theta}_{13}) + I_3^2 \sin\bar{\delta} g(\theta_{13}, \bar{\theta}_{13}) . \tag{4.7}$$

f and g are just replacements:

$$f(\theta_{13}, \bar{\theta}_{13}) = \frac{\sin^2 2\bar{\theta}_{13} - \sin^2 2\theta_{13}}{\cos\theta_{13} \sin 2\theta_{13}} \quad \text{and} \quad g(\theta_{13}, \bar{\theta}_{13}) = \frac{\cos\bar{\theta}_{13} \sin 2\bar{\theta}_{13}}{\cos\theta_{13} \sin 2\theta_{13}} . \tag{4.8}$$

Solving for $\sin\delta$ leads to

$$\left(\frac{I_1^1}{I_3^1} - \frac{I_1^2}{I_3^2} \right) f = 0 . \tag{4.9}$$

For this to be true in general, $f = 0$ and hence

$$\sin^2 2\theta_{13} = \sin^2 2\bar{\theta}_{13} . \tag{4.10}$$

The combination of data from first and second oscillation maximum partially resolves the degeneracy. Although there is no longer a θ_{13} degeneracy, the energy degeneracy is still present since Eq. 4.5 is invariant under the transformation $\delta \to \pi - \delta$. The combination of the data from additional energy pairings is sufficient to break the energy degeneracy completely and is discussed in more detail in Appendix C. This analysis does not guarantee good CP-violation reach, however, since for a given pair $(\bar{\theta}_{13}, \bar{\delta})$ the sensitivity region at a given confidence level may still cross the $\delta = 0^o$ and/or $\delta = 180^o$ lines. In this case, CP-violation cannot be established. When the calculation is repeated for a neutrino and anti-neutrino beam configuration, the intrinsic degeneracy is found to be resolveable.

Moving to the hierarchy degeneracy, the clone solution satisfies [108]

$$N_1(\bar{\theta}_{13}, \bar{\delta}, \mathrm{sign}(\Delta m_{31}^2), \bar{\theta}_{23}) = N_1(\theta_{13}, \delta, -\mathrm{sign}(\Delta m_{31}^2), \bar{\theta}_{23}) , \tag{4.11}$$

$$N_2(\bar{\theta}_{13}, \bar{\delta}, \mathrm{sign}(\Delta m_{31}^2), \bar{\theta}_{23}) = N_2(\theta_{13}, \delta, -\mathrm{sign}(\Delta m_{31}^2), \bar{\theta}_{23}) . \tag{4.12}$$

Since we are comparing the event rates from different assumptions on the mass hierarchy, we have

$$I_1^m \neq \bar{I}_1^m , \quad I_3^m \neq \bar{I}_3^m \quad \text{and} \quad I_4^m = \bar{I}_4^m . \tag{4.13}$$

Repeating the calculation as for the energy degeneracy, one finds that the I_3^m and $\bar{I}_3^m$ dependency vanishes leaving

$$\sin^2 2\bar{\theta}_{13} = \frac{I_1^1}{\bar{I}_1^1} \sin^2 2\theta_{13} \,. \tag{4.14}$$

The θ_{13}-degeneracy is not fully resolved in this analysis; a fake solution is found to exist (replacing the shorthand) at

$$\sin^2 2\theta_{13} \quad \simeq \quad \sin^2 2\bar{\theta}_{13} \left(1 + 4\frac{A}{\Delta_{31}} \right) \,, \tag{4.15}$$

$$\sin\delta \quad \simeq \quad \sin\bar{\delta} \,, \tag{4.16}$$

where terms up to first order in A/Δ_{31} have been kept. The hierarchy degeneracy is therefore expected to affect the determination of $\bar{\theta}_{13}$ at a mild level and negligibly that of $\bar{\delta}$. Again, this result matches expectations; the event rate for the inverted hierarchy will be less than for the normal case for a given $\bar{\theta}_{13}$ and $\bar{\delta}$ (or vice versa). Consequently, the event rate can be recovered with larger $\sin^2 2\theta_{13}$ (or smaller depending on the true $\text{sign}(\Delta m_{23}^2)$). Note that in this analysis, we have solved for $\sin\delta$. One could equally well match the event rate with a small change in δ or, in general, both $\sin^2 2\theta_{13}$ and δ. Indeed, in a full numerical simulation, the location of the degenerate solution generally includes a change in both coordinates. For the short and intermediate baselines for which the probability expansion is valid, the matter effect is weak at second oscillation maximum with only a small or moderate effect at first maximum. It is therefore expected that the combination of events from first and second oscillation maximum is insufficient to determine the type of neutrino mass ordering. However, when one includes information on the neutrino oscillation probability at other energies this degeneracy could be broken for competitive ranges of θ_{13}. In particular, matter effects increase with energy and the high energy bins will turn out to be important in breaking the sign degeneracy. (This feature was discussed in [89].)

Finally, although not the focus of the thesis, this procedure can be repeated for the octant degeneracy, with any clone solution will satisfying [107]

$$N_1(\bar{\theta}_{13}, \bar{\delta}, \text{sign}(\Delta m_{31}^2), \bar{\theta}_{23}) \quad = \quad N_1(\theta_{13}, \delta, \text{sign}(\Delta m_{31}^2), \pi/2 - \bar{\theta}_{23}) \,, \tag{4.17}$$

$$N_2(\bar{\theta}_{13}, \bar{\delta}, \text{sign}(\Delta m_{31}^2), \bar{\theta}_{23}) \quad = \quad N_2(\theta_{13}, \delta, \text{sign}(\Delta m_{31}^2), \pi/2 - \bar{\theta}_{23}) \,. \tag{4.18}$$

A clone solution exists and is non-trival:

$$\sin^2 2\theta_{13} \simeq \tan^2 \bar{\theta}_{23} \sin^2 2\bar{\theta}_{13} + (1 - \tan^2 \bar{\theta}_{23}) \sin^2 2\bar{\theta}_{12} \left(\frac{\Delta_{21}}{\Delta_{31}}\right)^2 \frac{\pi^2}{4}, \qquad (4.19)$$

$$\sin \delta \simeq \frac{\sin \bar{\delta}}{\tan \bar{\theta}_{23}} \left(1 + \frac{\pi^2}{8} \left(1 - \frac{1}{\tan^2 \bar{\theta}_{23}}\right) \frac{\sin^2 2\bar{\theta}_{12}}{\sin^2 2\bar{\theta}_{13}} \left(\frac{\Delta_{21}}{\Delta_{31}}\right)^2\right). \qquad (4.20)$$

These expressions are valid in the whole allowed range of the oscillation parameters for $\sin^2 2\bar{\theta}_{13} < 10^{-3}$ and only terms up to $O(\Delta_{21}/\Delta_{31})^2$ have been retained. As has already been discussed, an asymmetry between the two possible θ_{23} octants is not present in the atmospheric and interference contributions to the probability. In order to resolve the octant degeneracy requires either small θ_{13}, so that these two contributions are suppressed, or substantial event rates at low energies. For the European baselines, with the exception of CERN-Phyhasalmi, the appropriate energy range is below the detector threshold. European baselines are therefore expected only to provide information on the θ_{23}-octant for small values of θ_{13}.

The results of this idealised analysis suggest that a neutrino run alone is sufficient to resolve degeneracies and, provided the event rates are high enough, to obtain a good physics reach for the unknown oscillation parameters. A more detailed analysis was carried out taking into account finite energy resolution, statistical and systematic errors, backgrounds, the energy dependence of the integrand in Eq. 4.1 and multiple bins. Presented shortly, that analysis confirmed the general trends suggested by the semi-analytical calculations. It is necessary, however, to attach an additional caveat to the above analysis. Above it was determined whether or not the number of events for the true pair $(\bar{\theta}_{13}, \bar{\delta})$ could be matched by the event vector of a fake pair (θ_{13}, δ). If not, it was 'claimed' that any degeneracy was resolved. In reality, one resolves degeneracy at a given confidence level and so some degenerate regions can remain. In particular, since we work with χ^2-functions, as opposed to rates directly, the degeneracies may still persist owing to the smaller χ^2 at the low energies, even if a probability analysis like above separates them.

4.3. Strategy and simulations

The analysis presented here is a re-simulation of the setup presented in [89]. As mentioned previously, this is primarily for consistency with the assumptions of the later chapters. Specifically, the analysis presented here sets $\theta_{23}^{tr} = 45^o$ so there is no octant degeneracy. The simulations are carried out using the GLoBES long baseline neutrino oscillation public code.
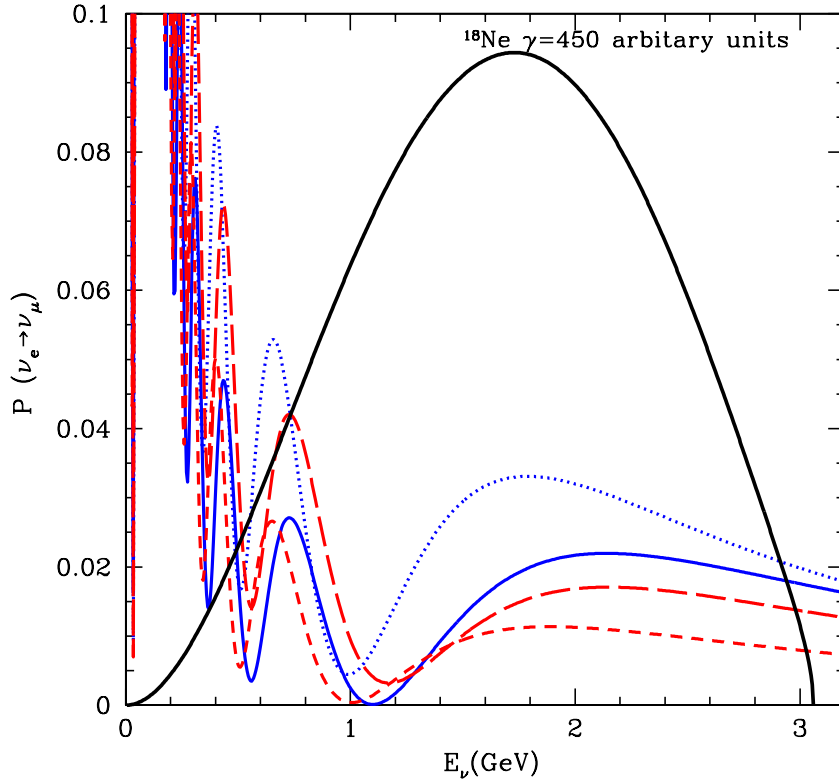
Figure 4.1.: Transition probability of ν_e into ν_μ as a function of the neutrino energy for normal hierar-
chy and $\delta = 0°$ (blue solid line), normal hierarchy and $\delta = 90°$ (blue dotted line), inverted
hierarchy and $\delta = 0°$ (red short dashed line) and inverted hierarchy and $\delta = 90°$ (red long
dashed line). Also shown in arbitrary units the unoscillated beta-beam neutrino spectrum
from ^{18}Ne decays and $\gamma = 450$. Figure taken from [89].

First, the common features of the two studies will be motivated and presented. In Fig. 4.1,
$\nu_e \rightarrow \nu_\mu$ appearance probabilities are shown for the CERN-Boulby baseline (1050 km) for the
cases $\delta = 0^o$ and $\delta = 90^o$; and for the normal mass ordering (blue lines) and inverted mass
ordering (red lines). Superimposed on this is the $\gamma = 450$ un-oscillated neutrino flux from the
decays of ^{18}Ne. The units of the flux are arbitrary.

The maximum neutrino energy in the laboratory frame is 3.06 GeV with an average neu-
trino energy $\langle E_\nu \rangle \simeq \gamma E_0 \sim 1.5$ GeV. The second oscillation maximum is around 600-700 MeV
for this baseline depending on the true values of the oscillation parameters. First maximum
is around 2 GeV. With the choice $\gamma = 450$, first oscillation maximum is not aligned with the
peak of the neutrino flux. Although larger boosts return larger numbers of events at the high
energies they also suffer from more beam and misidentification backgrounds. Also, the form

of the probability at first oscillation maximum and in the tail is dominated by the atmospheric contributions and so events at higher energies do not provide any additional information on the interference contributions of the appearance probability. The choice of $\gamma = 450$ is not rigorous but, all the above considered, it is a good compromise between large event rates and reduced backgrounds.

From Fig. 4.1, it is seen that with a detector energy threshold of 400 MeV both the first and second oscillation maximum can be studied. As mentioned above, there is little need to carefully reconstruct the probability for energies beyond first oscillation maximum; a single bin to the maximum neutrino energy will suffice. A generic detector was assumed in the first study and the un-oscillated event rate was phrased as an exposure. This allowed for the study of the effect of different ion intensities, detector studies and run times.

After the above considerations, in both studies, the following Beta Beam configuration was used

- CERN-Boulby baseline ($L = 1050$ km)

- ^{18}Ne ions boosted to $\gamma = 450$ as the ν_e source

- A detector with low energy threshold that could reconstruct both QE and non-QE events was assumed with the following detector binning

  - An energy threshold of 400 MeV;

  - 200 MeV bins from 400 MeV up to 2 GeV;

  - A final bin of 1.06 GeV.

- A 100 % efficiency was assumed for all energies.

- A 2 % normalisation error on the flux was taken as was an intrinsic beam background of 0.1 % of the un-oscillated flux. The beam background is mainly attributed to neutral current pion production and electrons misidentication as muons.

A Water Čerenkov is disfavoured at this baseline because the reliance on quasi-elastic events for energy reconstruction result in small cross-sections at energies above ~ 1.5 GeV. In the absence of a specific detector choice, it is standard practice to use 100 % efficiency. A smaller, but constant efficiency, can be absorbed into the exposure. To see how this works, in both studies, two exposures are considered:

1. $5 \cdot 10^{21}$ ions-kton-yr

2. $1 \cdot 10^{21}$ ions-kton-yr

The first exposure could be achieved with a 10 year run with $5 \cdot 10^{18}$ useful decays per year and a far detector with fiducial mass 100 kton. An imperfect efficiency can be incorporated into the interprettion of the results by assuming a larger decay rate, longer run time, or larger detector mass.

The simulations presented in this chapter are different in an number of respects compared to the original study [89]. As mentioned previously, this is primarily for consistency with the other studies in this thesis. Below the main differences are listed.

- $\theta_{23} = 45^o$ in this thesis but not in the original study [89]. The analysis in the original study therefore needed to incorporate any octant degeneracy into the analysis.

- The codes used in [89] used a statisitical smearing to generate a $\chi^2_{min} \neq 0$ so that all analyses used $\Delta\chi^2$. In this thesis, all simulations generate 'true' data using the pair $(\theta^{tr}_{13}, \delta^{tr})$ without simulating an experimental fit.

- No energy resolution was incorporated into the orginal study, whilst here the public TASD GLoBES-detector file is used. Consequently, an energy resolution for muon detection is taken as $\Delta E = 3\,\%/\sqrt{E}$ in this chapter.

- The analyses presented in Figs. 4.2, 4.5, 4.6 and the righthand panel of Fig. 4.7 were not carried out in [89]. They are included here to demostrate some of the features of the proposal, whilst the original paper focussed on the physics reach.

- In [89], studies examining the ability to determine the mass hierarchy and the octant of θ_{23} were carried out. The focus in this thesis is solely on CP-violation.

In the next section, the results are presented with demonstrations of the benefit of combining low and high energy bins, the ability to rule of CP-violation, and analyses examining the behaviour of the true solutions and hierarchy clones. These results are also compared to a similar configuration that uses both neutrino and anti-neutrino runs.

4.4. Results

In Fig. 4.2, the benefit of combining low energy and high energy bins is demonstrated. Defining the low energy bins to be the bins up to the first oscillation minimum, i.e 0.4 GeV to 1.2 GeV; and the high energy bins to be from this energy to the maximum neutrino laboratory
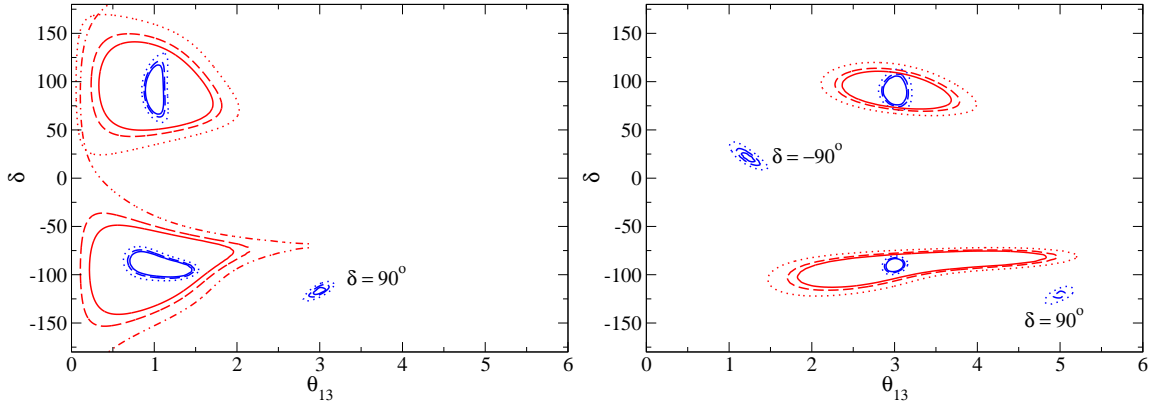
Figure 4.2.: 90 %, 95 % and 99 % confidence levels for an exposure of $5 \cdot 10^{21}$ ions-kton-yrs for the low energy bins (red) and high energy bins (blue). The simulations have been performed for $\delta^{\mathrm{tr}} = 90^o$ and -90° for the cases $\theta^{\mathrm{tr}} = 1^o$ (left) and $\theta_{13}^{\mathrm{tr}} = 3^o$ (right). Normal mass ordering has been assumed and any energy degeneracy has been labelled. The plot demonstrates how the lower energy bins rule out the intrinsic degeneracy associated with the high energy bins although little overall sensitivity is contributed.

energy; 90 %, 95 % and 99 % confidence levels for an exposure of $5 \cdot 10^{21}$ ions-kton-yr are presented. The setup has been simulated for $\theta_{13}^{\mathrm{tr}} = 1^o$ (left) and $\theta_{13}^{\mathrm{tr}} = 3^o$ (right) for $\delta^{\mathrm{tr}} = -90^o$ and 90° assuming the true hierarchy to be normal.

It is seen that the data from the high energy bins often allow for an energy degeneracy, more so for larger θ_{13}. This is to be expected since for large θ_{13} and energies around the first oscillation maximum, the atmospheric contribution to the appearance probability dominates. The interference contribution provides the sensitivity to CP-violation, but its influence is weak in the high bins. The interference contribution, and the solar contribution, is more dominant at the low energies. For all (θ_{13}, δ) pairs considered, there is only one sensitivity region, albeit a large one. Although the form of the appearance probability is helpful for determining the true values of θ_{13} and δ at these energies, the low event rates are not. The gain in using events from both regions is in their combination. The sensitivity regions from the high energy bins are small and provide good resolution on the true values of θ_{13} and δ. For a high energy run alone, the presence of an energy degeneracy can inhibit sensitivity as these solutions could be consistent with CP-conservation at 99 % level. Their locations, however, are typically far from the true solution. This means that the role of the low energy bins is to select the correct region in the (θ_{13}, δ) plane. No or very little sensitivity comes from these energies. All the sensitivity is derived from the events in the high energy bins.

In Fig. 4.3, the sensitivity is presented for the combination of the low and high energy bins for $\theta_{13}^{\mathrm{tr}} = 1^o$ and 3°; and $\delta^{\mathrm{tr}} = -90^o$, 0°, 90° and 180°. The true hierarchy is assumed to be

normal; however, in all cases a fit has been attempted assuming the inverted hierarchy. These solutions, when they exist, are shown in red for the same confidence levels. An exposure of $5 \cdot 10^{21}$ ions-kton-yr has been assumed. This setup demonstrates good sensitivity for all cases considered. For large θ_{13}, the hierarchy clone solutions do not appear for all choices of true values. From Fig. 4.1, the choice of hierarchy has a more pronounced effect around first oscillation maximum. Specifically, the discrepancy in the appearance probability is much larger, especially for large θ_{13}. There the location of the hierarchy clone solution would be far from the true solution at the high energies. Around second oscillation maximum, the matter effect is much smaller: the probabilities for normal and inverted hierarchies for a given θ_{13} and δ are very similar. Consequently, the hierarchy clone around second oscillation maximum is very close to the true solution. Therefore the combination of high and low energy bins is sufficient to rule out the hierarchy clone. This, however, is a θ_{13}-dependent statement as can be see from Fig. 4.3. The magnitude of the atmospheric term varies as $\sin^2 2\theta_{13}$. As θ_{13} is lowered, the discrepancy between the two oscillation probabilities decreases. As a consequence, the location of the hierarchy clone solution moves closer to the true solution. When the atmospheric contribution is sufficiently weak, the data from second oscillation maximum, dominated by the interference effects and solar effects, is unable to distinguish the true solution from the fake solution. At 99 % confidence level, the hierarchy clone solution exists for all cases. This is not a problem in general since the fake solutions are close to the true solutions for small values of θ_{13} and do not greatly interfere with sensitivity to CP-violation. From Fig. 4.3, the hierarchy clones that are indistinguishable from CP-conservation at 99 % confidence level belong to true solutions which themselves are indistinguishable from CP-conservation at 99 % confidence level. For $\theta_{13}^{\text{tr}} = 1^o$ and $\delta^{\text{tr}} = 180^o$, the position of the hierarchy degeneracy appears to not follow the pattern in being located close to the true solution. In fact, if the analysis is repeated for other $90^o < \delta^{\text{tr}} < 180^o$, the position of the degeneracy appears at $\delta = \pi - \delta^{\text{tr}} + \varepsilon$ where, ε is a small correction. This feature is was not explored in the original paper and has not been investigated further here. This feature is nominally assigned to the lack of an anti-neutrino run, but this cannot be confirmed without a detailed analysis of the oscillation probability. Whatever its origin, the effect on the CP-sensitivity is largely unaffected as the position of the degeneracies are typically away from CP-conservation if the true solution is also. In summary, the sensitivity to θ_{13} and δ looks competitive from this initial analysis. The next step is to examine the single ion setup's ability to rule out CP-conservation.

Fig. 4.4 shows the region in the $(\sin^2 2\theta_{13}, \delta)$ plane for which CP-conservation can be ruled out at 99 %. As a comparison, the same analysis has been performed for a 5+5 experimental run, all other experimental parameters the same. The 5 year anti-neutrino run was simulated with boost $\gamma = 350$ and ^{6}He as the source ($\gamma = 350$ is the maximum boost available with a
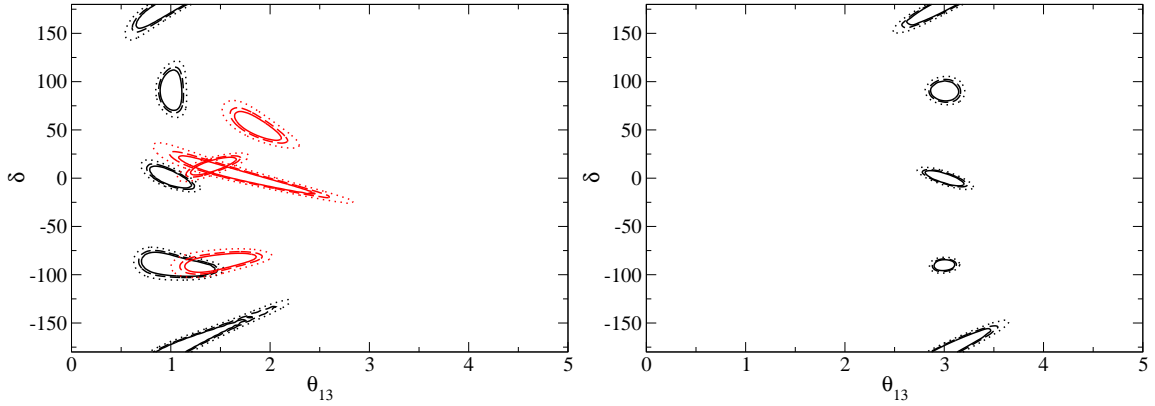
Figure 4.3.: 90 %, 95 % and 99 % confidence levels for an exposure of $5 \cdot 10^{21}$ ions-kton-yrs for $\theta_{13}^{\mathrm{tr}} = 1^o$ (left) and $\theta^{\mathrm{tr}} = 3^o$ (right). The 'true' mass ordering has been taken as normal with sensitivity simulated for $\delta^{\mathrm{tr}} = -90^o$, 0°, 90° and 180° in both cases. Each event spectrum has also been fitted to the 'wrong' inverted mass ordering and these are shown in red.

1 TeV machine for ^{6}He and so a completely matching anti-neutrino flux cannot be sourced). The same useful decay rate was assumed for both ions. The analyses have been carried out with $\theta_{23} = 45^o$ and the hierarchy degeneracy taken into account in the manner described in Chap. 2. The sensitivity region for the 5+5 setup takes a smooth, virtually symmetric form, whilst the single ion setup takes on a anti-symmetric and sometimes jagged appearance. In addition, there are enclaves of poor sensitivity at large $\sin^2 2\theta_{13}$ where good sensitivity would be expected regardless of the strategy employed. Further, there is a region for $\sin^2 2\theta_{13} > 10^{-3}$ and $-180^o < \delta < -135^o$ where sensitivity is poor owing to persistent degeneracies. The asymmetry is easy to understand. The switch $\delta \to -\delta$ leaves all terms in the appearance probability expansion unchanged apart from the $\sin \delta$ contribution to the interference term. This asymmetry in the probability will therefore lead to an asymmetry in the the procedure for minimising and locating the degenerate solutions. The reason for the pockets of poor sensitivity is less clear and is studied below. On the whole, the sensitivity regions for both setups are similar; the minimal $\sin^2 2\theta_{13}$ for which CP-conservation can be ruled out is $\sim 10^{-4}$ in both cases. The minimum $\sin^2 2\theta_{13}$ for which CP-conservation can be ruled out is slightly larger for the dual boost machine though primarily because of the smaller cross-sections of anti-neutrinos and the smaller boost for half of the run time. The single ion setup suffers more at the sensitivity limit and gives an overall smaller coverage of the (θ_{13}, δ) plane. This is not significant, except for the region mentioned above, and does not appear to be a phenomenological obstacle preventing this from being a valid experimental option. Below, the sensitivity is investigated further for the enclaves and the regions at the boundary.
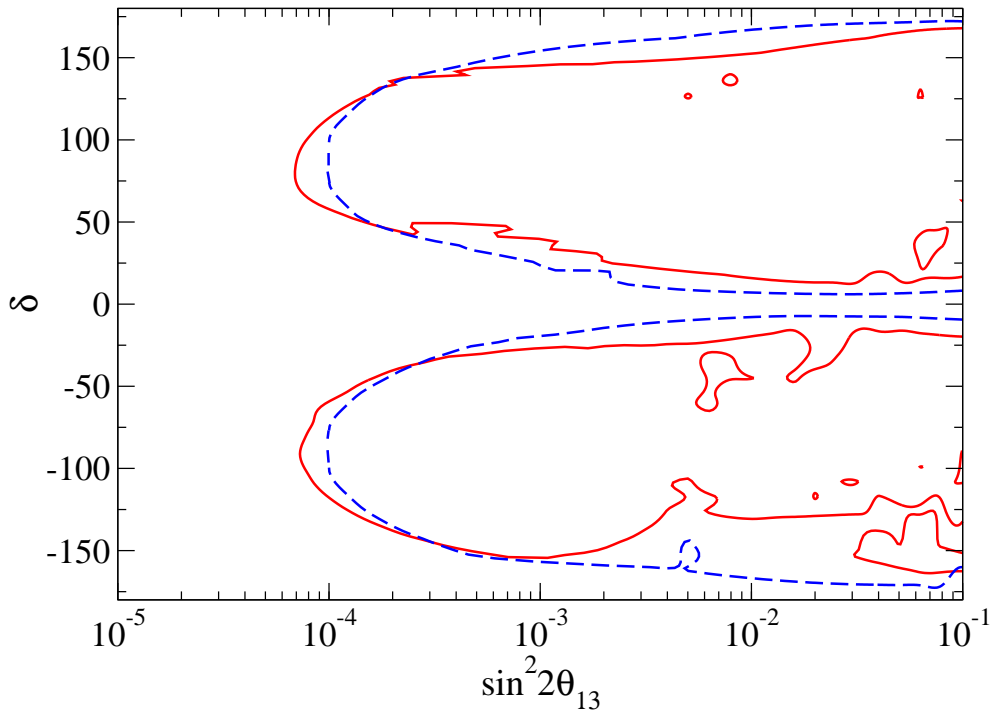
Figure 4.4.: 99 % confidence levels for the ability to rule out CP-conservation. The red lines show the sensitivity for the single ion setup whilst the blue dashed lines represent the results of the same analysis for the dual ion setup. An exposure of $5 \cdot 10^{21}$ ions-kton-yrs has been assumed with the hierarchy degeneracy incorporated into the analysis. The octant degeneracy is not included since $\theta_{23}^{\text{tr}} = 45^o$ has been taken. To read this plot: all points that share the same regions as the pairs $(10^{-3}, -90^o)$, $(10^{-3}, 90^o)$ and $(7 \cdot 10^{-3}, -150^o)$, the event rate vector is not consistent with CP-conservation.

Fig. 4.5 takes $\theta_{13}^{tr} = 1^o$ and considers the case $\delta^{tr} = 90^o$ for the true hierarchy being normal. This pair can be distinguished from CP-conservation for both setups. On the other hand, the same analysis is presented for $\theta_{13}^{tr} = 1^o$ and $\delta^{tr} = 160^o$. This pair is within the sensitivity region for the 5+5 setup, but lies just outside for the single ion beam. This case demonstrates the CP-sensitivity behaviour at the boundary. The location of the hierarchy clone is attempted in all cases (shown in red if they exist). The results for the single ion beam are presented on the left, and the 5+5 setup on the right. For both setups, the sensitivity for the true pair $(\theta_{13}^{tr}, \delta^{tr})$ is very similar. There is a hierarchy clone solution of similar size in each case. The single ion beam fake solution is larger, as expected, due to the absence of an anti-neutrino run. Since none of these solutions are close to the $\delta = 0^o$ or $\delta = 180^o$ lines, this pair can be distinguished from CP-conservation at 99 % confidence level. The same is not true for $\delta^{tr} = 160^o$ however. This pair lies on the sensitivity boundary for the 5+5 setup. This is evident from the right panel of Fig. 4.5 where the true solution just touches the CP-conserving $\delta = 180^o$ line. The hierarchy clone does not appear at 99 % confidence level. There is no sensitivity to CP-violation for the single ion setup because the true solution sensitivity region is large. In particular, it crosses the $\delta = 180^o$ line and spreads into the $\delta < 0^o$ region. In addition, there is also a large hierarchy clone solution present that cannot be distinguished from CP-conservation at 99 % confidence level. From this analysis, it is concluded that the principle reason for the shape of the single ion beam sensitivity boundary is the lack of an anti-neutrino run. Without this complementary information, the sensitivity regions are larger and cannot be distinguished from CP-violation for larger ranges of δ^{tr} at a given θ_{13}^{tr}.

Next, consider the behaviour in the poor sensitivity enclave around $\sin^2 2\theta_{13} = 7 \cdot 10^{-3}$ and $\delta = -40^o$. In Fig. 4.6, the 90 %, 95 % and 99 % confidence levels are presented for the 2 pairs $(7 \cdot 10^{-3}, -40^o)$ and $(1 \cdot 10^{-3}, -40^o)$. As before, an exposure of $5 \cdot 10^{21}$ ions-kton-yrs is considered and the true hierarchy is taken to be normal. The left panel shows the results for the single ion setup whilst the right panel holds the results for the dual ion setup. From the left panel, the failure to establish CP-violation at 99 % is a consequence of a hierarchy clone being consistent with $\delta = 180^o$. For smaller $\sin^2 2\theta_{13}$, the clone is far from CP-conservation. At larger values of $\sin^2 2\theta_{13}$, the clone solution is ruled out at 99 % and therefore poses no problem. In addition, for $\sin^2 2\theta_{13} = 10^{-3}$, there exists a small energy degeneracy but this does not interfere with the determination of CP-violation. No intrinsic or hierarchy degeneracy is present. Therefore, one concludes that the origin of the no sensitivity enclaves is a consequence of the single ion setup not being able to adequately remove the hierarchy clone solutions. As $\sin^2 2\theta_{13}$ increases, the relative size of the atmospheric and interference contributions of the appearance probability change causing the location of the
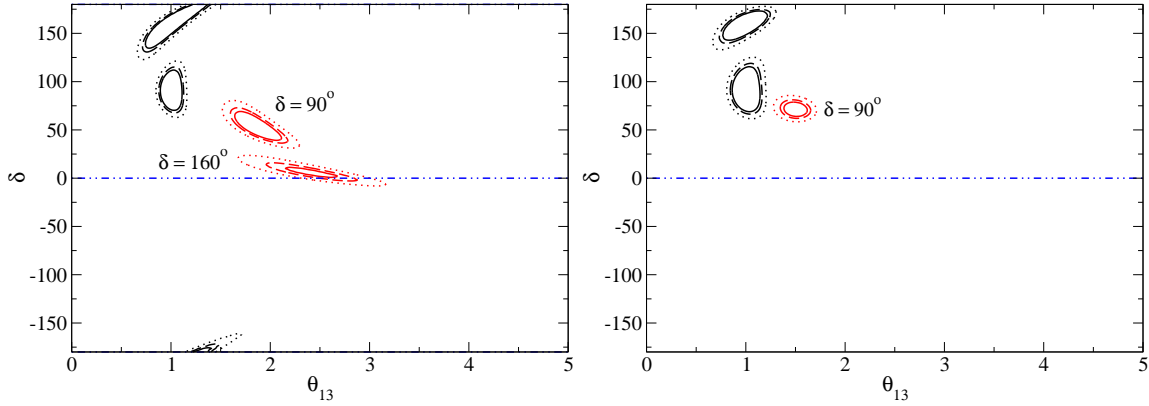
Figure 4.5.: Hierarchy degeneracy regions for a the single ion beta beam (left) and the dual ion beta beam (right). The analysis presented are the 90 %, 95 % and 99 % confidence levels for an exposure of $5 \cdot 10^{21}$ ions-kton-yrs and $\theta_{13}^{tr} = 1^o$. The 'true' mass ordering has been taken as normal with sensitivity simulated for $\delta^{tr} = 90^o$ and 160° in both cases. The blue line is $\delta = 0^o$. There is no sensitivity at 99 % if any 99 % confidence level contour crosses it. The $\delta = 90^o$ case represents a true pair that can be distinguished from $\delta = 0^o$ for both setups whilst the $\delta = 160^o$ case lies just outside the 99 % contour of the single ion setup. The hierarchy clone solutions are sho
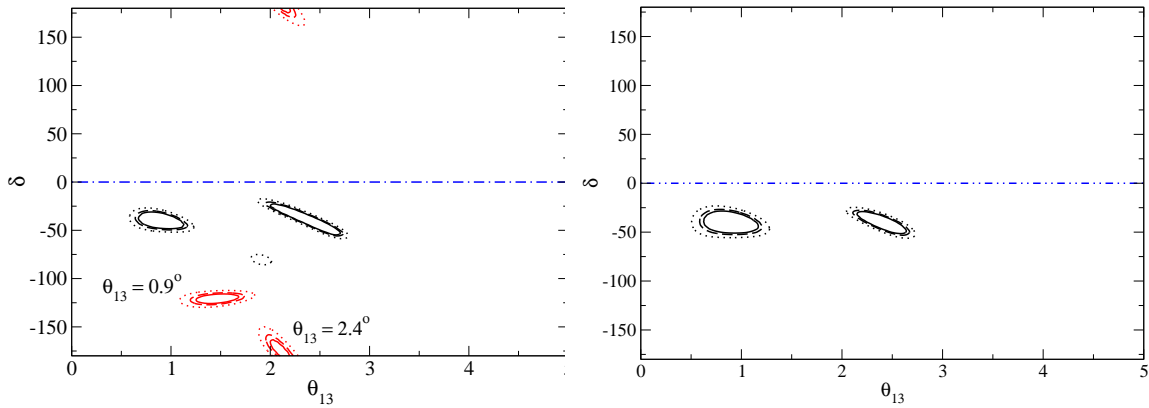
Figure 4.6.: Analysis of the lack of sensitivity in the region $\left(\sin^2 2\theta_{13}^{tr}, \delta^{tr}\right) \sim \left(7 \cdot 10^3, -40^o\right)$. The 90 %, 95 % and 99 % confidence levels for an exposure of $5 \cdot 10^{21}$ ions-kton-yrs and $\delta^{tr} = -40^o$ for the cases $\theta_{13}^{tr} = 0.9^o$ and 2.4^o. The 'true' mass ordering is taken to be normal. On the left the analysis has been performed for the single ion setup whilst the right panel shows the results for the dual ion setup.

hierarchy clone to migrate towards CP-conservation. For sufficiently large $\sin^2 2\theta_{13}$, the clone solution is ruled out at 99 % confidence level.

The simulations performed up to now have used an exposure of $5 \cdot 10^{21}$ ions-kton-yrs which has to be considered optimistic. For a 100 kton detector with 100 % efficiency, this exposure could be achieved if $5 \cdot 10^{18}$ useful ion decays are available each year for 10 years. This rate is not implausible but it should be considered as an upper limit, especially for a large

boost. The exposure is not a problem here since this study is concerned with determining the behaviour of a single ion beta beam. Never-the-less, it is instructive to examine the behaviour for a smaller exposure. A realistic setup could then be considered as intermediate to the two exposures studied. In the left panel of Fig 4.7 , the sensitivity to CP-violation is presented for an exposure of $1 \cdot 10^{21}$ ions-kton-yrs.

The smallest value of $\sin^2 2\theta_{13}$ for which CP-conservation can be ruled out is now 5 times larger, consistent with expectations (the size of a χ^2 function for a given hypothesis is proportional to the number of useful decays, when everything else remains unchanged). However, with reductions in the number of useful ions, degenerate solutions that were resolved at 99 % confidence level previously are now present and interfere with the sensitivity. The dual boost setup maintains roughly the same form but with additional enclaves of no sensitivity at $\sin^2 2\theta_{13} \sim 10^{-2}$. This feature is sometimes present in Beta Beams at intermediate baseline [111] as this is the region in which the interference and atmospheric contributions to the appearance probability are of similar magnitude. The smaller ranges of δ^{tr} for which there is sensitivity for the single ion setup is expected, as is the contour's haphazard shape. A feature that was present, but not so marked, in the high exposure simulation is very prominent here: the lack of sensitivity for $\sin^2 2\theta_{13} \sim 10^{-2}$ and $\delta < 0^o$. The reason for this is shown in the right panel of Fig. 4.6. The true solution for the pair $(10^{-2}, -90^o)$ is accompanied by a larger energy degeneracy at smaller $\sin^2 2\theta_{13}$ and δ. At 99 % confidence level, this clone solution is consistent with CP-conservation. Additionally, the pair $(10^{-2}, 135^o)$ has been simulated to examine the behaviour of true solutions that now exist outside the 99 % contour. No energy degeneracy is present, however there is now a sensitivity region that is just consistent with $\delta = 180^o$. The location of the hierarchy clone is shown which itself has an additional fake solution.

4.5. Summary

In the present chapter, the CP-violation reach of a Beta Beam without an anti-neutrino run has been investigated using the CERN-Boulby baseline as a case study. The principle was to bin the data sufficiently narrow to extract the oscillatory structure of the ν_μ appearance signal. Such a strategy requires access to data from a range of energies; specifically events around second oscillation maximum where the interference contribution to the oscillation probability is strong.
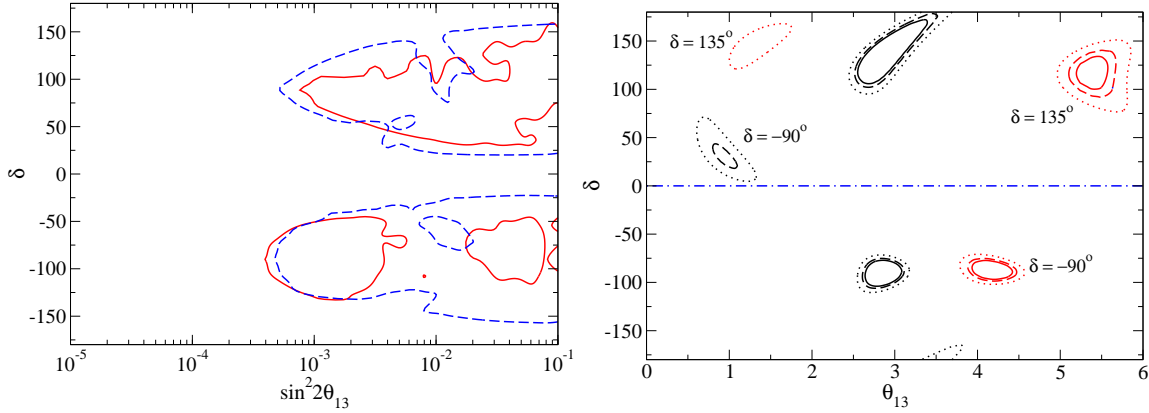
Figure 4.7.: 99 % confidence levels for the ability to rule out CP-conservation for the low luminosity run (left panel). The red lines show the sensitivity for the single ion setup whilst the blue dashed lines represent the results of the same analysis for the dual ion setup. An exposure of $1 \cdot 10^{21}$ ions-kton-yrs has been assumed with the hierarchy degeneracy incorporated into the analysis. The octant degeneracy is not included since $\theta_{23}^{tr} = 45^o$ has been taken. The right panel shows a number of two parameter fits for the single ion run as outline in the text. The black contours are the true solutions (hierarchy assumed to be normal) and the red lines the hierarchy clone solutions.

This study was motivated by suggestions that large caverns could be excavated below the current laboratory level at the Boulby mine. The caverns would be sufficiently large so to host detectors of several tens of kilotons. At a distance of 1050 km from CERN, both the first and second oscillation maxima can be studied with a low energy threshold detector located at Boulby. The second motivation was the uncertainty on the number of useful ion decays achievable for a Beta Beam. It may be the case that the un-oscillated event rate is significantly larger for one neutrino helicity than the other. In which case it is necessary to consider a single ion beam as a contender for a future neutrino facility. The usefulness of information from first and second oscillation maxima was demonstrated analytically using the appearance probability expansion. The combination of data bins is sufficient to resolve any energy degeneracy that is present for similar energies. There is some hierarchy degeneracy present but it is not sufficiently strong to be catastrophic to the CP-violation sensitivity.

In the numerical simulation, an exposure of $5 \cdot 10^{21}$ ions-kton-yrs was considered for the ^{18}Ne and a boost $\gamma = 450$. This was compared to a neutrino and anti-neutrino facility with equal run times. CP-violation sensitivity plots were constructed for both cases and the features were explored further with 2-parameter fits to chosen 'true' values. The asymmetrical and disorderly appearance of the sensitivity for the single ion run suggested that its degeneracy breaking abilities might pose problems for lower luminosities. To check this observation, a run was performed for an exposure reduced by a factor of 5. Degeneracy that was resolved

for the large exposure was no longer so for the low exposure. This is especially true for $\sin^2 2\theta_{13} \sim 10^{-2}$ and $\delta < 0^o$. A facility without an anti-neutrino run therefore requires a large exposure.

In conclusion, a Beta Beam that only uses a neutrino run is a viable option is a large luminosity can be realised. Although the discussion here has focussed on sensitivity to CP-violation, I believe this might be the best option to study the mass hierarchy at these short baselines. The mass hierarchy will be resolved by accumulating events from the high energies - those in excess of the first oscillation maximum - and combining them with the data from the lower energies where the matter effect is small thus breaking any degeneracy. I consider the setup presented here to be the desirable option because of the charge-to-mass ratios of the ions. With a 1 TeV machine, ^{18}Ne can be accelerated up to $\gamma = 590$ which corresponds to a maximum neutrino laboratory energy of 4 GeV. ^{6}He, on the other hand, can only be boosted to $\gamma = 355$ corresponding to a maximum anti-neutrino laboratory energy of 2.5 GeV. A dual ion Beta Beam with the maximum boosts therefore will have a lower event rate in the energy range beyond first oscillation maximum where the hierarchy will manifest itself and hence an inferior hierarchy reach. If this hypothesis is correct, then the single ion Beta Beam using neutrinos will have a better overall physics reach compared to its dual ion counterpart. The hierarchy reach was presented in the original study [89]; however, the comparison just described was not studied.

Chapter 5.

Electron capture machines

In a standard Beta Beam the neutrino flux is sourced from the decay of boosted radioactive ions. It is advantageous to produce a clean, collimated beam this way since a single boost is all that is necessary for a laboratory neutrino flux to span an energy range up to several GeV. As discussed in the previous chapter, degeneracy can be resolved through the analysis of their energy dependence of the oscillation signal. However, one is not free to choose the neutrino spectrum; the boost determines the maximum neutrino energy in the laboratory frame which in turn determines the un-oscillated event at all energies. For example, if the peak of the Beta Beam flux is chosen to align with first oscillation maximum, the flux at the second oscillation maximum is automatically determined by this choice. In a Beta Beam, complete freedom to choose the relative fluxes at different energies is not available. In addition, some neutrinos are 'lost' because they have no practical use or their information is hidden by systematics and backgrounds;

1. Neutrinos events below the detector threshold are not used in an analysis and so are lost in this sense. This affects the lower γ Beta Beams since the fraction of neutrinos at the detector below this energy in the laboratory frame is greater.

2. At high energies, there are additional backgrounds, such as charmed meson decay, which can have muons in the final state. It is therefore important not to rely on information from neutrinos with energies above the production thresholds.

3. In a Water Čerenkov detector, energy reconstruction is via quasi-elastic events. For energies greater than ~ 1.5 GeV, where hadronic processes begin to dominant the cross-section, neutrino events are severely reduced, especially at high γ where the proportion of neutrinos with energies in this range is higher.

4. Some might argue that neutrinos are lost at energies corresponding to oscillation minima and it is better to have more neutrinos at the maxima where there is a useful event even for $\delta = 0$ and/or negative (positive) hierarchies for neutrinos (anti-neutrinos). This is partly true, but (see Fig. 2.3) the position of the maxima and minima change with the CP-phase δ and the mass hierarchy and so the mimina also provides important information in this respect.

One way to alleviate these concerns is to use a source of mono-energetic neutrinos so that the boost of the ion can be altered to freely choose the laboratory frame energy of the neutrinos. Clearly, such and approach needs at least two boosts as both θ_{13} and δ are unknown. Such a beam would use ions that decay through a dominant electron capture channel as their source; an idea that is discussed in the next section.

5.1. The electron capture beam concept

The electron capture process was briefly introduced in Chap. 3. Electron capture is a decay channel available to proton-rich nuclei and it competes with positron decay depending on the energy available. For $Q < 2m_e$, positron decay is kinematically forbidden and so electron capture decays form the entire phase space. For electron capture decays, the rate is proportional to the Q^2 from the two body decay and Z^3 from the square of the electron orbital wave-function. For proton number Z, shell binding energy E_B, fine structure constant α and beta decay matrix element $\mathcal{M}$, the electron capture rate for Q-value Q is [153]

$$\Gamma_{\text{EC}} = \frac{G_F^2}{\pi^2}(Q - E_B)^2 (\alpha Z)^3 |\mathcal{M}|^2 . \tag{5.1}$$

The equivalent expression for beta decay is (with the same matrix element)

$$\Gamma_{\beta} = \frac{G_F^2}{2\pi^3} m_e^5 f(E_0, Z) |\mathcal{M}|^2 , \tag{5.2}$$

where the f is the normalisation

$$f(E_0, Z) = \int_1^{\omega_0} \omega\sqrt{\omega^2 - 1} (\omega_0 - \omega)^2 F(\omega, Z) d\omega . \tag{5.3}$$

In these expressions, m_e is the electron mass, $\omega = E_\nu/m_e$ and $F(\omega, Z)$ is the Coulamb correction term for the interaction of the ejected electron with the final state nucleus. To first order, the positron decay rate is proportional to fifth power of the Q-value; the relative rate for

$Q > 2m_e$ is approximately given by

$$\frac{\Gamma_{\text{EC}}}{\Gamma_{\beta}} \propto \frac{(\alpha Z)^3}{Q^3} \, , \tag{5.4}$$

where the matrix elements are assumed to be identical. For electron capture with Q-value Q_{EC} and boost γ, the neutrino flux in the laboratory frame at baseline L from source is given by [91, 154]

$$\frac{dN}{d\Omega dE_\nu} = \frac{N_{\text{ions}}}{\pi L^2}\gamma^2\,\delta(2\gamma Q_{\text{EC}} - E_\nu) \equiv \Phi(E_\nu)\,\delta(2\gamma Q_{\text{EC}} - E_\nu) \, . \tag{5.5}$$

Trivially, the baselines available to electron capture machines are dependent on the Q-value of the ion and the maximum boost allowed from the acceleration. Two different phenomenological studies have been carried out to date and can be distinguished by their choice of Q-value.

The use of electron capture decays to source mono-energetic neutrino fluxes was suggested in [154] and subsequently in [155]. These papers proposed the use of ions with Q-values less than twice the electron mass where positron decay is kinematically forbidden. No phenomenological study was carried out initially; however, a half-life (in the laboratory frame) of order months or up to a year was suggested. Small Q-value electron capture machines are ruled out by this criteria since the optimal laboratory half-life is $O(1\,sec)$ which in the laboratory frame is $\sim$ minutes. An interesting feature was highlighted, and was explored further in [155], namely that with low Q and high boost electron capture machines, most of the neutrinos cross the detector. This means that, in principle, positional information can be used to extract the energy dependence of the signal as the energy of the neutrino in the laboratory frame drops as on goes off-axis (see Appendix B). In [155] a study exploring this idea was carried out using ^{110}Sn as the source ion. In the decay rest frame, ^{110}Sn has $Q = 267$ keV (for the K-shell) and a half-life of 4.11 hours. Three setups were considered, all assuming a 500 kton Water Čerenkov detector located at either 250 km or 600 km from source, and boosts in the range $900 < \gamma < 2500$. Such high boosts are necessary because of the very low Q-value; this analysis assumes that the LHC is available to accelerate the ions[1]. A detailed study was carried out using the GLoBES simulation package; sensitivities to CP-violation were found to be equivalent to the IDS Neutrino Factory setup, although the authors acknowledge the idea to be "extreme". In summary, the very high boosts required, even for the moderate baselines of

---

[1]The use of the SPS for a Beta Beam does not disrupt LHC operations. Time on the LHC for Beta Beams is not going to happen in reality and so very high boost setups such as [155] should be taken as a demonstration of a principle rather a viable facility option.

Europe, and the low Q-values mean that electron capture long baseline facilities of this type are not realistic.

Prior to the above studies, a second option using higher Q-valued ions was discussed and was later expanded into studies for the CERN-Frejus and CERN-Canfranc baselines [91]. For ions with Q-value greater than twice the electron mass, the electron capture channel competes with a positron decay background (Eq. 5.1); the branching ratio for electron capture channels drops sharply as the Q-value increases. With Q-values $\sim 3 - 4$ MeV and a 1 TeV accelerator, one would be able to place a mono-energetic neutrino beam on first oscillation maximum for baselines up to 1000 km, making the idea an attractive one in Europe with the source based at CERN. However, the positron decay background would make the idea unattractive since the number of useful electron capture decays would not be high enough for competitive physics reach. It could be argued that the positron decay neutrinos could be used to boost sensitivity by providing coverage of the second oscillation maxima with concentration of the electron capture neutrino on and around first oscillation maxima. This is the strategy will be explored in detail in Chap. 6. A number of nuclides that decay quickly[2] through large Gamow-Teller resonances have been discovered, see for example [156], that could source dominant electron capture channels at higher Q-values. A collection of some of these ions are presented in Tab. 5.1. ^{150}Dy formed the basis of the study [91]. This particular ion was chosen as the resonance did not have a width and because of its lower Q-value. Recall from Eq. 5.5 that the neutrino flux is proportional to the square of the boost for a fixed baseline and number of useful decays. Lower Q-values require higher γ to achieve the same laboratory neutrino energies, and so lower Q-values are favoured in this sense, provided the accelerator is capable of achieving the boosts. This particular study is the start off point and motivation for this chapter. Before proceeding with the phenomenology though, it is necessary to point out some extra technological challenges associated with electron capture machines and hybrids.

5.1.1. Partially stripped ions

For Beta Beams, the ions will have all their electrons removed before the acceleration. The probability that the ions will acquire an electron due to the imperfect vacuum conditions in the acceleration and subsequent storage is effectively nil. Facilities that make use of electron

---

[2]Quickly is a vague word that is sometimes used in this context. It should be treated to mean relative to ions with similar Q-values. Ions with similar $Z^3 Q^2$ will have similar electron capture rates from the K-shell. An ion that can decay through a resonance will have a much larger matrix element, however, which quickens the rate.

Parent nucleus	Half-life	EC BR	EC intensity	Ex Daughter level (keV)	Q-value (keV)
^{148}Dy	3.1 m	100 %	92.5 %	620	2678
^{148}Er	4.6 s	100 %	8.8 %	0.00	6800
^{150}Er	19 s	100 %	59.5 %	476+X	4108
^{150}Dy	7.2 m	64 %	64 %	397+Y	1794
^{152}Yb	3.1 s	100 %	29 %	482	5470
^{154}Er	3.7 m	99.53 %	96.8 %	26.9	2032

Table 5.1.: Candidate electron capture beam ions. Based on a similar table from [156].

capture decays and bound beta decays, however, will require the acceleration of partly stripped ions. This is a necessity for electron capture machines and hybrid machines since orbital electrons are required for the electron capture to take place. For a bound beta decay machine, high proton number ions are required to source a useful bound beta decay flux (see Sec. 5.5), and so the likelihood of being able to produce a fully stripped ion is low. Indeed, for the Beta Beam hybrid study, to be discussed in the next chapter, 16 electrons were assumed to be left bound to the ion for experimental reasons, although this restriction is an arbitrary one. The principle reason for this is to minimise losses due to space charge effects - the ion-ion electromagnetic interactions causing dispersion of the beam.

The acceleration of partly stripped ions is not a problem per se [158]. In particular, [159] reported that there has been intense study on partly stripped ions at GSI for the FAIR facility [160] and at Brookhaven for the RHIC program. The issue in the context of the Beta Beam related technologies is the intensities of the useful neutrinos required and the demands imposed on the accelerator chain. Imperfect vacuum conditions, which will deteriorate as the acceleration cycle progresses, is the major cause for concern. As a consequence, at high energies, the electron stripping cross-section is large [159] and is the dominant source of losses during the acceleration and storage - the act of removing an electron from a partly stripped ion changes its charge-to-mass ratio: the magnetic field configuration no longer matches the field needed to keep accelerate the ion or hold it in the storage ring. These 'vacuum losses' can be considered as an extra decay channel, and it is useful to assign a 'vacuum half-life' to it. In [159] it was reported that a vacuum half-life of 1 minute during acceleration and 3 minutes during storage ring should be taken as a conservative estimate of the effect. The annual rate of neutrinos (Eq. 3.22) needs to be modified to include this important loss :

$$R = \frac{I_{\text{in}}l}{T_{\text{rep}}} \frac{\lambda_{\text{EC}}/\gamma}{\lambda_{\text{EC}}/\gamma + \lambda_{\text{vac}}} \left(1 - e^{m T_{\text{rep}} (\lambda_{\text{EC}}/\gamma + \lambda_{\text{vac}})} \right) T_{\text{run}} \qquad (5.6)$$

Here, λ_{EC} and λ_{vac} are the decay constants for the electron capture decay and vacuum losses respectively. For intense beams, especially high charged beams, stability is a major problem. The Coulamb interactions of the particles in the beam cause a divergence from the ideal conditions. Following [150], consider a stream of particles with a uniform particle density ρ_0 each with a velocity v_z and charge q. It is natural to take the coordinate system as cylindrical with a point labelled by (r, ψ, ϕ). By symmetry, the electric field is only in the radial direction and, from Coulomb's Law, is given by

$$E_r = \frac{1}{2\varepsilon_0}\rho_0 r \; . \tag{5.7}$$

The magnetic field is azimuthal; from Ampere's Law we find

$$B_\psi = \frac{1}{2}\mu_0\rho_0 v_z r \; . \tag{5.8}$$

The Lorentz force is in the radial direction and is given by

$$F_r = q(E_r - v_z B_\psi) = \frac{1}{2}\varepsilon_0 q\frac{\rho_0}{\gamma^2}\, r \; . \tag{5.9}$$

The above relations are written for S.I. units with ε_0 and μ_0 the permittivity and permeability of free space, respectively. The contribution from the Coulomb interaction on the test particle is the net force in the rest frame. In the laboratory frame, the generated magnetic field opposes the electric field; the contributions exactly cancel for a beam travelling at the speed of light. From the right-hand side of Eq. 5.9, the magnitude of the Lorentz force increases with charge and intensity, but decreases with boost. Space charge is therefore a great concern for ions considered for electron capture machines, hybrids and bound beta beams, especially early on in the acceleration chain where the boosts are still close to unity. In addition the ions are high-Z ions and, with their relatively long lifetimes (compared to standard ions), will have high densities (the ions during acceleration will be effectively continuous with bunching to the required duty factor taking place on injection to the storage ring). Typically, boosts are of the same order for all types of machine proposed for long baseline experiments.

In reality, the above analysis is simplistic and a more detailed consideration taking into account bunching of the beam and the size of the vacuum chamber is required [162]. One should instead use the Laslett tune-shift [161]:

$$\Delta Q = -\frac{Z^2}{A_p}\frac{3r_p}{4\beta^3\gamma^3 c}\frac{R}{\tau_b}\frac{N_b}{\varepsilon}\; . \tag{5.10}$$

Here, Z is the charge of the ion, A_p is the ion-to-proton mass ratio, r_p is the classical proton radius, c is the speed of light, R is the mean radius of the machine, N_b is the number of ions per bunch of duration τ_b, and ε is the physical emittance of the beam. Fundamental accelerator dynamics is beyond the scope of this thesis; loosely speaking the larger the tune shift, the more the beam is unstable. For intense ion beams, the Coulomb repulsion is a major source of instability.

At present, no extensive R&D has been performed for electron capture machines, hybrids and bound beta beams. A brief survey [163], however, has been carried as a project in the CERN Summer Student programme. In the analysis, the annual neutrino intensities and the incoherent tune-shifts were calculated for the four rare-earth nuclei put forward in [91]. A source rate of 10^{13} ions per second from the proposed EURIOSOL facility, a boost $\gamma = 100$, $\tau_b = 0.8$ and emittances the same order as for ^{6}He and ^{18}He were all assumed. With these assumptions, the tune shifts are about a factor of three higher for the rare-earth ions than for ^{6}He and ^{18}He, and the annual neutrino rates are $\sim 10^{15}$ neutrinos per year [163].

5.2. Optimisation of an electron capture machine

The discovery of ions far from the stability line that decay through a giant Gamow-Tellar resonance opened up the possibility of using 1 TeV machines such as an upgraded Super Proton Synchrotron (SPS) to source the intermediate baselines in Europe. As mentioned previously, [91] considered this probability for the CERN-Frejus (130 km) and CERN-Canfranc (650 km) baselines with ^{150}Dy as the chosen ion. Since only a neutrino flux is available in an electron capture setup, the approach was to exploit the different energy dependence of the CP-odd and CP-even properties of the appearance probability (Eq. 2.34) by running at two different boosts. The purpose of those studies was not to optimise an electron capture long baseline setup, rather to demonstrate the phenomenological feasibility of the idea: the use of multiple boosts to extract the energy dependence of the event spectra. However, the electron capture beam was not optimised in terms of the boosts and the run times. This is the purpose of this chapter.

In this section, an electron capture facility will be optimised using two boosts. For simplicity, the number of useful decays will be fixed at $N_{\text{ions}} = 10^{18}$, irrespective of the boost; a 440 kton Water Čerenkov detector is assumed (with no energy reconstruction all CC events are taken as signal); and no atmospheric backgrounds will be included. Since the expsoure and the atmopsheric background are critical for the projective CP-sensitivity, they will be taken into

account varied once the optimal energies have been found. The neutrino oscillation parameters have been set to the current values [15].

For both electron capture and Beta Beams, the parent ions will accelerated in the existing or upgraded CERN infrastructure before accumulated and stored in a ring whose long, straight sections source the neutrino flux. For electron capture machines with ion boost γ, the mono-energetic neutrino flux at a detector distance L from the source is given by Eq. 5.5. Since the neutrino energy in the laboratory frame is given by $E_\nu = 2\gamma E_0^{\mathrm{EC}}$, for fixed baseline and number of useful decays, the ions with lower Q-values result in larger fluxes. The choice of ion is thus a balance between Q-value and the available acceleration. A selection of possible ions is presented was Tab. 5.1. ^{148}Dy and ^{154}Er have very similar characteristics; the bulk of all decays being an electron capture, half-lives ~ 3 minutes and neutrino energies of ~ 2 MeV in the rest frame. The lower Q-value ion, ^{150}Dy, will be taken in this paper for consistency with [91] and the higher γ's required compensate for the lower electron capture branching ratio. The remaining 36 % for ^{150}Dy is α-decay and so does not source a primary neutrino background, the daughter has 100 % α-decay with a 74 year half-life. The other ions in Tab. 5.1 have undesireable intensity and Q-value combinations. These higher Q-value ions also have a large beta decay background and are more suitable for the hybrid machine introduced in the next chapter.

For a ^{150}Dy^{66+} ion, the maximum boost attainable[3] with an upgraded 1 TeV SPS is $\gamma_{\mathrm{max}} = 440$ corresponding to a laboratory frame energy of $E_\nu = 1.23$ GeV. For a pure electron capture machine with no backgrounds the choice of detector does not depend on the energy reconstruction capabilities as the event energy is determined by the boost. In reality, some reconstruction might be necessary for the electron capture events to reduce the atmospheric background, especially if low production rates or issues with the acceleration force a large duty cycle. This point will be discussed further in Sec. 5.3. Since the maximum laboratory frame energy is 1.23 GeV, baselines in excess of CERN-Canfranc are unrealistic propositions. Therefore matter effects are small, but not negligible, but not enough to achieve competitive sensitivities to the mass hierarchy. Electron capture machines of this type are therefore 'CP-violation machines'.

---

[3]The maximum boost for a fully stripped ^{150}Dy ion is in fact $\gamma = 468$; however, it is necessary to leave several electrons bound to the nucleus to source the electron capture decay. If one leaves the 2 K-shell electrons and 2 in the L-shell, this reduces the maximum boost to 440.
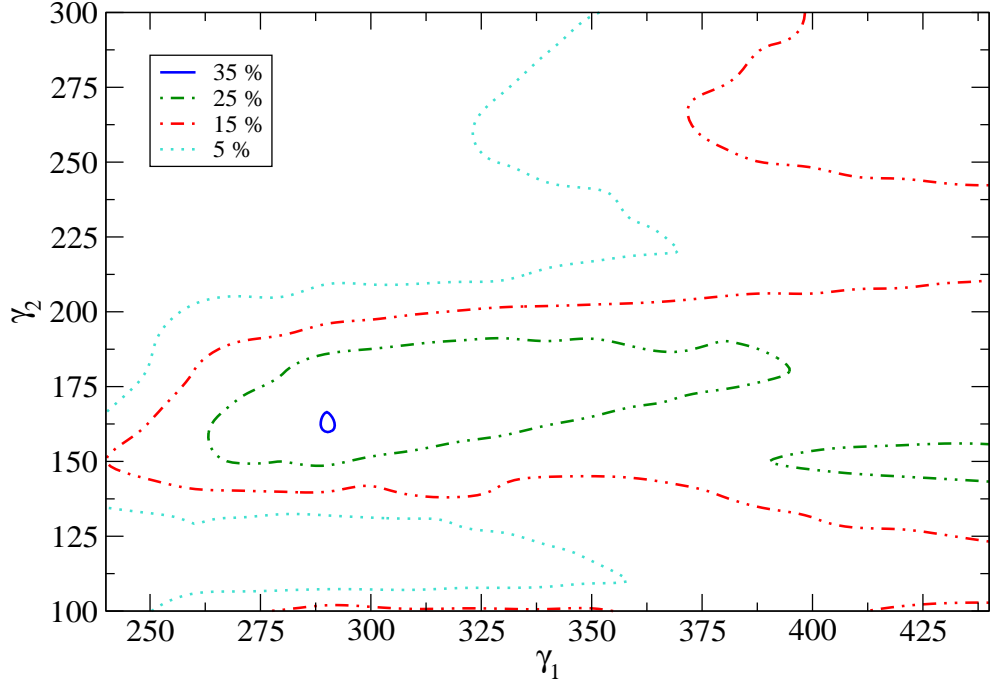
Figure 5.1.: 5 %, 15 %, 25 % and 35 % (θ_{13}, δ) plane coverage for f=0.3. Coverage is defined as the fraction of the sample grid points for which one can rule out CP-conservation at 99 % C.L.

5.2.1. A dual boost electron capture machine

In this section, the sensitivity to CP-violation of an electron capture machine as a function of two boosts, γ_1 and γ_2, and the run time fraction, f, will be explored. For a given boost pair (γ_1, γ_2), number of targets $\mathcal{N}_T$, and run time fraction f, the simulated events are given by

$$n_{\gamma_i} = \mathcal{N}_T \, \eta_i \, t \int_0^\infty \Phi(E_\nu) \, \sigma(\nu_\mu) \, P_{\nu_e \to \nu_\mu}(E_\nu) \, \delta(E - E_\nu) \, dE \, , \qquad (5.11)$$

where $\eta_1 = f$, $\eta_2 = 1 - f$ and t is the total run time. The relatively short simulation time will be exploited to 'optimise' the electron capture machine. For a pair (γ_1, γ_2), the CP-sensitivity plot is constructed by scanning the (θ_{13}, δ) plane. At each point on the grid, CP-violation is tested at the 99% C.L.. The fraction of points for which deviation from CP-conserving can be determined is the 'coverage' for the pair (γ_1, γ_2). This procedure is repeated for many such pairs. Note that any information on the shape of the 99% contours is lost in this analysis. In particular, it does not guarantee that the 'optimal' pair will yield a CP-sensitivity symmetry in $\delta = 0^o$, nor that the minimum $\sin^2 2\theta_{13}$ will be found. In Fig. 5.1, the 5 %, 15 %, 25 % and 35% coverage contours are presented for the case $f = 0.3$. There are two distinct regions in the (γ_1, γ_2) plane; the first corresponds to the placement of the neutrino flux at the highest energy allowed in combination with a flux at second oscillation maximum. This combination
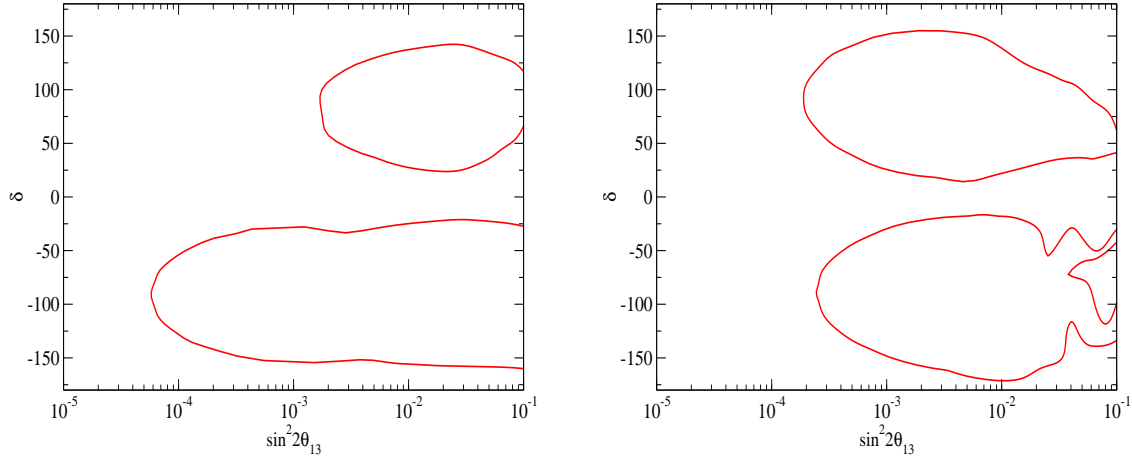
Figure 5.2.: CP-violation sensitivity at 99% for the γ pairs $(\gamma_1, \gamma_2) = (440, 150)$ (left) and $(\gamma_1, \gamma_2) = (280, 160)$ (right).

corresponds to the naive expectation that good sensitivity should result from combining first and second oscillation maximum, as discussed in the previous chapter. However, there is a (additional) large region of (γ_1, γ_2) space in which sizeable coverage can be achieved. Specifically, for a high boost, $260 < \gamma_1 < 400$ and a narrower range of low boosts, $150 < \gamma_2 < 185$; there is at least 25 % coverage of the (θ_{13}, δ) plane. This rises to 35 % for $(\gamma_1, \gamma_2) \sim (280, 160)$. This result is repeated for the cases $f = 0.4$ and $f = 0.5$ with little variation. The small region with 35 % coverage at $(280, 160)$ is the best CP-coverage of the run time fractions and boost pairs studied.

In Fig. 5.2 the CP-sensitivity plots are shown for the two pairs $(440, 150)$ and $(280, 160)$. These correspond to the centre of the 'naive' choice of boosts and the 37 % coverage region on the coverage plot (Fig. 5.1), respectively. It is seen that the first option produces an asymmetrical sensitivity region, the best sensitivity for $\delta < 0^o$; any degeneracy is resolved in larger regions of parameter space. However, the minimal $\sin^2 2\theta_{13}$ is larger for $\delta > 0^o$ and this choice of boosts. For $\delta < 0^o$, the lack of sensitivity around $\sin^2 2\theta_{13} \sim 10^{-2}$ that was present in the original study [91] is not present. The minimal $\sin^2 2\theta_{13} \sim 10^{-2}$ for which CP-conservation can be ruled out at 99 % is also slightly smaller.

In Fig.5.3, the 90%, 95% and 99% C.L. 2 parameter fits for this boost pair are presented. The overall sensitivity and the contributions from each boost are shown and have been computed on the assumption of normal mass ordering. The four true value pairs $(\sin^2 2\theta_{13}^{\mathrm{tr}}, \delta^{\mathrm{tr}}) = (10^{-3}, 60^o)$, $(10^{-3}, -60^o)$, $(10^{-2}, 60^o)$ and $(10^{-2}, -60^o)$ are shown. The choice of boosts corresponds to placing the electron capture flux on second oscillation maximum and, approximately, first oscillation maximum. The quantities $\Delta m_{13}^2 L/4E_1$ and $\Delta m_{13}^2 L/4E_2$ are therefore π
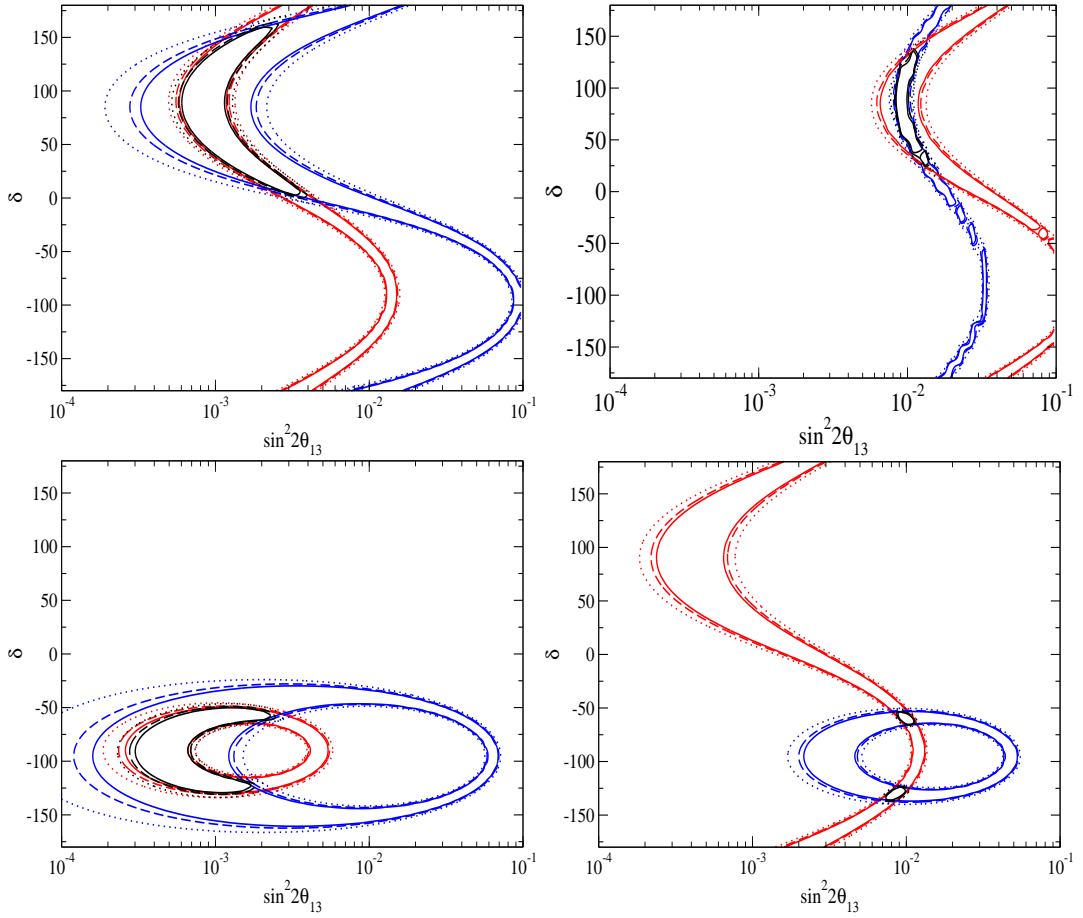
Figure 5.3.: 90%, 95% and 99% C.L. 2 parameter fits for $(\gamma_1, \gamma_2) = (440, 150)$ for the CERN-Canfranc baseline (650 km). Plots have been produced on the assumption that $\sin^2 2\theta_{13}^{\text{tr}} = 10^{-3}$ (left), 10^{-2} (right), $\delta^{\text{tr}} = 60^o$ (top) and $\delta^{\text{tr}} = -60^o$ (bottom). The blues curves correspond to $\gamma = 440$, the red to $\gamma = 150$ and the black to the overall sensitivity. Normal mass ordering has been assumed.

out of phase with each other. The sinusoidal shape in solely the cause of interference effects; the solar and atmospheric features of the appearance probability have no δ dependance.

From the right-hand panel of Fig. 5.2, it is seen that the combination of two lower boosts results in a more symmetrical sensitivity region in the (θ_{13}, δ) plane. For large values of $\sin^2 2\theta_{13}$, the effects of degeneracies are still present, especially for $\delta < 0^o$. This is of little concern, however, since measurement of $\sin^2 2\theta_{13} > 10^{-2}$ will be explored with the next generation reactor and accelerator long baseline experiments. The minimum $\sin^2 2\theta_{13}$ for which CP-violation can be established is now a factor of 4 larger. This feature is a result of a large region of equivalent solutions being present at small values of $\sin^2 2\theta_{13}$ (smaller boosts imply smaller event rates which weaken the sensitivity). By choosing two relatively small boosts, the setup has been optimised to explore the interference features of the appearance probability. In doing so, there is now a poorer resolution on θ_{13} which comes predominantly from the atmospheric features where there is no degeneracy between θ_{13} and δ. This is seen in Fig. 5.3, where the 90%, 95% and 99% C.L. 2 parameter fits are presented for the same pairs of true values as before and for normal mass ordering. The good CP-sensitivity for the boost pair is a result of the CP-features of the appearance probability being out of phase with each other. In particular, the inflexion point of the sensitivity region for one boost corresponds to the turning point of the other. There are, in general, two such points; the second corresponds to an energy degeneracy at large $\sin^2 2\theta_{13}$. This solution, however, can be ruled out by near future reactor and accelerator experiments. Note that any energy degeneracy that remains does not cross the lines $\delta = 0^o$ or $\delta = 180^o$ and therefore does not interfere with the sensitivity. The relatively poor sensitivity to CP-violation, is therefore not a consequence of any energy degeneracy; instead it can be attributed to poor $\sin^2 2\theta_{13}$ resolution and low event rates.

5.3. Useful decays and atmospheric backgrounds

In the previous sections, the optimisation of the electron capture machine was carried out assuming that 10^{18} useful ion decays per year will be available and that the number of atmospheric background events is zero. As discussed in Sec. 5.1.1, this useful decay rate is challenging and would require technology and R&D beyond that required for the standard Beta Beam ions. Zero atmospheric backgrounds is not a realistic assumption; with no energy reconstruction nor background rejection, every atmospheric event that passes the cuts will be misidentified as an ν_μ appearance event. Assuming a duty factor of 10^{-3}, i.e. only 0.1 % of the decay ring is filled with ions, there will about 0.03 atmospheric neutrino events per kton-
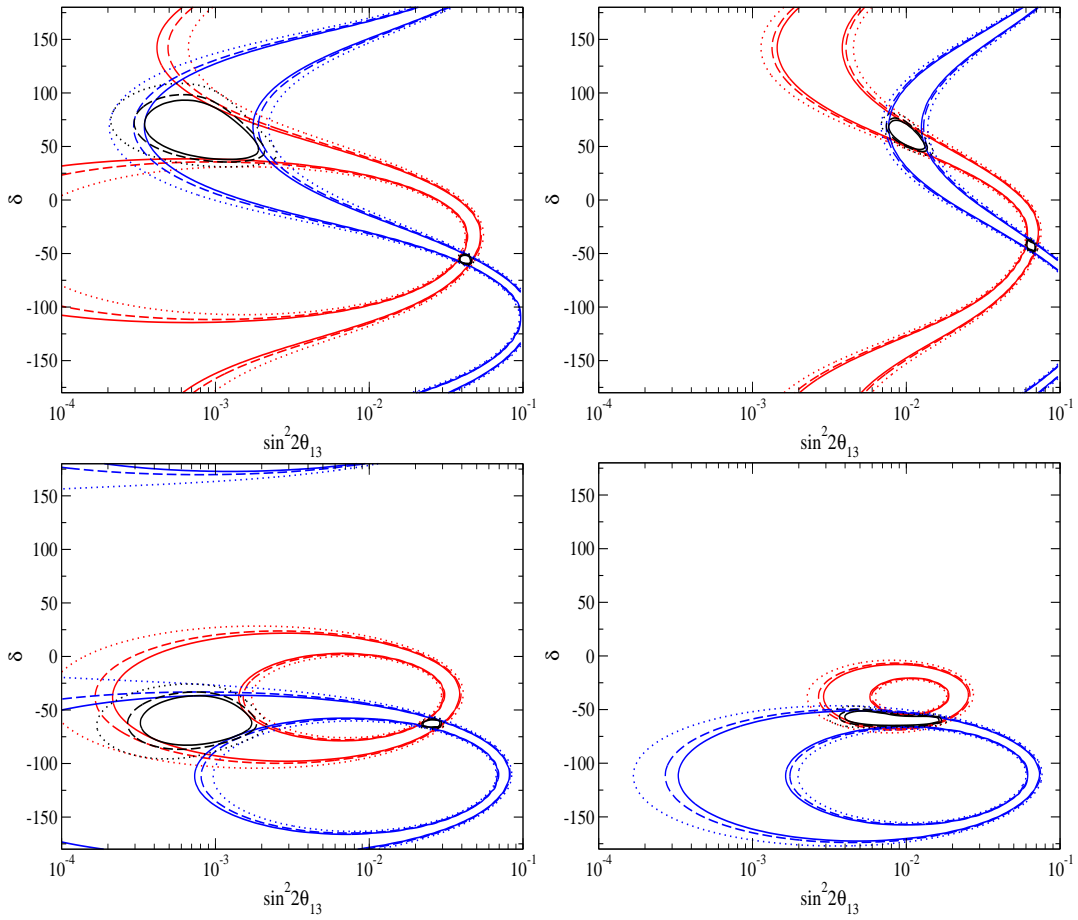
Figure 5.4.: 90%, 95% and 99% C.L. 2 parameter fits for $(\gamma_1, \gamma_2) = (280, 160)$ for the CERN-Canfranc baseline (650 km). Plots have been produced on the assumption that $\sin^2 2\theta_{13}^{\mathrm{tr}} = 10^{-3}$ (left), 10^{-2} (right), $\delta^{\mathrm{tr}} = 60^o$ (top) and $\delta^{\mathrm{tr}} = -60^o$ (bottom). The blues curves correspond to $\gamma = 280$, the red to $\gamma = 160$ and the black to the overall sensitivity. Normal mass ordering has been assumed.

year [86]. With a 440 kton detector this amounts to 13.2 events per year. This is a constant that will need to be added to the number of events for all count rates in the simulation. The effect of the atmospheric background is felt at the sensitivity boundary. In these regions, the number of events is the same order as the atmospheric background. The inclusion of the atmospheric background reduces the value of the χ^2 and pushes the boundary, at a given δ, to higher $\sin^2 2\theta_{13}$. This can be seen trivially with the Gaussian form of a χ^2. For true event rate n_i, test event rate ξ_i and overall systematic f_{sys}, the Gaussian χ^2 is given by

$$\chi^2 = \sum_{\text{bins}} \frac{(n_i - \xi_i)^2}{\xi_i + (f_{\text{sys}} \cdot \xi_i)^2} \ . \tag{5.12}$$

Inclusion of a constant background, B, is the replacement $n_i \rightarrow n_i' = n_i + B$ and similarly for ξ_i. This constant translation of the event rates leaves the numerator of the χ^2 unchanged whilst increasing the denomenator. The result is that is the χ^2 is reduced.

The physics reach of the electron capture beam cannot be stated until the atmospheric background is included. Further, it is not known what is a realistic useful decay rate per year - it is reasonable to assume that 10^{18} may well be close to an upper limit though. A technique to improve the decay rate is to increase the duty factor which in turn introduces a larger atmospheric background rate. Since the useful decay rate is not known, the approach requested by the experimentalists [165] is to treat the useful decay rate and number of atmospheric events as independent.

This analysis has been carried out and the results are presented in Fig. 5.5. The two pairs (440,150) and (280,160) with $f = 0.3$ have been re-simulated incorporating the number of background events per year and varying the number of useful ion decays. It is seen that the electron capture machine, like all Beta Beam type machines, is statistics dominated; the coverage of the $(\sin^2 2\theta_{13}, \delta)$ plane is reduced considerably with drops in the decay rate. For example, if the average number of atmospheric background events per year is 10, reducing the useful decay rate by a factor of 2 reduces the coverage by almost 10 % of the plane for both cases. When the coverage is only 35 % for 10^{18} useful decays, this is a substantial drop. A similar result, but with a lower reduction in coverage, is obtained if instead it is necessary to achieve the desired useful decay rate by increasing the duty factor.

To see this more explicitly, in Fig. 5.6, CP-sensitivity plots have been constructed (for both boost pairings) that include a constant atmospheric background of 13.2 events per year for a range of useful ion decay rates. The choice of boost pairs presented here provide excellent resolution of the energy degeneracy. As a consequence, a lower event rate merely reduces
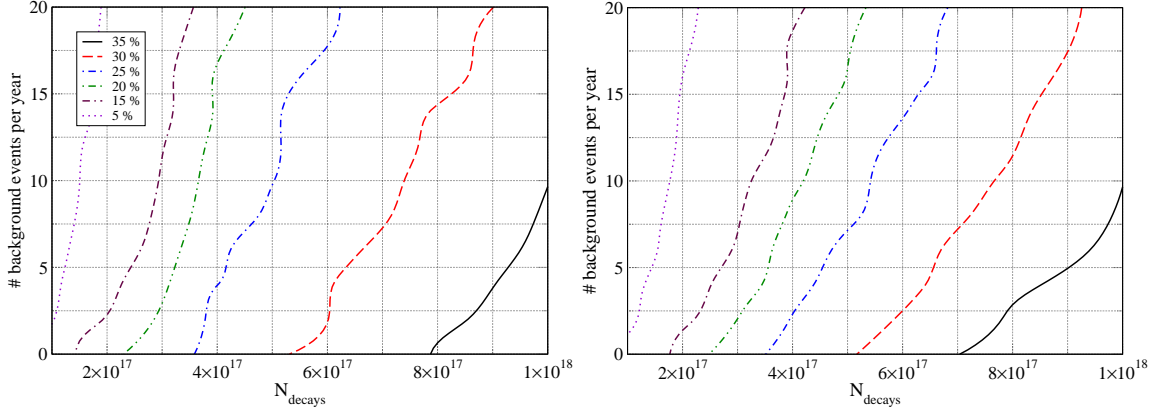
Figure 5.5.: CP-violation coverage for a dual electron capture machine with $f = 0.3$ for $(\gamma_1, \gamma_2) = (440, 150)$ (left) and $(280, 160)$ (right). Coverage is defined as the fraction of the sample grid points for which one can rule out CP-conservation at 99 %.
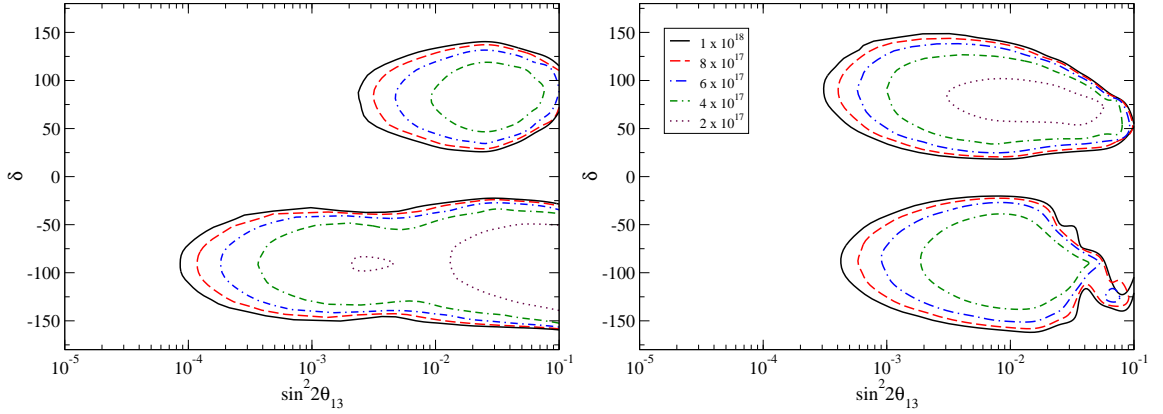
Figure 5.6.: CP-violation sensitivity at 99 % confidence level for $f = 0.3$ and $N_{\text{atm}} = 13.2$ per year for $(\gamma_1, \gamma_2) = (440, 150)$ (left) and $(280, 160)$ (right). In both cases, the sensitivity curve has been constructed for a range of useful decay rates.

to overall sensitivity of the setup, rather than let degeneracies ruin the sensitivity. The first manifestation of any degeneracy is for $N_{\text{decays}} = 2 \times 10^{17}$ for (440,150) at $\sin^2 2\theta_{13} \sim 10^{-2}$ and $\delta < 0^o$.

These plots indicate that the physics reach of the electron capture machine is a struggle between sourcing a plentiful useful decay rate whilst keeping the atmospheric background to a minimum. With binning of the neutrino signal, the constant decay rate per year can be reduced whilst keeping the useful decay rate fixed. There are two drawbacks to this idea:

1. The use of QE-events would be necessary;

2. An event reconstruction efficiency needs to be included.

The electron capture machines need to use large Water Čerenkov detectors to achieve a competive event rate: the cross-sections are small at the lower energies studied at short baselines. The energy reconstruction of neutrino events at a Water Čerenkov is through selection of quasi-elastic events which with an efficiency of about 60-70 %. This is in addition to the loss of events from not using pion or hadron events (see Fig. 2.5). At $\gamma = 440$, this amounts to 70 % fewer appearance events. There will also be a small further loss owing to finite energy resolution (some neutrinos will be recorded in adjacent bins). Binning the signal will reduce background but the reduction in events is essentially equivalent to using a smaller useful decay rate. There is therefore likely no gain in using either approach.

The boost parings with the largest CP-violation coverage are either asymmetrical in δ or symmetrical, but with a larger $\sin^2 2\theta_{13}$ limit. It is clear that unless vast improvements in the available number of useful decays per year are achieved or envisaged, the physics reach of electron capture machines cannot compete with the standard Beta Beams over equivalent baselines which can rule out CP-conservation down to $\sin^2 2\theta_{13} \sim 10^{-4}$ and are close to symmetric in δ. The reason for this is the absence of an anti-neutrino run. The need for information complementary to first oscillation data, forcing runs at smaller boosts, has reduced the overall event rate across the whole experimental run. One option to explore is whether it is possible to construct a facility with a mono-energetic anti-neutrino flux at first oscillation in combination with an equivalent neutrino flux from electron capture. The two fluxes would be complimentary with the need for additional runs at lower energies unnecessary. The event rate across the entire run of any experiment would be higher, with less susceptibility to variations in the useful decay rate. One process put forward as a complementary source of mono-energetic anti-neutrinos is the bound beta decay process (BBD) [94].

5.4. Benefits of an anti-neutrino run

In the previous sections, the physics reach of an electron capture machine was optimised; first through the variation of the boosts, then secondly by incorporating the atmospheric backgrounds and the possible restrictions on the number of ions. It was found that good coverage for CP-violation was possible provided the target of $O(10^{18})$ useful ion decays per year could be met. This is known to be very challenging and will required much R&D beyond that required for a standard Beta Beam; a recycling ring will almost certainly be necessary to minimise accelerator dead-time, in addition to new ion production techniques. In electron capture beams, one has the freedom to choose the energy of the neutrinos in the laboratory

frame by altering the boost. This has the advantage that neutrinos are no longer wasted as in a Beta Beam, but this is also the main disadvantage. In order to reach competitive sensitivities, substantial runs at lower energies, where the event rate is smaller, are necessary to extract complementary information from the appearance probability. Beta Beams in general are 'statistics dominated' which means the physics reach is high volatile to the event rate. This feature is manifest in electron capture machines, as seen in Fig. 5.5, where changes in physics reach are dramatic even with small changes in the useful decay rate. One option to explore is whether it is possible to construct a facility with a mono-energetic anti-neutrino flux at first oscillation in combination with an equivalent neutrino flux from electron capture decays, thus making the need for runs at low energies redundant. The two fluxes would be complementary with the need for additional runs at lower energies unnecessary. The event rate across the entire run of any experiment would be higher, with less susceptibility to variations in the useful decay rate. One process that has been identified as capable of sourcing mono-energetic anti-neutrinos is the bound beta decay process (BBD), introduced in Chap. 3, and will form the focus for the following sections.

The possibility of using BBD as a neutrino source for a long baseline neutrino oscillation experiment was first suggested in [94] where the authors proposed the use of ions that can BBD as well as electron capture and continuum beta decay (CBD). The paper defined the 'CP-evenness' as

$$\eta(E,\gamma) = \frac{\mathcal{F}(\nu_e;E)\sigma(\nu_\mu;E) - \mathcal{F}(\bar{\nu}_e;E)\sigma(\bar{\nu}_\mu;E)}{\mathcal{F}(\nu_e;E)\sigma(\nu_\mu;E) + \mathcal{F}(\bar{\nu}_e;E)\sigma(\bar{\nu}_\mu;E)}, \tag{5.13}$$

where the $\mathcal{F}$ are fluxes and the σ cross-sections at definite energies. Since $\mathcal{F}(\nu)\sigma(\nu)$ is the unoscillated number of events at the detector, it was suggested that an optimum neutrino beam is one with $\eta \approx 0$ (equal un-oscillated neutrino and anti-neutrino events). The authors were considering mono-energetic neutrinos, and the form of the expression reflects this.

A beam, or combination of beams, with $\eta \approx 0$ can determine the existence of CP-violation, for oscillations in vacuum, since the detector response will be symmetrical for $\delta = 0^o$ and 180°, provided θ_{13} is sufficiently large. In this case, CP-violation will manifest itself as a discrepancy between the number of μ^- and μ^+ events. In general, however, since neutrino interactions with matter are not CP-invariant, the appearance channels for neutrinos and anti-neutrinos will be different, even for $\delta = 0^o$ and 180°.

To contrast the CP-even and dual boost electron capture machine approaches, the CERN-Canfranc baseline ($L = 650$ km) is considered and CP-sensitivity analyses have been simulated for two exposures:
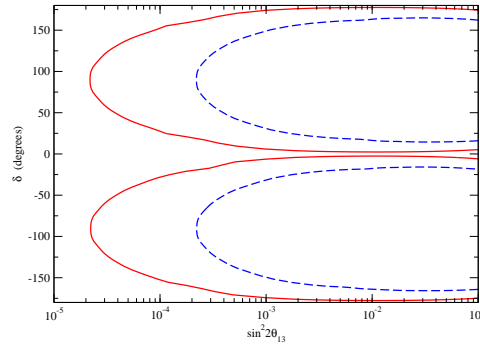
Figure 5.7.: CP-violation sensitivity at 99% confidence level for a hypothetical CP-even setup. The red solid lines correspond to an exposure of $4.4 \cdot 10^{21}$ ions-kton-years, whilst the dashed blue lines depict $5.0 \cdot 10^{20}$ ions-kton-years.

- High statistics: $4.4 \cdot 10^{21}$ ions-kton-years;

- Low statistics: $5.0 \cdot 10^{20}$ ions-kton-years.

For example, the high statistics exposure could be achieved with a 10 year run, 10^{18} useful decays per year and a 440 kton Water Čerenkov detector. Here, the number of ions refers to the electron capture ions. To achieve a CP-even setup, the same boost for neutrinos and anti-neutrinos has been assumed but the number of decays for anti-neutrinos has been increased to compensate for the lower cross-section. A χ^2 analysis has been performed using the Gaussian form with an overall systematic error of 2% included.

As seen from Fig. 5.7, the CP-even setup has symmetry between $\delta > 0$ and $\delta < 0$. The anti-neutrinos compensate for the poor sensitivity from the neutrinos in regions of parameter space, and vice versa. In addition, the anti-neutrino run, also at $\gamma = 440$, allows for higher event rates for a given exposure. Clearly, in this hypothetical setup, the CP-sensitivity coverage is far to superior to the dual boost electron machine and any Beta Beam. In order to source such a machine, however, one would need $O(10^{18})$ useful mono-energetic anti-neutrinos and separate them out from any continuum beta decay background. As mentioned previously, one possible source could be fully stripped ions that can then decay via bound beta decay. Is this a realistic proposition? It is my view that it is not and this will be justified in the following sections.

5.5. Technological challenges

In this section, the possibilty of using BBD will be discussed and some of the technological challenges articulated. First, the physics of bound beta decay will be briefly summarised before the demands on the acceleration chain and the impact on the anti-neutrino fluxes will be focussed on. In the third part, the effect of the energy resolution of the detector will examined with the likely demands on the acceleration chain investigated.

5.5.1. Bound beta decay

Recall that bound beta decay is the process

$$I_P^{Z+} \longrightarrow I_D^{Z+} + \bar{\nu}_e, \tag{5.14}$$

in which the electron is captured into an orbital and the $\bar{\nu}_e$ spectrum is mono-energetic. The process is heavily suppressed in neutral atoms owing to weak bindings and the small wave function overlaps of the outer electron orbitals. With complete ionisation, BBD can take a significant branching of the decay rate. BBD can be thought of as the inverse process of electron capture and therefore the ratio of the rates is equivalent to Eq. 5.1:

$$\frac{\Gamma_B}{\Gamma_\beta} = \frac{Q_B^2 |\Psi_n(0)|^2}{f(Q_C, Z)} . \tag{5.15}$$

For a fully ionised atom, the BBD decay Q-value Q_B^{Z+} is related to the continuum beta decay Q-values Q_C and Q_C^{Z+} via

$$\begin{aligned} Q_B^{Z+} &= Q_C \quad + |B_n(I')| - |\Delta B^{tot}(I', I)| , \\ &= Q_C^{Z+} + |B_n(I')| , \end{aligned} \tag{5.16}$$

where $|B_n(I')|$ is the binding energy of the electron captured into orbital n of the daughter nucleus and $|\Delta B^{tot}(I', I)|$ is the difference in binding energies of the complete parent and daughter atoms. The smallness of $|B_n(I')|$ is one of the principle reasons why using BBD is not a realistic proposition. This will be discussed in the context of energy resolution shortly.

To make the following discussion more explicit, some ion 'choices' are presented in Tab. 5.2. It is stressed that a concrete setup is not being considered here - the table is just for illustration. An optimal ion will have a half-life ~ 1 second [146]; however, the paucity of

Ion	Q-value (MeV)	Channel %	Half-life	$\Gamma_{BBD}/\Gamma_{CBD}$
^{20}O	2.757	99.97	13.51 sec	$9.4 \cdot 10^{-5}$
^{34}Si	2.993	100	2.77 sec	$3.6 \cdot 10^{-4}$
^{52}Ti	1.831	100	1.7 min	$8.8 \cdot 10^{-3}$
^{56}Cr	1.506	100	5.94 min	$7.0 \cdot 10^{-3}$
^{55}Cr	2.603	99.96	3.497 min	$2.1 \cdot 10^{-3}$
^{62}Fe	2.023	100	68 sec	$4.5 \cdot 10^{-3}$
^{98}Zr	2.250	100	30.7 sec	0.010
^{99}Nb	3.403	100	15.0 sec	$4.1 \cdot 10^{-3}$
^{120}Cd	1.760	100	50.8 sec	0.026
^{121}In	2.434	100	23.1 sec	0.014
^{206}Tl	1.533	99	4.199 min	0.080
^{207}Tl	1.423	99.72	4.77 min	0.138
^{209}Tl	1.832	98.8	2.20 min	0.118

Table 5.2.: A selection of ions selected based on their half-lives and dominant decay channels. The quoted Q-values are for CBD and need to modified as discussed in Sec. 5.5.1 fully stripped ions.

choice means the half-lives may be much higher. A scan of the database [157] for ions with single dominant decay channels and half-lifes in the range 0.5 sec $< t_{1/2} <$ 8 min was made[4]. Very few ions matched the criteria.

Acceleration and flux

In a Beta Beam, the radioactive ions are accelerated then stored in a ring to decay. To source a useful flux from the storage rings requires an optimal half-life $O(1 \text{ sec})$. The ions put forward for electron capture machines and BBD machines are not optimal in that they have half-lives up to several minutes and so the number of useful neutrinos sourced is several orders to low [163]. This problem could be dealt with R&D in the acceleration stage: increased production rates, reduction of losses during acceleration, and loosening of constraints on the duty factor could all lead to a boost in useful decay rate. An accumulation ring is also an option

---

[4]The asymmetry about $t_{1/2} = 1$ second is necessary so to increase the chances of finding a suitable ion.
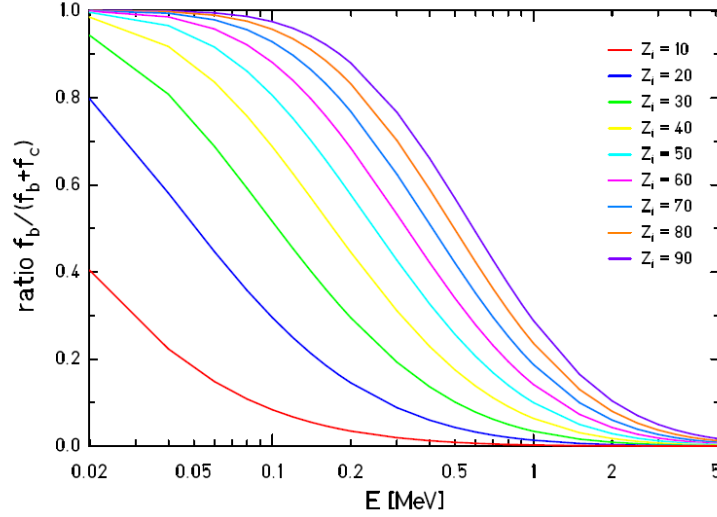
Figure 5.8.: Bound beta decay branching ratios as a function of the available energy and the proton number. These results are a fully relativistic calculation and have been taken from [138].

to compensate for the accelerator complex dead time of approximately 8 seconds [158]. For electron capture machines, the aim is to choose ions with near 100% branching ratios. This is not a luxury available to BBD sources however. As shown in Fig. 5.8, and can be seen from Tab. 5.2, the branching ratio for BBD is typically small unless the Q-value is very small or the proton number of the ion is large. However, if one wishes to source a long baseline experiment, very small Q-value ions are not an option (Tab. 5.1). Low or modest branching ratios are therefore an intrinsic feature of BBD long baseline candidate ions. For example, consider ^{207}Tl which has the highest branching ratio of the selected ions. 10^{18} useful decays is the target rate for any long baseline Beta Beam type experiment. If this could be achieved, one is still an order of magnitude short for the useful mono-energetic anti-neutrinos. In addition, to extract a useful BBD rate requires hydrogen-like atoms. Large proton numbers point to severe space charge problems, especially in the low energy part of the accelerator chain. This is in addition to the losses through ion decays in the acceleration [164]. These effects collectively force the need for an extra factor of 10 in production [165] requiring an extensive R&D program and large duty factors (up to 10%). For the electron capture proposals, this is less of a problem since electrons can be left bound to the nucleus. For an electron capture machine, the stripping of the nuclides is only a necessity for the acceleration of the ions. For a fully stripped ion, vacuum losses are not a concern since the probability of the ion capturing an electron is effectively nil [158].

Additional concerns can be brought up with respect to the boosts. For an ion boost γ, an energy E_ν in the laboratory frame is related to its rest frame counterpart by $E_\nu = 2\gamma E^{\text{rf}}$. For a

given accelerator, the maximum boost possible for an ion $^A_Z X^{N+}$ is given by

$$\gamma_{\text{ion}}^{\max} = \frac{N}{A} \gamma_p^{\max}, \tag{5.17}$$

where $\gamma_p^{\max}$ is the maximum boost of the proton and N is the number of electrons removed from the atom. For the 1 TeV machines available to Beta Beams, such as an upgraded SPS, $\gamma_p^{\max} = 1066$. Ions that beta decay lie on the neutron-rich side of the line of stability on a Segre chart, and typically have $Z/A \sim 0.4 - 0.5$. Therefore, energies ~ 1 MeV in the rest frame correspond to energies ~ 0.8 GeV in the laboratory frame at maximum boost. The attainable boosts also put tough restrictions on the energy resolution of the detector when using BBD ions, a point to which we now turn.

Detectors and energy resolution

In the previous section, a number of issues surrounding the acceleration were highlighted. BBD will now be examined in the context of the technology that is or may be available to the Beta Beam class of machines and what energy resolutions are required. In what follows, the lower limit, $\gamma_{\text{ion}}^{max} = 400$ is taken.

The ions considered in [94] could BBD, CBD and decay through electron capture. Four ions were identified with BBD Q-values ranging from 1.67 MeV to 2.46 MeV. The branching ratios were therefore low. The motivation behind this proposal was to use the BBD and electron capture spectra with the end part of the CBD spectrum to fix $\eta \approx 0$. Such a beam will contain both neutrinos and anti-neutrinos. For such a strategy, it is therefore mandatory to discriminate the μ^- and μ^+ events at the detector, as for Neutrino Factories. The Magnetised Iron Neutrino Detectors (MIND) studied for use with Neutrino Factories have thresholds > 3 GeV [56]. Neutrino energies set to first oscillation maximum will therefore be below the MIND threshold (with $\gamma = 400$) for baselines $L < 1500$ km. Magnetised variants of LAr detectors and TASD are alternatives that could provide the techniques to deal with this issue.

In what follows, it will be assumed that the neutrino and anti-neutrinos are sourced from separate ions. If one sources the electron capture neutrinos with ions which possess a Gamow-Teller resonance, as discussed earlier, then one has freedom to choose the energy of the neutrino flux, provided it is possible with the available boosts, and to alter the run time to fix $\eta = 0$. This method is therefore constrained by the choice of BBD ion, the baseline and energies required.

The shortest long baseline being considered for the future long baseline neutrino oscilla-tion program is CERN-Frejus at 130 km. Using the current values of the oscillation parame-ters [15], the energy of first oscillation maximum for the $\bar{\nu}_e \to \bar{\nu}_\mu$ channel at 130 km is 0.25 GeV. With a boost $\gamma = 400$, $Q_B > 0.315$ MeV is necessary for the mono-energetic anti-neutrino flux to get placed on first oscillation maximum at Frejus. From Fig. 5.8, it can be seen that for Z=90, BBD will make up $\sim 75\%$ of the anti-neutrino flux. Therefore the CBD fraction will be at least 25 % for all cases in which the mono-energetic neutrinos are to be placed on first maximum. From Tab. 5.2, all the ions identified have much larger Q-values. The mini-mum CBD fraction, from these choices is a much higher 85%. All these ions could place a mono-energetic source on (or around) the first oscillation maximum for the CERN-Canfranc baseline ($L = 650$ km). The CERN-Boulby baseline ($L = 1050$ km) requires a minimum $Q_C \sim 2.5$ MeV. From the ions selected, no more than 1 % BBD would be possible. Therefore, in all conceivable cases, a substantial flux from the CBD is to be expected and it is important to understand what energy resolutions are required if the use BBD ions is to be advocated.

Consider a setup in which the separation of the CBD and BBD (capture into a $1s_{1/2}$ state) channels at the detector is a requirement. In the rest frame, the two channels are split by the difference between the CBD and the BBD Q-values: the electron binding energy $B_1(Y)$. Therefore, for a detector with energy resolution ΔE, to separate the channels one requires

$$\Delta E < 2\gamma B_1(Y). \tag{5.18}$$

For example, ^{207}Tl^{81+} has $B_1(Y) = 99$ keV. For a detector with $\Delta E = 150$ MeV, a boost $\gamma > 750$ is required. Since $B_1(Y) \propto (Z+1)^2$, where Z is the proton number of the parent, the γ factors required will be larger than this for other ions. With the accelerators expected to be available to the community, such as an upgraded SPS and the Tevatron, CBD and BBD cannot be separated for this example. A substantial portion of the anti-neutrino flux will always, therefore, be sourced from the CBD. If creating hydrogen like ions is problematic, the BBD neutrinos will be suppressed, or effectively reduced to nil. In that case, one would have a high Z anti-neutrino Beta Beam.

5.6. Summary and remarks

In this chapter, the work of collaborators [91] examining the CP-violation reach of an electron capture machine has been extended. In [91], a 440 kton fiducial mass Water Čerenkov detector was considered for the CERN-Frejus and CERN-Canfranc baselines. The mono-energetic

neutrinos were sourced from ^{150}Dy and two boosts were considered for equal run times. The results of that study indicated that discovery of CP-violation would be possible (for some δ) down to $\sin^2 2\theta_{13} \sim 10^{-4}$, competitive with large boost European Beta Beam proposals [86]. However, the initial study did not include systematic errors and atmospheric backgrounds, nor did it attempt to find the optimal boost pairing and the respective run times. That was the principle task of this chapter.

Since the simulation of electron capture machines is not as complex nor time consuming as the simulation of a neutrino facility with a spectrum and energy reconstruction, it is possible to perform a CP-violation analysis for many different pairs of boosts on a reasonable time scale. The CP-coverage was simulated for the CERN-Canfranc baseline with a 440 kton fiducial mass Water Čerenkov detector and with ^{150}Dy as the source ion. Two large coverage regions of the (γ_1, γ_2) plane were found: the naive pairing of first and second oscillation maximum; and a boost close to second oscillation maximum and a boost just beyond the first oscillation minimum, on the rise towards first oscillation maximum. The maximum CP-coverage for the cases considered was for a run time fraction $f = 0.3$ and $(\gamma_1, \gamma_2) \sim (280, 160)$. The shape of the (θ_{13}, δ) coverage regions were not equivalent, however. For the combination of first and second oscillation maximum, the CP-violation reach was asymmetrical in δ with sensitivity down to $\sin^2 2\theta_{13} \sim 10^{-4}$ for $\delta < 0^o$ but only $\sin^2 2\theta_{13} \sim 10^{-3}$ for $\delta > 0^o$. The $(\gamma_1, \gamma_2) \sim (280, 160)$ pairing, on the other hand, had a symmetrical CP-violation reach with sensitivity down to $\sin^2 2\theta_{13} \sim 3 \times 10^{-4}$.

The above results were obtained for 10^{18} useful ion decays per year and no atmospheric backgrounds. If one assumes a duty factor $S_f = 10^{-3}$, there will be 13.2 atmospheric neutrino events per year in a 440 kton detector. Since an electron capture machine needs R&D in addition to that for the standard Beta Beam, it is not clear whether 10^{18} useful ion decays per year can be achieved with a suppression of 0.1 %. The next stage was therefore to examine the coverage as a function of the number of useful ions and atmospheric backgrounds, treating both as independent variables. It was found that the number of useful decays was the more important experimental parameter: in both pairings considered, a halving of the useful decay rate reduced the coverage by around 10 %; whereas a doubling of the atmospheric background only diminishes the coverage by a few %. For the symmetrical CP-coverage facility, a useful decay rate of $N_{\mathrm{decays}} = 6 \times 10^{17}$ is required to reach the $\sin^2 2\theta_{13} \sim 10^{-3}$ level, assuming a 13.2 atmospheric event rate per year.

The limitation of the electron capture method is the need to run for substantial periods of time at low energies. An option would be to combine an electron capture experiment with an equivalent mono-energetic anti-neutrino beam at the same energy. Such a flux will

complement the neutrino flux rendering the need for runs at low energies unnecessary. An idea put forward in [94] to use the anti-neutrino flux from ions that bound beta decay was critiqued. The useful decay rates of mono-energetic anti-neutrinos will be very low and inseparable from the continuum flux unless either the boost is extremely large (beyond a 1 TeV machine) or energy resolution is exceptional. These two points are also correlated with the lack of ions with an appropriate half-life for a Beta Beam-type machine.

The plausibility of an electron capture machine rests on the ability to achieve a sufficiently high useful decay rate. The ions in the Gamow-Teller resonance region of the Segre plot are not very interesting for nuclear Physicists [165] and so little research has been carried out searching for fast decays with a resonance and production methods for these ions; although there is a possibility some R&D will be performed in the near future [166]. Without this extra work, I see no reason to promote the electron capture machine over a standard Beta Beam for short European baselines.

Chapter 6.

Hybrid Beta Beams

In the previous chapter, the physics reach and experimental obstacles of mono-energetic neutrino long baseline oscillation facilities were presented. It was pointed out that the configuration of such machines are limited by the Q-values of candidate ions and the need for the decay to be dominated by a Gamow-Teller resonance. In this chapter, the physics reach of facilities using source ions not in possession of a resonance will be considered; such machines shall be referred to as '*hybrids*'. For ions with $Q \sim 3 - 4$ MeV, one would expect the the branching ratios of the positron decay and electron capture decay to be of similar size. Source ions with a dominant positron decay would constitute a high-Z Beta Beam and will not be considered as they are of no interest.

There are a number of reasons for studying facilities that use both positron decay and electron capture decay to source their neutrino flux:

- The option should be investigated in its own right.

- To see if there any benefit in concentrating the high energy neutrinos of a standard Beta Beam into a narrow energy range in combination with a low energy Beta Beam flux.

- A hybrid setup may possess degeneracy breaking properties not available to simpler neutrino spectra. Specifically, is there a physics motivation for attempting this more challenging facility?

- The simulation of the hybrid provides a toy setup to explore the synergy between the low and high energy neutrino events; and equivalently, the role of the atmospheric, interference and (to a lesser extent) the solar features of the appearance probability.

All these motivations (to some extent) overlap, differing only in their perspective. On embarking on this study, I took the view that hybrid setups should be studied for completeness

with the main physics focus on the fourth motivation. For a similar number of useful decays and a similar energy range in the laboratory frame, one would expect similar physics reach to a standard Beta Beam. It is was shown in Chap. 3 that with good energy resolution, a $\gamma = 450$ Beta Beam could achieve sensitivity down to $\sin^2 2\theta_{13} \sim 10^{-4}$ for CP-violation. I expected the hybrid to perform in a similar manner but possibly with complex 99 % C.L. sensitivity regions in the (θ_{13}, δ) plane. In such an eventuality, there is no reason push the community towards a hybrid Beta Beam which would require extra experimental resources and ingenuity for similar physics reach that could be obtained with less effort. This view was borne out by the simulations.

In this chapter I will summarise the study of hybrid Beta Beams carried out in [92] with the focus on CP-violation. The physical case study will be introduced and the strategy followed will be presented. The results of the simulations include analyses looking into the separate contributions of the two channels and CP-violation sensitivity. The chapter will finish with some remarks about the feasibility of a hybrid Beta Beam and its place in any strategy towards a future long baseline neutrino oscillation experiment.

6.1. The Beta Beam and electron capture combination

In this section, the hybrid Beta Beam setup studied in [92] will be presented. I will briefly review the physics of the ions that can decay through both positron decay and electron capture taking care over the definition of the Q-value and endpoint energy. Two ions were identified for this study: ^{156}Yb and $^{148m}_{65}$Tb. Their physical properties will be summarised before a physics strategy based on the first will be sketched.

Recall that in an electron capture decay an electron is consummed from the initial state whereas for a positron decay the electron needs to be created in the final state. Therefore, for the same nuclear transition, the maximum neutrino energy available in the positron decay is the energy available to the neutrinos in the electron capture minus twice the electron mass. Define, as usual, the endpoint energy for the positron decay, E_0, as the energy available to the decay. Then the maximum energy available to the neutrinos in the positron decay is given by $Q_\beta = E_0 - m_e$, where m_e is the mass of the electron. The energy of the neutrinos from the electron capture decay is then given by

$$Q_{\text{EC}} = E_0 + m_e = Q_\beta + 2m_e \,. \tag{6.1}$$

Decay (i-channel)	Daughter	Q_i^{eff} (MeV)	BR
β^+	$^{156}_{69}\text{Tm}^*$	2.44	52%
EC	$^{156}_{69}\text{Tm}^*$	3.46	38%
α	$^{152}_{68}\text{Er}$	4.81	10%

Table 6.1.: Decay summary for $^{156}_{70}\text{Yb}$. The Q_{EC}-value for the transition between ground states is 3.58 MeV and taking into account the excitation energy of the final nuclear state (0.12 MeV), the effective $Q_{\text{EC}}^{\text{eff}}$-value is 3.46 MeV [169, 156].

When there are two decay channels, the advertised Q-value is Q_{EC}, but this will also need to be corrected for any excitations. For example, the decay energy of ^{156}Tb in the web-based databases [157] is given as 3.58 MeV. Studies have shown that the decay is in fact into an excited state of Thuliam with energy 0.12 MeV. The appropriate energies are therefore $Q_{\text{EC}} = 3.48$ MeV and $Q_\beta = 2.44$ MeV.

For an ion with dominant positron decay and electron capture decay channels (both from the same nuclear transition) one expects the branching ratios to satisfy

$$\frac{\Gamma_{\text{EC}}}{\Gamma_\beta} \propto \frac{(\alpha Z)^3}{Q^3} \ . \tag{6.2}$$

For ions with $E_0 \sim 3-4$ MeV, similar branching ratios are expected. When searching for ions, it should borne in mind that for high-Z nuclei that are proton rich, α-decay is a possible decay channel. Candidate ions with no α-decay channel are therefore preferred, or if they exist, low α-decay Q-values are required. This ensures the α-decay is slow so that the weak decay processes can dominate. Given these constraints, and the need for ion half-lives in the region of a second to several minutes, one would expect to find many potential ions. In reality, a scan of the nuclear databases returns very little. Nuclear studies of the target area of the Segre chart have been carried out; however, they are not comprehensive enough in the context of hybrid Beta Beams. Accurate breakdowns of the different decay channels, both the nature of the decay and the nuclear transition are lacking. Positron decays and electron capture decays are often reported together; for example, the details for ^{156}Yb reported in Table 6.1 will not match the online databases. The branching ratios presented here instead come from a recent study [156].

Decay (i-channel)	Daughter	Q_i^{eff} (MeV)	BR
β^+	$^{148}_{64}$Gd*	2.05	32%
EC	$^{148}_{64}$Gd*	3.07	68%

Table 6.2.: Decay summary for $^{148m}_{65}$Tb. The Q_{EC}-value for the transition between ground states is 5.77 MeV and the effective $Q_{\text{EC}}^{\text{eff}}$-value to the excited state is 3.07 MeV [170, 168, 171].

The relevant data for ^{156}Yb and $^{148m}_{65}$Tb are presented in Tables 6.1 and 6.2 respectively. (All the known nuclear structure information on the $A = 148$ and $A = 156$ nuclides has been reviewed in Ref. [168] and Ref. [169], respectively, where the data obtained in various reaction and decay experiments is presented, together with adopted level schemes.) $^{156}_{70}$Yb is a nuclide with spin-parity 0^+, which decays 90% via electron capture plus β^+-decay [169], split as 38% via electron capture and 52% via β^+-decay [156]. The remaining 10% goes into alpha particles. The α-decay has a relatively small branching ratio as a result of its small Q-value. The higher end-point energies of hybrid candidate ions also helps from a acceleration point of view; the half-lives are in general closer to the optimum half-life than the mono-energetic electron capture ion candidates. The electron capture-β^+-decay transition has only one possible daughter state with spin-parity 1^+, i.e., a Gamow-Teller transition into an excited state of Thulium, $^{156}_{69}$Tm*. As previously mentioned, the excitation energy of the final nuclear state (0.12 MeV) needs to be taken into account; the effective Q_{EC}-value is 3.46 MeV [169].

The $^{148m}_{65}$Tb isomer with spin-parity 9^+ was also identified, having a Q_{EC}-value of 5.77 MeV [168, 170]. Although the decay to the ground state of $^{148}_{64}$Gd is highly forbidden, the presence of a Gamow-Teller resonance allows the decay into an excited state with effective Q-value 3.07 MeV [171]. This nuclide, however, is longer lived with a half-life of 2.2 minutes. This ion was ruled out since the electron capture channel is more dominant than desired; providing insufficient information to obtain the good sensitivities aspired to by future long baseline experiments. It was shown in the previous chapter that multiple runs are necessary for an exclusive or dominant electron capture channel to achieve a good physics reach. Use of this ion is was expected to return poor results and hence the study of the hybrid approach in this chapter will focus on ^{156}Yb.

Machine	γ_{max}	$2\gamma_{max}Q_{EC}^{eff}$ (GeV)	$2\gamma_{max}Q_{\beta+}^{eff}$ (GeV)
SPS	166	1.15	0.81
Upgraded SPS	369	2.55	1.80

Table 6.3.: Maximum boosts and neutrino endpoint energies for ^{156}Yb available for the current SPS setup and a proposed 1 GeV upgraded SPS.

6.1.1. Choice of γ and baseline

In the study [92], we adopted the arbitrary restriction that 16 electrons should be left on the ion to assist in the acceleration and storage [165]. As mentioned in the previous chapter, this is an experimental request and not a necessity. The maximum boost, γ_{max}, available is thus given by

$$\gamma_{max} = \frac{E_{acc}}{m_p} \frac{Z-16}{A} \,, \tag{6.3}$$

where m_p is the mass of the proton and E_{acc} is the 'maximum' energy accessible with the accelerator. In the analysis, the maximum boosts available from the current SPS and upgraded SPS will be considered. These are presented in Table 6.3 for reference.

With the maximum energies possible, CERN-Frejus (130 km) and CERN-Canfranc (650 km) are the feasible baselines for facilities based on the current SPS. With an upgraded SPS, the CERN-Gran Sasso (730 km), Polkewice (950 km) and CERN-Boulby (1050 km) baselines can then be used. In this study, we focussed on the following baselines and boosts;

1. **Boost $\gamma = 166$ with current SPS**

   - CERN-Frejus (130 km)

   - CERN-Canfranc (650 km)

2. **Boost $\gamma = 369$ with an upgraded SPS**

   - CERN-Canfranc (650 km)

   - CERN-Boulby (1050 km)

From Fig. 6.1b and Tab. 6.3, the current magnetic rigidity of the SPS can place the electron capture neutrino flux on first oscillation maximum for the CERN-Canfranc baseline (650 km) with the Beta Beam spectrum peaking around the second oscillation maximum. For such a
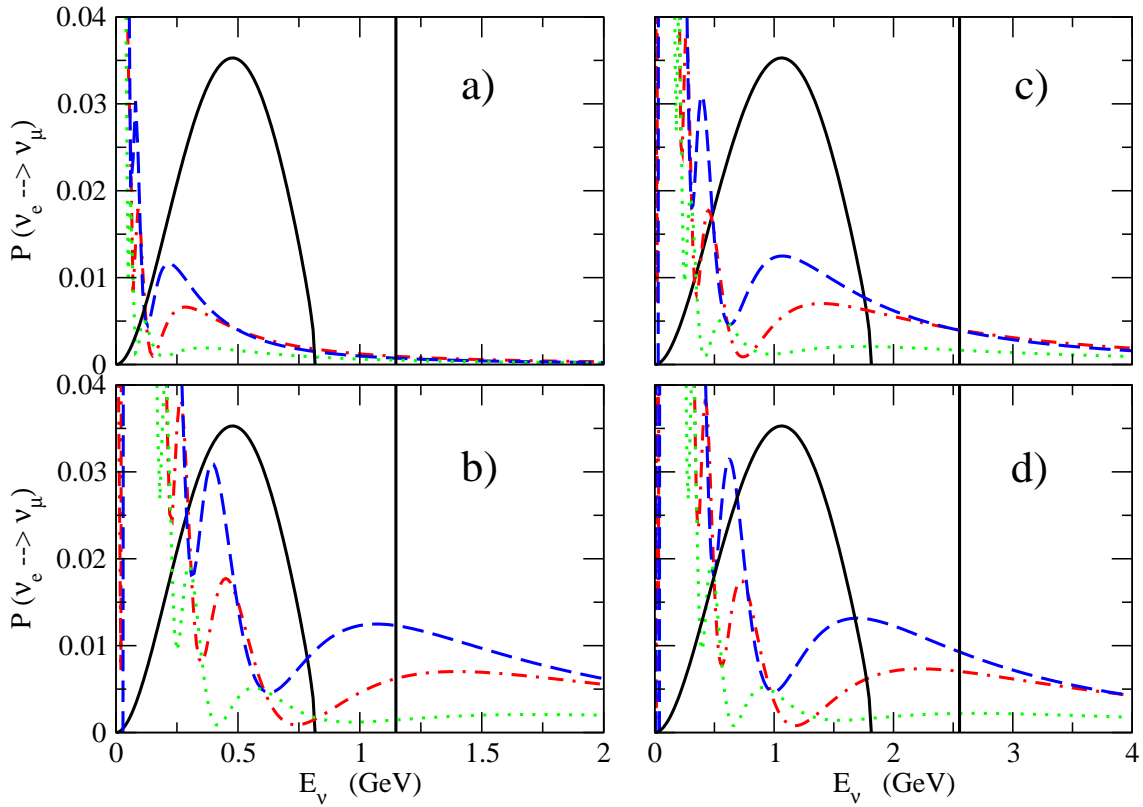
Figure 6.1.: $\nu_e \to \nu_\mu$ appearance probabilities for the *(Panel a)* CERN-Frejus (130 km), *(Panel b)* CERN-Canfranc (650 km), *(Panel c)* CERN-Canfranc (650 km) and *(Panel d)* CERN-Boulby (1050 km) baselines. In all cases, the dash-dotted lines correspond to $\delta = 0°$, dashed lines to $\delta = 90°$ and dotted lines to $\delta = -90°$. The value $\sin^2 2\theta_{13} = 0.01$ was taken for all curves. The unoscillated ν_e flux in the laboratory frame is also shown (solid lines) for ^{156}Yb given a boost $\gamma = 166$ (left panels) and $\gamma = 369$ (right panels) in arbitrary units. Figure reproduced from [92].

choice, a detector with a low energy threshold is necessary to exploit the oscillatory structure of the appearance probability. For the CERN-Frejus baseline, on the other hand, events from first oscillation maximum are available only. The electron capture neutrino flux is far into the probability tail and it contribution is expected to be minimal. With a 1 TeV SPS, the electron capture beam could be placed at first oscillation maximum, or on the probability tail, for the CERN-Boulby baseline (1050 km) or, using the Tevatron, for the FNAL-Homestake baseline (1280 km).

6.1.2. Choice of detector

From the previous chapter, the electron capture machine does not necessarily need energy reconstruction of the neutrino events at the detector; the neutrino energy is given by the choice of ion and boost factor leaving no need for this. Energy reconstruction can be used to reduce the atmospheric background, but this is done at the expense of lower efficiencies in the detector which in turn does not guarantee improved physics reach. For the hybrid approach, energy reconstruction is necessary for the Beta Beam flux, but not, in principle, to separate the energy of the line spectrum from the continuous spectrum. To see this[1] suppose an event is identified to be an QE elastic event with energy $E_\nu(\text{QE})$, then it must be the case that the true energy $E_\nu^{\text{true}} \geqslant E_\nu(\text{QE})$. There are then two cases

1. If $E_\nu(\text{QE}) < 2\gamma E_0^\beta$ then the event originates from the Beta Beam or is some form of background.

2. If $E_\nu(\text{QE}) > 2\gamma E_0^\beta$ then the event must have come from the electron capture flux (or a background) and there is no need to reconstruct the energy exactly since the true energy is known.

The separation between the energy of the electron capture events from the end-point events of the Beta Beam is $2m_e\gamma$ in the laboratory frame. Since this is large, i.e. several bins, the separation of the two fluxes should be possible with minimum error. This was assumed throughout the study.

In the analysis, two strategies with regard the detector type were followed. A generic detector technology, which could be LAr or TASD, with a fiducial mass of 50 kton and a 500 kton (fiducial) Water Čerenkov detector. For the generic detector, the energy reconstruction is assumed to come from the charged current events whilst the Water Čerenkov can only use the

---

[1]This argument is attributed to Jose Bernabeu.

quasi-elastic events. However, the information from the inelastic events is included in a single bin since no spectral information can be taken from these. Perfect efficiency is assumed for the 50 kton detector (which can be easily scaled), and 70 % efficiency for the Water Čerenkov detector.

Based on the selected boost factors and baselines, the type of detectors were assigned in the following manner in the analysis

1. **50 kton detector (LAr or TASD) with 2×10^{18} ions/yr**

   - Setup I: CERN-Frejus (130 km) and $\gamma = 166$

   - Setup II: CERN-Canfranc (650 km) and $\gamma = 166$

   - Setup III: CERN-Canfranc (650 km) and $\gamma = 369$

   - Setup IV: CERN-Boulby (1050 km) and $\gamma = 369$

2. **500 kton Water Čerenkov detector with 2×10^{18} ions/yr**

   - Setup III-WC: CERN-Canfranc (650 km) and $\gamma = 369$

   - Setup IV-WC: CERN-Boulby (1050 km) and $\gamma = 369$

The choice of the number of ions per year, 2×10^{18} ions/yr, is arbitrary as the ion production rate for ^{156}Yb has not been studied. This choice is similar to the target rates for the standard Beta Beam. Since the hybrid is essentially a Beta Beam with a non-trivial flux, it is expected that a similar useful decay rate is required to achieve competitive results.

A running time of 10 years for all the experimental configurations was considered. In all setups, an energy threshold of 250 MeV is taken with 200 MeV bins above that value, except for non-QE events in Water Čerenkov detectors which are grouped in a single bin. For the electron capture events a single bin was always taken. All the simulations in this chapter were carried out by Catalina Espinoza. Although not significant, there is a slight difference compared to the earlier chapters in how the hierarchy degenerate solutions are located. In the location of the degenerate solutions, the mimisation was performed by marginalising over all the unknown oscillation parameters. The errors on θ_{12}, θ_{23}, Δm_{32}^2 and Δm_{31}^2 were incorporated via the addition of priors as described in Chap. 2. Once the degenerate solution was located, the 2 parameter fits and the CP-violation analyses were carried out keeping these parameters fixed.

6.2. Contribution of the channels

Firstly, the study of the combination of the channels is presented. The performance of the Beta Beam (upper row), electron capture (middle row) and their combination (lower row) is shown for $\theta_{13} = 1°$ and $\delta = 90°$ for setup I (left column) and setup II (right column), at 90%, 95% and 99% confidence level (CL) in Fig. 6.2. Setups I and II use a low boost factor, $\gamma = 166$ and a 50 kton detector. The sensitivity to θ_{13} and δ is very limited as a consequence. Specifically, CP-violation can be established only for a small range of values of the δ phase and only if θ_{13} is close to the present bounds. As seen from the right panels of Fig. 6.2, the Beta Beam channel contributes very little to the overall sensitivity of the setup. This is a consequence of the γ^2-dependence of a Beta Beam flux and the small cross-sections at the energies centred on second oscillation maximum. With a scarce count rate from the Beta Beam, the bulk of the sensitivity comes from the electron capture channel. The hierarchy clone solution has been included but does not change the findings at these short baselines.

In Fig. 6.3, the contours for Setup III as presented for $\delta = 90°$ and for the cases $\theta_{13} = 1°$ (left column) and $3°$ (right column). Similarly to Fig. 6.2, in Fig. 6.3, the contributions from both the β^+-decay (upper row) and electron capture (middle row) channels are shown in addition to the total sensitivity (lower row). The effect of placing the electron capture flux in the tail of first oscillation maximum has also given the Beta Beam flux coverage of the second oscillation maximum and substantial portions of the first oscillation maximum. Comparing the $\gamma = 166$ and $\gamma = 369$ cases for the CERN-Canfranc baseline, the influence of the Beta Beam neutrinos and electron capture neutrinos are interchanged. From Fig. 6.1, the Beta Beam spectrum covers the first oscillation maximum. The Beta Beam contribution is now much more pronounced with substantial information coming from the first oscillation maximum in addition to a now larger count rate from the second oscillation maximum.

This setup best demonstrates how the Beta Beam and electron capture beam combine. Separately, both fluxes suffer from a continuum of allowed solutions. From Fig. 6.2, the gain in combining the two channels is in the difference in the phase and amplitude between the two sinusoidal regions. The combination constrains the correct solution to a much narrower region of parameter space than either of the two techniques separately. However, for $\theta_{13} = 3^o$ some energy degeneracy still remains at 99 % confidence level.

Finally, the same analysis is performed for setup IV and is presented in Fig. 6.4. The CERN-Boulby baseline (1050 km) and $\gamma = 369$ should be considered as an intermediate case - the position of the electron capture neutrino flux is neither on first oscillation maximum nor
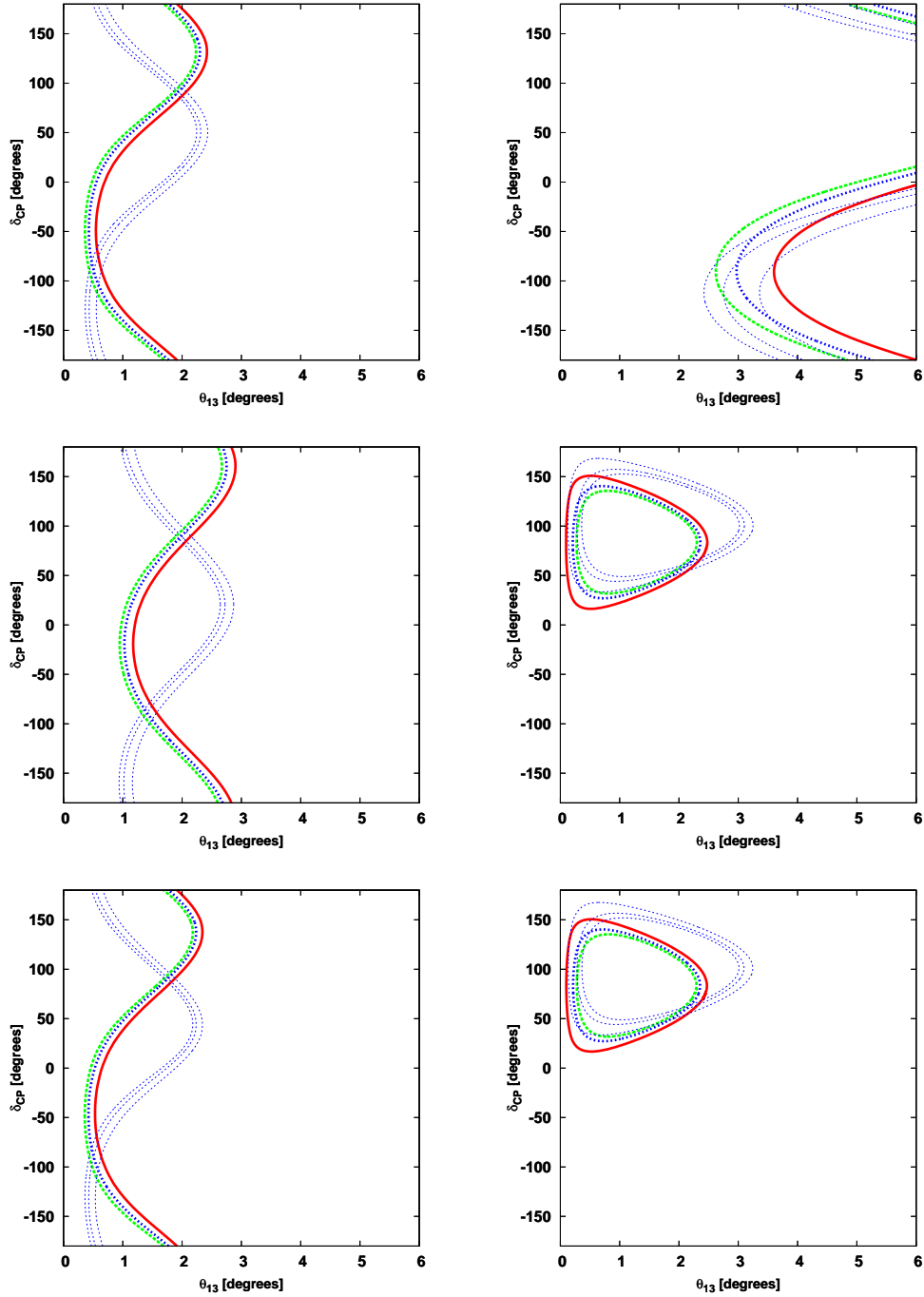
Figure 6.2.: 90%, 95% and 99% CL contours for setup I (left panels) and setup II (right panels). The parameters $\theta_{13} = 1°$ and $\delta = 90°$ have been taken assuming normal mass ordering and $\theta_{23} = 45°$. The thick lines in red, blue and green correspond to the case of true normal hierarchy, while the fine blue dotted lines indicated the clone solution for the wrong inverted hierarchy. The upper row is the contribution of the beta-beam, the middle row is that of the electron capture channel while the lower row, being the combination, shows the overall sensitivity. The contours for the hierarchy clone solution are also shown (dashed blue lines).
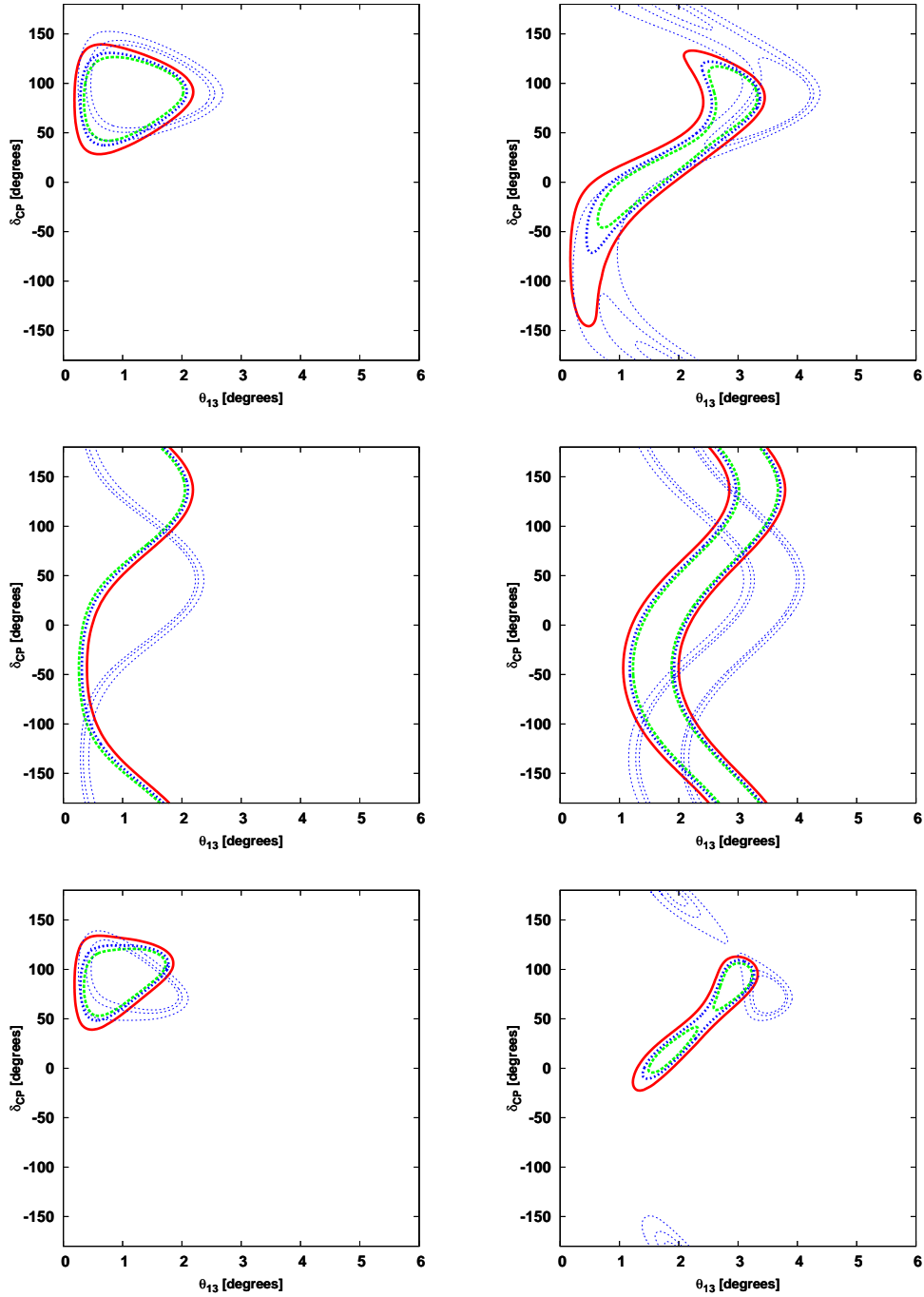
Figure 6.3.: 90%, 95% and 99% CL contours for the setup III. The left column is simulated for $\theta_{13} = 1°$ and $\delta = 90°$ assuming normal mass ordering and $\theta_{23} = 45°$. The right column is the same but for $\theta_{13} = 3°$. The upper row is the contribution of the beta-beam, the middle row is the electron capture channel with the lower row being the combination, showing the overall sensitivity. The contours for the hierarchy clone solution are also shown (dashed blue lines).

far into the probability tail. The Beta Beam in this case therefore has coverage of both the first and second oscillation maxima regions. Here the electron capture channel shows similar behaviour to its sensitivity in setup III. Although some information from first oscillation maximum is available to the Beta Beam (the characteristic sinusoidal shape of first oscillation maximum and higher energies is not dominant), the bulk on the sensitivity is derived from the events around second oscillation maximum. This means that the combination of channels is also important here. The lack of concurrence of the Beta Beam and electron capture allowed regions means that their combination constrains δ and θ_{13} in small ranges.

6.3. Sensitivity to CP-violation

In this section, the sensitivity to CP-violation will be presented for the $\gamma = 369$ setups only as, from the previous section, the sensitivity is very limited for the $\gamma = 169$ options.

The CP-violation discovery potential is shown in Fig. 6.5 for the 50 kton generic detectors, and in Fig. 6.6 for the 500 kton Water Čerenkov detector. In both figures, the CERN-Canfranc baseline is displayed in the left panel and the CERN-Boulby baseline is on the right. In all cases, the results are presented for the Beta Beam only (blue dotted lines); the overall sensitivity of the combination (red solid lines); both without (thin lines) and with (thick lines) taking the hierarchy degeneracy into account. This presentation has the benefit of separating out the effect of the hierarchy and energy degeneracies. For example, in all cases, the inclusion of the electron capture channel improves the sensitivity as the impact of the energy degeneracy and the continuum of allowed solutions is severely weakened or removed. This is to be expected from the discussion of the previous section. With a single channel, the 99 % confidence level region often crossed the $\delta = 0^o$ or $\delta = 180^o$ lines or both. Consequently, CP conservation cannot be ruled out. The addition of the electron capture channel constrained the solution to close to its true value, limiting the closeness of the 99 % contours to CP-conservation.

The sensitivity to CP-violation is greatly affected by the presence of the hierarchy degeneracy. This is seen in all cases, especially for $\delta < 0^o$ where its inclusion results in loss of sensitivity by a couple of orders of magnitude in $\sin^2 2\theta_{13}$. To understand this, in Figs. 6.7 and 6.8, the 90 %, 95 % and 99 % confidence level contours are shown for setups III-WC and IV-WC. In both cases, the setups have been simulated for $\theta_{13}^{tr} = 1^o$ (left) and $\theta_{13}^{tr} = 3^o$ (right), and $\delta^{tr} = -90^o$, 0°, 90° and 180°. For CERN-Canfranc, the degenerate solutions exist within similar δ ranges for $\delta^{tr} = 90^o$, whereas for $\delta^{tr} = -90^o$, the location of the fake solution exist at different δ. Specifically, the degenerate 99 % confidence regions for CERN-Canfranc cannot
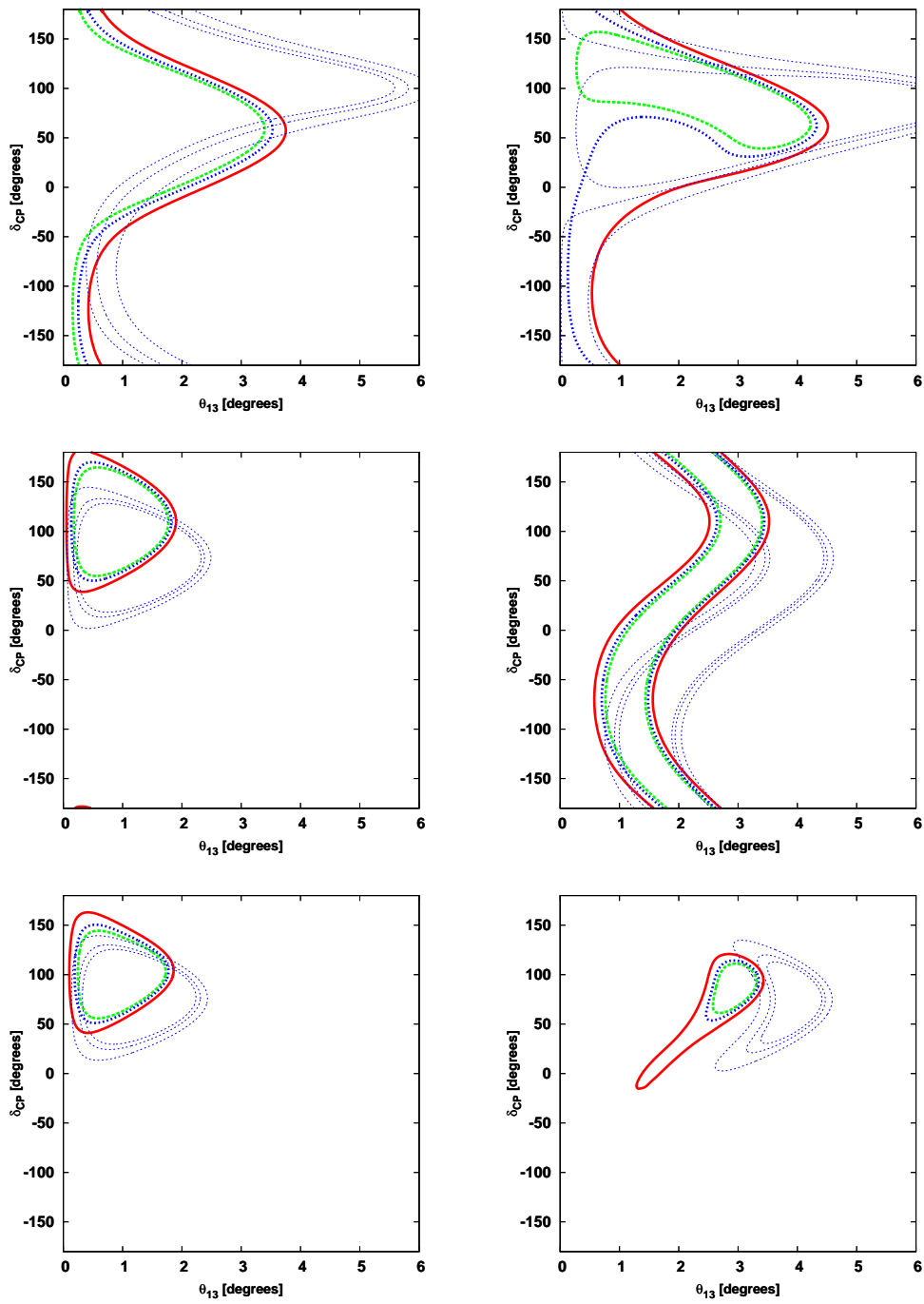
Figure 6.4.: Same as Fig. 6.3 but for setup IV.
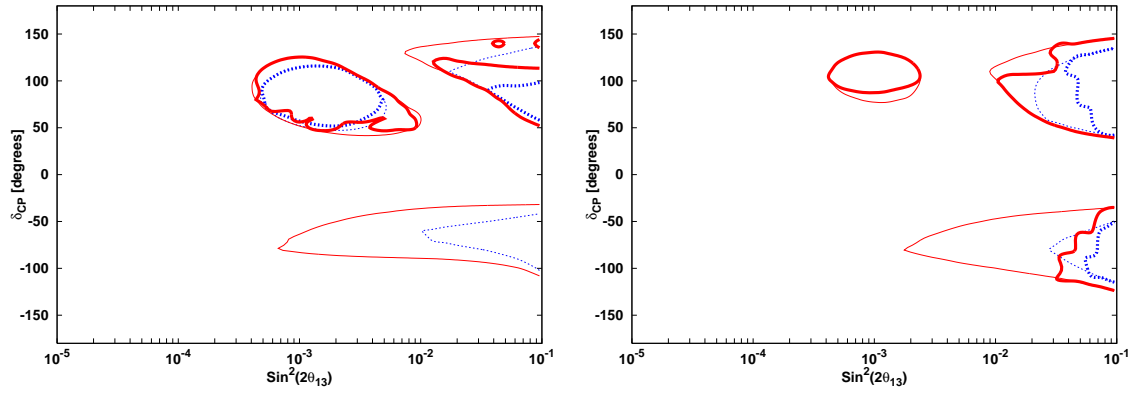
Figure 6.5.: CP-violation discovery potential at 99% CL for setup III (left panel) and IV (right panel). In each case, we present the results for the beta-beam only (blue dotted lines) and the combination with the electron capture result (red solid lines), both without (thin lines) and with (thick lines) taking the hierarchy degeneracy into account.
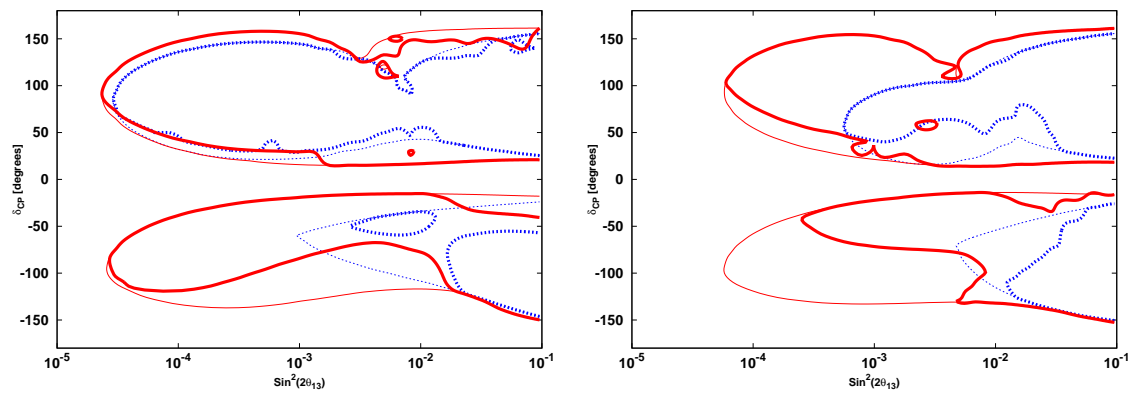
Figure 6.6.: Same as Fig. 6.5 but for setup III-WC (left panel) and setup IV-WC (right panel).
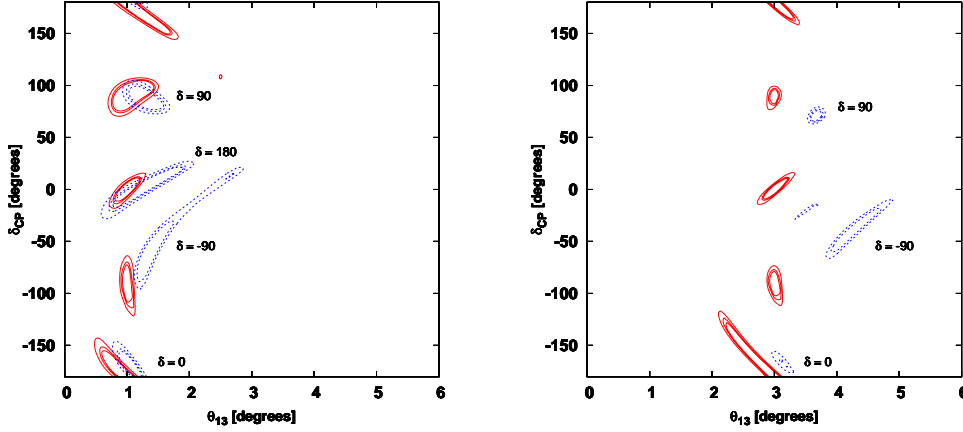
Figure 6.7.: 90%, 95% and 99% CL contours for setup III-WC with solutions from discrete degeneracies included for $\theta_{13} = 1°$ (left panel) and $\theta_{13} = 3°$ (right panel) for different values of the CP-phase, $\delta = -90°, 0°, 90°, 180°$.

be distinguished from CP-conservation except at large θ_{13}. With its larger matter effect, the CERN-Boulby baseline, the hierarchy degeneracy is stronger; however, with reconstruction of the oscillation spectrum, this baseline is in a better position to resolve them. This is seen in the right panel of Fig. 6.8 where only the $\delta^{tr} = 90^o$ hierarchy clone remains. Therefore the results with and without the hierarchy clone are not significantly different for this baseline, except for some $\delta^{tr} < 0^o$ where the problem persists.

Overall, it is noted that the CERN-Canfranc baseline has a better reach for CP-violation than CERN-Canfranc since at fixed boost, the un-oscillated flux scales as $1/L^2$. The CERN-Boulby baseline is better at resolving the hierarchy degeneracy, however this does not completely compensate for the small event rates. The sensitivity to CP-violation is therefore worse, but by no means poor. Trivially, the WC with its much larger count rates, achieves significantly better results: CP-sensitivity down to $\sin^2 2\theta_{13} \sim 10^{-4}$.

6.4. Summary and conclusions

In the present chapter a new type of experimental setup which combines a Beta Beam with an electron capture beam has been studied.. This can be achieved naturally by using nuclei which can decay into both channels. The nuclide ^{156}Yb was chosen as it has favourable beta decay and electron capture branching ratios, and only a small alpha decay contribution. This combination is very powerful as the EC channel provides a high energy signal at a well known energy, while the Beta Beam provides coverage of the first and second oscillation maxima.
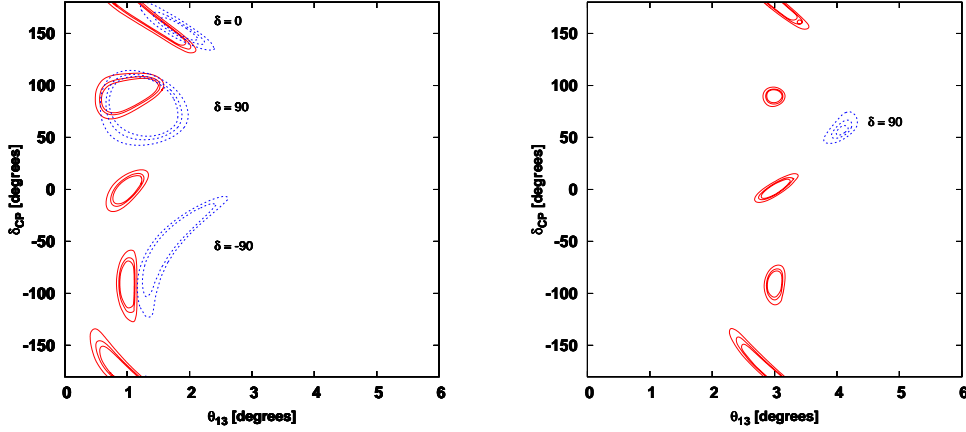
Figure 6.8.: Same as Fig. 6.7 but for setup IV-WC.

The allowed regions in the (θ_{13}, δ) plane for the two separate channels have a limited overlap resulting in a good resolution of the energy degeneracy.

A detailed study of the dependence of the physics reach of this experimental technique by considering six different setups was performed: two values for the ion boost factor $\gamma = 166$ and 369; two choices for the detector: a 50 kton TASD or LAr and a 500 kton WC detector; and three baselines: CERN-Frejus, CERN-Canfranc, CERN-Boulby. This allowed the impact of the count rate, choice of baseline and the tuning of the energy of the beta-beam and EC beam to the oscillatory pattern to be studied. The setups with low gamma and 50 kton detectors have very poor physics reach, owing to the limited event rates. The information on CP-violation is mainly provided by the high energy EC signal. We studied the options with $\gamma = 369$, the highest value of the boost factor allowed by an upgraded SPS. For these neutrino energies, two types of detectors were considered: a 50 LAr/TASD option, which has good energy resolution for the high energy part of the neutrino spectrum; and a 500 kton WC detector, which provides a larger number of events.

Setups III and III-WC, which use the CERN-Canfranc baseline, have larger count rates and a better tuning of the beam to the oscillatory pattern, with respect to their CERN-Boulby counterparts: setups IV and IV-WC. This results in a very good ability to measure the parameters (see Fig. 6.6). In particular these setups provide the best sensitivity to CP-violation for positive values of δ. However, for negative δ, owing to the relatively short distance, the type of hierarchy can be resolved only for very large values of θ_{13}. The sign degeneracy prevents discovery of CP-violation in this case (see Fig. 6.7). The CERN-Boulby setups, IV and IV-WC, suffer from smaller count rates and poor tuning of the Beta Beam to the oscillation pattern. Comparing the two baseline options, if the hierarchy is known to be normal from other neutrino

experiments, the CERN-Canfranc option has an improved physics reach, while if the ordering is not known, the CERN-Boulby baseline outperforms the shorter option. For the high event rate scenario, one gets sensitivity to CP-violation down to values of $\sin^2 2\theta_{13} \sim 3 \times 10^{-5}$ at 99% CL for a WC detector at Canfranc, and $\sin^2 2\theta_{13} \sim 10^{-4}$ for a WC detector at Boulby.

In conclusion, the novel idea of using a single beam which combines neutrinos from beta and electron capture decays has been presented and the physics reach of several possible setups has been demonstrated. This could naturally be done with the use ^{156}Yb, which has comparable Beta Beam and electron capture branching ratios. As both beams are produced from a single isotope, this combination cannot be further optimised. The simulations performed in this chapter have taken similar experimental parameters as a 'standard' Beta Beam; namely useful decays $\sim 10^{18}$ and a duty factor $S_f = 10^{-3}$. In reality this requires considerable R&D on top of that necessary for the standard Beta Beam, and may not even be attainable. Either the number of useful decays or the duty factor or both may need to be relaxed. In which case, the sensitivity will be poorer. It is not practical to carry out an analysis that varies the exposure and atmospheric neutrino rate independently because of the extended run time of the simulations. The extent to which the exposure is important can be gauged by comparing Figs. 6.5 and 6.6. It is seen that lowering the exposure not only reduces the sensitivity but brings degeneracy in the region $\sin^2 2\theta_{13} \sim 10^{-2}$ to the fore. The difference in fiducial detector volumes is a factor of 10, but the Water Čerenkov use only QE-events and has been taken to have an efficiency of 70 %. Therefore the average difference, at a given neutrino energy, is around 5. The increase in minimal $\sin^2 2\theta_{13}$ is far more than this. Therefore one must conclude that degeneracy is a major problem for hybrids unless the exposure is large. Taking the degeneracy problems and extra necessary R&D into account, there appears to be no good reason to promote this idea instead of a standard Beta Beam.

Chapter 7.

Conclusions

The last decade has seen a shift in our understanding of neutrinos. A series of experiments have resolved the long standing solar neutrino problem and determined the origin of the atmospheric neutrino anomaly. The combination of data from solar, atmospheric, reactor and accelerator experiments provide compelling evidence for neutrino oscillations. The existence of neutrino oscillations implies that neutrinos are massive and that they mix; the mass states and the flavour states are misaligned. Three neutrino mixing and oscillations can be described by 3 mixing angles, a CP-violating phase (and possibly two Majorana phases) and two independent mass-squared splittings. Current oscillation data indicates that neutrino mass splittings are hierarchal in nature; the three neutrino mixing can be viewed as two approximate decoupled 2 neutrino oscillation schemes, each with a mass-squared splitting and mixing angle.

Despite all this progress, a number of important questions are still un-answered. What is the absolute neutrino mass scale and its origin? What is the nature of neutrinos (Dirac or Majorana)? In the context of long baseline neutrino oscillation experiments, it is important to determine the third mixing angle that manifests itself as a interference between the solar and atmospheric sectors; whether CP-symmetry is violated in the lepton sector; and whether the neutrino mass ordering in normal or inverted.

It is the goal of the future long baseline neutrino oscillation programme to address these questions. To this end, Superbeams, Neutrino Factories and Beta Beams are all being studied in detail with the intention of sourcing intense neutrino beams that are to be aimed at distant detectors where searches for sub-dominant appearance events will be made. The phenomenological analysis and optimisation of future long baseline experiments is not straightforward; the extraction of the unknown mixing parameters suffers from the problem of degeneracies with up to 8 solutions being able to fit a given data set. The primary goals of phenomenological research into the future neutrino machines is to develop strategies to resolve these

degeneracies and simultaneously push for the best sensitivity to the unknown mixing parameters.

In Chaps. 1 and 2 a brief survey of the phenomenology of neutrino oscillations was given. This included a brief history and a summary of two neutrino oscillations. This discussion included the 'standard' derivation of the oscillation probabilities in the vacuum; and how the result needs to be modified for passage through matter. The present analysis of the experimental data was presented and the future goals of the neutrino oscillation program were highlighted. In Chap. 2, the discussion was extended to three neutrino oscillations and included both numerical and analytical results. A sketch of the derivation of the $\nu_e \to \nu_\mu$ appearance probability was given and the important features of its form were pointed out. An introduction to the problem of degeneracies followed and a brief overview of the many strategies to resolve them was imparted. A detailed discussion of how to perform a numerical simulation of a future facility, including the calculation of the event spectrum and the statistical analysis, concluded the chapter.

Chap. 3 introduced the technological aspects of the Beta Beam. A Beta Beam aims to exploit much existing accelerator infrastructure, or proposed upgrades to it. There are three distinct phases: ion production; the acceleration of the ions; and the bunching and storing of the ions. The chapter began with a brief summary of the Beta Beam flux and the physical parameters that determine the neutrino energy range in the laboratory frame. Two general classes of long baseline Beta Beam were identified (continental and inter-continental) and a short survey of the main phenomenological studies to date was presented. Each sector of a Beta Beam front-end was considered in turn before the chapter finished with some comments of number of useful beta decays available to an experiment.

In the Chap. 4, the first phenomenological analysis was presented. This study was a re-working of a case study performed for the CERN-Boubly baseline, but under different assumptions and through the use of numerical simulations consistent with the later chapters. The ability of a moderate baseline to resolve energy degeneracy was investigated with the conclusion that coverage of the (θ_{13}, δ) plane similar to dual ion setups was possible; especially for large exposures when degeneracy is less of an issue. This study confirmed the expectations from an analytical study using the expansion of the appearance probability. The underlying principle is that data from high energy bins provides the CP-violation sensitivity whilst the data from low energy bins, although they provide no additional sensitivity, select the correct region of the (θ_{13}, δ) plane.

These ideas were extended in Chap. 5 where existing work from collaborators were continued and examined in more phenomenological detail. The studies resolved around the use of ions with fast Gamow-Teller resonant electron capture decay modes to source mono-energetic neutrinos for the CERN-Canfranc baseline. The matter effect and hierarchy degeneracies were included for the first time and a scan of the boost pair space to find the maximum CP-violation coverage was performed. The next step was to examine the affect of altering the number of useful decays and the number of atmospheric events. An electron capture neutrino beam does not need to be reconstructed at the detector since the neutrino energy is known. However, this means that all ν_μ events will misidentified as $\nu_e \rightarrow \nu_\mu$ appearance events. This limits the sensitivity, especially if the duty factor of the storage ring needs to be relaxed to achieve the sought useful ion decay rate. The chapter finished with a critique of the suggestion from a Japanese collaboration to use bound beta decays to source a mono-energetic anti-neutrino beam. Such a beam would greatly increase physics reach since neutrino runs at low boost would not be necessary. The idea falls-down on the need for fully stripped ions with low Q-values. Space charge issues, very precise energy resolution and useful decay rates much larger than standard Beta Beams make the proposal unrealistic in practice.

The final chapter examined the possibility of combining a Beta Beam with an electron capture beam using a single ion. For ions that can electron capture decay but do not possess a Gamow-Teller resonance, the beta decay sources a background - the magnitude of which is dependent on the total energy available to the ion decay. A summary of the CP-violation studies of a recent paper was presented and included an analysis of how the different decay channels combine to yield the overall physics reach of the facility.

Since the conception of the idea by Zucchelli in 2002, a number of different Beta Beam facilities have been proposed for use in long baseline neutrino oscillation experiments. Since the neutrino flux at source is not contaminated by other flavours or CP-conjugate channels, a magnetised far detector is not necessary. As a consequence there is complete freedom to choose the experimental parameters within the hard limits set by the technology. This is not to say that the feasibility of a Beta Beam is a given; merely that from a phenomenological point of view there is flexibility in one's choice of ion, boost baseline and detector technology. The choices made influence the physics reach of a given facility and, vice versa, a facility with a specific set of physics capabilities can be proposed through judicious choice of the experimental parameters. Not all Beta Beams are equally plausible, of course, since influences outside merely choosing the experimental parameters need to be taken into account in the long run.

As an example, consider the following question

'What is the maximum γ available to a Beta Beam sourced from ^{18}Ne?'

This question was dealt with in Chap. 3: the maximum boost available to an ion is the maximum boost available for a proton multiplied by its charge to mass ratio. For a 1 TeV machine, the maximum boost available to ^{18}Ne is therefore $\gamma_{max} = 592$. If one is being precise, this is in fact the theoretical maximum boost, which is not necessarily the same as the maximum boost. This result is the maximum boost available to a single ion circulating in a 1 TeV accelerator. This is not a Beta Beam. A Beta Beam is a machine that aims to source $\sim 10^{18}$ useful ion decays in a straight section of a storage ring directed at a far detector. The goal is to achieve this rate with a given boost, duty factor and storage ring configuration. A Beta Beam is thus a facility that consists of production, ionisation, several stages of acceleration and injection into a storage ring. The number of useful decays is a function of the accelerator technology, the size of the decay ring and magnetic fields available. It may well be the case that, to achieve $\sim 10^{18}$ useful ion decays,

$$\gamma_{max}^{\beta B} < \frac{Z}{A} \, \gamma_{max}^{p} \, .$$

The point is that the experimental parameters are all correlated between themselves and with outside influences such as the local geology of the site, civil engineering issues, the requirements for related areas of nuclear and high energy physics, the amount of resources required for collider sector, and so on. Until these correlations are understood, the optimal physics reach of a Beta Beam cannot be determined.

All the studies to date have made assumptions on the availability of technology at the time of construction. The results presented are only as valid as the assumptions made. The studies presented in this thesis do not follow this philosophy. The goal was not to claim absolute physics reach, rather to explore the properties of the facilities.

In this thesis, the ability to rule out CP-conservation for single ion Beta Beams; multi-boost electron capture machines; and a hybrid Beta Beam and electron capture machine were presented. The main strategy adopted was the use of the energy spectrum of appearance events for facilities using a neutrino run only. The energy dependence of the oscillation probability can then be used to constrain the true region in (θ_{13}, δ) space and break any energy or hierarchy degeneracies that may have been present. For a standard Beta Beam, this approach had not been studied elsewhere. For electron capture machines and hybrid machines, this is the only way to achieve sensitivity as there is no corresponding and practical anti-neutrino source available.

The studies in this thesis contribute to the overall physics study of future long baseline neutrino oscillation experiments. The use of a single ion Beta Beam is a viable alternative to the combination of a neutrino and anti-neutrino run. In the event that a run in one of the neutrino or anti-neutrinos becomes unworkable, for either a physics or non-physics reason, the single ion proposal is an attractive option for Beta Beam if a high luminosity can be achieved. Specifically, since a single ion beam with neutrinos has a larger event rate at high energies, it may well be superior in overall physics reach compared to a two ion facility. The feasibility of the electron capture and hybrid beams is not clear. Such facilities need extra R&D on all aspects of the front-end to ascertain how plausible it is to achieve $\sim 10^{18}$ useful ion decays in one straight section of a storage ring when the ions are at a large boost. For an electron capture machine to be a viable alternative, it is necessary to demonstrate that it has capabilities beyond a standard Beta Beam that warrant the extra necessary technological research. It is my view that hybrid machines should not be considered for further study. The form of the neutrino flux is not sufficiently different as to provide physics opportunities not available to a standard Beta Beam. In this context it is less attractive since the non-standard flux shape and the lack of an equivalent anti-neutrino run gives the CP-sensitivity region a complex form. Degeneracies are a problem even with a good energy resolution. If reactors and near future Superbeams fail to measure θ_{13}, a hybrid beam could miss out on detection if $\sin^2 2\theta_{13} \sim 10^{-3} - 10^{-2}$. In a standard Beta Beam, this problem is either not present or considerably less pronounced.

Within the next few years, new experimental data and R&D on future technologies will bring into focus both our priorities and technologies capabilities. Until then, the feasibility of the Beta Beam and its related technologies will remain open questions. The results of this thesis indicate that a single ion Beta Beam type facility may have a place in the future neutrino oscillation experimental programme.

Appendix A.

Numerical calculation of the oscillation probabilities

The computation of the oscillation probabilities used in this thesis formed the base of a more extensive code that attempted to numerically evolve an initial neutrino state from production at the centre of the sun to its surface. In such a computation, the neutrino evolution is complicated by its coupling to an external environment: the neutrino absorption and re-emission via neutral current and charge current interactions; ν_τ regeneration and a finite size production region at the centre of the sun all need to be included. The appropriate formalism for this is the evolution in space of the neutrino density matrix [172].

A.1. The density matrix

For some operator $\hat{O}$, the density operator $\hat{\rho}$ is defined by

$$\langle O \rangle = \operatorname{Tr} \hat{\rho}\, \hat{O} \;, \tag{A.1}$$

with

$$\operatorname{Tr} \hat{\rho} = 1 \;. \tag{A.2}$$

Consider a system with wave-function ϕ and expand it in a basis $|k\rangle$ that spans the space containing ϕ

$$|\phi\rangle = \sum_k |k\rangle\langle k|\phi\rangle . \tag{A.3}$$

Substituting this in the usual expression for the expectation,

$$\langle o \rangle = \langle \phi | \hat{O} | \phi \rangle , \tag{A.4}$$

gives

$$\langle o \rangle = \sum_k \sum_l \langle \phi | l \rangle \langle l | \hat{O} | k \rangle \langle k | \phi \rangle \tag{A.5}$$

$$= \sum_k \sum_l \rho_{lk} O_{kl} , \tag{A.6}$$

with

$$\rho_{lk} \equiv \langle \phi | l \rangle \langle k | \phi \rangle . \tag{A.7}$$

Note that the diagonal elements of ρ are the probabilities for the system to be in a given state;

$$\rho_{kk} = |\langle \phi | k \rangle|^2 = P_k , \tag{A.8}$$

and the off-axis elements represent a projection of a particular state on the vector $|\phi\rangle$. Note also that some information is redundant:

$$\rho_{lk} = \langle \phi | l \rangle \langle k | \phi \rangle = \langle l | \phi \rangle^* \langle k | \phi \rangle = (\langle l | \phi \rangle \langle k | \phi \rangle^*)^* = (\langle \phi | k \rangle \langle l | \phi \rangle)^* = \rho_{kl}^* . \tag{A.9}$$

With these definitions, it is straightforward to show that the density matrix evolves in time in relation to the Hamiltonian according to

$$i\frac{\partial \hat{\rho}}{\partial t} = -[\hat{\mathcal{H}}, \hat{\rho}] . \tag{A.10}$$

A.2. Calculation of the probability

To use the previous relation to obtain the neutrino oscillation probabilities, it is necessary to convert it from evolution in time to evolution in space and with correct units. We wish to measure neutrino energies in GeV, baselines in km and mass-squared splittings in eV^2. In natural units and converting to the fore-mentioned unit choices, Eq. A.10 becomes

$$i\frac{\partial \hat{\rho}}{\partial L} = -5.07 \left[\hat{\mathcal{H}}, \hat{\rho} \right] . \tag{A.11}$$

The density matrix is

$$\rho = \begin{pmatrix} \rho_{ee} & \rho_{e\mu} & \rho_{e\tau} \\ \cdot & \rho_{\mu\mu} & \rho_{\mu\tau} \\ \cdot & \cdot & \rho_{\tau\tau} \end{pmatrix} = \begin{pmatrix} \rho_{ee} & \rho_{e\mu}^{\Re} + i\rho_{e\mu}^{\Im} & \rho_{e\tau}^{\Re} + i\rho_{e\tau}^{\Im} \\ \cdot & \rho_{\mu\mu} & \rho_{\mu\tau}^{\Re} + i\rho_{\mu\tau}^{\Im} \\ \cdot & \cdot & \rho_{\tau\tau} \end{pmatrix}, \tag{A.12}$$

where the off-diagonal elements have been written as the real and imaginary parts. The below diagonal elements have not been written as they provide no additional information. Inserting the Hamiltonian from Eq. 2.1.1, returns 9 simultaneous differential equations for the elements of the density matrix. These simultaneous equations will be a function of the mixing angles, the mass squared splittings, the neutrino energy and the matter potential. These equations are solved numerically using code based on the solution of stiff equations taken from [173]. The evolution has initial conditions

$$\rho(L=0) = \begin{pmatrix} 1 & 0 & 0 \\ 0 & 0 & 0 \\ 0 & 0 & 0 \end{pmatrix} \quad \text{or} \quad \rho(L=0) = \begin{pmatrix} 0 & 0 & 0 \\ 0 & 1 & 0 \\ 0 & 0 & 0 \end{pmatrix} \tag{A.13}$$

for initial ν_e or ν_μ beams respectively. For the ν_e beam, at baseline L,

$$\rho_{ee}(L) = P_{\nu_e \to \nu_e} , \tag{A.14}$$

$$\rho_{\mu\mu}(L) = P_{\nu_e \to \nu_\mu} , \tag{A.15}$$

$$\rho_{\tau\tau}(L) = P_{\nu_e \to \nu_\tau} . \tag{A.16}$$

Appendix B.

Neutrino flux in the laboratory frame

The calculation of the un-oscillated neutrino flux in the laboratory is a two stage process: first perform the appropriate Lorentz transformation, then convert the angle the neutrino makes with the beam direction in the ion rest frame to the corresponding angle in the laboratory frame.

Consider a neutrino with energy E^* and 3-momentum $\vec{p}^* = (p_x^*, p_y^*, p_z^*)$ in the centre of mass frame. Neglecting the neutrino mass, we can write $E^* = |\vec{p}^*|$ and

$$
\begin{aligned}
p_x^* &= E^* \sin\theta^* \cos\phi , \\
p_y^* &= E^* \sin\theta^* \sin\phi , \\
p_z^* &= E^* \cos\theta^* .
\end{aligned}
\tag{B.1}
$$

Without loss of generality, take $\phi = 0^o$ and consider the boost to be in the $\theta = 0^o$ direction. The 4 momentum in the laboratory frame is then found via the Lorentz transformation

$$
\begin{pmatrix}
E \\
E\sin\theta \\
0 \\
E\cos\theta
\end{pmatrix}
=
\begin{pmatrix}
\gamma & 0 & 0 & \beta\gamma \\
0 & 1 & 0 & 0 \\
0 & 0 & 1 & 0 \\
\beta\gamma & 0 & 0 & \gamma
\end{pmatrix}
\begin{pmatrix}
E^* \\
E^*\sin\theta^* \\
0 \\
E^*\cos\theta^*
\end{pmatrix} ,
\tag{B.2}
$$

so that the energy of the neutrino in the laboratory frame is given by

$$
\gamma E^* (1 + \beta\cos\theta^*) .
\tag{B.3}
$$

This is still in terms of the rest frame angle and therefore needs to be trasnformed a little further. Now

$$\frac{dE}{d\cos\theta} = \frac{dE}{d\cos\theta^*}\frac{d\cos\theta^*}{d\cos\theta} = \gamma E^*\frac{d\cos\theta^*}{d\cos\theta} \ . \tag{B.4}$$

Using the result of the Lorentz trasnformation we can write

$$\cos\theta = \frac{\gamma E^*(\beta + \cos\theta^*)}{\sqrt{(\gamma E^*(\beta + \cos\theta^*))^2 + (E^*\sin\theta^*)^2}} = \frac{\beta + \cos\theta^*}{1 + \beta\cos\theta^*} \ . \tag{B.5}$$

Inverting this we get

$$\cos\theta^* = \frac{-\beta + \cos\theta}{1 - \beta\cos\theta} \ , \tag{B.6}$$

and hence

$$\frac{d\cos\theta^*}{d\cos\theta} = \left[\gamma^2(1 - \beta\cos\theta)^2\right]^{-1} \ . \tag{B.7}$$

From equation B.4, the exact energy at an angle θ in the laboratory frame is

$$E(\theta) = \frac{E^*}{\gamma}\frac{1}{1 - \beta\cos\theta} \ . \tag{B.8}$$

Large γ and small θ allows the further approximation

$$E(\theta) = \frac{2\gamma E^*}{1 + \gamma^2\theta^2} \ , \tag{B.9}$$

where $\beta \approx 1 - \frac{1}{2\gamma^2}$ and $\cos\theta \approx 1 - \frac{\theta^2}{2}$ have been used.

We require that the neutrino spectrum which will take the form

$$\frac{dN}{dE_\nu d\cos\theta} = \Phi(E_\nu) \ . \tag{B.10}$$

Boosting from the centre of mass frame to the laboratory frame is equivalent to the transformation

$$E_\nu \longrightarrow E_\nu\gamma(1 - \beta\cos\theta) \ ,$$
$$dE_\nu \longrightarrow \gamma(1 - \beta\cos\theta)dE_\nu \ . \tag{B.11}$$

Consequently the laboratory spectrum is related to the centre of mass spectrum via

$$\Phi_{lab}(E_\nu, \theta) = \frac{\Phi_{cm}(E_\nu \gamma [1 - \beta \cos \theta])}{\gamma [1 - \beta \cos \theta]} \ . \tag{B.12}$$

Note that the spectrum maintains its functional form, the only difference being the scale - a factor of $\gamma(1 - \beta \cos \theta)$ that alters the overall magnitude of the flux and also the argument. Note that the flux off-axis is equivalent to a flux on-axis but with a smaller boost.

Off-axis conventional beams

The manner of neutrino production for conventional and Superbeams allows one to source fluxes in narrow energy ranges by placing the far detector off axis (with respect to the centre of the beam.) To see this, first note that the neutrino energy in the rest frame of its source pion is a constant, given by

$$E_\nu^* = \frac{m_\pi}{2} \left(1 - \frac{m_\mu^2}{m_\pi^2} \right) \approx 30 \text{ MeV} \ , \tag{B.13}$$

where m_π and m_μ are the pion and muon masses respectively. This can be combined with Eq. B.9 to find the neutrino energy in the laboratory frame as a function of the off-axis angle:

$$E_\nu(\theta) = \left(1 - \frac{m_\mu^2}{m_\pi^2} \right) \frac{E_\pi m_\pi^2}{m_\pi^2 + E_\pi^2 \theta^2} \ . \tag{B.14}$$

For $\theta = 0^o$, the range of neutrino energies is determined by the range of pion energies selected by the focussing horns. As one goes off-axis, the neutrinos become bunched into narrower energy ranges. This can be see by noting that dE_ν/dE_π vanishes for $\theta = m_\pi/E_\pi$. Whereas for $\theta = 0^o$ the neutrino energy was linear with the pion energy, for non-zero off-axis angles, there is a peak neutrino energy given by

$$E_\nu^{\text{peak}} \approx \frac{30 \text{ MeV}}{\theta} \ . \tag{B.15}$$

The neutrinos are therefore concentrated into the energy range $[0, E_\nu^{\text{peak}}]$, irrespective of the energy of the source pion. This is the principle of off-axis conventional and Superbeams. This trick cannot be applied to Beta Beams nor Neutrino Factories due to the different nature in which they are sourced.

Appendix C.

Energy degeneracy discussion from arXiv:0912.2676

In this appendix, discussion of the energy degeneracy from the electron capture article is presented verbatim for reference. In Chap. 4 the discussion focuses on first and second oscillation maximum, as it did in the original paper [89]. The discussion here is more general.

The energy degeneracy

It is well known that the analysis of data from a future long baseline facility suffers from the problem of degeneracies [106, 107, 108, 109]; the asymmetry between neutrino and anti-neutrino probabilities, the unknown sign of Δm_{31}^2, and the unknown octant of θ_{23} can all lead to multiple fits to experimental data. For binned data, the number of neutrino (anti-neutrino) events in the ith neutrino (anti-neutrino) energy bin for the pair $(\bar{\theta}_{13}, \bar{\delta})$ is given by

$$N_i(\bar{\theta}_{13}, \bar{\delta}) = \mathcal{N}_T\, t \int_{E_i}^{E_i+\Delta E} \varepsilon(E_\nu)\sigma_{\nu_\mu(\bar{\nu}_\mu)}(E_\nu)\, P_{e\mu}^{\pm}(E_\nu, \bar{\theta}_{13}, \bar{\delta})\, \Phi_{\nu_e(\bar{\nu}_e)}(E_\nu)\, dE_\nu\ , \qquad (C.1)$$

where $\mathcal{N}_T$ is the number of targets in the detector, t is the time of data taking, $\varepsilon(E_\nu)$ is the detector efficiency, $\sigma(E_\nu)$ is the interaction cross section, $\Phi(E_\nu)$ is the beam spectrum and ΔE is the bin width. Using the shorthand $\Delta_{ji} \equiv \Delta m_{ji}^2/(2E)$, the oscillation probability $P_{\nu_e \to \nu_\mu} \equiv P_{e\mu}$

163

can be expanded in the small parameters $\bar{\theta}_{13}$, Δ_{12}/Δ_{13}, Δ_{12}/A and $\Delta_{12}L$ [66],

$$
\begin{aligned}
P_{e\mu}^{\pm}(\bar{\theta}_{13}, \bar{\delta}) =\ & \sin^2 2\bar{\theta}_{13} \sin^2 \bar{\theta}_{23} \left(\frac{\Delta_{31}}{B_{\mp}} \right)^2 \sin^2 \left(\frac{B_{\mp}L}{2} \right) \\
& + \jmath \frac{\Delta_{21}}{A} \frac{\Delta_{31}}{B_{\mp}} \sin \left(\frac{AL}{2} \right) \sin \left(\frac{B_{\mp}L}{2} \right) \cos \left(\pm\bar{\delta} - \frac{\Delta_{31}L}{2} \right) \\
& + \cos^2 \bar{\theta}_{23} \sin^2 2\bar{\theta}_{12} \left(\frac{\Delta_{21}}{A} \right)^2 \sin^2 \left(\frac{AL}{2} \right) ,
\end{aligned}
\tag{C.2}
$$

where $\jmath = \cos \bar{\theta}_{13} \sin 2\bar{\theta}_{12} \sin 2\bar{\theta}_{23} \sin 2\bar{\theta}_{13}$, the $\pm$ corresponds to neutrinos/anti-neutrinos and $B_{\mp} \equiv A \mp \Delta_{31}$. Here we are using $A = \sqrt{2}G_F \bar{n}_e(L)$ (the constant density approximation for the index of refraction) where $\bar{n}_e = 1/L \int_0^L n_e(L')dL'$ is the average electron density and $n_e(L)$ is the electron density along the baseline.

Labelling N^+ to be the number of neutrino events, and N^- to be the number of anti-neutrino events; 4 pairs of equations can be solved

$$
N^{\pm}(\bar{\theta}_{13}, \bar{\delta}, |\Delta m_{31}^2|, \theta_{23}) = N^{\pm}(\theta_{13}, \delta, |\Delta m_{31}^2|, \theta_{23}) , \tag{C.3}
$$

$$
N^{\pm}(\bar{\theta}_{13}, \bar{\delta}, |\Delta m_{31}^2|, \theta_{23}) = N^{\pm}(\theta_{13}, \delta, -|\Delta m_{31}^2|, \theta_{23}) , \tag{C.4}
$$

$$
N^{\pm}(\bar{\theta}_{13}, \bar{\delta}, |\Delta m_{31}^2|, \theta_{23}) = N^{\pm}(\theta_{13}, \delta, |\Delta m_{31}^2|, 90^o - \theta_{23}) , \tag{C.5}
$$

$$
N^{\pm}(\bar{\theta}_{13}, \bar{\delta}, |\Delta m_{31}^2|, \theta_{23}) = N^{\pm}(\theta_{13}, \delta, -|\Delta m_{31}^2|, 90^o - \theta_{23}) ; \tag{C.6}
$$

which in general lead to 8 solutions that can fit the data. In order, the first set of equations results in the 'intrinsic clone'; the second returns the 'hierarchy clones'; the third gives the 'octant' clones; and the fourth equation allows for 'mixed' clones. Solutions to the first set of equations are depicted graphically in Fig. 1 for $\sin^2 2\theta_{13} = 10^{-2}$, $\delta = 50^o$, $\theta_{23} = 45^o$ and $L = 650$ km. The black lines correspond to E = 1.3 GeV (first oscillation maximum) and the red lines are for E = 1.8 GeV. Solid lines are for neutrinos and dashed lines are for anti-neutrinos.

From Fig. C.1, there is another type of degeneracy not discussed in the literature. Consider the first set of equations above but now also for energies E_1 and E_2 :

$$
N_{1,2}^{\pm}(\bar{\theta}_{13}, \bar{\delta}, |\Delta m_{31}^2|, \theta_{23}) = N_{1,2}^{\pm}(\theta_{13}, \delta, |\Delta m_{31}^2|, \theta_{23}) . \tag{C.7}
$$

Attempting to find a solution to these equations will return only the true solution since the location of the intrinsic clone is energy dependent. This is the main strategy in resolving the intrinsic degeneracy. Suppose, one does not have an anti-neutrino channel. This set reduces
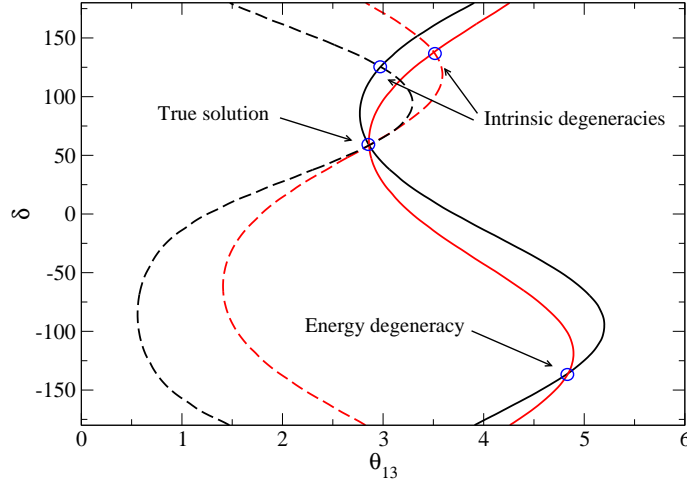
Figure C.1.: Equi-probability curves for the CERN-Canfranc baseline (650 km) for $\sin\theta_{13}^{tr} = 0.05$ and $\delta^{tr} = 50^o$. The other oscillation parameters have been set to their current central values [15]. The black curves use $E_\nu = 1.3$ GeV and the red curves use $E_\nu = 1.8$ GeV. Solid lines are for neutrinos, dashed lines are for anti-neutrinos.

from 4 to 2 equations, and in general will possess a clone solution. This can been seen as the intersection of the red and black solid curves at $(\theta_{13}, \delta) = (4.8^o, -140^o)$. The location of this degeneracy will be different for neutrino and anti-neutrino runs. Therefore the inclusion of both resolves the degeneracy and hence it is not present in most setups discussed in the literature. For single ion Beta Beams and electron capture studies [89, 91, 92], this degeneracy needs to be resolved by the experiment or constrained to values of θ_{13} larger than near future experimental limits. This degeneracy shall hereafter be referred to as the 'energy degeneracy' to distinguish it from the usual intrinsic degeneracy which has a different origin.

Ideally, we would want the energy degeneracy to not be present in the data. To find a condition for this to be so, first rewrite the probability (Eq. C.2) as

$$P_{e\mu} = I_1 \sin^2 2\bar{\theta}_{13} + I_2 \sin 2\bar{\theta}_{13} \cos\bar{\delta} + I_3 \sin 2\bar{\theta}_{13} \sin\bar{\delta} + I_4 \tag{C.8}$$

so that all the non-essential constants are tied up in the I_i. As a first step, we attempt to solve Eq. C.7 for mono-energetic neutrinos only with energies E_1 and E_2. Labelling the respective coefficients as I_i^1 and I_i^2 we obtain the relation

$$\left[\frac{I_1^1}{I_3^1} - \frac{I_1^2}{I_3^2}\right](\sin^2 2\theta_{13} - \sin^2 2\bar{\theta}_{13}) + \left[\frac{I_2^1}{I_3^1} - \frac{I_2^2}{I_3^2}\right](\sin 2\theta_{13} \cos\theta_{13} \cos\delta - \sin 2\bar{\theta}_{13} \cos\bar{\theta}_{13} \cos\bar{\delta}) = 0 .$$

$$\tag{C.9}$$

For the energy degeneracy to be resolved, we must have $\theta_{13} = \bar{\theta}_{13}$ which is true if either

1. $I_2^1/I_3^1 = I_2^2/I_3^2$, i.e. $\Delta m_{31}^2/4E_1$ and $\Delta m_{31}^2/4E_2$ differ by π;

2. $I_1^1/I_3^1 = I_1^2/I_3^2$.

In general $I_1^1/I_3^1 \neq I_1^2/I_3^2$ so we are left with the first condition. The set of equations (C.7) can accommodate the solution

$$\delta = \pi - \bar{\delta} - 2\tan^{-1}\left(\frac{I_2^1}{I_3^1}\right) , \tag{C.10}$$

in addition to the trivial solution $\delta = \bar{\delta}$ for the case $\theta_{13} = \bar{\theta}_{13}$. Therefore the energy degeneracy for a pair of neutrino energies is only completely resolved if condition 1 above and

$$\bar{\delta} = \frac{\pi}{2} - \tan^{-1}\left(\frac{I_2^1}{I_3^1}\right) \tag{C.11}$$

hold. Therefore, the energy degeneracy is present in general for two beams of mono-energetic neutrinos; however, this is not necessarily a nuisance. The combination of mono-energetic neutrino beams placed almost on first oscillation maximum and on second oscillation maximum provides some of the largest CP-violation sensitivity coverage. In such a case, the CP-even part of the probability vanishes and the energy degeneracy is located at $\delta = \pi - \bar{\delta}$. Since this change will leave the probability invariant, the degenerate region will be the same strength and will be symmetrically placed about the $\delta = \pi/2$ or $-\pi/2$ lines. The two regions will always be either be CP-conserving or CP-violating at the same time.

In [89, 92] only neutrinos were used. In those studies, the strategy was to exploit the energy dependence of the oscillation signal to break degeneracy and push for a good physics reach; specifically though the combination of bins centred around first and second oscillation maximum. The above argument says that the combination of the maxima is insufficient to completely break the energy degeneracy, but the θ_{13}-part of the degeneracy is broken. The reason why the degeneracy was only present for very small values of $\sin^2 2\theta_{13}$ in these studies was because the data was binned. If one thinks of the data set as predominantly pairs of bins separated by $\delta\Delta m_{31}^2/4E = \pi$, the location of the energy degeneracy is different for each pair and only the true solution is statistically significant. Or more simply, from Eq. C.9, the combination of multiple energies completely breaks the degeneracy as its location is energy dependent. In this paper, only two electron capture boosts will be used and so this degeneracy is in general present.

List of figures

List of tables

Bibliography

[1] W. Pauli, Letter to L. Meitner and colleagues, 4th December 1930.

[2] H. Bethe and R. Peierls, Nature **133** (1934) 532.

[3] F. Reines and C. L. Cowan, Jr., Phys. Rev. **92** (1953) 830.

[4] C. S. Wu, E. Amber, R. W. Hayward, D. D. Hoppes, ,R. P. Hudson, Phys. Rev. **105** (1957) 1413 .

[5] V. M. Lobashev *et al.*, Phys. Lett. B **460** (1999) 227; V. M. Lobashev *et al.*, Nucl. Phys. Proc. Suppl. **91** (2001) 280.

[6] C. Kraus *et al.*, Eur. Phys. J. C **40** (2005) 447 [arXiv:hep-ex/0412056].

[7] A. Osipowicz *et al.* [KATRIN Collaboration], arXiv:hep-ex/0109033; J. Angrik *et al.* [KATRIN Collaboration], KATRIN design report 2004.

[8] M. Sisti [MARE Collaboration], Nucl. Phys. Proc. Suppl. **168** (2007) 48.

[9] Q. R. Ahmad *et al.* [SNO Collaboration], Phys. Rev. Lett. **87**, 071301 (2001) [arXiv:nucl-ex/0106015]; *ibid.* **89**, 011301 (2002) [arXiv:nucl-ex/0204008]; and *ibid.* **89**, 011302 (2002) [arXiv:nucl-ex/0204009].

[10] S.Hatakeyama *et al.* [Kamiokande Collaboration] Phys. Rev. Lett. **81** (1998) 2016 [arXiv:hep-ex/9806038]; Y. Fukuda *et al.* [Super-Kamiokande Collaboration], Phys. Rev. Lett. **82** (1999) 2644 [arXiv:hep-ex/9812014].

[11] Y. Fukuda *et al.* [Super-Kamiokande Collaboration], Phys. Rev. Lett. **81**, 1562 (1998) [arXiv:hep-ex/9807003].

[12] Y. Ashie *et al.* [Super-Kamiokande Collaboration], Phys. Rev. D **71**, 112005 (2005). [arXiv:hep-ex/0501064].

[13] B. Pontecorvo, Zh. Eksp. Teor. Fiz.

33 (1957), 549.

[14] C. Amsler *et al.* [Particle Data Group], Phys. Lett. B **667** (2008) 1.

[15] T. Schwetz, M. Tortola and J. W. Valle New J. Phys. **10** (2008) 113011 [arXiv:0808.2016 [hep-ph]].

[16] P. Zucchelli, Phys. Lett. B **532** (2002) 166.

[17] R. Davis, Phys. Rev. Lett. **12** (1964) 303.

[18] J. N. Bachall and R.K. Ulrich, Rev. Mod. Phys. **60** 297 (1998).

[19] B. T. Cleveland *et al.*, Astrophys. J. **496**, 505 (1998).

[20] J. N. Abdurashitov *et al.* [SAGE Collaboration], J. Exp. Theor. Phys. **95**, 181 (2002) [Zh. Eksp. Teor. Fiz. **122** (2002) 211] [arXiv:astro-ph/0204245].

[21] W. Hampel *et al.* [GALLEX Collaboration], Phys. Lett. B **447**, 127 (1999); T. A. Kirsten [GNO Collaboration], Nucl. Phys. Proc. Suppl. **118**, 33 (2003).

[22] S. N. Ahmed *et al.* [SNO Collaboration], Phys. Rev. Lett. **92**, 181301 (2004) [arXiv:nucl-ex/0309004]; B. Aharmim *et al.* [SNO Collaboration], Phys. Rev. C **72**, 055502 (2005) [arXiv:nucl-ex/0502021].

[23] K. Eguchi *et al.* [KamLAND Collaboration], Phys. Rev. Lett. **90**, 021802 (2003) [arXiv:hep-ex/0212021]; T. Araki *et al.* [KamLAND Collaboration], Phys. Rev. Lett. **94**, 081801 (2005) [arXiv:hep-ex/0406035].

[24] R. Becker-Szendy *et al.*, Nucl. Phys. Proc. Suppl. **38** (1995) 331.

[25] M. C. Sanchez *et al.* [Soudan 2 Collaboration], Phys. Rev. D **68**, 113004 (2003) [arXiv:hep-ex/0307069].

[26] M. Ambrosio *et al.* [MACRO Collaboration], Phys. Lett. B **434**, 451 (1998) [arXiv:hep-ex/9807005].

[27] K. Daum *et al.* [Frejus Collaboration.], Z. Phys. C **66** (1995) 417.

[28] M. Aglietta *et al.* [The NUSEX Collaboration]' Europhys. Lett. **8** (1989) 611.

[29] S. Fukuda *et al.* [Super-Kamiokande Collaboration], Phys. Rev. Lett. **85** (2000) 3999 [arXiv:hep-ex/0009001].

[30] M. H. Ahn *et al.* [K2K Collaboration], Phys. Rev. D **74**, 072003 (2006) [arXiv:hep-

ex/0606032].

[31] S. Eliezer and A. R. Swift, Nucl. Phys. B **105** (1976) 45; H. Fritzsch and P. Minkowski, Phys. Lett. B **62** (1976) 72; S. M. Bilenky and B. Pontecorvo, Phys. Rept. **41** (1978) 225.

[32] C. Giunti, AIP COnf. Proc. **1026** (2008) 3 [arXiv:0801.0653 [hep-ph]].

[33] B. Kayser Phys. Rev. D **24** (1981) 110 Y. Takeuchi, Y. Tazaki, S. Y. Tsai and T. Yamazaki, Prog. Theor. Phys. **105**, 471 (2001) [arXiv:hep-ph/0006334].

[34] M. Beuthe, Phys. Rept. **375** (2003) 105 [arXiv:hep-ph/0109119]; W. Grimus and P. Stockinger, Phys. Rev. D **54**, 3414 (1996) [arXiv:hep-ph/9603430]; W. Grimus, P. Stockinger and S. Mohanty, Phys. Rev. D **59**, 013011 (1999) [arXiv:hep-ph/9807442].

[35] R. G. Winter Lett. Nuovo Cim. **30** (1981) 101; C. Giunti, C. W. Kim, U. W. Lee, Phys. Rev. D **44** (1991) 3635; C. Giunti, C. W. Kim, Found. Phys. Lett. **14** (2001) 213.

[36] C. Giunti and C. W. Kim, Found. Phys. Lett. **14** (2001) 213 [arXiv:hep-ph/0011074].

[37] L. Wolfenstein, Phys. Rev. D **17**, 2369 (1978); S. P. Mikheev and A. Yu Smirnov Nuovo Cim. **C9** (1986) 17.

[38] J. N. Bahcall and C. Pena-Garay, New J. Phys. **6** (2004) 63 [arXiv:hep-ph/0404061]; G. Fogli and E. Lisi, New J. Phys. **6**, 139 (2004).

[39] G. Drexlin, Nucl. Phys. Proc. Suppl. **118** (2003) 146.

[40] Y. Fukuda *et al.* [Kamiokande Collaboration], Phys. Rev. Lett. **77**, 1683 (1996).

[41] S. Fukuda *et al.* [Super-Kamiokande Collaboration], Phys. Lett. B **539**, 179 (2002).

[42] M. Apollonio *et al.* [CHOOZ Collaboration], Phys. Lett. B **466**, 415 (1999) [arXiv:hep-ex/9907037]; M. Apollonio *et al.* [CHOOZ Collaboration], Eur. Phys. J. C **27**, 331 (2003) [arXiv:hep-ex/0301017].

[43] F. Boehm *et al.*, Phys. Rev. Lett. **84**, 3764 (2000) [arXiv:hep-ex/9912050]; Phys. Rev. D **62**, 072002 (2000) [arXiv:hep-ex/0003022]; and *ibid.* **64**, 112001 (2001) [arXiv:hep-ex/0107009].

[44] D. G. Michael *et al.* [MINOS Collaboration], Phys. Rev. Lett. **97**, 191801 (2006) [arXiv:hep-ex/0607088].

[45] G. L. Fogli, E. Lisi, A. Marrone, A. Palazzo and A. M. Rotunno, Phys. Rev. Lett. **101**, 141801 (2008) [arXiv:0806.2649 [hep-ph]].

[46] H. L. Ge, C. Giunti and Q. Y. Liu, arXiv:0810.5443 [hep-ph].

[47] Y. Hayato *et al.*, Letter of Intent, available at `http://neutrino.kek.jp/jhfnu/`.

[48] D. S. Ayres *et al.* [NOvA Collaboration], hep-ex/0503053. FERMILAB-PROPOSAL-0929, March 21, 2005. Revised nova Proposal available at `http://www-nova.fnal.gov/NOvA_Proposal/Revised_NOvA_Proposal.html`.

[49] S. B. Kim [RENO Collaboration], AIP Conf. Proc. **981** (2008) 205 [J. Phys. Conf. Ser. **120** (2008) 052025].

[50] X. Guo *et al.* [Daya-Bay Collaboration], arXiv:hep-ex/0701029.

[51] Y. Grossman, Phys. Lett. B **359** (1995) 141 [arXiv:hep-ph/9507344]; S. Davidson, C. Pena-Garay, N. Rius and A. Santamaria, JHEP **0303** (2003) 011 [arXiv:hep-ph/0302093]; P. Huber and J. W. F. Valle, Phys. Lett. B **523** (2001) 151 [arXiv:hep-ph/0108193]; M. C. Gonzalez-Garcia *et al.*, Phys. Rev. Lett. **82** (1999) 3202 [arXiv:hep-ph/9809531]; M. C. Gonzalez-Garcia, Y. Grossman, A. Gusso and Y. Nir, Phys. Rev. D **64** (2001) 096006 [arXiv:hep-ph/0105159]; P. Huber, T. Schwetz and J. W. F. Valle, Phys. Rev. D **66** (2002) 013006 [arXiv:hep-ph/0202048]; J. Kopp, M. Lindner and T. Ota, Phys. Rev. D **76** (2007) 013001 [arXiv:hep-ph/0702269]; N. C. Ribeiro, H. Minakata, H. Nunokawa, S. Uchinami and R. Zukanovich-Funchal, JHEP **0712** (2007) 002 [arXiv:0709.1980 [hep-ph]]; J. Kopp, M. Lindner, T. Ota and J. Sato, Phys. Rev. D **77** (2008) 013007 [arXiv:0708.0152 [hep-ph]]; J. Kopp, T. Ota and W. Winter, Phys. Rev. D **78** (2008) 053007 [arXiv:0804.2261 [hep-ph]].

[52] A. Palazzo and J. W. F. Valle, arXiv:0909.1535 [hep-ph].

[53] F. Ardellier *et al.* [Double Chooz Collaboration], arXiv:hep-ex/0606025.

[54] L. Scotto Lavina [OPERA Collaboration], Nucl. Phys. Proc. Suppl. **188** (2009) 185; R. Acquafredda *et al.*, JINST **4** (2009) P04018; D. Autiero, M. Komatsu, P. Migliozzi and F. Terranova, *In *Thomas, J.A. (ed.) et al.: Neutrino oscillations* 173-196*.

[55] P. Huber, M. Lindner, T. Schwetz and W. Winter, arXiv:0907.1896 [hep-ph]; P. Huber, M. Mezzetto and T. Schwetz, JHEP **0803** (2008) 021 [arXiv:0711.2950 [hep-ph]]; V. Barger, P. Huber, D. Marfatia and W. Winter, Phys. Rev. D **76** (2007) 053005 [arXiv:hep-ph/0703029]; V. Barger, P. Huber, D. Marfatia and W. Winter, Phys. Rev.

D **76** (2007) 031301 [arXiv:hep-ph/0610301]; P. Huber, M. Lindner, M. Rolinec and W. Winter, Phys. Rev. D **74** (2006) 073003 [arXiv:hep-ph/0606119]; P. Huber, J. Kopp, M. Lindner, M. Rolinec and W. Winter, JHEP **0605** (2006) 072 [arXiv:hep-ph/0601266]; P. Huber, M. Lindner, M. Rolinec, T. Schwetz and W. Winter, Phys. Rev. D **70** (2004) 073014 [arXiv:hep-ph/0403068]; P. Huber, M. Lindner, T. Schwetz and W. Winter, Nucl. Phys. B **665** (2003) 487 [arXiv:hep-ph/0303232]; P. Huber, M. Lindner and W. Winter, Nucl. Phys. B **654** (2003) 3 [arXiv:hep-ph/0211300]; P. Huber, M. Lindner and W. Winter, Nucl. Phys. B **645** (2002) 3 [arXiv:hep-ph/0204352]; S. K. Agarwalla, S. Choubey, A. Raychaudhuri and W. Winter, JHEP **0806** (2008) 090 [arXiv:0802.3621 [hep-ex]]; W. Winter, Phys. Rev. D **78** (2008) 037101 [arXiv:0804.4000 [hep-ph]].

[56] A. Bandyopadhyay *et al.* [ISS Physics Working Group], Rept. Prog. Phys. **72** (2009) 106201 [arXiv:0710.4947 [hep-ph]].

[57] B. Achkar *et al.*, Nucl. Phys. **B434** (1995) 503.

[58] P. Huber, M. Lindner, T. Schwetz and W. Winter Nucl. Phys. B **665** (2003) 487.

[59] R. Garoby, SPL at CERN, http://cdsweb.cern.ch/record/1210469 .

[60] http://projectx.fnal.gov .

[61] V. Barger, M. Dierckxsens, M. Diwan, P. Huber, C. Lewis, D. Marfatia and B. Viren, Phys. Rev. D **74** (2006) 073004 [arXiv:hep-ph/0607177].

[62] K. Hagiwara, N. Okamura and K. i. Senda, Phys. Rev. D **76** (2007) 093002 [arXiv:hep-ph/0607255].

[63] S. Geer, Phys. Rev. D **57**, 6989 (1998) [Erratum-ibid. D **59**, 039903 (1999)] [arXiv:hep-ph/9712290]; A. De Rújula, M. B. Gavela and P. Hernández, Nucl. Phys. B **547**, 21 (1999) [arXiv:hep-ph/9811390]; V. Barger, S. Geer, R. Raja and K. Whisnant, Phys. Rev. D **62**, 013004 (2000) [arXiv:hep-ph/9911524]; M. Freund, M. Lindner, S. T. Petcov and A. Romanino, Nucl. Phys. B **578**, 27 (2000) [arXiv:hep-ph/9912457].

[64] Muon Collider Task Force Report (FERMILAB-TM-2399-APC), https://mctf.fnal.gov/annual-reports/mctf-report-207_v9.doc .

[65] S. Geer, O. Mena and S. Pascoli, Phys. Rev. D **75**, 093001 (2007) [arXiv:hep-ph/0701258]; A. D. Bross, M. Ellis, S. Geer, O. Mena and S. Pascoli, Phys. Rev. D **77**, 093012 (2008) [arXiv:0709.3889 [hep-ph]].

[66] A. Cervera, A. Donini, M. B. Gavela, J. J. Gomez Cadenas, P. Hernandez, O. Mena and S. Rigolin, Nucl. Phys. B **579** (2000) 17 [Erratum-ibid. B **593** (2001) 731] [arXiv:hep-ph/0002108].

[67] https://www.ids-nf.org/wiki/FrontPage/Documentation .

[68] P. Huber, M. Lindner, M. Rolinec and W. Winter, Phys. Rev. D **74** (2006) 073003 [arXiv:hep-ph/0606119].

[69] S. F. King, Rept. Prog. Phys. **67** (2004) 107 [arXiv:hep-ph/0310204]; G. Altarelli and F. Feruglio, New J. Phys. **6** (2004) 106 [arXiv:hep-ph/0405048]; R. N. Mohapatra *et al.*, arXiv:hep-ph/0412099; R. N. Mohapatra and A. Y. Smirnov, Ann. Rev. Nucl. Part. Sci. **56** (2006) 569 [arXiv:hep-ph/0603118].

[70] M. Jerkins, J. R. Klein, J. H. Majors and M. G. Raizen, arXiv:0901.3111 [nucl-ex].

[71] M. Lindroos, B. McElrath, C. Orme and T. Schwetz, arXiv:0904.1089 [hep-ph].

[72] S. M. Bilenky, C. Giunti, J. A. Grifols and E. Masso, Phys. Rept. **379** (2003) 69 [arXiv:hep-ph/0211462].

[73] F. Feruglio, A. Strumia and F. Vissani, Nucl. Phys. B **637** (2002) 345 [Addendum-ibid. B **659** (2003) 359] [arXiv:hep-ph/0201291].

[74] S. Pascoli, S. T. Petcov and T. Schwetz, Nucl. Phys. B **734** (2006) 24 [arXiv:hep-ph/0505226].

[75] W. Maneschg, A. Merle and W. Rodejohann, Europhys. Lett. **85** (2009) 51002 [arXiv:0812.0479 [hep-ph]].

[76] G. L. Fogli, E. Lisi, A. Marrone, A. Melchiorri, A. Palazzo, P. Serra and J. Silk, Phys. Rev. D **70** (2004) 113003 [arXiv:hep-ph/0408045].

[77] S. Hannestad, arXiv:0710.1952 [hep-ph].

[78] J. E. Campagne *et al.*, JHEP **0704**, 003 (2007).

[79] S. K. Agarwalla, S. Choubey and A. Raychaudhuri, Nucl. Phys. B **771**, 1 (2007).

[80] S. K. Agarwalla, A. Raychaudhuri and A. Samanta, Phys. Lett. B **629**, 33 (2005); S. K. Agarwalla, S. Choubey and A. Raychaudhuri, Nucl. Phys. B **798**, 124 (2008); S. K. Agarwalla, S. Choubey, S. Goswami and A. Raychaudhuri, Phys. Rev. D **75**, 097302 (2007).

[81] M. Mezzetto, J. Phys. G **29**, 1771 (2003); M. Mezzetto, Nucl. Phys. Proc. Suppl. **143**, 309 (2005); M. Mezzetto, Nucl. Phys. Proc. Suppl. **155**, 214 (2006).

[82] A. Donini, E. Fernandez-Martinez, P. Migliozzi, S. Rigolin and L. Scotto Lavina, Nucl. Phys. B **710**, 402 (2005).

[83] A. Donini, E. Fernandez, P. Migliozzi, S. Rigolin, L. Scotto Lavina, T. Tabarelli de Fatis and F. Terranova, arXiv:hep-ph/0511134; A. Donini, E. Fernandez-Martinez, P. Migliozzi, S. Rigolin, L. Scotto Lavina, T. Tabarelli de Fatis and F. Terranova, Eur. Phys. J. C **48**, 787 (2006); A. Donini *et al.*, Eur. Phys. J. C **53** (2008) 599 [arXiv:hep-ph/0703209].

[84] S. K. Agarwalla, S. Choubey and A. Raychaudhuri, Nucl. Phys. B **805**, 305 (2008); P. Coloma, A. Donini, E. Fernandez-Martinez and J. Lopez-Pavon, JHEP **0805**, 050 (2008).

[85] S. Choubey, P. Coloma, A. Donini and E. Fernandez-Martinez, arXiv:0907.2379 [hep-ph].

[86] J. Burguet-Castell, D. Casper, E. Couce, J. J. Gómez-Cadenas and P. Hernandez, Nucl. Phys. B **725**, 306 (2005); J. Burguet-Castell, D. Casper, J. J. Gómez-Cadenas, P. Hernandez and F. Sanchez, Nucl. Phys. B **695**, 217 (2004).

[87] A. Jansson, O. Mena, S. J. Parke and N. Saoulidou, Phys. Rev. D **78**, 053002 (2008).

[88] A. Donini and E. Fernandez-Martinez, Phys. Lett. B **641**, 432 (2006).

[89] D. Meloni, O. Mena, C. Orme, S. Palomares-Ruiz and S. Pascoli, JHEP **0807**, 115 (2008).

[90] F. Terranova, A. Marotta, P. Migliozzi and M. Spinetti, Eur. Phys. J. C **38** (2004) 69 [arXiv:hep-ph/0405081].

[91] J. Bernabeu, J. Burguet-Castell, C. Espinoza and M. Lindroos, JHEP **0512** (2005) 014 [arXiv:hep-ph/0505054]; J. Bernabeu and C. Espinoza, Phys. Lett. B **664** (2008) 285 [arXiv:0712.1034 [hep-ph]].

[92] J. Bernabeu, C. Espinoza, C. Orme, S. Palomares-Ruiz and S. Pascoli, JHEP **0906** (2009) 040 [arXiv:0902.4903 [hep-ph]].

[93] C. Orme, arXiv:0901.4287 [hep-ph].

[94] A. Fukumi, I. Nakano, H. Nanjo, N. Sasso,, S. Sato and M. Yoshimura, J. Phys. Soc.

Jpn. **78** (2009) 013201 [arXiv:hep-ex/0612047].

[95] A. Donini, E. Fernandez-Martinez and S. Rigolin, Phys. Lett. B **621** (2005) 276 [arXiv:hep-ph/0411402].

[96] T. Schwetz, JHEP **0705** (2007) 093 [arXiv:hep-ph/0703279].

[97] A. Donini, D. Meloni and P. Migliozzi, Nucl. Phys. B **646** (2002) 321 [arXiv:hep-ph/0206034].

[98] D. Autiero *et al.*, Eur. Phys. J. C **33** (2004) 243 [arXiv:hep-ph/0305185].

[99] D. Meloni, Phys. Lett. B **664** (2008) 279 [arXiv:0802.0086 [hep-ph]].

[100] A. Donini, K. I. Fuki, J. Lopez-Pavon, D. Meloni and O. Yasuda, JHEP **0908** (2009) 041 [arXiv:0812.3703 [hep-ph]].

[101] C. Giunti and C. W. Kim, *Fundamentals of Neutrino Physics and Astrophysics*, Oxford (2007).

[102] S. M. Bilenky, Sov. J. Part. Nucl. **18**, 188 (1987) [Fiz. Elem. Chast. Atom. Yadra **18**, 449 (1987)]; S. M. Bilenky and S. T. Petcov, Rev. Mod. Phys. **59**, 671 (1987) [Erratum-ibid. **61**, 169.1989 ERRAT,60,575 (1989 ERRAT,60,575-575.1988)]; V. D. Barger, K. Whisnant, S. Pakvasa and R. J. N. Phillips, Phys. Rev. D **22**, 2718 (1980); C. W. Kim and W. K. Sze, Phys. Rev. D **35**, 1404 (1987); H. W. Zaglauer and K. H. Schwarzer, Z. Phys. C **40**, 273 (1988); T. Ohlsson and H. Snellman, J. Math. Phys. **41**, 2768 (2000) [Erratum-ibid. **42**, 2345 (2001)] [arXiv:hep-ph/9910546]; T. Ohlsson and H. Snellman, "Neutrino oscillations with three flavors in matter: Applications to Phys. Lett. B **474**, 153 (2000) [arXiv:hep-ph/9912295]; Z. z. Xing, Phys. Lett. B **487**, 327 (2000) [arXiv:hep-ph/0002246]; T. Ohlsson, Phys. Scripta **T93**, 18 (2001); K. Kimura, A. Takamura and H. Yokomakura, "Exact formula of probability and CP violation for neutrino oscillations in Phys. Lett. B **537**, 86 (2002) [arXiv:hep-ph/0203099]; K. Kimura, A. Takamura and H. Yokomakura, "All you ever want to know about neutrino oscillation probabilities in Phys. Rev. D **66**, 073005 (2002) [arXiv:hep-ph/0205295]; P. F. Harrison, W. G. Scott and T. J. Weiler, "Exact matter-covariant formulation of neutrino oscillation Phys. Lett. B **565**, 159 (2003) [arXiv:hep-ph/0305175].

[103] E. K. Akhmedov, R. Johansson, M. Lindner, T. Ohlsson and T. Schwetz, JHEP **0404** (2004) 078 [arXiv:hep-ph/0402175].

[104] E. K. Akhmedov, A. Dighe, P. Lipari and A. Y. Smirnov, "Atmospheric neutri-

nos at Super-Kamiokande and parametric resonance in Nucl. Phys. B **542**, 3 (1999) [arXiv:hep-ph/9808270]; O. L. G. Peres and A. Y. Smirnov, Phys. Lett. B **456**, 204 (1999) [arXiv:hep-ph/9902312]; E. K. Akhmedov, P. Huber, M. Lindner and T. Ohlsson, Nucl. Phys. B **608**, 394 (2001) [arXiv:hep-ph/0105029]; O. L. G. Peres and A. Y. Smirnov, Nucl. Phys. Proc. Suppl. **110**, 355 (2002) [arXiv:hep-ph/0201069]; O. L. G. Peres and A. Y. Smirnov, "Atmospheric neutrinos: LMA oscillations, U(e3) induced interference and Nucl. Phys. B **680**, 479 (2004) [arXiv:hep-ph/0309312]; O. Yasuda, "Three flavor neutrino oscillations and application to long baseline Acta Phys. Polon. B **30**, 3089 (1999) [arXiv:hep-ph/9910428]; M. Freund, M. Lindner, S. T. Petcov and A. Romanino, "Testing matter effects in very long baseline neutrino oscillation Nucl. Phys. B **578**, 27 (2000) [arXiv:hep-ph/9912457]; M. Freund, "Analytic approximations for three neutrino oscillation parameters and Phys. Rev. D **64**, 053003 (2001) [arXiv:hep-ph/0103300].

[105] A. Takamura and K. Kimura, JHEP **0601** (2006) 053 [arXiv:hep-ph/0506112].

[106] J. Burguet-Castell, M. B. Gavela, J. J. Gomez-Cadenas, P. Hernandez and O. Mena, Nucl. Phys. B **608** (2001) 301 [arXiv:hep-ph/0103258].

[107] G. L. Fogli and E. Lisi, Phys. Rev. D **54** (1996) 3667 [arXiv:hep-ph/9604415].

[108] H. Minakata and H. Nunokawa, JHEP **0110** (2001) 001 [arXiv:hep-ph/0108085].

[109] M. Freund, P. Huber and M. Lindner, Nucl. Phys. B **615** (2001) 331 [arXiv:hep-ph/0105071]. T. Kajita, H. Minakata and H. Nunokawa, Phys. Lett. B **528** (2002) 245 [arXiv:hep-ph/0112345]; H. Minakata, H. Nunokawa and S. J. Parke, Phys. Rev. D **66** (2002) 093012 [arXiv:hep-ph/0208163]; P. Huber, M. Lindner and W. Winter, Nucl. Phys. B **645** (2002) 3 [arXiv:hep-ph/0204352]; M. Aoki, K. Hagiwara and N. Okamura, Phys. Lett. B **606** (2005) 371 [arXiv:hep-ph/0311324]; O. Yasuda, New J. Phys. **6** (2004) 83 [arXiv:hep-ph/0405005]; O. Mena and S. J. Parke, Phys. Rev. D **72** (2005) 053003 [arXiv:hep-ph/0505202].

[110] A. Donini, D. Meloni and S. Rigolin, JHEP **0406** (2004) 011 [arXiv:hep-ph/0312072];

[111] P. Coloma, Talk given at NuFACT 09, IIT, Chicago.

[112] K. T. McDonald, arXiv:hep-ex/0111033.

[113] A. Rubbia, arXiv:hep-ph/0106088.

[114] J. Kopp, Talk given at IDS meeting plenary meeting, CERN, 23-24 March 2009.

[115] A. Badertscher *et al.*, arXiv:0804.2111 [hep-ph].

[116] M. Aoki, K. Hagiwara and N. Okamura, Phys. Lett. B **554** (2003) 121 [arXiv:hep-ph/0208223].

[117] M. Ishitsuka, T. Kajita, H. Minakata and H. Nunokawa, Phys. Rev. D **72** (2005) 033003 [arXiv:hep-ph/0504026].

[118] O. Mena Requejo, S. Palomares-Ruiz and S. Pascoli, Phys. Rev. D **72** (2005) 053002 [arXiv:hep-ph/0504015]; O. Mena, S. Palomares-Ruiz and S. Pascoli, Phys. Rev. D **73** (2006) 073007 [arXiv:hep-ph/0510182].

[119] P. Huber and W. Winter, Phys. Rev. D **68** (2003) 037301 [arXiv:hep-ph/0301257].

[120] A. M. Dziewonski and D. L. Anderson, Phys. Earth Planet. Interiors **25** (1981) 297.

[121] A. Takamura and K. Kimura, JHEP **0601** (2006) 053 [arXiv:hep-ph/0506112].

[122] P. Lipari, M. Lusignoli and F. Sartogo, Phys. Rev. Lett. **74** (1995) 4384 [arXiv:hep-ph/9411341].

[123] P. Lipari, Nucl. Phys. Proc. Suppl. **112** (2002) 274 [arXiv:hep-ph/0207172].

[124] P. Huber, M. Lindner and W. Winter, Comput. Phys. Commun. **167**, 195 (2005) [arXiv:hep-ph/0407333]; P. Huber, J. Kopp, M. Lindner, M. Rolinec and W. Winter, Comput. Phys. Commun. **177** (2007) 432 [arXiv:hep-ph/0701187].

[125] http://www.mpi-hd.mpg.de/lin/globes/download.html .

[126] http://www.imsc.res.in/ ino/OpenReports/INOReport.pdf .

[127] S. Amerio *et al.* [ICARUS Collaboration], Nucl. Instrum. Meth. A **527** (2004) 329; F. Arneodo *et al.* [ICARUS collaboration], arXiv:hep-ex/0103008.

[128] A. Rubbia, arXiv:hep-ph/0402110; A. Ereditato and A. Rubbia, Nucl. Phys. Proc. Suppl. **139** (2005) 301 [arXiv:hep-ph/0409143]; A. Ereditato and A. Rubbia, Nucl. Phys. Proc. Suppl. **154** (2006) 163 [arXiv:hep-ph/0509022].

[129] P. .G. Hoel, *Introduction to Mathematical Statistics, 2nd ed.*, Wiley, 1954.

[130] S. Baker and R. D. Cousins, Nucl. Instrum. Meth. **221** (1984) 437.

[131] P. R. Bevington and D. K. Robinson, *Data Reduction and Error Analysis for the Physical Sciences, 3rd ed.*, McGraw-Hill, 2003.

[132] G. L. Fogli, E. Lisi, A. Marrone, D. Montanino and A. Palazzo, Phys. Rev. D **66**, 053010 (2002) [arXiv:hep-ph/0206162].

[133] P. Huber, M. Lindner, M. Rolinec and W. Winter, Phys. Rev. D **73** (2006) 053002 [arXiv:hep-ph/0506237].

[134] M. Jung *et al.*, Phys. Rev. Lett. **69** (1992) 2164.

[135] F. Bosch *et al.*, Phys. Rev. Lett. **77** (1996) 5190.

[136] T. Ohtsubo *et al*, Prog. Theo. Phys. Supp **146**, 493 (2002) Prog. Theo. Phys. Supp **146**, 493 (2002).

[137] T. Ohtsubo *et al.*, Phys. Rev. Lett. **95** (2005) 052501.

[138] D. Boutin, Dissertation Justus-Lieberg Universität Giessen.

[139] J. N. Bachall, Phys. Rev. **124** (1961) 495.

[140] http://www.eurisol.org/site02/index.php .

[141] A. Stahl, talk given at EUROnu WP4 kick-off metting, CERN, 23rd October 2008.

[142] C. Rubbia, A. Ferrari, Y. Kadi and V. Vlachoudis Nucl. Instrum. Meth. A **568** (2006) 475 [arXiv:hep-ph/0602032]; C. Rubbia, arXiv:hep-ph/0609235.

[143] S. K. Agarwalla and P. Huber, arXiv:0909.2257 [hep-ph].

[144] S. Hancock, 'The EURISOL Beta Beam', EURISOL Town Meeting, April 2009.

[145] A. Fabich, private communciation.

[146] B. Autin *et al.*, J. Phys. G **29** (2003) 1785 [arXiv:physics/0306106].

[147] Beta Beam task group presentations, http:beta-beam.web.cern.ch/beta-beam/Presentations/presentations.htm

[148] E. Wildner, *Beta beam R&D status*, in proceedings of *10th International Workshop on Neutrino Factories, Superbeams and Beta beams, Valencia Spain, 30th June - 5th July, 2008*, PoS(Nufact08)007.

[149] M. Hass, D. Berkovits, T. Y. Hirsh, V. Kumar, M. Lewitowicz, F. de Oliveira and S. Veintraub, J. Phys. G **35** (2008) 014042; T. Hirsh, M. Hass, D. Berkovits, Y. Nir-El, L. Weissman, F. de Oliveira, in proceedings of *10th International Workshop on Neutrino Factories, Superbeams and Beta beams, Valencia Spain, 30th June - 5th July,*

2008, PoS(Nufact08)090.

[150] H. Wieldemann, *Particle Accelerator Physics 3rd Ed.*, Springer, 2007.

[151] N. Spooner, private communication.

[152] A. Chance and J. Payet, *Prepared for European Particle Accelerator Conference (EPAC 06), Edinburgh, Scotland, 26-30 Jun 2006*; A. Chance, in proceedings of "10th International Workshop on Neutrino Factories, Superbeams and Beta Beams, June 30 -July 5 2008", Valencia, Spain, POS(Nufact08)088.

[153] M. Fukugita and T. Yanagida, *Physics of Neutrinos and Applications to Astrophysics*, Springer, 2003.

[154] J. Sato, Phys. Rev. Lett. **95** (2005) 131804 [arXiv:hep-ph/0503144].

[155] M. Rolinec and J. Sato, JHEP **0708** (2007) 079 [arXiv:hep-ph/0612148].

[156] A. Algora *et al.*, Proc. XXXII Symposium on Nuclear Physics, Cocoyoc, Morelos, Mexico (2009); M. E. Estévez *et al.*, DPG Spring Meeting, Bochum, Germany (2009); A. Algora, E. Estévez and B. Rubio, *private communication*.

[157] The Berkeley Laboratory Isotopes Project, http://ie.lbl.gov/education/isotopes.htm .

[158] M. Lindroos, AIP Conf. Proc. **981** (2008) 93.

[159] M. Lindroos, J. Bernabeu, J. Burguet-Castell and C. Espinoza, PoS **HEP2005** (2006) 365.

[160] D. Neuffer, FERMILAB-FN-0808-APC .

[161] M. Benedikt, A. Fabich, S. Hancock, M. Lindroos, *The EURISOL Beta-beam Facility Parameter and Intensity Values, Version 2*, EURISOL DS/TASK12/TN-05-03, available from http://beta-beam.web.cern.ch/beta-beam/docs.htm .

[162] E. Wilson, *An Introduction to Particle Accelerators*, OUP.

[163] M. A. Fraser, *A survey of the introduction of rae-earth nuclei into the beta beam accelerator chain in order to attain a monochromatic neutrino beam*, EURISOL DS task note 12-25-2008-0011, available from http://beta-beam.web.cern.ch/beta-beam/docs.htm .

[164] M. Lindroos, J. Bernabeu, J. Burguet-Castell and C. Espinoza, PoS **HEP2005** (2006) 365.

[165] M. Lindroos, private communication.

[166] J. Bernabeu, private communication.

[167] B. Rubio and W. Gelletly, Lect. Notes Phys. **764** (2009) 99.

[168] M. R. Bhat, Nucl. Data Sheets **89** (2000) 797.

[169] C. W. Reich, Nucl. Data Sheets **99** (2003) 753.

[170] H. Keller *et al.*, Z. Phys. A **352** (1995) 1.

[171] E. Nácher *et al.*, GSI Sci. Report 2001, 8.

[172] M. Cirelli, N. Fornengo, T. Montaruli, I. Sokalski, A. Strumia and F. Vissani, Nucl. Phys. B **727** (2005) 99 [Erratum-ibid. B **790** (2008) 338] [arXiv:hep-ph/0506298].

[173] W. H. Press *eta l.*, *Numerical Recipes in FORTRAN: The Art of Scientific Computing 2nd Ed.*, CUP (1992).